

DOCTORAL THESIS

Multifunctional Energy Router for Residential Applications

Mahdiyyeh Najafzadeh

TALLINN UNIVERSITY OF TECHNOLOGY
DOCTORAL THESIS
25/2022

Multifunctional Energy Router for Residential Applications

MAHDIYYEH NAJAFZADEH



TALLINN UNIVERSITY OF TECHNOLOGY

School of Engineering

Department of Electrical Power Engineering and Mechatronics

Power Electronics Group

This dissertation was accepted for the defence of the degree 16/05/2022

Supervisor: PhD Indrek Roasto
Department of Electrical Power Engineering and Mechatronics
Tallinn University of Technology
Tallinn, Estonia

Co-supervisor: Dr. Oleksandr Husev
Department of Electrical Power Engineering and Mechatronics
Tallinn University of Technology
Tallinn, Estonia

Opponents: Prof. Ilya Galkin
Riga Technical University
Faculty of Power and Electrical Engineering
Riga, Latvia

Prof. Luigi Piegari
Polytechnic University of Milan
Faculty of Electronics, Information, and Bioengineering
Milan, Italy

Defense of the thesis: 16/06/2022, Tallinn

Declaration:

Hereby I declare that this doctoral thesis, my original investigation and achievement, submitted for the doctoral degree at Tallinn University of Technology has not been submitted for doctoral or equivalent academic degree.

Mahdiyyeh Najafzadeh

signature



European Union
European Regional
Development Fund



Investing
in your future

Copyright: Mahdiyyeh Najafzadeh, 2022

ISSN 2585-6898 (publication)

ISBN 978-9949-83-835-6 (publication)

ISSN 2585-6901 (PDF)

ISBN 978-9949-83-836-3 (PDF)

Printed by Koopia Niini & Rauam

TALLINNA TEHNIKAÜLIKOO
DOKTORITÖÖ
25/2022

Multifunktsionaalne energiaruuter eramutele

MAHDIYYEH NAJAFZADEH



Contents

List of Publications	7
Author's Contribution to the Publications	8
Abbreviations	9
1 Introduction	10
1.1 Background	10
1.2 Motivation of the Thesis	11
1.3 Aims, Hypotheses and Research Tasks.....	11
1.4 Contribution and Dissemination	12
1.5 Experimental Setup	12
1.6 Outline.....	13
2 Energy Router Concept	14
2.1 Energy Router Role in the Energy Internet	14
2.2 ER Structures	15
2.3 The Industrial Hybrid Inverters' Configurations	16
2.4 The Proposed ER Topology	18
2.5 ER Control Structure	19
2.6 ER Control Techniques	20
2.7 Summary	21
3 Operation Modes of ER	23
3.1 General Transition Modes.....	23
3.2 Different ER Configurations and Operation Modes	25
3.3 Summary	27
4 Control System Tuning and Implementation	29
4.1 VSIs' Control Block Diagrams	29
4.1.1 CCM Control of VSI	29
4.1.2 VCM Control of VSI: MPC Implementation	30
4.1.3 VCM Control of VSI: Enhanced MPC Implementation	35
4.1.4 DC-link Voltage Control Using FLC Regulator	40
4.1.5 Dc-link Control Considering Constant Power Loads.....	43
4.2 Battery Control Diagram	47
4.2.1 Active Decoupling with Battery Utilization	47
4.3 PV Control Diagram.....	48
4.4 Summary	48
5 Conclusions	52
References	53
Acknowledgements.....	57
Abstract	58
Lühikokkuvõte.....	59
Appendix	61
Curriculum vitae.....	155
Elulookirjeldus.....	156

List of Publications

The following is a list of author's publications, on the basis of which the thesis has been prepared:

- I Najafzadeh, M.; Ahmadihangar, R.; Husev, O.; Roasto, I.; Jalakas, T.; Blinov, A. Recent contributions, future prospects and limitations of interlinking converter control in hybrid AC/DC microgrids. IEEE Access, 2021.
- II Roasto, I.; Husev, O.; Najafzadeh, M.; Jalakas, T.; Rodriguez, J. Voltage source operation of the energy-router based on model predictive control. Energies, 2019, 12 (10), 1892.
- III M. Najafzadeh, O. Husev, R. Strzelecki, I. Roasto, N. Strzelecka, D. Vinnikov, Grid-Forming Operation of Energy-Router Based on Model Predictive Control with Improved Dynamic Performance. Submitted for publication.
- IV M. Najafzadeh, I. Roasto, T. Jalakas, Energy Router Based Energy Management System for Nearly Zero Energy Buildings, 2019 IEEE 60th International Scientific Conference on Power and Electrical Engineering of Riga Technical University (RTUCON), Riga, Latvia, 2019, pp. 1–6, DOI: 0.1109/RTUCON48111.2019.8982366.
- V M. Najafzadeh, O. Husev, I. Roasto, T. Jalakas, Improved DC-Link Voltage Transient Response and Stability Issues in Energy Router with Fuzzy Logic Control Method, 2020 IEEE 60th International Scientific Conference on Power and Electrical Engineering of Riga Technical University (RTUCON), Riga, Latvia, 2020, pp. 1–6, DOI: forthcoming.
- VI M. Najafzadeh, O. Husev, I. Roasto, Dmitri Vinnikov, DC Nano Grid Control in the Residential Energy Router with the Presence of Constant Power Loads, IEEE 7th International Energy Conference (ENERGYCON 2022) in Riga Technical University (ENERGYCON), Riga, Latvia, 2022, pp. 1–6, DOI: 10.1109 / ENERGYCON48111.2019.8982258.
- VII M. Najafzadeh, O. Husev, I. Roasto, D. Vinnikov, T. Jalakas, DC-link Capacitor Minimization In Residential Energy Router Through Battery Utilization, CPE POWERENG 2021, Italy, Florence. pp. 1–6, DOI: forthcoming.

Author's Contribution to the Publications

Contributions to the papers in this thesis are:

- I Mahdiyyeh Najafzadeh as the main author has reviewed, classified, and concluded the prospects of the literature. She was responsible for submission and contact with editors in the peer-review process.
- II Mahdiyyeh Najafzadeh as the co-author was responsible for small signal modeling equations and stability analysis of the system. She has co-authored the writing.
- III Mahdiyyeh Najafzadeh as the main author has improved the control technique and developed it with software in the experimental setup. She was responsible for experimental validation results and writing.
- IV Mahdiyyeh Najafzadeh as the main author has provided small signal and stability analysis and simulation results in PLECS. She wrote and presented the paper at the 2019 IEEE 60th International Scientific Conference on Power and Electrical Engineering of Riga Technical University (RTUCON) in Riga, Latvia.
- V Mahdiyyeh Najafzadeh as the main author has reviewed the literature and provided the simulation results in PLECS. She wrote and presented the paper at the 2020 IEEE 60th International Scientific Conference on Power and Electrical Engineering of Riga Technical University (RTUCON) in Riga, Latvia.
- VI Mahdiyyeh Najafzadeh as the main author was responsible for the literature review, methodology, and simulation results. She also wrote and presented the paper at ENERGYCON 2022 in Riga, Latvia.
- VII Mahdiyyeh Najafzadeh as the main author has reviewed the literature and provided the simulation results in PLECS. She wrote and presented the paper at CPE POWERENG 2021, Italy, Florence.

Abbreviations

AC	Alternating Current
BIC	Bidirectional Interlinking Converter
CCM	Current Controlled Mode
CPL	Constant Power Load
DC	Direct Current
DG	Distributed Generation
EMI	Electromagnetic Interference
ER	Energy Router
ES	Energy Storage
FLC	Fuzzy Logic Controller
iMPC	Indirect Model Predictive Control
MPC	Model Predictive Control
NZEB	Nearly-Zero-Energy-Building
PCB	Printed Circuit Board
PCC	Point of Common Coupling
PF	Power Factor
PFC	Power Factor Correction
PI	Proportional Integrator
PID+R	Proportional Integrator Derivative and Resonant
PLL	Phased Locked Loop
PV	Photovoltaic
SCADA	Supervisory Control and Data Acquisition
SOGI	Second-Order Generalized Integrator
THD	Total Harmonic Distortion
VCM	Voltage Controlled Mode
VSC	Voltage Source Converter

1 Introduction

1.1 Background

The increasing temperature of the planet and climate change are concerning issues caused by greenhouse gases. Referring to the European Environment Agency report, energy production in form of heat and electricity are the main sources of greenhouse gases. The main alternative to traditional power generation is renewable energy sources. However, the electrical output (voltage, current, and frequency) of renewable sources varies in a wide range and needs stabilization before it can be used by a load or injected into the grid. The stabilization will be done by power electronic converters, which means that the number of converters will grow together with renewable sources. The main goals of the modern power electronics are:

- Increasing efficiency while maintaining economic feasibility.
- Increasing reliability of the systems.

The first goal can be met by utilizing new semiconductor components e.g. GaN, SiC MOSFETS, which allow higher switching frequencies, operation temperatures, increased efficiency, and lower costs. The second goal is mainly related to control system development and its effectiveness. Recently, Texas Instruments has brought dual core microcontrollers for power electronics on the market, which have opened new opportunities to implement complicated nonlinear control algorithms for fast and more precise control [1].

Together with the growing number of distributed renewable sources the structure of the power grid will be changing as well. Centrally controlled grid is regrouping into smaller independent segments called microgrids. Microgrids have local sources and storage units available, which means they can also work independently from the main grid. All sources, storages, and loads are interfaced with power electronics converters. The power electronics converter that connects the microgrid with the main grid is called an energy router (ER). ER is the key component for successful energy management in microgrids.

Such ER-coupled microgrids have many advantages compared to traditional transformers interfaced grids. They have volume and weight reduction, better power density, and higher efficiency over the full operation range, i.e. from no-load to full power. Moreover, power electronics allows implementing various active functions that are not possible with conventional line-frequency transformers:

- Active and reactive power control.
- Voltage control (compensation of voltage sags and peaks, harmonic control).
- Current control (harmonic cancelation, short-circuit protection).
- Integration of distributed generation (MPP tracking, energy storage management).
- Protection functions (island detection, frequency, voltage, and current monitoring, short circuit protection).

In general, the size of the microgrid is not clearly defined. The microgrid could be a city, a village, or even a house. The current doctoral thesis focuses on the ER implementation in residential buildings, which can be seen as small-scale microgrids with a power level of less than 50 kW.

1.2 Motivation of the Thesis

The ER concept and role in microgrids is well-known and described in many scientific publications. On the other hand, its application in residential applications is still relatively little studied, which was the main motivator for the current doctoral thesis. Residential application mainly refers to buildings. Today the building sector is considered as one of the biggest energy consumers. In Europe, the annual consumption is over 40 % of the total energy [2]. To meet EU targets for energy saving and decarbonization, new requirements have been imposed for buildings. By 2021 all new buildings must satisfy nearly zero energy building (NZEB) requirements i.e. energy-efficient buildings with energy storage and generation capability [3]-[4]. However, without proper energy management, such building can never utilize their full potential. An energy router is a suitable technology to provide the needed flexibility and control for residential buildings.

A further motivation of the thesis is to achieve a broader paradigm shift in the buildings sector. By introducing ER concept, the residential buildings could be transferred into a small-scale microgrid (i.e., a nanogrid). Only then the full potential of NZEB could be achieved. From the scientific point of view, there are many challenges to solve from both the hardware and software sides. However, this thesis focuses mainly on control system-related issues. The versatility of different operation modes requires a complex and multilevel control system, which is especially inspiring for the author.

1.3 Aims, Hypotheses and Research Tasks

Partly the concept of the energy router has been implemented by the industry in form of hybrid solar inverters. These are inverters with integrated energy storage that allows them to work as well in on-grid as in off-grid modes. However, the energy router includes much more functionalities than it can be found in conventional hybrid inverters e.g. ancillary services, reactive power control, harmonics injection, smart energy management, etc. Also the ER structure provides more modes of operations compared to its industrial counterparts. This Ph.D. work aims to introduce ER topology with enhanced functionality and optimize its performance with the proposed control system.

Hypothesis:

1. The flexibility of conventional energy router topologies can be extended, and new operation modes can be introduced by the means of adding an auxiliary bypass switch to the converter.
2. The dc-link voltage regulation of conventional linear control techniques could be improved by artificial-intelligence-based control.
3. An inevitable part of the energy router is a battery energy storage. In addition to covering load-side energy shortages, the battery with proper control could be used also for the dc-link voltage ripple mitigation.
4. A model predictive control can provide better performance compared to traditional linear controllers in the grid-forming operation.

Research Tasks:

1. Review of power electronics aspects and control techniques of conventional hybrid micro-/nanogrid converters.
2. Development and implementation of needed control functions in the ER at the point of common coupling (PCC), such as current control, PV, and battery control.
3. Improvement of the ER performance in the grid-forming operation mode.
4. Design an artificial-intelligence-based control for the dc-link voltage control.
5. Evaluate the possibility of battery utilization as a decoupling tool for dc-link voltage control.
6. Experimental verification of the proposed control and operation modes of the ER.

1.4 Contribution and Dissemination

This research contributes to the single-phase AC/DC/AC ER interface for residential applications. It also investigates different scenarios of the ER operation modes and the deficits of the linear control system, has proven the better performance of the nonlinear control system, and verified the proposed control method compared with the linear control system.

Scientific novelties:

- ✓ Developing Fuzzy Logic Controller (FLC) for dc-link voltage control of the ER.
- ✓ Implementing Model Predictive Control (MPC) for the ac grid-forming operation of the ER.
- ✓ Utilization of battery as a decoupling tool for dc-link voltage control.
- ✓ The required control technique selection and suitable ER configuration in different scenarios.

Practical novelties:

- ✓ Developing the ER topology by adding a static transfer switch.
- ✓ Reducing Total Harmonic Distortion (THD) of the voltage in grid-forming operation with nonlinear loads.

The main findings of this work have been published in four IEEE international conference papers and three international journal articles, which are provided in the author's publication list.

1.5 Experimental Setup

This work is verified via an experimental prototype shown in Figure 1.1, containing two boards. The top PCB is the measuring and control board, whereas the bottom is the power PCB. The measuring and control board contains voltage and current sensors and a microcontroller. The required inputs' currents are measured by Hall effect current transducers ACS720. The inputs' voltage is sensed by optically isolated precision voltage sensors ACPL-C87A. TMS320F2837 microcontroller unit is implemented on the control board. 1200 V MOSFETs IMZ120R030M1H are utilized for switches.

In the experimental verification process, a range of different lab equipment has been used. Dc supply Electro-Automatik EA-PSI 9080-60, autotransformer, and different load resistors are utilized. The digital oscilloscope Tektronix MSO4034B with current probes Tektronix TCP0150A, TCP0030A, and voltage probe Tektronix P5205A are used to demonstrate the required voltage and currents signals.

1.6 Outline

This thesis encompasses five chapters. The first chapter provides a general introduction to the work. The second gives the ER concept description, topologies, and control techniques in detail. In the third section, operation modes of the ER are investigated. Accordingly, the control system tuning and its implementation are performed in the fourth chapter. Finally, the conclusions are discussed in the fifth chapter.



Figure 1.1 The 5-kW experimental prototype.

2 Energy Router Concept

2.1 Energy Router Role in the Energy Internet

Increasing wide-scale DG application requires double-side energy-sharing and energy-information directions, promoting the idea of an 'energy internet'. This energy internet enhances the smart grid to a web-based one. The smart grid is mostly dominated by centralized power generation and some large-scale DGs. As a result, the required communication system is a single-direction network and it is mainly controlled regionally. However, emerging wide-scale DGs need two-direction energy flow, two-direction communication networks such as the internet, smart metering, and real-time monitoring. Furthermore, the energy internet provides open access to large-scale DGs, the energy market, and trading platforms for both end-users and operators, leading to more openness, increased efficiency, and opportunities to increase wide-scale or small-scale-power DGs [5][6].

This energy internet is multiple sets of smart communities such as buildings [4]. The smart community has different names, such as energy subnet [7], and nanogrid [8]. An NZEB is also considered to be another example of smart communities. An NZEB requires three key technologies: plug-and-play interface (power delivery infrastructure), a double-direction communication network or a web, and an ER as shown in Figure 2.1 [9].

The plug-and-play structure connects the main grid, ESs, DGs, and loads. The increasing penetration of sources and loads with dc-nature confirms the future of the plug-and-play structure. However, the existing main grid is ac, which promotes the hybrid structure. The main reason is that the hybrid structure is more compatible with the existing grid. Synchronization issues, reactive power circulating, more power loss, and more power transfer stages are the downsides of the ac structure. However, the existing grid system needs high modifications to upgrade to the dc structure. The non-zero crossing feature of dc is the main challenge in the dc circuit breakers of dc structures.

The communication feature is distributed among DGs, ESs, and loads. This feature is embedded in the ER. This communication network allows the ER to control the system and to communicate and coordinate with other ERs and higher-level controllers [9][4]. An ER which is called, based on the energy internet concept, a Bidirectional Interlinking Converter (BIC) device, acts as an intelligent manager in the system.

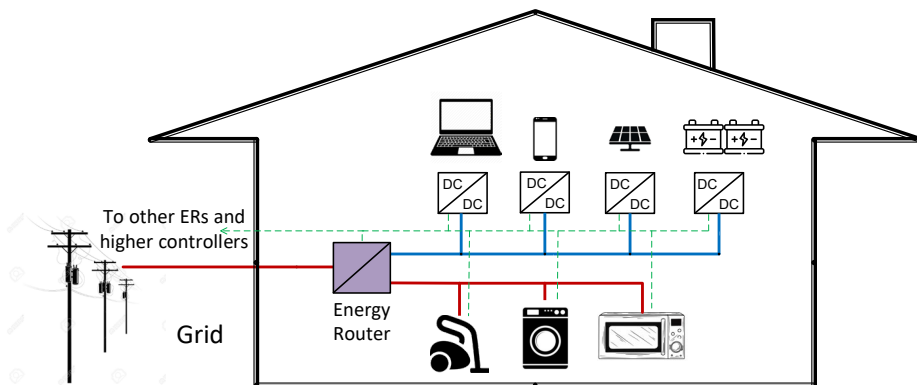


Figure 2.1. NZEB features.

It has different names such as MER (multiport energy router) [7], ECC (energy control center) [10], BEMS (building energy management system) [11][12], IEM (intelligent energy management) [6]. The main features of ERs for NZEBs applications are:

- Programmable master supply among grid, battery, and PV.
- Programmable multiple operation modes based on the loads, PV, battery, and grid presence.
- Programmable charging current and voltage based on different battery types.
- Enables working off-grid as Uninterruptable Power Supply.
- Upgrades to having multiple communication types.
- Smart metering.
- Real-time monitoring and control of sources and loads.

2.2 ER Structures

As small-scale grids (less than 20kW) like NZEBs are considered nanogrids, their ER structures and their control techniques are similar to interlinking converters in microgrids [8]. The BIC's topologies in hybrid microgrids are proposed depending on the galvanic isolation requirement, grid-input voltages, load-side voltages, and the dc-link voltages. A review in [1] summarized the majority of suggested studies and worked on the hybrid configuration, as shown in Figure 2.2. This structure contains two main bars, ac and dc; whereas ac loads and sources connect to the ac bar, dc loads and sources connect to the dc bar. To enhance dc bar voltage stability, a third DS bar is suggested in some works as an energy buffer, energy balancer, and fault ride-through tool. This bar is a slack type that is linked with DSs such as batteries and supercapacitors.

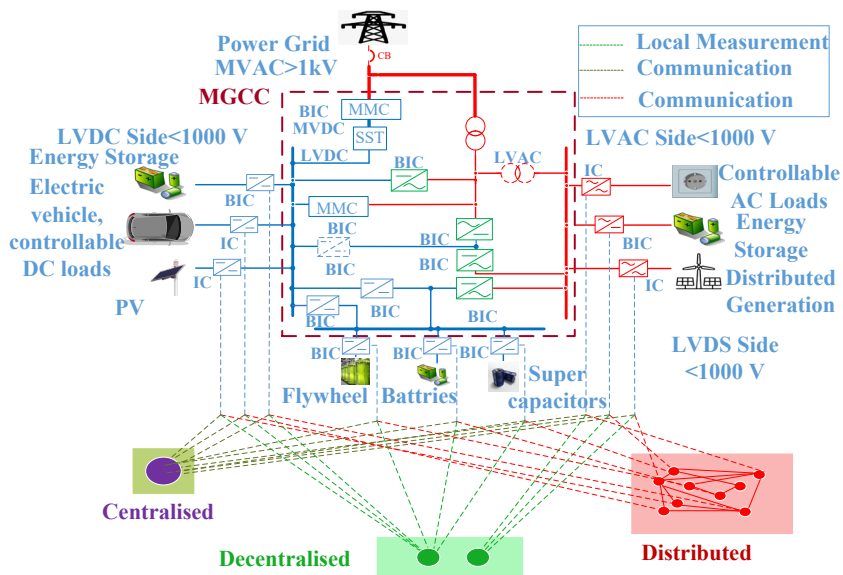


Figure 2.2. Conventional hybrid microgrid configuration [1].

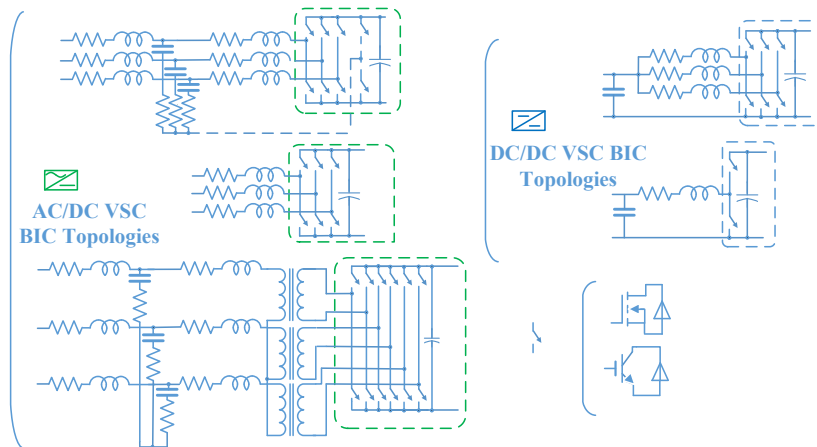


Figure 2.3. Common topologies in microgrid structures [1].

As the stable voltages for the aforementioned bars have to be provided in both grid-tied and isolated mode, the back-to-back or one full-bridge Voltage Source Converters (VSCs) are the most popular topologies, as demonstrated in Figure 2.3. On the other hand, CSCs' configurations are less popular for dc-side ripple current and the resulting ac-side harmonics reasons. Nevertheless, the current-limiting nature and the resulting increased reliability in the CSCs configurations have motivated researchers to study them in different applications such as PV, wind, and fuel cell interfaces with the main grid.

2.3 The Industrial Hybrid Inverters' Configurations

The purpose of this section is to provide a comparative analysis of hybrid solar inverters on the market. Several of the most popular commercial hybrid solar inverters on the market have been chosen for comparison. The selected power range is from 3 kW to 5 kW, which is the typical PV power range for residential applications. All characteristics of commercial hybrid inverters obtained from the open sources are shown in Table 2.1 [13]–[22]. These inverters illustrate a variety of solutions that are available on the market. The most popular manufacturers were selected for analysis.

Most of the inverters are single-phase with an average maximum efficiency of around 97%. It should be noted that maximum efficiency is the efficiency that can be observed only in one operation point. European Weighted Efficiency or California Energy Commission (CEC) efficiency is another, more important, parameter.

From Table 2.1 The most common commercial hybrid inverters. it is clear that there are two types of inverters – first with low battery voltage range such as Sungrow SH5K-30, Redback SH5000, and Imeon 3.6. The low voltage range (42 V - 58.8 V) leads to a high charging/discharging current. It is supposed that they use isolated battery interface converters. In the case of Redback SH5000, it is 85 A and 100 A respectively. The second type is inverters with high battery voltage, for example, Solis RHI-1P5K-HVES-5G. Its battery voltage varies from 120 V to 500 V. In this case charging and discharging currents are only 20 A. Compatible batteries for inverters are mostly Li-ion. However, 3 phase Fronius SYMO Hybrid requires a LiFePO4 type of battery. All of the selected inverters use the same standard communications – RS485 connection or a CAN Bus.

Table 2.1 The most common commercial hybrid inverters.

NO	Device	ac Nominal power, W	Max. efficiency, %	Number of phases	Battery type	Battery Voltage Range, V	Max. battery power, W	Battery communication	Comments
1	Huawei SUN2000 -5KTL-L1	5000	97.8	1	Li-ion	350 - 450	5000	RS485	The battery is connected to dc-link.
2	Fronius SYMO Hybrid 5.0-3-S	5000	96	3	LiFePO4	240 - 345	4800	RS485	Different battery packs can be used.
3	Sungrow SH5K-30	5000	97.1	1	Li-ion	32 – 70	4500	CAN/RS485	
4	Redback SH5000	5000	97	1	Li-ion	42 – 58.8	4600	CAN	
5	ABB REACT2- UNO- 5.0-TL	5000	96.6	1	Li-ion	170 - 575	5000	RS485	
6	Solis RHI- 1P5K- HVES-5G	5000	97.5	1	Li-ion	120 - 500	7000	CAN/RS485	Continuous maximum battery power is 6 kW.
7	Imeon 3.6	3000	94.5	1	Li-ion	42 – 62	3840	RS485	
8	SolaX X3 Hybrid 5.0T	5000	97	3	Li-ion	200 - 500	5000	CAN/RS485	
9	Sunny Boy Storage 5.0	5000	97.5	1	Li-ion	100 - 550	5000	CAN/RS485	

The possible structure of the hybrid solar inverters is illustrated in Figure 2.4. It shows the solar terminals, grid-connected Voltage Source Inverter (VSI), and a buck-boost cell which realizes Maximum Power Point Tracking (MPPT) function and common dc-link. In addition, most commercially available inverters have terminals for a backup operation.

In the case of string solar hybrid inverters, the battery can be connected with an additional interface converter that is integrated with the Energy Storage, as shown in Figure 2.4a [23] and Figure 2.4b [24], [25]. The example of a structure without an additional interface converter is realized in Huawei SUN2000-5KTL-L1. Simplicity and cost are the main advantages, while limited battery type and voltage is the main drawback. An example of the external ESS with an additional interface converter, as in Figure 2.4a, is Fronius SYMO Hybrid 5.0-3-S. In this case, the company provides the ESS system as an additional feature, while the inverter has dc-link terminals for connection. Other hybrid

solar inverters, such as Sungrow SH5K-30, have isolated integrated battery interface converters. This corresponds to the structure illustrated in Figure 2.4b. Due to this, the high step-up of the battery voltage can be realized.

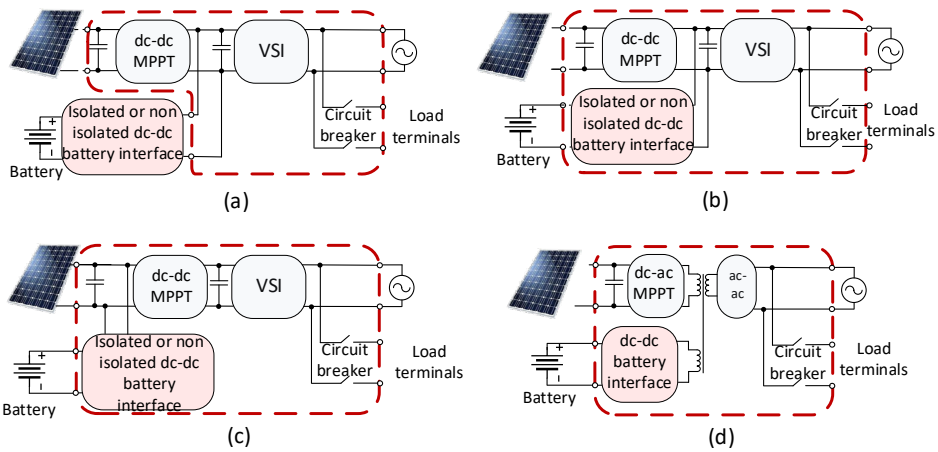


Figure 2.4. Typical structure of the hybrid solar inverter. a) without battery interface, b) integrated with battery interface connected to dc-link, c) integrated with battery interface connected to PV, d) isolated hybrid solar interface.

In addition, Figure 2.4c. shows the internal structure of the hybrid inverter where the internal interface battery converter can be connected to the solar panel terminals.

There are several types of microinverters. The concept of microinverters is the same as solar inverters. The difference consists of the power and voltage levels. Usually, they are intended for single solar panel connection in a range from 10 V to 60 V and low-voltage battery. Due to the significant voltage difference between the input side and the grid, the step-up transformer is utilized. This concept is illustrated in Figure 2.4d. Despite an interesting idea that seems to be suitable for residential application, some difficulties are reported in [26], [27]. The main constraints are connected with battery overheating in case of tied coupling with solar panels.

2.4 The Proposed ER Topology

As the small-scale power in NZEB, the DS bar can be combined with the dc bar. The proposed ER topology is an isolated topology, consisting of a single-phase two back-to-back full-bridge Voltage Source Converters (VSCs), connecting via a 400 V dc-link. By back-to-back connection of inverters, electrical isolation between the main grid and ac-load is provided. However, a lack of blocking leakage-current techniques or equalizing two sides of ground voltage can cause the high-frequency common-mode voltage noise. The former methods can be solved by a different configuration of leakage-current blocking switches during the freewheeling period or by galvanic isolation [1] whereas the latter is performed by the virtual common ground on the ac and dc sides [28], [29]. This high-frequency voltage produces high-frequency leakage current damaging equipment, more power loss, Electromagnetic Interference (EMI) issues, lower quality of the ac-side current, and jeopardizes human safety [30]. Line frequency transformer and high-frequency transformer are two ways of providing galvanic isolation. However,

the line-frequency transformers are bulky and high-frequency transformer topologies need complicated switching. The cost and power loss are other negative issues of galvanic transformer utilization.

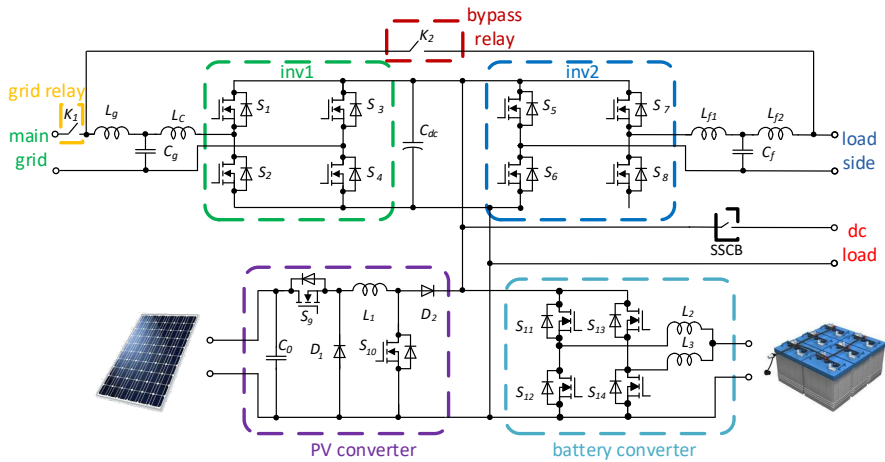


Figure 2.5. The energy router topology.

Dc-link capacitors are used to stabilize the dc-link voltages by decoupling the high to intermediate frequency dynamics between the dc and ac sides.

The ER topology is demonstrated in Figure 2.5 showing inv1 is connected to the main grid through an LCL filter, whereas inv2 is connected to the ac-load via its LCL filter. Inv1 is connected to the main grid by K_1 the grid relay. K_2 bypasses the back-to-back inverters. A two-switch noninverting buck-boost converter is utilized for the PV converter. An interleaved bidirectional buck-boost converter is used as the battery converter. SS CB is a solid-state circuit breaker to turn on and off dc-loads.

2.5 ER Control Structure

ER controls different active functions that can be divided into energy management and protection. These control objectives are:

Energy management functions:

- Active and reactive power control at PCC
- Voltage control
- Current control
- Grid-synchronization
- Integration of DGs and MPPT tracking
- Integration of ESSs and SOC control
- Seamless transition between different operation modes
- Economic energy dispatch
- Power quality control

- Harmonic mitigations
- Increased the reliability (off-grid operation, redundant supply, modular structure)

Protection functions:

- Islanding detection [31]
- Fault detection (over-voltage, current, and frequency protection)
- Black start management

The control structure in the hybrid microgrid depends on the communication network which can be implemented as decentralized, centralized, and distributed [32], as shown in Figure 2.2. All the aforementioned functions are divided into three time-scale layer tasks discussed in [1]. The first layer (local control) is responsible for providing stability through decentralized, master-slave, centralized, or distributed control structures. The second layer recovers the voltage and frequency deviation of the local controller, whereas the third layer communicates with Supervisory Control and Data Acquisition (SCADA) to optimize the total energy price and minimize the power loss [33]. To increase the reliability of the system, a free-communication or decentralized structure is suggested for the local controller while the performance of the second and third layers depends on the communication network.

The proposed control structure for NZEB is a centralized type in which all elements are managed by the ER. Based on this control structure, the ER can receive the hierarchical command from upper-level controllers to contribute to peak shaving, reactive or active power control, and economical control strategy based on weather conditions, energy price, and load profile. Different control strategies are utilized among different converters within the ER for different operation modes. In this work, the focus is on the local control of the ER considering the upper-level set points.

2.6 ER Control Techniques

The main control objective in an ER is power-sharing, through which the voltage and frequency stability can be satisfied. Power-sharing is achieved by three concepts: current or voltage control loop, droop, and virtual synchronous generator. The control techniques are divided into linear and nonlinear methods. Studies have shown the greater performance of nonlinear controllers in terms of dynamic response in power electronics converters. The traditional Proportional Integrator Derivative and Resonant (PID+R) is the linear technique nevertheless, MPC, FLC, and RL are the nonlinear techniques.

When the ER works in grid-tied mode, it follows the voltage grid so the exchange current is controlled. In isolated mode, providing a stable voltage is the control parameter so the ER works in grid-forming or voltage-controlled mode.

The droop concept is used for ac, dc, and hybrid nano-/microgrids as ac, dc, and hybrid droop. Depending on the availability of the communication system it can be an active droop which is more accurate in terms of transient response, voltage deviations, and power-sharing, at the expense of lower reliability [34][35]. As a result, the output voltage and frequency of the active droop method are closer to the reference values without secondary layer control [36]. On the other hand, free communication droop performance is dependent on the line parameters, resulting in inaccurate voltage regulation.

The widespread PID+R regulator is also called a dual loop. To track the reference current or voltage, an outer voltage loop and an inner current loop in different frames provide the required switching functions.

An MPC technique provides the optimized switching states based on minimized cost function in every sampling time. The common cost function contains the amplitude or root mean square of the difference between the reference and predicted parameters with their coefficients and limitations [37]. The predicted parameters are calculated in each sampling time based on the state equations of the system. The main challenge is to determine the coefficients. Higher prediction horizon steps result in enhanced performance and stability at the expense of higher processing time. MPC can include or exclude the modulator in the finite control set MPC or continuous control set MPC consequently [38]. As a result, the switching frequency is variable; however, in the other type of MPC the switching frequency is constant. Comparison between the finite control set and the continuous control set MPC shows higher harmonics and THD in the controlled parameter infinite control set. On the other hand, the variable switching frequency provides degree of freedom that can be integrated into the cost function to mitigate the power loss and consider thermal balance among switches[39].

FLC is another nonlinear technique that uses linguistic variables instead of numbers, replicating human intuition.

RL is a new topic, consisting of environment, agent, action, reward, penalties, and states. It concentrates on maximizing the rewards for agents based on their actions in predefined environment states [1]. This topic is a trend in the control of dc-dc converters and dc grids [40]-[41].

Different control techniques and comparisons are summarized in Table 2.2.

2.7 Summary

In this chapter, the concept of the energy router and the energy internet is discussed. The most common counterparts of ER in scientific research and industry are investigated. Following this, the ER structure and its functions is reviewed. Finally, the state-of-the-art control techniques of power electronics interfaces are classified and summarized.

Table 2.2 Comparison of different control techniques [1].

Technique	Pros	Cons	Application
PID+R	<p>Less computational time</p> <p>Fixed switching frequency</p> <p>Easy to implement</p>	<p>Dependency on the mathematical analysis</p> <p>Dependency on the dynamics of the system</p> <p>The complicated control system in terms of the cascaded control structure, feedback loops, and PWM structure</p> <p>Time-consuming parameter tuning of PID+R</p> <p>Slow in the dynamic response</p>	<p>Most mature technique in both ac and dc practice</p>
MPC	<p>Multi-objective optimization control technique</p> <p>Fast transient response</p> <p>Simplifies the control structure by combining the modulator block</p>	<p>More computational burden</p> <p>Needs a high sampling frequency</p> <p>FCS produces extra harmonics</p> <p>Difficulty and uncertainty in the determination of weighting factors in the cost function</p> <p>Dependent on the accuracy model of the system</p>	<p>Both ac and dc application</p>
RL	<p>Able to learn without pre-required knowledge</p> <p>Able to combine with other techniques</p>	<p>Convergence dependency on the initialization</p>	<p>New technique in dc grids</p>
FLC	<p>Does not need an accurate mathematical model of the system</p> <p>Does not need an accurate model of training</p> <p>An easy technique for control of complicated systems</p> <p>Simple rule-based membership functions</p> <p>Less sensitivity to disturbances</p> <p>Able to combine with PID+R controllers</p>	<p>Time-consuming in setting the membership functions</p> <p>Not optimized in terms of identifying membership functions</p> <p>Complicated in increasing numbers of inputs and outputs</p>	<p>Dc application</p>

3 Operation Modes of ER

3.1 General Transition Modes

ER operation modes can be classified into 4 main modes, as shown in Figure 3.1 when the ER is stopped, it is in standby mode. In other words, standby mode is the start point of ER operation after ER is paused by the user or tripped by a fault. Standby mode goes to the grid-tied mode if the grid connection is safe by pressing the start command and it goes to the islanded mode if the grid connection is not safe. The ER internal conditions are checked at each sampling time. In the case of major errors, the ER goes to fault mode and it is blocked. Moreover, it islands the error elements in minor fault conditions and after erasing the minor faults, then these islanded elements reconnect to the system. In the case of major faults, after clearing the fault, the ER can go into standby mode by the reset button. In the case of islanding detection or island command, the ER moves to fault mode. Moreover, when the grid is stabilized then the black-start command (Automatically or by user) connects the ER to the main grid.

Based on the availability of the battery, PV, and the main grid different configuration schemes are available as shown in Figure 3.2 and Figure 3.3. Figure 3.2 shows the grid-tied operation modes, in which K1 is closed. Figure 3.3 demonstrates the islanded operation mode where K1 is open. These figures show different configurations based on different scenarios in Table 3.1 and Table 3.2 which will be described in further detail. Furthermore, the K2 relay bypassing two back-to-back VSCs provides the following operation modes:

1-parallel operation of inverters. As a result, the required nominal power of the switches can be decreased. In the case of grid-tied operation, both inverters work in Current Controlled Mode (CCM). In the case of islanded mode, one inverter can work in VCM and the other in CCM.

2-redundant mode of inverters, which makes it possible to use the other inverter when it is required.

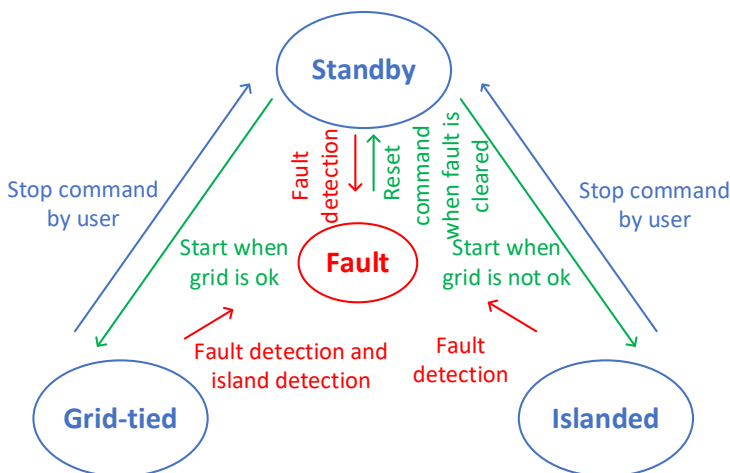


Figure 3.1 ER main operation modes.

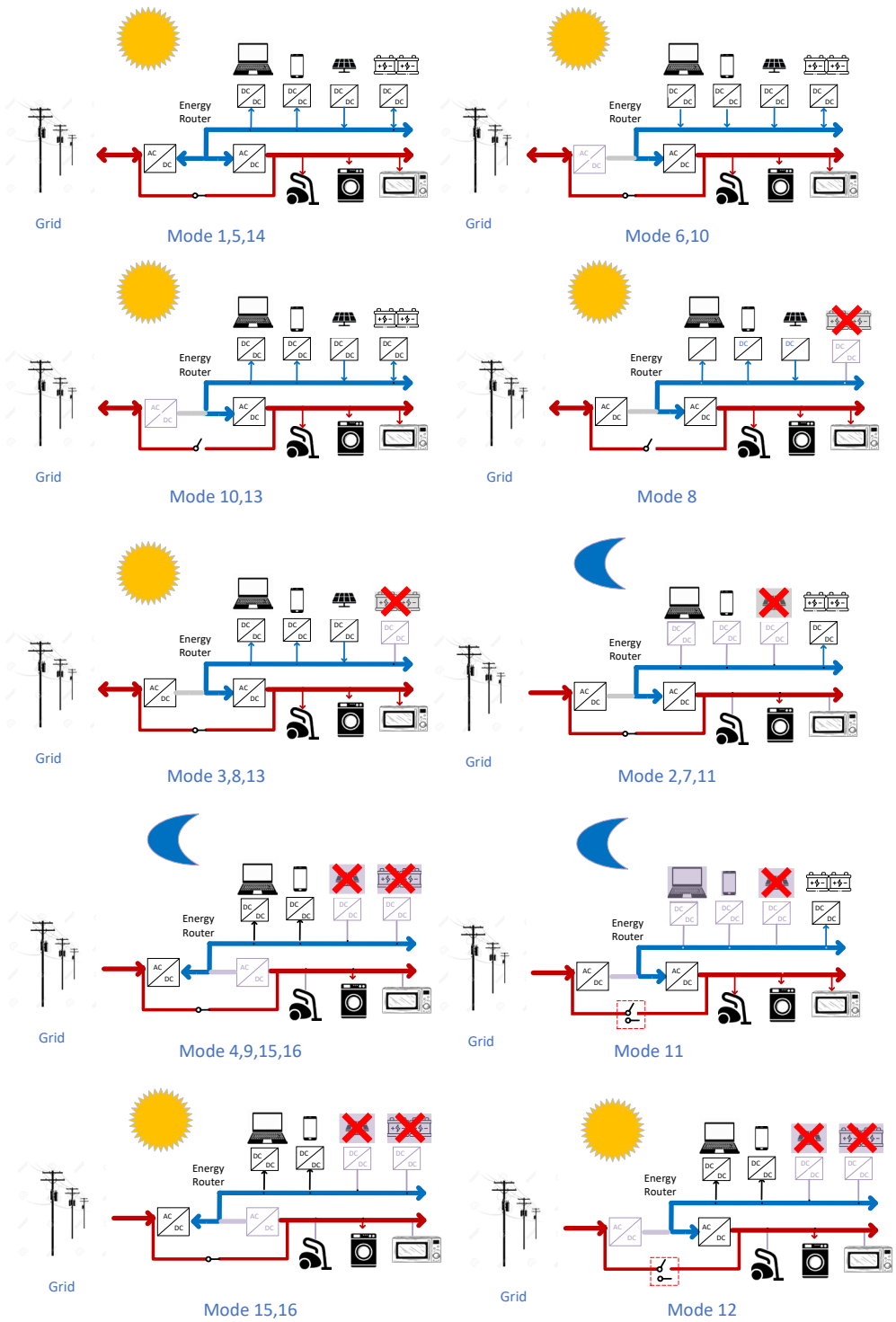


Figure 3.2 Grid-tied operation modes of ER.

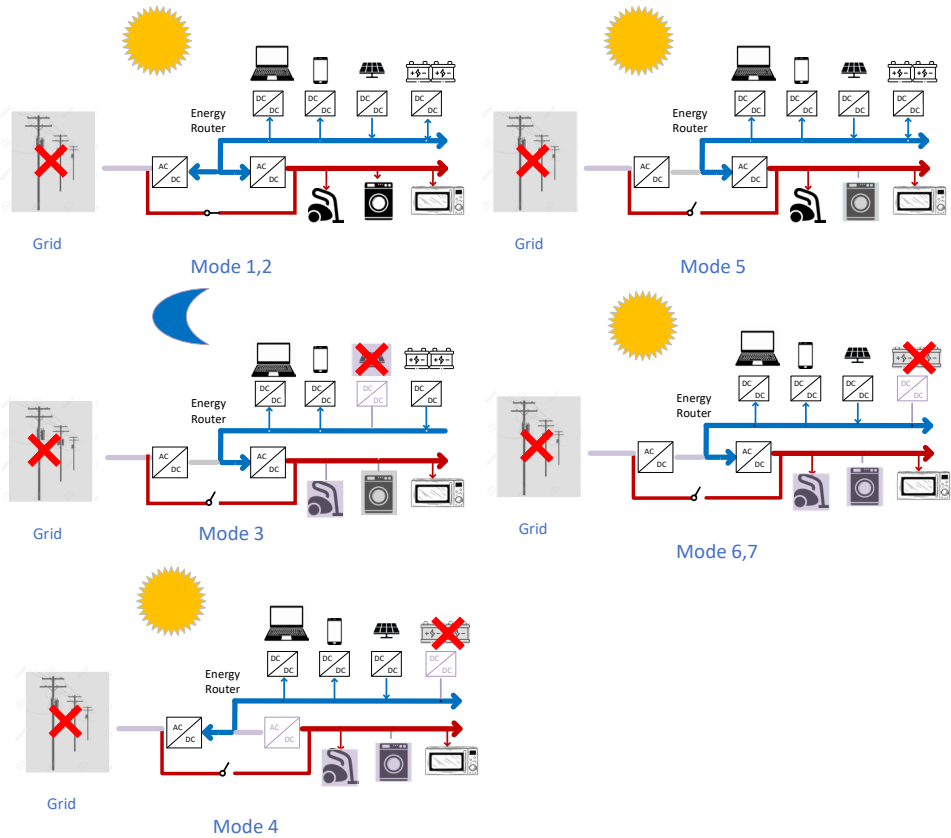


Figure 3.3 Isolated operation modes of ER.

3.2 Different ER Configurations and Operation Modes

The peak load for a residential application is assumed to be 5 kW based on a consumption profile of a four-member family in Estonia [42]. The nominal power of converters is 3.6 kW. The PV and the battery MPPT are 3.6 kW. The target is to balance generation-load via different modes. Based on the ac load (p_{ac}), dc load (p_{dc}), MPPT PV (p_{pv}) and SOC of battery, the master device is selected. The master device is responsible for stabilizing the dc-link voltage via working in Current Controlled Mode (CCM). Inv2 is also responsible for providing ac-link voltage working as Voltage Controlled Mode (VCM) in the case it is not bypassed by K2. Based on this, different configurations of ER are suggested in Table 3.1 and Table 3.2. Comparison of typical dc-load versus ac-load in residential appliances in [43] shows the majority of residential appliances are ac, and the typical dc-load power range is low. As a result, the peak of typical dc-powered appliances is assumed to be less than 3.6 kW.

Another issue is the policy of battery utilization to maximize profits and prolong its lifetime. The battery degradation consists of calendric aging and cyclic aging. Calendric aging depends on various stress factors such as SOC, stored time, and temperature [44][42]. As a result, to enhance the li-ion battery lifetime, the SOC should be kept in a limited range. Consequently, the SOC limit is considered to be between 20% and 90% [45].

Table 3.1 Grid-tied operation-mode configurations of the ER (K1 closed).

Peak hours	Modes No.	p_{ac} (kW)	$p_{pv} + p_{es}$ (kW)	SOC (%)	Es mode	PV mode	K2 relay	inv1	Inv2
	1	≥ 3.6	$\leq p_{ac} + p_{dc}$	≥ 20	CCM	MPPT	Closed	Master CCM	CCM
	2				CCM	No PV	Closed	-	Master CCM
	3				-	MPPT	Closed	-	Master CCM
	4				-	No PV	Closed	Master CCM	-
	5	≤ 3.6	$\leq p_{ac} + p_{dc}$	≥ 20	Master CCM	MPPT	Closed	CCM	CCM
	6				CCM	MPPT	Closed	-	Master CCM
	7				CCM	No PV	Closed	-	Master CCM
	8				-	MPPT	closed	-	Master CCM
	9				-	No PV	Closed	Master CCM	-
	10				Master CCM	MPPT	Open or closed	-	VCM or CCM
	11				Master CCM	No PV	Open or closed	-	VCM or CCM
	12				-	MPPT	Open or closed	-	VCM or CCM
13	-				MPPT	Open or closed	-	VCM or CCM	

Off-peak hours	Modes No.	-	$p_{ac} + p_{es} - p_{pv}$ (kW)	SOC (%)	Es mode	PV mode	K2 relay	inv1	Inv2
	14	-	≥ 3.6	< 90	charging	MPPT	Closed	Master CCM	CCM
	15	-	< 3.6	< 90	charging	If available MPPT	Closed	Master CCM	-
	16	-		≥ 90	-	If available MPPT	Closed	Master CCM	-

The battery is utilized to decrease the house electricity cost by considering the time-of-use tariff and maximizing PV exploitation. As the understudy system is in Estonia and the Baltic region, the time-of-use tariff includes two-level as high and low prices. As a result, the battery is discharged during the peak tariff time range as well as when the PV is absent or it cannot satisfy the load demand [44]. On the other hand, it is charged when there is a surplus of PV generation as well as during the off-peak tariff scheme, which is 00-07 in the specified region [42]. It should be noted that modes 4 and 7 in islanded operation mode are load shedding modes in which the generated power is less than consumption. In this mode, the emergency loads can be energized.

3.3 Summary

The general operation policy of the ER is studied in this chapter. Different configurations and optimized control techniques are considered according to the grid-tied or islanded mode, peak hours, total generation and consumption in the house.

Table 3.2 Isolated operation-mode configurations of the ER (K1 open).

No.	p_{ac} (kW)	$p_{pv} + p_{es}$ (kW)	SOC (%)	Es mode	PV mode	K2 relay	Inv1	Inv2
1	≥ 3.6	$\geq p_{ac} + p_{dc}$	≥ 20	Master CCM	MPPT	Closed (parallel)	CCM	VCM
2			≥ 20	Master CCM	MPPT	Closed (parallel)	CCM	VCM
3					No PV	Open	-	VCM
4				< 20	-	MPPT	Open	VCM
5	≤ 3.6	$\geq p_{ac} + p_{dc}$	≥ 20	Master CCM	If available MPPT	Open	-	VCM
6			< 20	Master CCM	MPPT	Open	-	VCM
7			$\leq p_{ac} + p_{dc}$	< 20	-	MPPT	Open	-

4 Control System Tuning and Implementation

The general proposed control system of ER is shown in Figure 4.40. To enhance the readability of the figure, the control system of each converter is separated with the same color as the dashed line of converters.

The ER contains multiple converters which are interconnected by the dc-link [46]. As a result, the dc-link voltage stability is the core stability factor of the ER. Consequently, the responsible converter for the dc-link voltage is considered a master. Inv1 as master can also work as PFC and ancillary service to the grid when it is needed.

The general specification of the ER used for simulations is shown in Table 4.1.

4.1 VSIs' Control Block Diagrams

VSIs can work in CCM, VCM, and parallel, as described for different operation modes in Table 3.1 and Table 3.2. These control block diagrams are demonstrated in Figure 4.40.

4.1.1 CCM Control of VSI

CCM control block consists of master or slave mode. In the master mode, a PI regulator is implemented to control the dc-link voltage. This PI regulator provides the reference current amplitude. On the other hand, in the slave mode, the master element provides the reference current to the internal current controller. A Second-Order Generalized Integrator (SOGI) based Phased Locked Loop (PLL) is utilized to extract the grid phase angle and provide a current reference to the current controller of the VSI target. The internal current loop consists of the PR regulator with the harmonic compensation as follows.

$$G_{PR}(s) = K_p + \sum_{h=1,3,5,7,9} K_{hi} \frac{2\omega_c s}{s^2 + 2\omega_c s + (h\omega_0)^2}. \quad (1)$$

This CCM control system enables the VSI to operate as PFC in PCC [IV]. In this work, the equivalent circuit shown in Figure 4.2 is implemented. PLECS is used as the simulation software. The simulation results with different Power Factors (PFs) are shown in Figure 4.1 and Figure 4.3. The experimental result with unity PF is shown in Figure 4.4.

Table 4.1 ER specifications.

Symbol	Parameter	Value
V_g, V_{out}	Grid and Load side voltage (RMS)	230 V, 50 Hz
L_g, L_{f2}	Grid -side and output-side LCL inductor	0.6 mH
L_c, L_{f1}	Converter -side LCL inductor	1.44 mH
C_g	Grid-side LCL filter capacitor	3 μ F
C_f	Output-side LCL filter capacitor	9.6 μ F
V_{dc}	DC link voltage	400 V
F_{sw}	Switching frequency	20 kHz

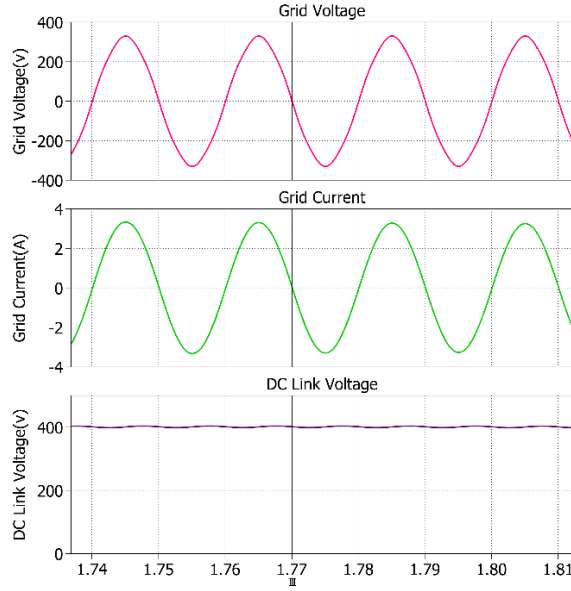


Figure 4.1 Grid Voltage and Current, DC Link Voltage with PF=1 [IV].

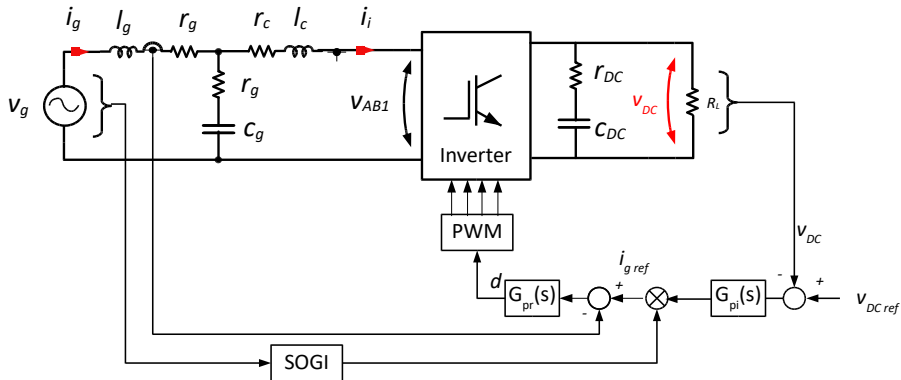


Figure 4.2 Equivalent model of ER and the control system.

4.1.2 VCM Control of VSI: MPC Implementation

The primary VCM control block of VSI was similar to CCM, containing dual-loop. However, the zero-pole map investigation of the system confirms the pole's tendency toward right-half-plan by decreasing the load to idle mode [11]. As a result, an indirect continuous control set (constant switching frequency) MPC is suggested. Figure 4.5 demonstrates the equivalent circuit of the VSI and the indirect MPC structure. Inductors' current of LCL filter i_{Lf1} , i_{Lf2} , ac-output voltage v_{out} , dc-link voltage v_{dc} are measured signals, used by the indirect MPC block. The dynamic of the system is described by the state-space equations. The state-space variables in the continuous form are:

$$x(t) = [i_{Lf1}(t), i_{Lf2}(t), v_{cf}(t)]^T. \quad (2)$$

With the measured signals, the predicted value for the next sample is calculated by state-space equations as:

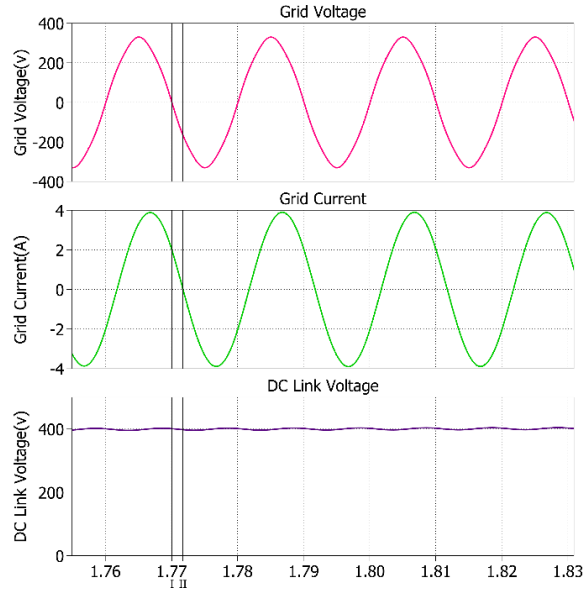


Figure 4.3 Grid Voltage and Current, DC Link Voltage with PF=-0.15 [IV].

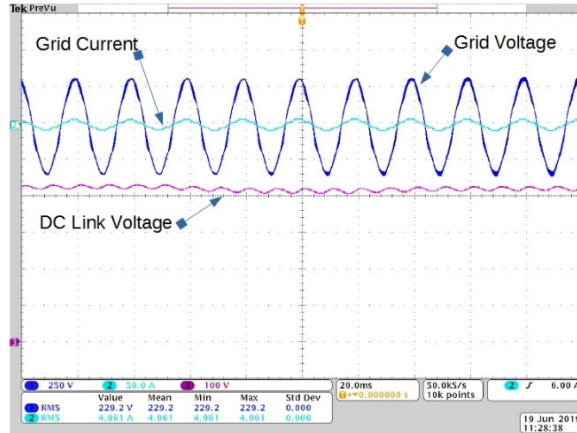


Figure 4.4 Grid Voltage and Current, DC Link Voltage with PF=1 [IV].

$$x(n + 1) = F \cdot x(n) + G \cdot u(n), \quad (3)$$

where $u(n)$ is the input vector.

$$u(n) = [v_{ab}(n), v_{out}(n)]^T. \quad (4)$$

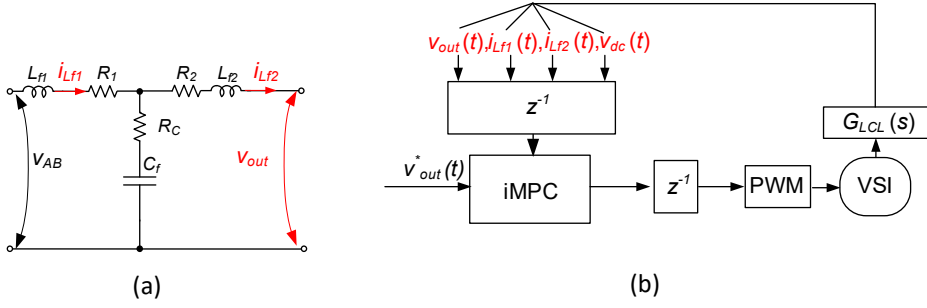


Figure 4.5 Equivalent circuit of the VSI (a) The MPC structure (b) [11].

F and G are the dynamic matrices corresponding to the small-signal model of the system in discrete form:

$$F = \begin{bmatrix} f_1 & f_2 & f_3 \\ f_4 & f_5 & f_6 \\ f_7 & f_8 & 1 \end{bmatrix}, G = \begin{bmatrix} g_1 & 0 \\ 0 & g_4 \\ 0 & 0 \end{bmatrix}, \quad (5)$$

where:

$$f_1 = 1 - (R_1 + R_C) \frac{T_S}{L_1}; f_2 = \frac{R_C T_S}{L_1}; f_3 = -\frac{T_S}{L_1}; \quad (6)$$

$$f_4 = 1 - (R_2 + R_C) \frac{T_S}{L_2}; f_5 = \frac{R_C T_S}{L_2}; f_6 = \frac{T_S}{L_2}; \quad (7)$$

$$f_7 = \frac{T_S}{C_f}; f_8 = -\frac{T_S}{C_f}; \quad (8)$$

$$g_1 = \frac{T_S}{L_1}; g_4 = -\frac{T_S}{L_2}, \quad (9)$$

T_S is the sampling time.

As one of the state variables in the LCL filter is dependent, we select voltage capacitor as the dependent variable which can be derived from the above equations.

The predicted output voltage is calculated as:

$$v_{out}(n+1) = v_c(n+1) - \frac{(i_{L2}(n+1) - i_{L2}(n))}{-g_4}. \quad (10)$$

The error voltage is:

$$\Delta v_{out}(i) = v_{out}(i) - v_{out.ref}(i), (n+1 \geq i \geq n+p). \quad (11)$$

The error voltage in different prediction horizons should be minimized. As a result, the cost function $J[d]$ is described as:

$$J[d] = |\Delta v_{out}(n+1)| + \dots + |\Delta v_{out}(n+p)|, \quad (12)$$

where p is the prediction horizon. To provide voltage drops on inductors and some other operation voltage deviation during load connection, a reference voltage v_{ab} during the evaluation of the cost function is considered as:

$$v_{ab}(i, d) = v_{out_ref}(i) + \Delta v_{ab}(i, d). \quad (13)$$

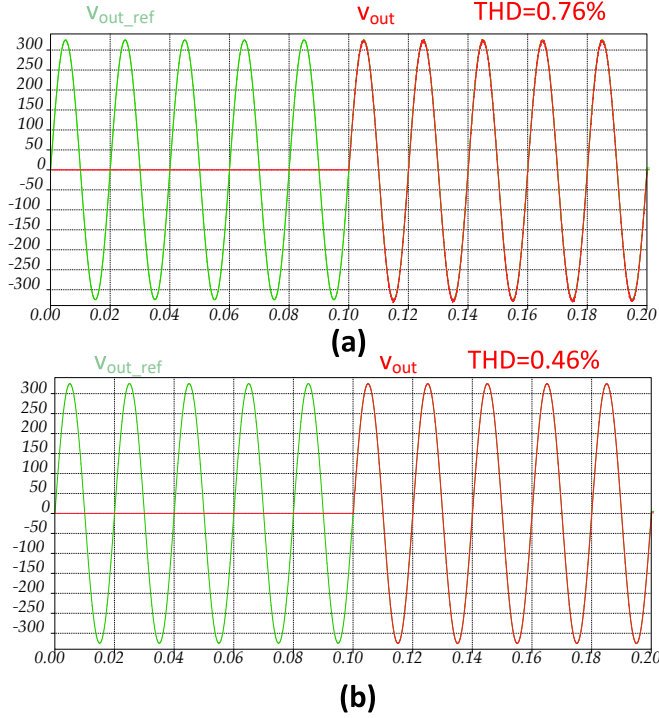


Figure 4.6 Output voltage waveform with prediction horizon $p=1$, $\Delta v_{ab_max} = 40$ V (a). $\Delta v_{ab_max} = 5$ V (b).

A set of 21 possible deviations as $\Delta v_{ab}(i, d)$ is assumed in which step deviations are constant. In each sampling time, all of these deviations are used to calculate $v_{out}(i)$ then the one closer to the reference value is selected. The $\Delta v_{ab}(i, d)$ is different in each sampling time but the range of $\Delta v_{ab}(i, d)$ is constant as follows:

$$-\Delta v_{ab_max} < \Delta v_{ab}(i, d) < \Delta v_{ab_max}. \quad (14)$$

The iteration numbers per sampling time are:

$$N = 21^p. \quad (15)$$

This means the iteration of 21 for $p=1$ and for $p=2$ the iteration number is raised to 441. Figure 4.6 and Figure 4.7 demonstrate the simulation results of output voltage with different Δv_{ab_max} and different prediction horizons. In terms of the THD evaluation of output voltage, a decrease in the voltage deviations with higher prediction horizons leads to lower THD at the expense of higher iteration numbers and higher processing tasks as shown in Figure 4.6 and Figure 4.7.

To decrease the processing time of the microcontroller, $p=1$ is selected in practice. The experimental results of the MPC algorithm on the ER setup in idle mode, and the transition from idle to a 700 W resistive load, are demonstrated in Figure 4.8 and Figure 4.9. The experimental results confirm that the prediction horizon of 1 can provide suitable output voltage with less burden of processing time on the microcontroller.

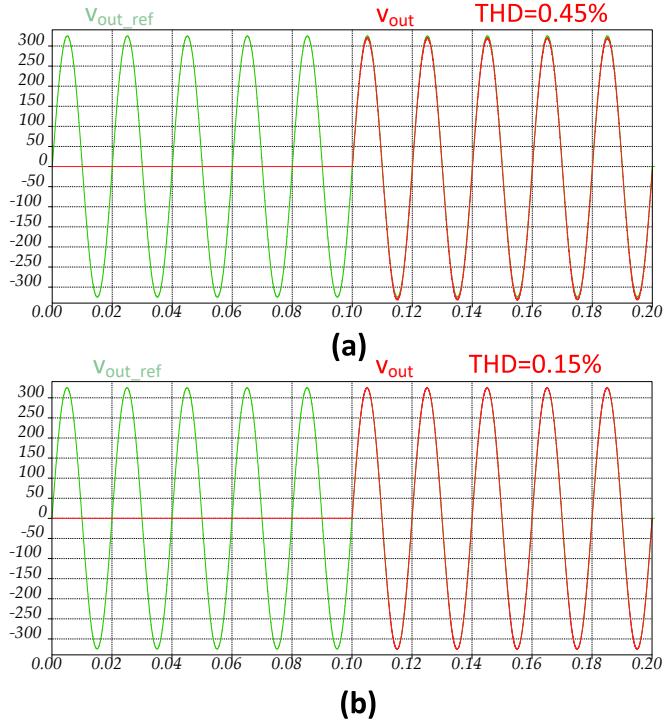


Figure 4.7 Output voltage waveform with prediction horizon $p=2$, $\Delta v_{ab \max} = 40 \text{ V}$ (a). $\Delta v_{ab \max} = 5 \text{ V}$ (b).

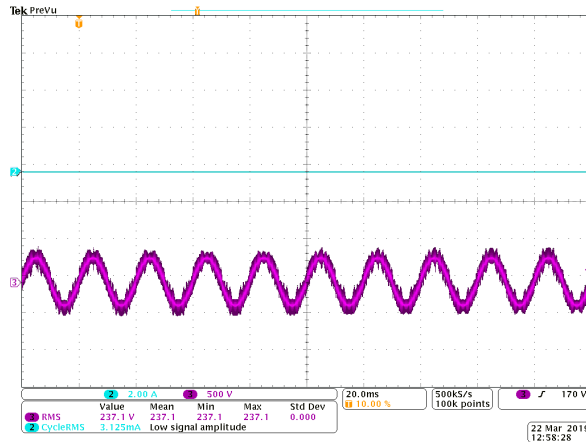


Figure 4.8 The ER ac voltage and current in idle mode of operation [11].

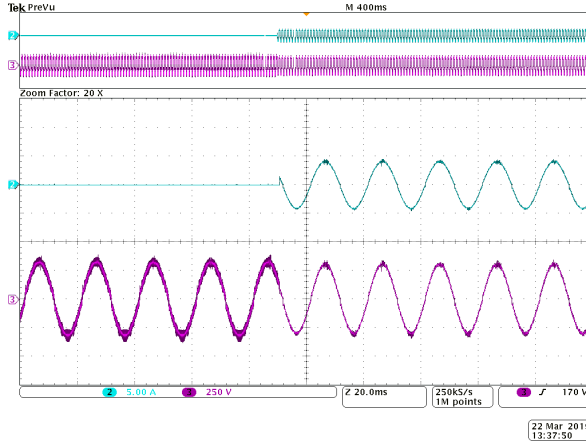


Figure 4.9 The output voltage and current at the power step from 0 to 700 W [II].

4.1.3 VCM Control of VSI: Enhanced MPC Implementation

To consider the ER performance in nonlinear loads when back-to-back inverters work, an enhanced control technique of VSI2 is required, as shown in Figure 4.10. As a result, the improved indirect MPC (iMPC) is suggested. In this technique, the MPC controls both LCL filter capacitor voltage and the output voltage. As a result, the cost function is defined as [III]:

$$J [d] = k_{out} |\Delta v_{out}(n + p)| + k_c |\Delta v_c(n + p)|. \quad (16)$$

The cost function contains an error voltage of output and an error voltage across the capacitor of LCL filter with k_{out} and k_c weighting coefficients. The p element corresponds with the horizon of prediction.

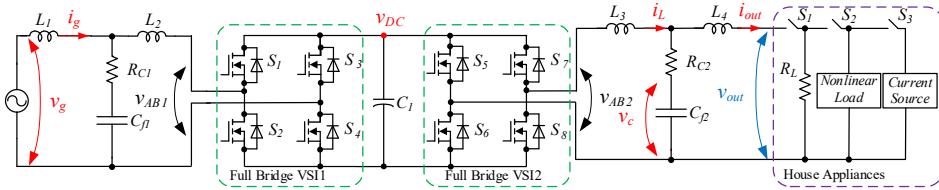


Figure 4.10 The back-to-back inverters' mode of operation with nonlinear loads [III].

The proposed control system of the VSI1 and VSI2 is depicted in Figure 4.11. As Figure 4.11 shows the dc link voltage, inductors currents and capacitor voltage of the LCL filter are measured for the iMPC system.

After discretization and state-space equations as (2), (3), (4), (5), (6), (7), (8), (9), the predicted input vectors are calculated.

$v_{out}^*(t)$ is the reference output voltage. The reference voltage capacitor is calculated as follows:

$$v_c^*(t) = v_{out}^*(t) - (i_L(t) - i_{out}^*(t)) \times R_{C2} + L_4 \frac{d}{dt} i_{out}^*(t) + R_4 \times i_{out}^*(t). \quad (17)$$

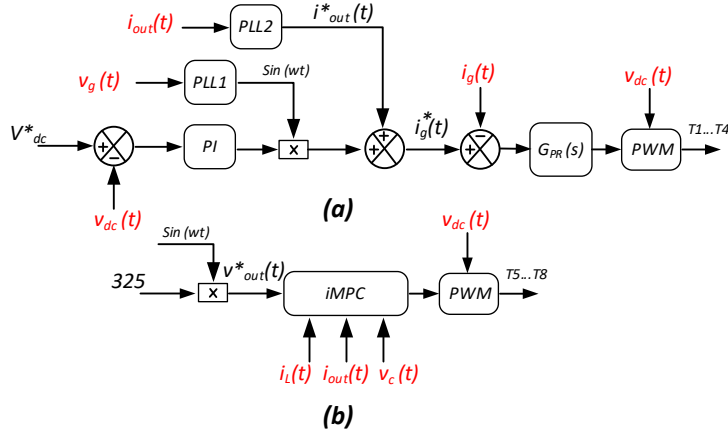


Figure 4.11 The proposed control system for VSI1 (a) and VSI2 (b).

In the next step, the predicted capacitor voltage and the predicted output voltage are calculated as a function of inverter voltage. At the end, the errors are calculated as:

$$\begin{aligned}\Delta v_{out}(n+1) &= v_{out}(n+1) - v_{out}^*(n+1), \\ \Delta v_C(n+1) &= v_C(n+1) - v_C^*(n+1).\end{aligned}\quad (18)$$

The flow chart diagram of the MPC is shown in Figure 4.12.

After measuring the parameters, the output voltage is estimated. Then, based on this estimated voltage, the predicted states at $n+1$ are calculated for all possible values of v_{AB2} , where v_{AB2} is expressed as:

$$v_{AB2}(n+1) = v_C^*(n+1) + \Delta v_{AB2}(i). \quad (19)$$

Finally, the output inverter voltage that minimizes the cost function will be applied to the modulator. To decrease the processing time of the microcontroller, the loop number is decreased to 5. During each sampling time, 5 possible output inverter voltage deviations $\Delta v_{AB2}(i)$ are considered which are calculated one by one. These deviations are similar in all sampling times.

To evaluate the influence of weighting factors on the quality of the output voltage, THDs of the output voltages are compared in the case of $k_{out} = 0, k_C = 1$ and $k_{out} = 1, k_C = 0$ in simulation. At the beginning a resistor load of 529 W is added the at 0.35 s, a 180 W nonlinear load is connected to the ac port.

The simulation results of the main grid voltage and current, output voltage and current, capacitor voltage with $k_{out} = 0, k_C = 1$ and $k_{out} = 1, k_C = 0$ are demonstrated in Figure 4.13 and Figure 4.14 respectively. In both cases, when the resistor load is connected, the ac voltage and current is sinusoidal but with nonlinear load connection, the ac voltage and capacitor get distorted.

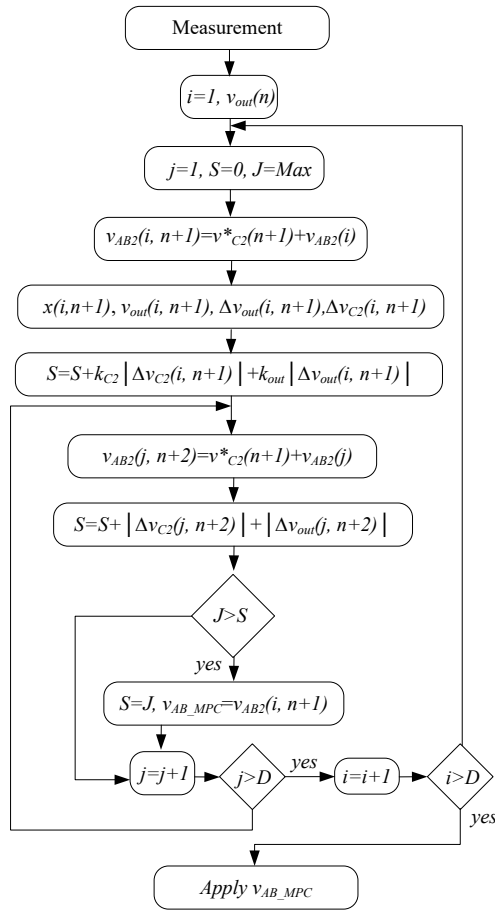


Figure 4.12 Flow chart diagram of the proposed iMPC for $p = 2$ [III].

Comparison of the THD of output voltage and capacitor voltage shows the higher THD of the output voltage in different coefficients. In contrast, the THD of the main grid remain constant in both cases. To evaluate the transient performance of the proposed control algorithm, the simulation is started in idle mode, then at 0.25 s the resistor and finally at 0.35 s the nonlinear load is connected to the ac port. The result for $k_{out} = 0.2$, $k_C = 0.8$ is demonstrated in Figure 4.15. Figure 4.15 confirms the suitable transient performance of the control system in this scenario. Output voltage and capacitor voltage and grid current get distorted with nonlinear load, however THD of output voltage and grid current is within the accepted range.

The next scenario is steady state and transient performance of the control system in the case of starting with idle mode then current-source connection at 0.25 s to the output side. The grid voltage and current, output voltage and current and the capacitor voltage shapes for $k_{out} = 0.2$, $k_C = 0.8$ are depicted in Figure 4.16. The output voltage and capacitor voltage THD are acceptable but the grid current THD is distorted highly. This result demonstrates the proposed control technique requires improvements to be compatible with PI+PR regulator in the case of injection power to the main grid.

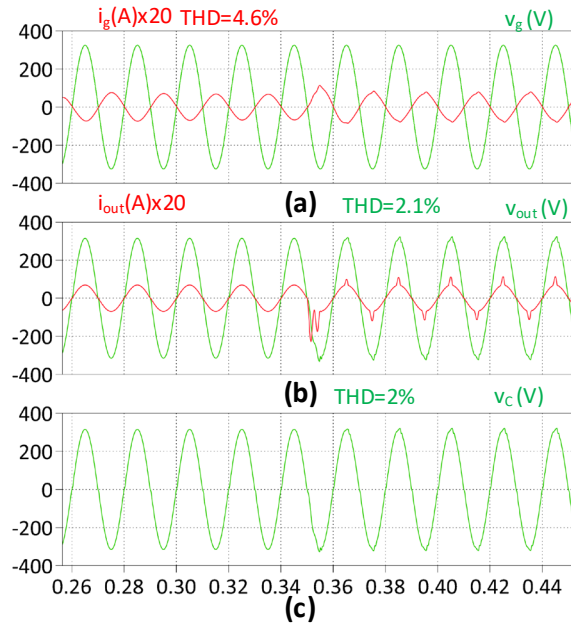


Figure 4.13 Voltage and current shape at main grid (a), output (b), capacitor of the filter with $k_{out} = 0$, $k_c = 1$ [III].

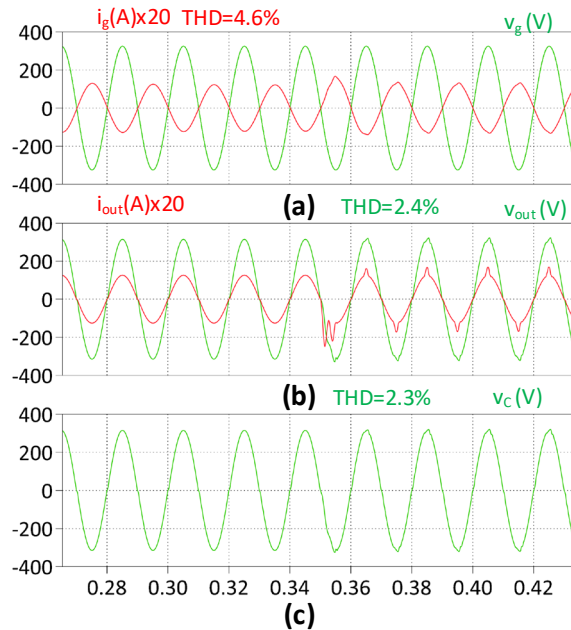


Figure 4.14 Voltage and current shape at main grid (a), output (b), capacitor of the filter with $k_{out} = 1$, $k_c = 0$ [III].

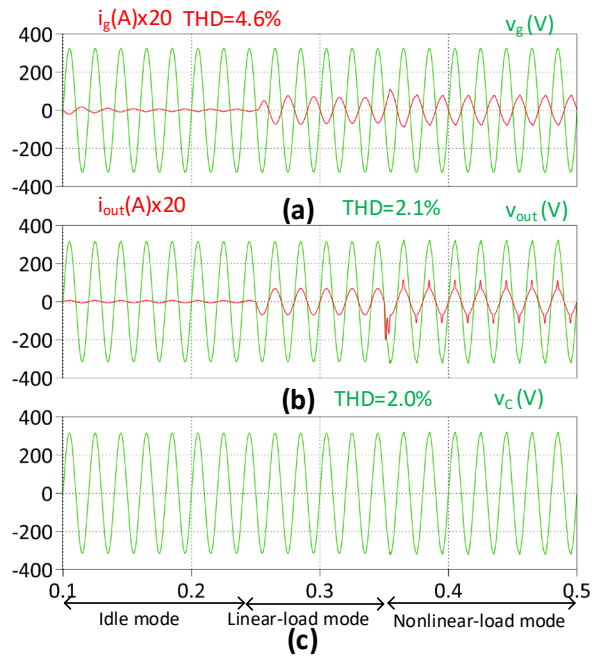


Figure 4.15 Voltage and current shape transition at main grid (a), output (b), capacitor of the filter with $k_{out} = 0.2$, $k_c = 0.8$ in idle mode, linear load and nonlinear load [III].

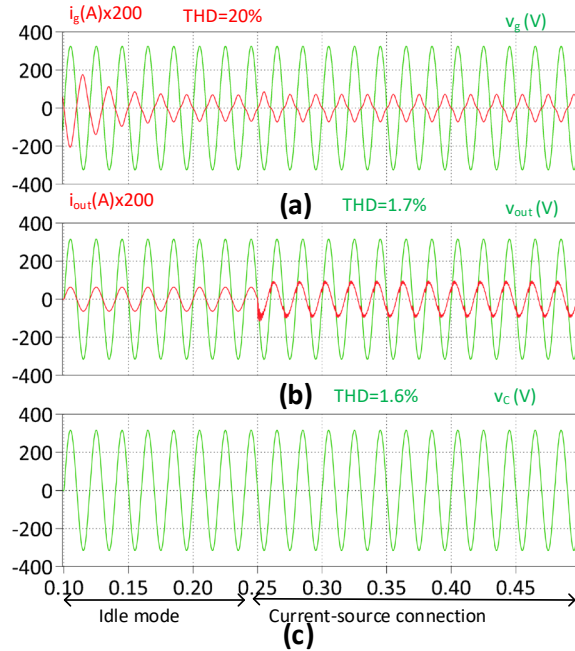


Figure 4.16 Voltage and current shape transition at main grid (a), output (b), capacitor of the filter with $k_{out} = 0.2$, $k_c = 0.8$ in idle mode, and current-source connection [III].

4.1.4 DC-link Voltage Control Using FLC Regulator

PFC algorithm based on PI regulator works well when there is no dc-load, however adding or changing dc-load causes the dc-link voltage to become unstable [V]. The main reason is the fixed and inflexible coefficients of the PI regulator. Consequently, FLC is suggested to be implemented instead of the PI regulator, as shown in Figure 4.17.

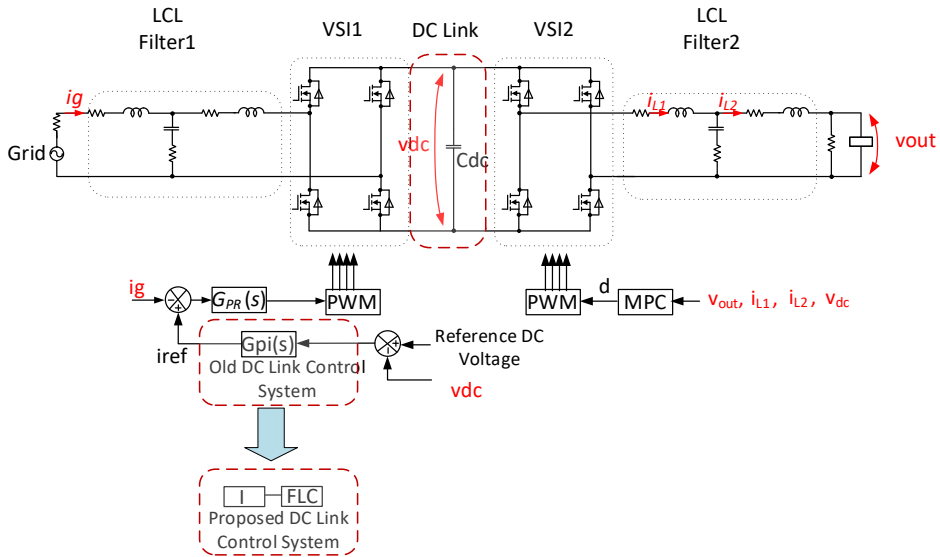


Figure 4.17 FLC implementation in ER control system.

Figure 4.18 shows the FLC inputs and output. The output of FLC is the derivative of grid-current amplitude which gives the grid-current amplitude via an integrator as shown in Figure 4.17. The proposed FLC has two inputs: the dc-link voltage error signal and the derivative of this signal. The derivative of the error signal helps the FLC to make accurate decisions. To clarify, Figure 4.19 demonstrates four different operating points in an assumed dc-link voltage error signal. In this figure, points 1 and 2 have the same error signal but different derivatives. Points 3 and 4 have the same error but different slopes of the error signal. Table 4.2 indicates the preferred FLC output for the aforementioned different operating points, in which points 1 and 2 need different outputs. A similar deduction is used for points 3 and 4. A Mamdani method with seven intervals for inputs and output membership functions is used. The intervals of membership function of the error signal are demonstrated in Figure 4.20, which are called negative high (NH), negative medium (NM), negative small (NS), zero (Z), positive small (PS), positive medium (PM), and positive high (PH).



Figure 4.18 Inputs and output of the FLC.

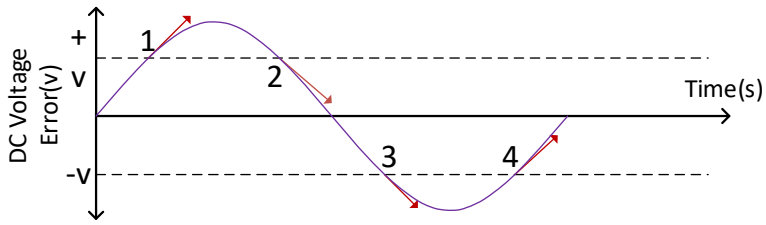


Figure 4.19 The error signal waveform.

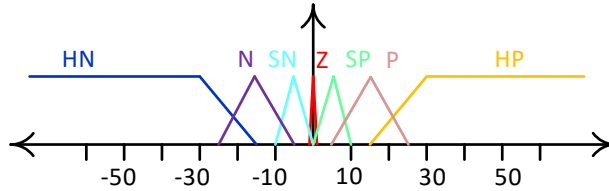


Figure 4.20 Membership function of error dc-link voltage signal.

Table 4.2 The required outputs for four different points [V].

	Error signal	The derivative of the error signal	Preferred grid reference current derivative
Point 1	+v	+	Decrease (-)
Point 2	+v	-	Zero (0)
Point 3	-v	-	Increase (+)
Point 4	-v	+	Zero (0)

Table 4.3 Table Rules for Low Load.

Error Signal \ Derivative Error Signal	Negative high	Negative medium	Negative small	Zero	Positive small	Positive medium	Positive high
Negative high	PH	PH	PH	PH	PH	PH	PM
Negative medium	PH	PM	PS	PS	PS	Z	Z
Negative small	PM	PS	PS	PS	Z	PS	Z
Zero	PS	Z	Z	Z	Z	Z	NS
Positive small	Z	Z	Z	NS	NS	NS	NM
Positive medium	Z	Z	NS	NS	NS	NM	NH
Positive high	NM	NH	NH	NH	NH	NH	NH

Table 4.4 Table Rules for High Load.

Error Signal \ Derivative Error Signal	Negative high	Negative medium	Negative small	Zero	Positive small	Positive medium	Positive high
Negative high	PH	PH	PH	PH	PH	PH	PH
Negative medium	PH	PM	PM	PM	PS	PS	PS
Negative small	PM	PM	PS	PS	Z	Z	Z
Zero	PS	PS	Z	Z	Z	NS	NS
Positive small	Z	Z	Z	NS	NS	NM	NM
Positive medium	NS	NS	NS	NM	NM	NM	NH
Positive high	NH	NH	NH	NH	NH	NH	NH

The higher the step-change in dc-load, the higher the reduction step in dc-link voltage will be. To compensate for the dc-link voltage reduction step, higher slope of grid-current amplitude is required. Based on this issue, the table rules for low dc-load and high dc-load are suggested in Table 4.3 and Table 4.4.

Three different dc-loads of 0.004, 0.4, and 2 kW are added at 0.35 s then at 0.5 s a 106 W ac-load is added to the ac-side. The required dc-link capacitor is decreased from 3000 μF to 1000 μF . The simulation results of the traditional PI regulator and FLC are shown in Figure 4.21, Figure 4.22, for 4 W dc-load, Figure 4.23 and Figure 4.24, for 400 W dc-load, and Figure 4.25 and Figure 4.26 for 2 kW dc-load. The total simulation results show better performance of FLC in dc-link voltage control and in terms of grid-current THD.

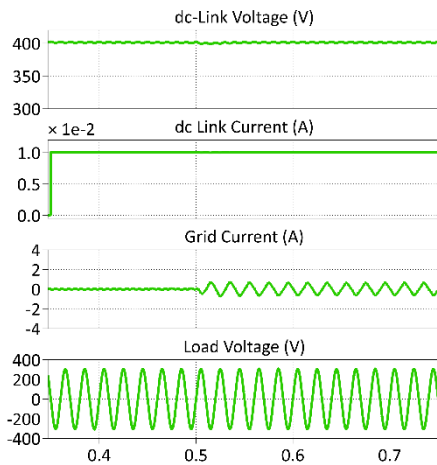


Figure 4.21. Simulation results for 4 W dc-load with the PI regulator.

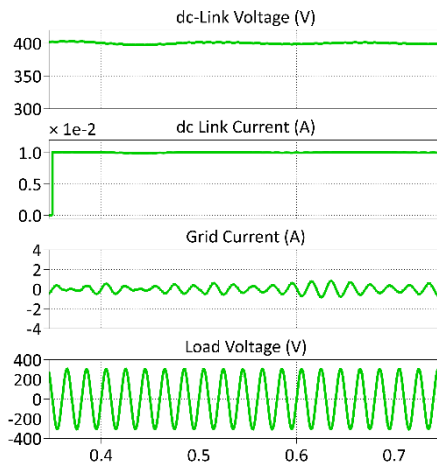


Figure 4.22. Simulation results for 4 W dc-load with FLC.

In the case of heavy load, the PI regulator cannot stabilize the dc-link voltage. The utilization of FLC and MPC confirms they can cooperate effectively.

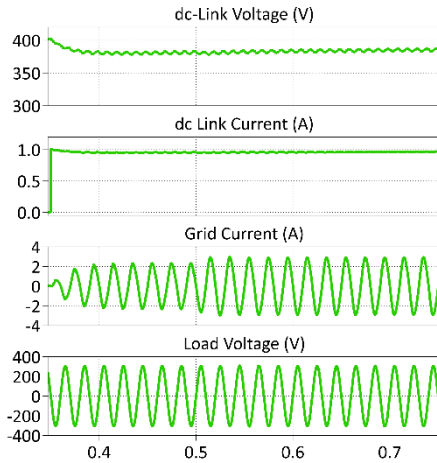


Figure 4.23 Simulation results for 400 W dc-load with the PI regulator.

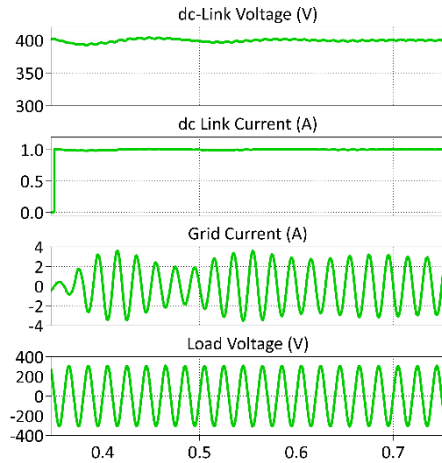


Figure 4.24 Simulation results for 400 W dc-load with FLC.

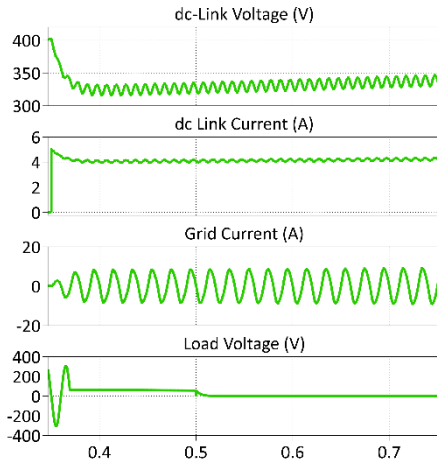


Figure 4.25 Simulation results for 2 kW dc-load with the PI regulator.

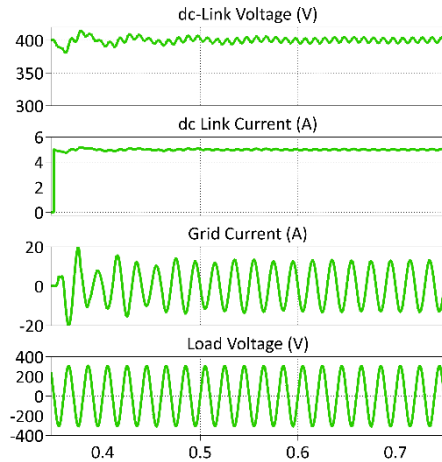


Figure 4.26 Simulation results for 2 kW dc-load with FLC.

4.1.5 Dc-link Control Considering Constant Power Loads

The growing number of electronic loads creates new challenges to the stability of grids and residential distributions systems [47]. The main reason is the negative equivalent resistor of the Constant Power Load (CPLs). The simulation results for CPLs connected to the dc-link with the classic PI regulator and PR in the current-controlled mode of VS11 show that although the dc-link stays stable the ac-current contains high THD [VI]. This is due to the linear characteristic of the control system for a highly nonlinear characteristic

of CPLs. As a result, FLC is suggested [VI]. As FLC is implemented to control the dc-link voltage, the inputs and output leave similarly. The membership functions are also similar. To simulate the CPL, a resistor with a high switching frequency buck converter is utilized.

A simple PI regulator is used to control the output voltage of the buck converters. The system configuration for the simulation is demonstrated in Figure 4.27.

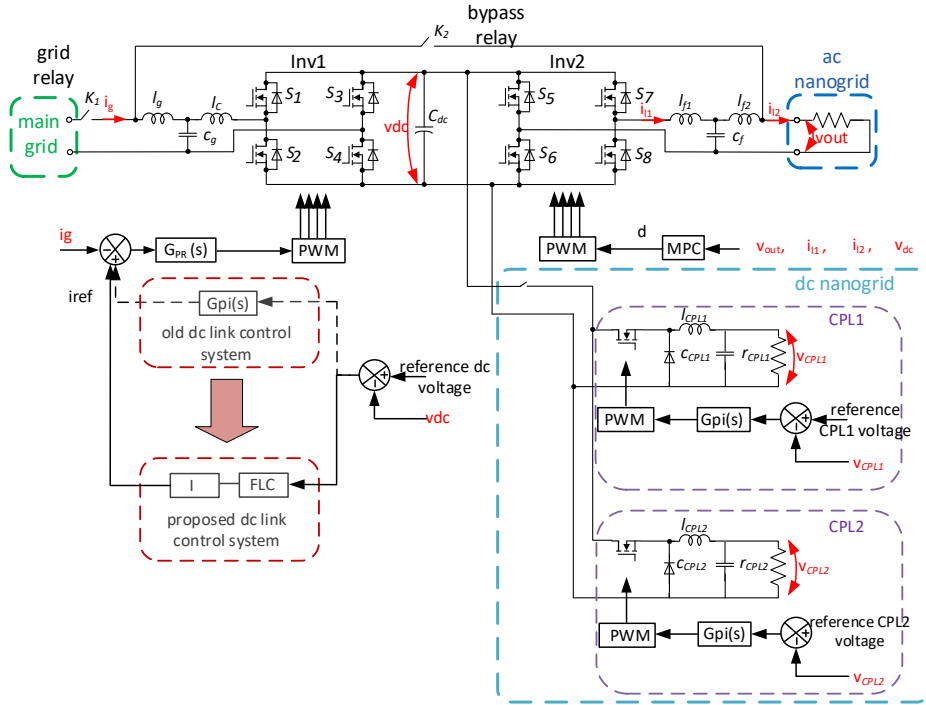


Figure 4.27 The energy router configuration, and control block diagram.

Table 4.5 Table rules for dc-voltage control.

Error Signal \ Derivative Error Signal	HN	N	SN	Z	SP	P	HP
HN	HP	HP	HP	HP	HP	HP	P
N	HP	P	SP	SP	SP	Z	Z
SN	P	SP	SP	SP	Z	SP	Z
Z	PS	Z	Z	Z	Z	Z	NS
SP	Z	Z	SN	SN	SN	SN	N
P	Z	Z	SN	SN	SN	N	HN
HP	N	HN	HN	HN	HN	HN	HN

As the power of CPLs in home appliances are low, the table rule used is based on the low-power loads demonstrated in Table 4.5. In Table 4.5 HN, N, SN, Z, SP, P, and HP are highly negative, negative, small negative, zero, small positive, positive, and highly positive respectively.

The CPL parameters used in the simulation are demonstrated in Table 4.6. The simulation is performed in two conditions: using the classic PI regulator control for dc-link voltage control and FLC implementation for dc-link voltage control. To test the compatibility with the MPC, MPC control technique is also used by Inv2 via adding 105W a resistor-load to the ac-load side.

The results in Figure 4.28 and Figure 4.29 show the better performance of FLC with PR in the current-controlled mode of Inv1 with lower THD of grid-current.

Table 4.6 CPLs' parameters used in the simulation.

CPLs' Parameters		
P_{CPL1}	CPL1 power	80 W
P_{CPL2}	CPL2 power	200 W
F_{sw}	Switching frequency	60 kHz
V_{CPL}	CPL voltage	20 V
k_p	Prportional Parameter	0.2
k_i	Integrator Parameter	0.8
r_{CPL1}	Resistor of the CPL1	5 Ω
l_{CPL1}	LC filter inductor of CPL1	0.1 mH
C_{CPL1}	LC filter capacitor of CPL1	1000 μ F
r_{CPL2}	Resistor of the CPL2	2 Ω
l_{CPL2}	LC filter inductor of CPL2	0.1 mH
C_{CPL2}	LC filter capacitor of CPL2	1000 μ F

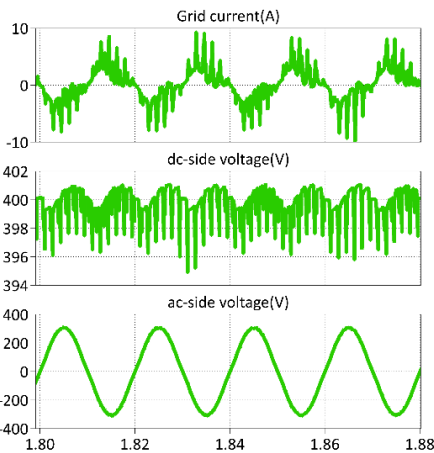


Figure 4.28 Simulation results of the classic PI regulator in steady-state.

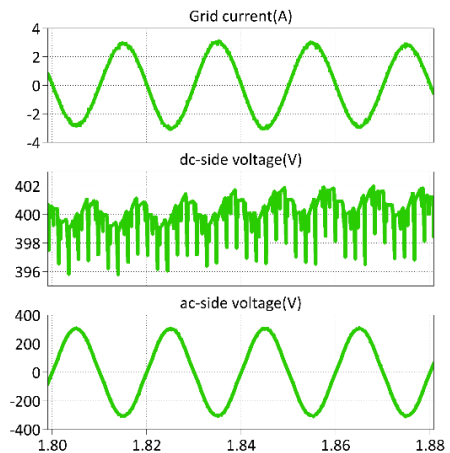


Figure 4.29 Simulation results of the classic FLC regulator in steady-state.

However, in both cases, the dc-link voltage is stable at its reference value of 400 V. In terms of MPC, it works well with the FLC. Moreover, FLC has more flexibility and better performance in PI voltage-control of CPLs.

Figure 4.30 and Figure 4.31 depict the transient behavior of the grid-current, dc-link voltage, and ac-load voltage in both cases. The results demonstrate that, despite the better performance of FLC in steady-state, PI works smoother in transient-condition.

Figure 4.32 and Figure 4.33 are selected to show the compatibility of the PI of CPL in controlling the load-voltage reference of 20v. The results demonstrate the better performance of FLC with CPLs' PI regulators.

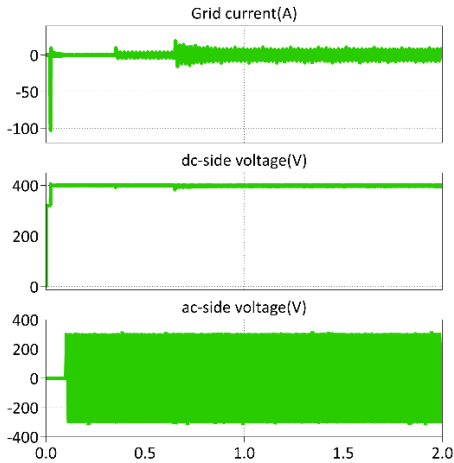


Figure 4.30 The transient results with the classic PI regulator.

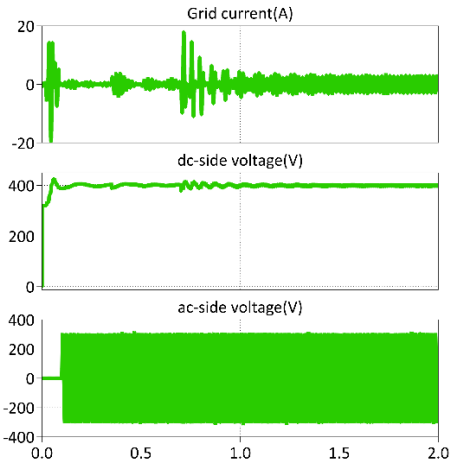


Figure 4.31 The transient results with the proposed FLC technique.

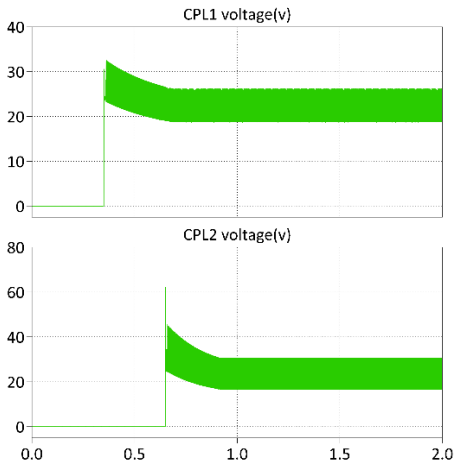


Figure 4.32 CPLs' voltages in classic PI regulator method.

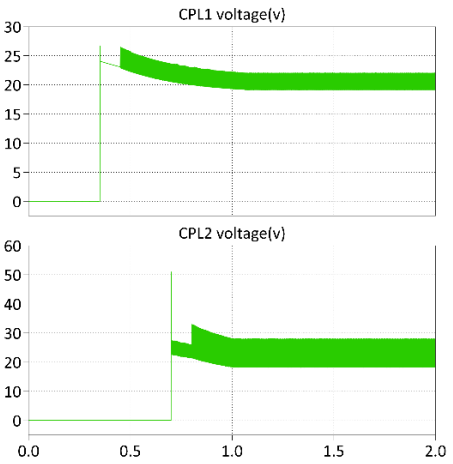


Figure 4.33 CPLs' voltages in the proposed FLC method.

4.2 Battery Control Diagram

If the battery works as a master, a PI regulator is implemented to control the dc-link voltage as shown in Figure 4.40. This PI regulator provides the reference current for current controllers in buck (charging) and boosts the (discharging) mode of the battery. As a slave, the battery receives the reference current from the master.

4.2.1 Active Decoupling with Battery Utilization

The literature review on the frequency of charging and discharging current of the li-ion battery shows that double frequency charging and discharging can have fewer degradation effects on the battery [VII]. Based on this conclusion, we suggest battery utilization as an active decoupling device for the double frequency ripple power of ac-dc conversion in dc-link.

The proposed control technique is demonstrated in Figure 4.34. In this work, it is assumed that VSI1 is connected to the grid, and VSI2 is connected to the ac-loads. VSI1 works as a master to stabilize the dc-link voltage. MPC is used for VSC control of the VSI2. A PR regulator compensator is implemented for double frequency reference current. The cutoff frequency of the low pass filter is 30 Hz.

The interleaved converter operations in buck and boost modes are shown in Figure 4.35.

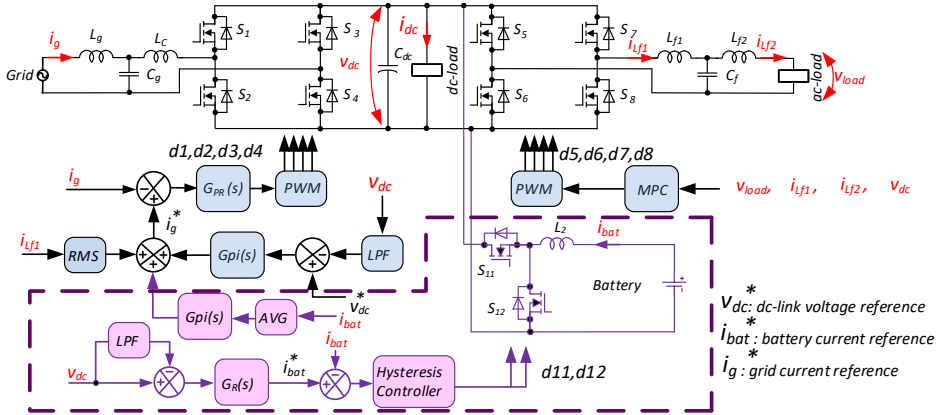


Figure 4.34 The control block diagram for active decoupling role of the battery.

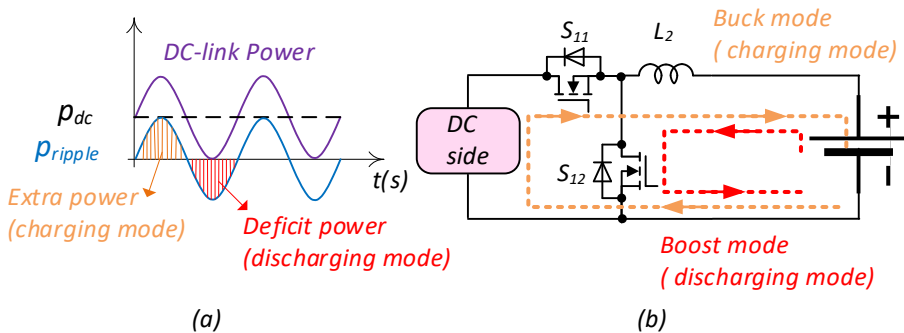


Figure 4.35 dc-link power relation with the interleaved converter (a), buck and boost modes of the battery converter.

When the power in the dc-link is extra, the converter works in buck mode. In the case of deficit power, it works in boost mode.

As the peak load of the house is assumed to be 5 kW, in three different steps the peak load is added to the ac-output. Limiting the dc-link voltage variation to ± 2 V, the proposed technique leads to a decrease in dc-link capacitors from 2000 to 400 μ F.

The simulation results of the grid voltage and current, and voltage-current of the output with 2000 μ F and with the proposed technique using 400 μ F are similar. Furthermore, the dc-link voltage transient condition results are demonstrated in Figure 4.36 and Figure 4.38. As Figure 4.37 and Figure 4.39 show the steady stable double frequency deviation in the proposed technique is limited to ± 1 V, which is less than the previous technique's ± 2 V. However, the transient voltage behavior is higher in the proposed technique.

4.3 PV Control Diagram

The control block of PV consists of master or slave mode, as shown in Figure 4.40. A PI regulator is implemented in master mode to generate the reference current; however, the reference current is determined by the master in the slave mode. Two PI regulators are implemented for a buck or to boost the operation of the PV.

4.4 Summary

In this chapter, several operation modes of ER were studied. PFC mode of INV1 satisfies the grid requirements. Different power of dc loads and constant power loads effects' on dc-link voltage are investigated. It is verified that the conventional PI regulator has a limitation in tracking the reference dc voltage so the FLC technique as a solution controls the dc voltage well. The grid-forming operation of ER in idle mode, linear load, nonlinear load and low-power current source have been studied. It is confirmed that the classic PR regulator can provide the sinusoidal voltage in a limited linear-load range. MPC results as a solution confirm its capability in grid-forming operation of ER.

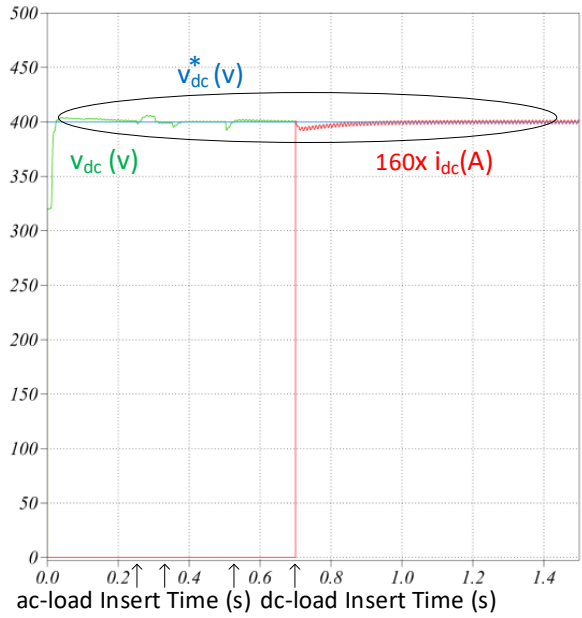


Figure 4.36 Dc-link Voltage and dc-load Current Simulation Results of the Traditional Control with 2000 μF dc-link capacitor.

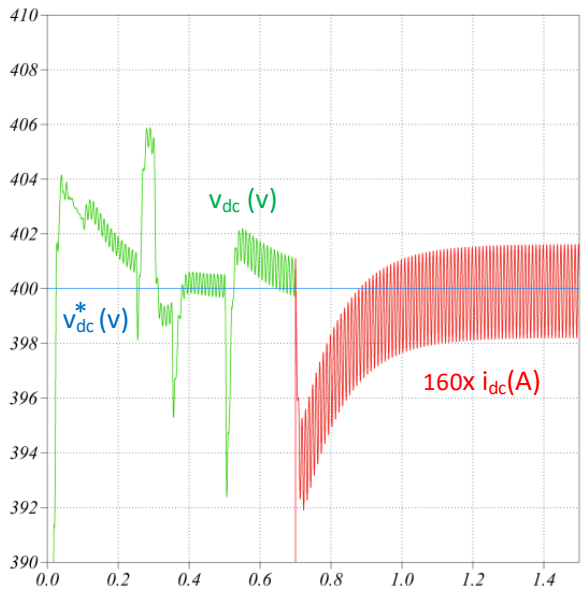


Figure 4.37 The detail view of Figure 4.36.

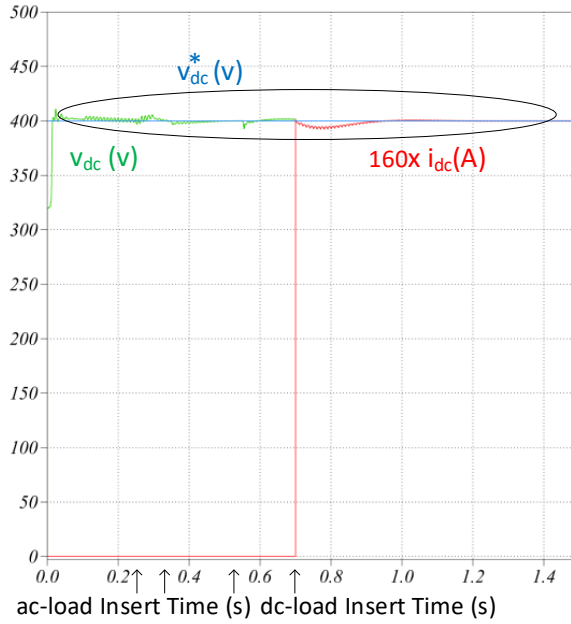


Figure 4.38 Dc-link Voltage and dc-load Current Simulation Results of the Traditional Control with 400 μF dc-link capacitor.

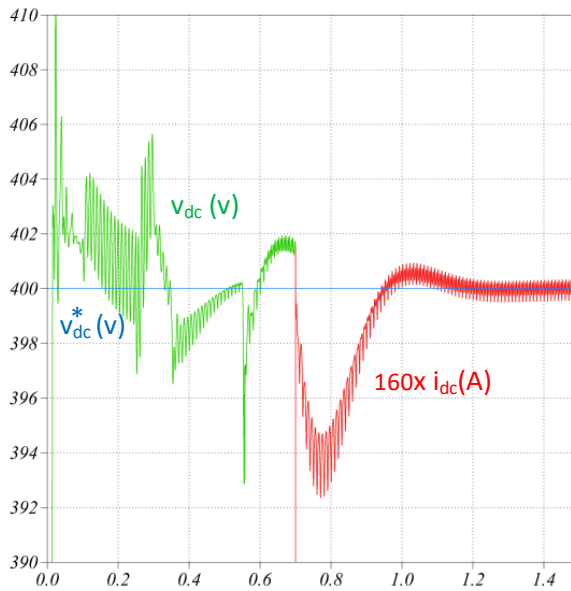


Figure 4.39 The detail view of Figure 4.38.

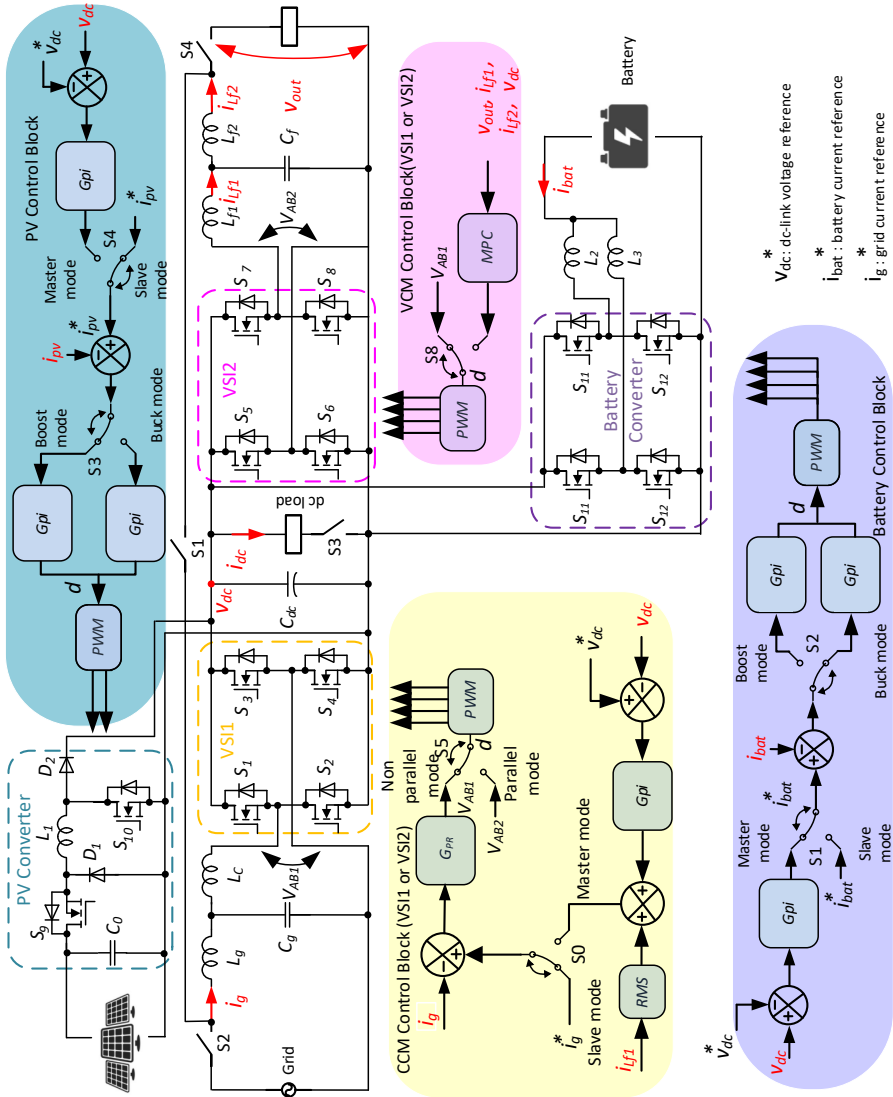


Figure 4.40 The proposed control system of the ER.

5 Conclusions

An ER with a bypass switch and a hybrid distribution system for home appliances is suggested. Dc-loads and resources connect to the dc-nanogrid and ac-load and sources can connect to the ac-nanogrid. The ER contains two back-to-back single-phase full-bridge inverters with a bypass switch, controlling the main grid current and the ac-nano grid voltage. This bypass switch adds flexibility in the ER operation compared with the industrial hybrid solar inverters for residential applications. It also includes a non-inverting buck-boost converter for MPPT tracking of PV and an interleaved converter for a battery. The ER structure with the capability of smart metering and communication system provides more flexibility in the ER operations, enhancing the house to a smart controllable entity in the power system. In this regard, it provides ancillary service to the main grid, and participation in peak shaving is feasible which result in the efficient management of the energy in the house.

The performance of the classical control techniques for different ranges of power for ac and dc loads is evaluated. The suitable operation of the ER as a PFC is confirmed in the experimental results. Moreover, the limitation of the PI regulator to provide the reference dc-link voltage in the presence of various power of dc loads and CPLs is confirmed. The intelligence-based control FLC is confirmed as a solution with better performance. Using a battery as a decoupling tool in the dc-link voltage control is another dc-voltage control technique.

In terms of the ac grid-forming operation of the ER, the classic PID+R has a limitation in providing ac-voltage with low THD in the case of various loads from idle mode to full load and ac-source connection. The experimental results of MPC implementation confirm its better performance compared with the PID+R regulators.

As a result, the conclusions of this study are summarized as:

- The ER interface for residential applications with the bypass switch provides more flexibility in the operation.
- The battery can be utilized as an active decoupling tool in the ER dc voltage control.
- The FLC technique performance is confirmed in dc-link voltage control in the case of various dc loads.
- The MPC technique for the grid-forming operation mode of the ER has suitable performance compared with the classic PID+R regulators with various ac-loads and resources.
- The compatibility of the FLC and MPC controllers with the linear PR and PI regulators is confirmed.
- Experimental verifications of the control techniques are verified.

Future research in the control of the energy router can be continued by:

- Implementation of the high-level control (energy management) system and further cost optimization.
- Feasibility of the FLC implementation on the experimental setup.
- Common mode leakage current evaluation and control if it is needed.

References

- [1] X. Wang, J. M. Guerrero, F. Blaabjerg, and Z. Chen, "A review of power electronics based microgrids," *J. Power Electron.*, vol. 12, no. 1, pp. 181–192, 2012, doi: 10.6113/JPE.2012.12.1.181.
- [2] "Energy Efficiency Trends in Buildings in Europe | Policy brief | ODYSSEE-MURE." <https://www.odyssee-mure.eu/publications/policy-brief/buildings-energy-efficiency-trends.html> (accessed Dec. 17, 2021).
- [3] R. A. Lopes, P. Magalhães, J. P. Gouveia, D. Aelenei, C. Lima, and J. Martins, "A case study on the impact of nearly Zero-Energy Buildings on distribution transformer aging," *Energy*, vol. 157, no. December 2016, pp. 669–678, 2018, doi: 10.1016/j.energy.2018.05.148.
- [4] C. Roncero-Clemente, N. Vilhena, V. Delgado-Gomes, E. Romero-Cadaval, and J. F. Martins, "Control and operation of a three-phase local energy router for prosumers in a smart community," *IET Renew. Power Gener.*, vol. 14, no. 4, pp. 1–11, 2020, doi: 10.1049/iet-rpg.2019.0589.
- [5] K. Wang *et al.*, "A survey on energy internet: Architecture, approach, and emerging technologies," *IEEE Syst. J.*, vol. 12, no. 3, pp. 2403–2416, 2018, doi: 10.1109/JSYST.2016.2639820.
- [6] H. M. Hussain, A. Narayanan, P. H. J. Nardelli, and Y. Yang, "What is energy internet? concepts, technologies, and future directions," *IEEE Access*, vol. 8, no. iv, pp. 183127–183145, 2020, doi: 10.1109/ACCESS.2020.3029251.
- [7] B. Liu *et al.*, "An AC–DC Hybrid Multi-Port Energy Router With Coordinated Control and Energy Management Strategies," *IEEE Access*, vol. 7, pp. 109069–109082, Aug. 2019, doi: 10.1109/access.2019.2933469.
- [8] I. Roasto, A. Rosin, and T. Jalakas, "Multiport Interface Converter with an Energy Storage for Nanogrids," *IECON 2018 - 44th Annu. Conf. IEEE Ind. Electron. Soc.*, vol. 1, pp. 6088–6093.
- [9] A. Q. Huang *et al.*, "The future renewable electric energy delivery and management (FREEDM) system: The energy internet," *Proc. IEEE*, vol. 99, no. 1, pp. 133–148, Jan. 2011, doi: 10.1109/JPROC.2010.2081330.
- [10] Dong, I. Cvetkovic, D. Boroyevich, W. Zhang, R. Wang, and P. Mattavelli, "Grid-interface bidirectional converter for residential DC distribution systems - Part one: High-density two-stage topology," *IEEE Trans. Power Electron.*, vol. 28, no. 4, pp. 1655–1666, Apr. 2013, doi: 10.1109/TPEL.2012.2212462.
- [11] L. Martirano *et al.*, "Demand Side Management in Microgrids for Load Control in Nearly Zero Energy Buildings," *IEEE Trans. Ind. Appl.*, vol. 53, no. 3, pp. 1769–1779, 2017, doi: 10.1109/TIA.2017.2672918.
- [12] M. A. Hannan *et al.*, "A review of internet of energy based building energy management systems: Issues and recommendations," *IEEE Access*, vol. 6, pp. 38997–39014, Jul. 2018, doi: 10.1109/ACCESS.2018.2852811.
- [13] "Affordable Solar and Battery Solutions | Redback Technologies." <https://redbacktech.com/> (accessed Mar. 24, 2022).
- [14] "Home | SUNGROW." <https://us.sungrowpower.com/> (accessed Mar. 24, 2022).
- [15] "Circuit Diagram Efficiency Curve Up to 30% More Energy with Optimizer Higher Yields."

- [16] "CHANGE YOUR ENERGY CHARGE YOUR LIFE Innovation for a Better Life Compact Size & Easy Installation," Accessed: Mar. 24, 2022. [Online]. Available: www.lgesspartner.com.
- [17] "EV Charging Single Phase Inverter SE3680H, SE4000H, SE5000H, SE6000H 2-in-1 EV Charger and Solar Inverter, Speeds Up Installation and EV Charging," Accessed: Mar. 24, 2022. [Online]. Available: <https://www.solaredge.com/sites/default/files/se-temperature-derating-note.pdf>.
- [18] "self-consumption autonomous house solar inverter hybrid batteries." <https://imeon-energy.com/> (accessed Mar. 24, 2022).
- [19] "NEW X-HYBRID," Accessed: Mar. 24, 2022. [Online]. Available: www.solaxpower.com.
- [20] "https://www.europe-solarstore.com/download/fronius/solarbattery/DS_Fronius_Energy_Package_EN_386411_snapshot.pdf."
- [21] "https://www.invertersupply.com/media/data/Datasheet_RHI-1P5K-HVES-5G.pdf."
- [22] "https://www.rectifier.co.za/wp-content/uploads/2019/08/REACT2-3.6-5.0-TL_BCD.00688_EN_RevD.pdf."
- [23] S. J. Chiang, K. T. Chang, and C. Y. Yen, "Residential photovoltaic energy storage system," *IEEE Trans. Ind. Electron.*, vol. 45, no. 3, pp. 385–394, 1998, doi: 10.1109/41.678996.
- [24] M. Makhlof, F. Messai, and H. Benalla, "Modeling and simulation of grid-connected photovoltaic distributed generation system," in *China International Conference on Electricity Distribution*, 2010, vol. 45, no. 2, pp. 378–386.
- [25] Y. Gurkaynak, Z. Li, and A. Khaligh, "A novel grid-tied, solar powered residential home with plug-in hybrid electric vehicle (PHEV) loads," in *2009 IEEE Vehicle Power and Propulsion Conference*, 2009, pp. 813–816, doi: 10.1109/VPPC.2009.5289765.
- [26] V. Vega-Garita, D. De Lucia, N. Narayan, L. Ramirez-Elizondo, and P. Bauer, "PV-battery integrated module as a solution for off-grid applications in the developing world," *2018 IEEE Int. Energy Conf. ENERGYCON 2018*, pp. 1–6, 2018, doi: 10.1109/ENERGYCON.2018.8398764.
- [27] V. Vega-Garita, S. Garg, N. Narayan, L. Ramirez-Elizondo, and P. Bauer, "Testing a PV-battery Integrated Module Prototype," *2018 IEEE 7th World Conf. Photovolt. Energy Conversion, WCPEC 2018 - A Jt. Conf. 45th IEEE PVSC, 28th PVSEC 34th EU PVSEC*, pp. 1244–1248, 2018, doi: 10.1109/PVSC.2018.8548111.
- [28] A. L. Julian, G. Oriti, and T. A. Lipo, "Elimination of common-mode voltage in three-phase sinusoidal power converters," *IEEE Trans. Power Electron.*, vol. 14, no. 5, pp. 982–989, 1999, doi: 10.1109/63.788504.
- [29] T. Kerekes, R. Teodorescu, M. Liserre, C. Klumpner, and M. Sumner, "Evaluation of three-phase transformerless photovoltaic inverter topologies," *IEEE Trans. Power Electron.*, vol. 24, no. 9, pp. 2202–2211, 2009, doi: 10.1109/TPEL.2009.2020800.
- [30] D. Dong, "Ac-dc Bus-interface Bi-directional Converters in Renewable Energy Systems," Virginia Polytechnic Institute and State University, 2012.
- [31] T. Jalakas, I. Roasto, and M. Najafzadeh, "Combined Active Frequency Drift Islanding Detection Method for NZEB Energy Router," *2019 IEEE 60th Annu. Int. Sci. Conf. Power Electr. Eng. Riga Tech. Univ. RTUCON 2019 - Proc.*, no. 1, 2019, doi: 10.1109/RTUCON48111.2019.8982258.

- [32] J. Wang, C. Dong, C. Jin, P. Lin, and P. Wang, "Distributed Uniform Control for Parallel Bidirectional Interlinking Converters for Resilient Operation of Hybrid AC/DC Microgrid," *IEEE Trans. Sustain. Energy*, vol. 13, no. 1, pp. 3–13, 2022, doi: 10.1109/TSTE.2021.3095085.
- [33] A. M. Taher, H. M. Hasanien, A. R. Ginidi, and A. T.M. Taha, "Hierarchical Model Predictive Control for Performance Enhancement of Autonomous Microgrids," *Ain Shams Eng. J.*, vol. 12, no. 2, pp. 1867–1881, 2021, doi: 10.1016/j.asej.2020.12.007.
- [34] N. L. Diaz, T. Dragicevic, J. C. Vasquez, and J. M. Guerrero, "Intelligent distributed generation and storage units for DC microgrids - A new concept on cooperative control without communications beyond droop control," *IEEE Trans. Smart Grid*, vol. 5, no. 5, pp. 2476–2485, Sep. 2014, doi: 10.1109/TSG.2014.2341740.
- [35] S. M. Malik, X. Ai, Y. Sun, C. Zhengqi, and Z. Shupeng, "Voltage and frequency control strategies of hybrid AC/DC microgrid: a review," *IET Gener. Transm. Distrib.*, vol. 11, no. 2, pp. 303–313, Jan. 2017, doi: 10.1049/iet-gtd.2016.0791.
- [36] E. Rokrok, M. Shafie-khah, and J. P. S. Catalão, "Review of primary voltage and frequency control methods for inverter-based islanded microgrids with distributed generation," *Renew. Sustain. Energy Rev.*, vol. 82, no. March 2017, pp. 3225–3235, Feb. 2018, doi: 10.1016/j.rser.2017.10.022.
- [37] S. Mariéthoz and S. Almér, "Model Predictive Control A Review of Its Applications in Power Electronics," *IEEE Industrial Electronics Magazine*, pp. 16–31, Mar. 2014.
- [38] L. Wang, T. Zhao, and J. He, "Investigation of Variable Switching Frequency in Finite Control Set Model Predictive Control on Grid-Connected Inverters," *IEEE Open J. Ind. Appl.*, vol. 2, no. July, pp. 178–193, 2021, doi: 10.1109/ojia.2021.3091154.
- [39] L. Wang, S. Member, J. He, S. Member, and T. Han, "Secondary Problem Formulation for Power Loss and Thermal Stress Reductions," vol. 56, no. 4, pp. 4028–4039, 2020.
- [40] D. J. Pradeep, M. M. Noel, and N. Arun, "Nonlinear control of a boost converter using a robust regression based reinforcement learning algorithm," *Eng. Appl. Artif. Intell.*, vol. 52, pp. 1–9, 2016, doi: 10.1016/j.engappai.2016.02.007.
- [41] C. Cui, N. Yan, B. Huangfu, T. Yang, and C. Zhang, "Voltage Regulation of DC-DC Buck Converters Feeding CPLs via Deep Reinforcement Learning," *IEEE Trans. Circuits Syst. II Express Briefs*, vol. 7747, no. c, 2021, doi: 10.1109/TCSII.2021.3107535.
- [42] N. Shabbir, L. Kutt, V. Astapov, M. Jawad, A. Allik, and O. Husev, "Battery Size Optimization with Customer PV Installations and Domestic Load Profile," *IEEE Access*, vol. 10, pp. 1–1, 2022, doi: 10.1109/access.2022.3147977.
- [43] J. J. Justo, F. Mwasilu, J. Lee, and J. W. Jung, "AC-microgrids versus DC-microgrids with distributed energy resources: A review," *Renew. Sustain. Energy Rev.*, vol. 24, pp. 387–405, 2013, doi: 10.1016/j.rser.2013.03.067.
- [44] U. G. K. Mulleriyawage and W. X. Shen, "Optimally sizing of battery energy storage capacity by operational optimization of residential PV-Battery systems: An Australian household case study," *Renew. Energy*, vol. 160, pp. 852–864, 2020, doi: 10.1016/j.renene.2020.07.022.

- [45] D. Leskarac, M. Moghimi, J. Liu, W. Water, J. Lu, and S. Stegen, "Hybrid AC/DC Microgrid testing facility for energy management in commercial buildings," *Energy Build.*, vol. 174, pp. 563–578, Sep. 2018, doi: 10.1016/j.enbuild.2018.06.061.
- [46] H. Wang, H. S. H. Chung, and W. Liu, "Use of a series voltage compensator for reduction of the dc-link capacitance in a capacitor-supported system," *IEEE Trans. Power Electron.*, vol. 29, no. 3, pp. 1163–1175, 2014, doi: 10.1109/TPEL.2013.2262057.
- [47] J. P. Leonard, "Nonlinear Modeling of DC Constant Power Loads with Frequency Domain Volterra Kernels," Florida State University, 2014.

Acknowledgements

I would like to thank my supervisors Indrek Roasto and Oleksandr Husev. Indrek accepted me to the Taltech power electronics group and laid out the vision of the thesis. Oleksandr's hard work and dedication to the field inspired and directed me to finish the thesis.

I also want to thank the head of the power electronics group Dmitri Vinnikov for all the organizational support and all the members of the PEG for their consultation and guidance and the fun times during my studies.

I would also express my deep gratitude to my families, my father, and my mother for their unlimited kindness and support I cannot reach this point of my life without them. All my sisters but especially Mona and Neda for their patience and emotional support. And my fiancé Karl joined me during my studies and always helped me outside of my studies.

Abstract

Multifunctional Energy Router for Residential Applications

This Ph.D. thesis focuses on the power electronics aspects to convert a conventional residential building into a smart, controllable and energy efficient building, also known as a residential nanogrid. In other words, it is a residential building that is equipped with local energy sources and a storage, and thus, it could operate independently from the main grid. The nanogrid not only consists of hardware but also requires smart energy management to control all the sources, loads and storage units. Today, all sources, storages, and loads are interfaced with power electronics converters, which are all independent and do not communicate with each other. Without communication smart energy management can be difficult to achieve. One solution to this problem is to add a multifunctional power electronics converter also between the building and the main grid. Such converter is also known as an energy router (ER). The concept has been known from microgrids but was little studied in relation to residential buildings, which was the main initiative for this thesis.

In the thesis the role of ER in residential applications was studied. Partly the concept of the ER has been already implemented by the industry in form of hybrid solar inverters. These are inverters with integrated energy storage that allows them to work as well in on-grid as in off-grid modes. However, the ER includes much more functionalities than it can be found in conventional hybrid inverters e.g. ancillary services, reactive power control, harmonics injection, smart energy management, etc. This Ph.D. work aimed to introduce ER topology with enhanced functionality and smart control system.

During the work various aspects of the ER were studied. From the input (power grid) side power factor compensation with bidirectional energy control was studied. The central part of the ER is the dc-link. Here the main focus was on different dc-link voltage control algorithms. The dc-link voltage fluctuations could be effectively reduced by a novel fuzzy logic-based algorithm. In addition, the author proposed a new method for dc-link voltage ripple mitigation by utilizing integrated battery storage. The output (i.e. building) side of the ER plays vital role regarding in-house power quality. Here the main challenge is to provide smooth transition from on-grid to off-grid mode. The author found that conventional control algorithms (proportional-resonance control) do not perform well under light load operation. Thus, a new approach, model predictive control, was successfully implemented and tested.

Although the thesis was mainly focused on the ER control, also some hardware modifications were proposed by the author. The author showed how the functionality of the conventional back-to-back ER topology could be extended by adding an auxiliary bypass switch. As a result, several new operation modes were derived.

This work also has a substantial practical value, as the application-oriented design of the proposed multiport ER topology was carried out and three full-scale prototypes were built while each time reducing volumes, increasing efficiency and improving EMC.

Lühikokkuvõte

Multifunktsionaalne energiaruuter eramutele

Selle doktoritöö fookuseks oli uurida kuidas jõuelektronika abil muundada tavaline eramu targaks, juhitavaks ja energiatõhusaks hooneks, mida võiks nimetada ka nanovõrguks. Teiste sõnadega on tegu eramuga, mis omab lokaalset energiaallikat ja salvestust ning on seega võimeline töötama ka iseseisvalt ilma elektrivõrguta. Nanovõrk ei tähenda ainult riistvara vaid nõuab ka paindliku energiahaldust, et juhtida oma allikaid, koormusseadmeid ja salvesteid. Tänapäeval on kõik allikad, koormusseadmed ja salvestid ühendatud võrku läbi muundurite, mis on iseseisvad ja üksteisega ei suhtle. Ilma suhtluskanalita on aga paindlik energiahaldus hoones raskesti saavutatav. Üheks lahenduseks sellele probleemile oleks lisada üks multifunktsionaalne jõuelektronikamuundur hoone ja elektrivõrgu vahele. Selline muundur on ka tuntud kui energiaruuter (ER). Selline kontsept on tuntud küll mikrovõrkudest aga on vähe uuritud eramute korral, mis oli ka käesoleva doktoritöö peamiseks motivaatoriks.

Doktoritöös uuriti ER rolli eramutes. Osaliselt hübriid-vaheldite kujul on selline ER kontsept juba ka tööstuses rakendust leidnud. Need on vaheldid, mis omavad integreeritud energiasalvestit, mis võimaldab neil töötada nii elektrivõrgu ühendusega (on-grid) kui ka ilma (off-grid). Kuid ER omab palju rohkem funktsioone kui neid leiab hübriid-vaheldite juures nt. elektrivõrgu toetamine, reaktiivenergia juhtimine, harmoonikute juhtimine, tark energiahaldus jt. Käesoleva doktoritöö eesmärgiks oli väljatöötada laiendatud funktsionaalsuse ja targa juhtimisega ER lahendus eramutele.

Töö käigus uuriti ER erinevaid aspekte. Sisendi (elektrivõrgu) poolelt uuriti võimsusteguri parendamist koos kahesuunalise energiavoo juhtimisega. ER keskne osa on alalisvooluvahelüli (dc-link). Siin oli uurimistöö fookuseks alalisvooluvahelüli pinge juhtimisalgoritmid. Alalisvooluvahelüli pingekõikumisi suudeti efektiivselt vähendada uudse hägusloogika algoritmi abil. Lisaks pakkus autor välja uue meetodi alalisvooluvahelüli pingepulsatsiooni vähendamiseks kasutades integreeritud akusalvestit. ER väljundis (hoone poolel) omab olulist rolli energiakvaliteedi juhtimine. Siin on põhiliseks väljakutseks saavutada sujuv üleminek võrguühenduselt võrguta režiimi. Autor tõestas, et senised algoritmid (nt. proportsionaal-resonant juhtimine) ei tule hästi toime väikese koormusega olukordades. Probleemi lahenduseks arendati välja ja testiti uudne mudeli põhine juhtimisalgoritm.

Kuigi doktoritöö oli põhiliselt keskendunud ER juhtimisele, pakkus autor välja ka mõned riistvaraga seotud uuendused. Autor näitas kuidas välise mõõdapääsulüliti lisamisega on võimalik ER topoloogia funktsionaalsust laiendada. Selle tulemusena arendati välja mitu uut töörežiimi.

Tehtud töö praktilist väärtust tõestavad kolm ER rakenduslikku seadme prototüüpi, mille käigus vähendati seadme mõõtmeid, parendati kasutegurit ja suurendati elektromagnetilist häirekindlust.

Appendix

Publication I

Najafzadeh, M.; Ahmadiyahangar, R.; Husev, O.; Roasto, I.; Jalakas, T.; Blinov, A. Recent contributions, future prospects and limitations of interlinking converter control in hybrid AC/DC microgrids. IEEE Access, 2021.

Received December 1, 2020, accepted December 30, 2020, date of publication January 4, 2021, date of current version January 14, 2021.

Digital Object Identifier 10.1109/ACCESS.2020.3049023

Recent Contributions, Future Prospects and Limitations of Interlinking Converter Control in Hybrid AC/DC Microgrids

MAHDIEH NAJAFZADEH¹, (Student Member, IEEE),
ROYA AHMADIAHANGAR¹, (Member, IEEE), **OLEKSANDR HUSEV¹**, (Senior Member, IEEE),
INDREK ROASTO, (Member, IEEE), **TANEL JALAKAS**, (Member, IEEE),
AND ANDREI BLINOV, (Senior Member, IEEE)

Department of Electrical Power Engineering and Mechatronics, Tallinn University of Technology, 19086 Tallinn, Estonia

Corresponding author: Mahdih Najafzadeh (mahdih.najafzadeh@taltech.ee)

This work was supported in part by the Estonian Research Council under Grant PRG675, Finest Twins grant H2020 No. 856602, EEA and Norway financial Mechanism Baltic Research Program in Estonia under Grant EMP474 and in part by the Estonian Centre of Excellence in Zero Energy and Resource Efficient Smart Buildings and Districts, ZEBE, of the European Regional Development Fund under grant 2020-2020.4.01.15-0016.

ABSTRACT This work analyzes interlinking converter control in hybrid AC/DC microgrids. The paper addresses the state-of-the-art general hybrid microgrid structure. The key power electronics topologies are used as bidirectional interface converters in the AC and DC parts. Different control structures of hybrid microgrids are categorized, followed by the classification of the main control functions, their control strategies, and the control techniques and a summary of their positive and negative aspects and applications. Control functions, strategies and techniques are classified in the interlinking-converter based. Finally, overall control objectives, time-scaled control structures, and their strategies are outlined. The prospects, main challenges, research gaps, and the trend of the hybrid microgrid structure and control are reviewed and summarized in the conclusions.

INDEX TERMS Bidirectional interface converter, control objectives, distributed generator, droop, hierarchical control, hybrid microgrid, island detection, power-sharing, power quality.

NOMENCLATURE

BIC	Bidirectional Interface Converter	ID	Islanding Detection
CCS	Continuous Control Set	MG	Microgrid
CM	Common Mode	MMC	Modular Multi-level Converter
CSC	Current Source Converter	MPC	Model Predictive Control
DG	Distributed Generator	MPPT	Maximum Power Point Tracking
DM	Differential Mode	NDZ	Non-Detection Zone
DS	Distributed Storage	PCC	Point of Common Coupling
EMC	Electro-Magnetic Compatibility	PID+R	Proportional Integral Derivative + Resonant Controller
EMI	ElectroMagnetic Interface	PWM	Pulse Width Modulation
FCS	Finite Control Set	P2P	Phase to Phase
FLC	Fuzzy Logic Control	ROCOF	Rate Of Change Of Frequency
GTO	Gate Turn-Off thyristor	SCADA	Supervisory Control and Data Acquisition
IC	Interface Converter	SOC	State Of Charge
		SST	Solid State Transformer
		SVM	Space Vector Modulation
		THD	Total Harmonic Distortion
		VSC	Voltage Source Converter
		VSG	Virtual Synchronization Generator

The associate editor coordinating the review of this manuscript and approving it for publication was Suman Maiti¹.

I. INTRODUCTION

Microgrids (MGs) have gained more attention in the past decade since they provide the facility for the exploitation of Distributed Generator (DG) to satisfy the growing rate of electricity demand. With improvements in technology, the share of electricity in global energy demand has increased from 17% in 2000 to 22% in 2018. Also, the electricity consumption growth rate of 80-90% is estimated in 2050 compared to 2018 [1]. Fig. 1 presents the global statistical data of electricity resources in 2018. More than 78% of electricity resources are coal, gas, and oil that produce greenhouse gas and air pollution, as shown in Fig. 1. For this reason, the trending usage of DGs in the power grid is justified. The growing rate of electricity demand, lower efficiency of the available power grid, and decreasing cost of the DG technology (PV and wind), with greenhouse gas regulation issues, motivate humans to upgrade the traditional power system to the smart grid through MGs [2].

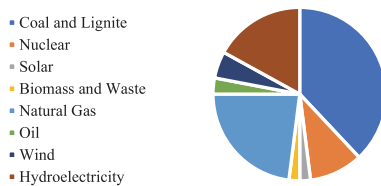


FIGURE 1. Share of electric power generation by resources in the world, 2018 [1].

On the other hand, developments in the power semiconductor technology have opened a new door of power-electronics applications in the power system. Digital signal processors in the control of Interface Converters (ICs) enhance their control algorithm complexity by decreasing the processing time [4]. The power-electronics ICs enable MGs to utilize and control the intermittent generated power of DG, typically with integrated Distributed Storages (DSs) [5]. Each MG consists of different DGs, loads, and DSs, which are connected through controllable ICs. This specification elevates MG functions acting as a controllable entity in the grid-tied or islanded operation mode. When an MG is connected to the main grid, it operates in the grid-tied mode and when it works standalone, it is in the islanded operation mode. Also, MGs can act as a consumer or a generator or a “plug and play” system [3], which provides a lot of freedom in the power system operation.

The increasing rate of DC sources and loads is a strong motivation to shift from mainstream AC MGs to hybrid or DC MGs. However, the AC nature of the existing power system promotes the hybrid MG concept as the first candidate since it is more compatible [3]. AC, DC, and hybrid MGs are different in their common links, which can be divided into three types: AC, DC, and the combination of both [6]. AC MGs are the most common types since they are compatible with the existing grid [3]. Synchronization issues, circulating reactive power, and bigger power losses are their

disadvantages. DC MGs attributed to future generations are gaining popularity because of the growing number of DC sources and electronic loads, e.g., PV panels, computers, cellphones, and batteries.

Although the existing distribution grid needs more modifications and higher investment costs, DC MGs are more reliable, efficient, and easier to control. Absence of synchronization issues, lower power loss of reactive power circulation, fewer required power-electronic-converter stages are the merits of DC MGs [6], [3]. But the non-zero crossing nature of the DC current is a challenge in DC breakers. DC MG topologies are described in detail in [7], [8].

However, due to the AC structure of the available power system, a hybrid MG has more potential to be adjusted to the current power system and leverage advantages of both AC and DC MGs [3], [9]–[15]. As some converters are omitted in the hybrid MG structure, the power loss of conversion is reduced and the power quality is increased [13]. The hybrid MG is a complex multi-objective system. It involves a variety of aspects of control, metering, communication, and protection, which have direct influence on other structures affecting each other.

The limitations of utilization of power electronics in hybrid MGs have not been reviewed in detail. This paper gives a comprehensive overview of the control issues of power-electronics devices inside hybrid MGs at the distribution level. In this regard, the incentive is to cover the entire range of various control aspects of power electronics devices in the MG application. In summary, the control studies of the hybrid MG have not addressed the power electronics state of the art. Neither have the objectives of the hybrid MG as a complex control system been reviewed in general terms. The aim of this review paper is to provide a comprehensive classification and comparison of control strategies and techniques in the hybrid MG, taking into account the state of art power electronics limitations and the feasibility of the existing methods for practical application.

The rest of the paper is organized as follows. Section II presents a common hybrid MG structure and different BIC topologies of the hybrid MG regarding power electronics units; in section III, different control structures are analyzed. Different control strategies with their techniques are discussed in section IV. Finally, prospects and conclusions are addressed in sections V and VI.

II. TOPOLOGIES

In most studies of BIC control, the hybrid MG is divided into three zones: AC sub-MG, DC sub-MG, and the Point of Common Coupling (PCC) to the main grid [10]–[12]. AC sub-MG consists of AC-link, DGs, DS, and loads connected to the AC-link. DC-link connected DGs, DSs, and loads from the DC sub-MG. The ICs among AC and DC sub-MG must be bidirectional to permit energy flow in both directions between AC and DC. In some studies, a separate DC-link is proposed for DSs (as LVDS side) to provide a DC-link slack. This extra DC-link enhances the voltage stability in the MG [16].

Different interface structures regarding connection among these three (or four) links have been reported. The most common topologies of AC/DC (between AC-link and DC-link) and DC/DC (Between two DC-links) converters are shown in Fig. 2. A simple 3-phase full-bridge BIC is a popular AC/DC topology presented in Fig. 2. In some studies, a non-inverting DC/DC buck-boost converter is also added to improve the DC-link controllability.

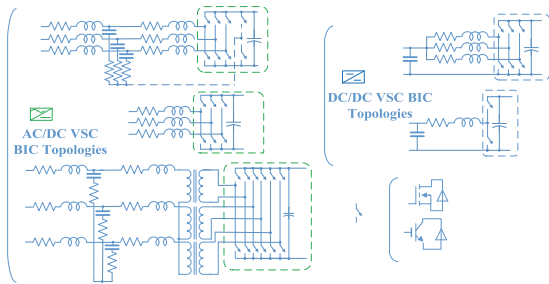


FIGURE 2. The common AC/DC and DC/DC BIC topology.

According to the literature, the PCC voltage level changes from medium levels (between 1 and 35 kV, based on the IEC 60038 [17]) to low voltages (between 100 and 1000 V, based on the IEC 60038 [17]), which is equal to the AC sub-MG voltages.

For a PCC with a medium-voltage-level power transformer, a Solid State Transformer (SST) and cascaded structures are the main options to step down the voltage. The power transformer can be added at the PCC to the main grid, which increases the reliability, leakage current inhibition, and protection degree of both the MG and the main grid through galvanic isolation from each other [18]–[21].

Providing galvanic isolation by a power transformer or high-frequency transformer helps to decrease the flowing leakage current of Common Mode (CM) voltages [18]. Besides, PVs are one of the most cost-effective and widespread resources in MGs and they have parasitic capacitors resulting in CM current. This leakage current produced by high-frequency CM voltage leads to high power loss, lower quality of grid current, ElectroMagnetic Interference (EMI), and other safety issues [20]. Moreover, for large leakage currents, the hybrid MG may trip due to ground current or fault protection [21]. As a result, this leakage current is targeted to be minimized. The two solutions are a bulky low-frequency transformer and a complicated modulated high-frequency transformer in SST. However, their cost, size (especially in residential and commercial applications), and low efficiency (for transformation level) are the main reasons why researchers are seeking transformer-less BIC solutions [18].

The industrial solution for PV arrays is to be equipped with line-frequency (power transformer) or high-frequency transformer at PCC since they isolate PV's parasitic capacitors path (parasitic capacitors between the PV and the ground)

through which leakage current can flow [19]. Regarding CM voltage reduction, different topologies such as H5, ... H8, neutral point clamped (three-level full-bridge) are introduced mostly to the inverter mode for PV applications with parasitic capacitors [18], [22]–[24]. In the solutions suggested, the common base topology is the full-bridge Voltage Source Converter (VSC). Then, different configurations of leakage-current blocking switches are added to separate AC and DC side during the freewheeling period [18], [25]. The virtual-ground connection was introduced by [26] and [27] for PV application; however, the proposed topology can be extended in hybrid MGs utilization as well. In this study, the neutral point of the LCL filter is connected to the neutral point of the DC-link capacitor and the neutral point of the three-phase three-level full-bridge inverter. This approach does not change the CM current; however, providing an alternative predominant capacitive path for the CM current decreases the high-frequency CM current flowing by the ground path. The main demerits of this method are the safety issue and the total power-loss increase because the virtual ground path consists of switches [27]. CM solutions are shown with a dashed line in Fig. 2.

Transferring AC power to DC power in one-phase AC/DC BICs provides a double line frequency ripple on the DC side [28]–[35]. This low-frequency ripple power increases the power loss and can decrease the DC sources, ES, and DC-link capacitor life [31], [35]. Moreover, to buffer this ripple power, a large size of the electrolyte capacitor is required; however, these capacitors are sensitive to temperature [36]. As a result, this ripple power increases the power loss in the capacitor and decreases the system reliability by gradually destroying the capacitor. Film capacitors can tolerate higher temperatures but their capacity is not high enough. So, one solution is to separate this ripple power from the constant one. Although different buffering solutions (active and passive methods) have been suggested in different studies [28]–[36], this issue is not entirely solved.

DC isolation and different DC voltage levels are achieved through SST implementation. These topologies need more complex modulation and control methods. It is also possible to increase the transferred power by using more BICs in parallel or different MG configurations. An interleaved buck-boost converter is another solution reported in [15] and [37]. In these studies, to provide different DC bus voltages connected to the common DC-link, a DC/DC n-phase interleaved BIC is presented. Reduction in the DC current-ripple with this interface structure leads to a decline in the required DC capacitor; however, adding an extra DC/DC power electronic level with its required filters results in a higher cost.

BIC can be divided into AC/DC and DC/DC parts to control both AC and DC buses. VSC or Current Source Converter (CSC) are the two main candidates as AC/DC BIC. The priority in MG control is to provide stabilized voltage in the islanded operation, which is promoted by the BIC appliance. As a result, most studies have concentrated on VSCs for MG's interface structure, as shown in Fig. 2. On the

other hand, DC side ripples in CSCs and the resulting AC side harmonics make CSCs less popular in the interface structure appliances. To solve this problem, efficient modulation [38] and the control method [39], [40] have been proposed.

On the other hand, the allowable configuration of short circuit switching and inherent current-limiting nature of CSCs and their reliability are shifting researchers' attention to using them for PV [67]–[70], wind [71], or Fuel Cell [72] interface with the main grid.

TABLE 1 categorizes previous studies based on their BIC interface structures, merits, and limitations of each structure, AC and DC voltages. Default voltages are phase-to-phase and phase-to-ground voltages denoted as P. Those BICs without the capability of islanding and fault isolation of the hybrid MG should be equipped with a circuit breaker or static transfer switch at PCC [73].

As shown in TABLE 1, the study in [41] proposes the back-to-back CSC between two MGs. It suggests an optimized Space Vector Modulation (SVM) to reduce the required DC-link inductance. In this study, the pulse patterns of rectifier and inverter CSCs are selected to minimize their voltage differences. The result confirms the lower DC-link ripple current at the expense of more complicated modulation and higher processing time. TABLE 1 shows that in the case of PCC with low AC voltage and a unified DC-link voltage level in hybrid MGs, the majority of studies suggest back-to-back or one full-bridge VSC in the non-isolated condition and with a line frequency in the isolated condition. The line-frequency transformer place is different, it can be between AC sub-MG and DC sub-MG or between PCC and the hybrid MG; depending on its place, it provides different isolation levels. Also, hybrid MGs with two DC-link voltage levels are equipped with DC/DC VSCs that are a simple buck-boost type or interleaved buck-boost in most cases.

In practice, in TABLE 1, [60] addresses a commercial building in Griffith University, Australia. The implemented topology in that study includes a line-frequency transformer to change the 11 kV at PCC to 0.4 kV for the AC-link, whereas AC/DC VSC connects the AC-link to the DC-link.

Since DSs contribute to the power balance, energy buffer, and fault ride-through, [61] and [62] consider a separate DS-link for DS sub-MG, as provided in TABLE 1. The main disadvantages of this topology are an increase in the complexity of power management, plug, and play capability, and the required control system. In TABLE 1, [66] presents an interface topology with a complex structure; however, MMC implementations and complicated structures are not popular among researchers since they need a complex control and modulation scheme. Standardization of hybrid MG's BIC topologies can simplify the analysis, evaluation, application, and categorization of their control structure.

Although in some studies, the DC-link voltage is decided based on the nominal voltage of the power electronics switches [51], the different levels of DC sub-MG voltages in TABLE 1 are noticeable. DC-link voltage is varied from 48 to 3500 V, which shows the lack of standard DC-link

voltage. Based on the limitation of the power-electronics device, power scale, and applications (residential, industrial, electric vehicle charging station), this standardization can unify future researches to some limited, standard DC-link voltage levels and help to reach some standard hybrid MG BIC topologies and hybrid MG structures as well. Different hybrid MG configurations are another research trend, in which different AC and DC sub-MGs are connected to a common link. This link can be DC or AC. In this way, it is possible to connect AC sub-MGs with different voltage magnitudes and frequency levels. The focus of this work is on the regular hybrid MG shown in Fig. 3, which depicts the power-electronic interface schemes of TABLE 1 regarding different connections among PCC, AC-link, DC-link, and DS-link. In this work, the topologies are classified according to their main elements: SST as a high-frequency transformer, DC/DC, or AC/DC BICs, as their configurations in a common hybrid MG shown in Fig. 3.

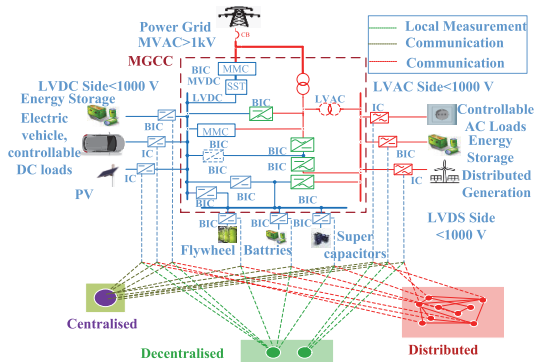


FIGURE 3. Conventional hybrid MG configuration and different possible coordinated control structures.

III. CONTROL STRUCTURES

The control structure of the hybrid MG can be independent of any communication network called communication-less-based. Also, it can be equipped with a communication network, a so-called communication-based control structure. In communication-based control structures, all converters are connected through the communication network. Centralized, master-slave, distributed control methods are communication-based [81].

Regarding the control aspect, the hybrid MG is controlled through different technical issues at different time scales and physical levels.

IEEE p2030.7 [74] categorized all the control objectives into three different control layer functions such that each layer acts in a specified time scale discussed in [11], [75]–[77].

The main task of the hybrid MG management system is to keep the hybrid MG stable, which is located in the primary control layer of control structures [75]. The strategies toward communication-less power-sharing function are dual loop and droop techniques, which will be discussed later.

TABLE 1. Comparison of the proposed categorization of the power electronics interface structures.

Power Electronics Interface Structure	Merits and Limitations								AC Voltages(V)		DC Voltages(V)		Ref.
	Isolation between sub-grids	Utility connection	Possibility of power measurement	Fault isolation	Islanding control	Grounding system possibility	Avoid overcurrent	Needs bulky DC-link inductance	PCC	AC Sub-MG	2nd. level	1st. Level	
Back-to-back CSC	No	By DC-link	Separable for DC and AC sub-MGs	Yes	Possible at PCC	No	Yes	Yes	208	208	-	-	[41]
									-	-	-	-	[42]
Full-bridge VSC	No	By AC-link	For DC sub-MGs	Partially for DC sub-MG	No	Partially	No	No	380	-	750	-	[43]
									170	-	280	-	[44]
									$220\sqrt{2}$	$220\sqrt{2}$	700	-	[45]
									220	220	380	-	[46]
									-	-	800	-	[47]
									400	-	360	-	[48]
									690	-	2500	-	[49]
									260	-	570	-	[50]
									255-270	-	600	-	[51]
									200	-	400	-	[52]
Full-bridge VSC + power transformer between AC and DC sub-MG	AC and DC sub-MG	By AC-link	For DC sub-MGs	Partially for DC sub-MG	No	Partially	No	No	208 P	208 P	-	300	[53]
									380	380	-	700	[54]
									220	270	-	750	[55]
									415	415	-	48 V	[56]
Full-bridge VSC + power transformer between the main grid and the hybrid MG	Utility and the hybrid MG	By AC-link	For the DC sub-MG	Partially for DC sub-MG	No	Partially	No	No	110	110	-	400	[57]
									25 k	690	-	1200	[58]
									-	-	-	-	[59]
An AC/DC VSC + DC/DC Converter: AC-link+ DC-link + DS-link	No	By AC-link	For the DC sub-MGs	Partially for DC and DS sub-MGs	No	Partially	No	No	11 k	400	-	650	[60]
									-	$230\sqrt{2}$ P	-	380	[61]
Back-to-back VSCs with their line-frequency transformer	Yes	By DC-link	Separable for DC and AC	Yes	Possible at PCC	Yes	No	No	11 k	3500	-	3500	[63]
									-	-	-	-	[62]
2 back-to-back VSCs + transformer between the main grid and hybrid MG	Utility and the hybrid MG	By DC-link	Separable for DC and AC	Yes	Possible at PCC	Yes	No	No	10 k	380	-	600	[64]
									-	-	-	-	[65]
2 Back-to-back AC/DC VSCs + autotransformer between main grid and the hybrid MG + An N phase interleaved DC/DC VSC	Utility and the hybrid MG	By DC-link	Separable for DC and AC sub-MGs	Yes	Possible at PCC	Yes	No	No	220	220	-	-	[15]
									-	-	450	200	[65]
-	-	-	-	-	-	-	-	-	980	450	-	[37]	
Modular Multi-level Converter (MMC) between 10 kV and high voltage DC-link, SST to LV DC-link + VSC for AC sub-MG	High voltage and the low one	By DC-link	Separable for DC and AC	Yes	Possible at PCC	Not clear	No	No	10 k	380	-	700	[66]
									-	-	-	-	[66]
2 back-to-back MMC AC/DC VSCs both connected to the grid	Utility and the hybrid MG	By DC-link	Separable for DC	Partially for DC sub-MG	Partially for DC sub-MG	Not clear	No	No	10 k	-	20 k	-	[16]

The communication-based power-sharing techniques contain droop in a centralized, master-slave, or distributed control structure [75]. However, to increase the reliability of the hybrid MG, a decentralized or autonomous control structure is suggested for use in the first (primary) control layer that is independent of the communication system [75], [78], [79].

The main function of the secondary layer is to recover the frequency and voltage deviation of the local control [77]. Since it is supposed to connect to the grid at this control level, synchronization, power quality, and other functions requiring grid-connection are listed in these control level tasks [75], [77]. However, this and the third layer operate slower; so, they require a slower communication network with low bandwidth for control coordination.

The tertiary control layer, also called the grid-interactive control [76], has the slowest pace compared to two other control levels and it is normally located out of MG like in the Supervisory Control and Data Acquisition (SCADA) system or upper control centers. The main function of this layer is to manage the power among different hybrid MGs' BICs based on the optimization calculations, energy cost, weather forecast; so, this control level is just interconnected to the grid-tied operation mode of the interface structures [12], [77].

Coordinated control plays an important role in smoothing the power transfer between ICs and maintaining stability under different load-supply balance conditions [12], as well as different operation modes [80]. The coordinated control method is a common solution to address frequency issues, particularly, in the islanded-mode of MG operation [81]. To increase the integration of renewable energy sources and different loads in the hybrid AC/DC MGs, multiple sub-MG topologies are attracting more interest. The downside of multiple sub-MG topologies is the complexity of control. Therefore, the coordinated control structure is necessary to overcome the challenge of maintaining stability among interacting sub-MGs [82].

Coordinated control is also necessary for the cluster of MGs to ensure optimal power exchanges among them [83]. Coordinated control structures are classified into centralized, decentralized, and distributed architecture. This classification depends on the data and information exchange between the controlled entities [5], [75].

A. CENTRALIZED

This structure naturally consists of a central controller and concentrates information in this node [84]. The central controller decides actions based on the control objectives and the information available from both AC and DC sub-MGs of the hybrid MG. A centralized structure is easy but expensive to implement.

B. DECENTRALIZED

The main characteristic of this structure is that it needs no communication links. The decentralized control methods require only local measurements [85]; therefore, it provides the ride through communication malfunction capability and

enhanced system reliability [62]. However, the drawback of the decentralized control structure is in the practical utilization: low accuracy of power-sharing and sensitivity to line impedance, poor performance in nonlinear load sharing, inherent load-dependent frequency, and amplitude deviations. Moreover, the effectiveness of this control structure is questionable under the circumstances that the power exchange between two sub-grids is required. There is a trend in recent research to develop tuning methodologies to adjust the droop characteristics to overcome the issues regarding nonlinear load sharing in a decentralized control structure [86].

C. DISTRIBUTED

This structure consists of independent advanced controllers, which are connected and therefore are aware of the mutual situation. A distributed control structure is particularly efficient for the multiple sub-grid topologies [94]. This structure enables some level of cooperation between different control entities, but the main issue is how to share data and define the access level of information. Meanwhile, distributed control is an emerging concept to enable the plug-and-play feature and handle topological variations through its scalable nature. Fig. 3 illustrates these three control structures for a hybrid AC/DC MG. TABLE 2. presents a comparison of the coordinated control structures of the hybrid AC/DC microgrid.

IV. CONTROL STRATEGIES

Some control objectives in the hybrid MG studied so far are power management, synchronization, parallel BIC operation, stability improvement, voltage, and current control, energy storage coordination, islanding detection, seamless transition between BIC operation modes, economic energy dispatch, black start management, fault detection, unbalanced voltage control, power quality, and harmonics mitigation. These control objectives can be divided into energy management and protection issues based on their related fields [9], [75], [120]. Different control strategies are implemented to control these objectives. Common strategies in BIC control will be discussed in this part.

A. POWER-SHARING

The power-sharing objective is possible by making a balance between production and consumption; in this way, voltage and frequency stability are also achieved. So, the power-sharing objective overlaps the stability issue, which will be discussed below. Power-sharing strategies are classified into three major concepts: current or voltage control, droop, and Virtual Synchronous Generator (VSG). The current or voltage control is the basic concept implemented in the droop and VSG concept as well. The droop technique concentrates on different ways of power-sharing among multiple BICs and ICs. The VSG concept is applied to enhance both the steady-state and transient stability of droop power-sharing [79].

TABLE 2. Comparison of coordinated control structures.

Structures	Disadvantages	Advantages	Applications	References
Centralized	Expensive and complex Difficult in expendability Decreased redundancy, reliability, and flexibility	Standardized procedures Easy implementations More accurate power-sharing Better power quality Faster transient response Less circulating current among ICs The optimal decision is guaranteed	Secondary and tertiary control Optimization functions and Economic dispatch Standalone MG	[84], [87], [88], [89], [90], [75], [91], [92], [93], [94], [95], [96]
Decentralized	The optimal decision is not guaranteed Less accurate in power management Slow in transient response Deviation in voltage and frequency control Poor power quality control More current circulation	Does not need communication Enables hierarchical control Least computational burden More reliable Less expensive and expandable Redundant, Flexible, and modular	Primary (Droop) control	[97], [98], [85], [99], [82], [86], [100], [94], [93], [95], [96]
Distributed	Insecurity in sharing information Signal Transmission delays Difficult in expendability Decreased reliability, redundancy, and flexibility	The optimal decision is possible Accurate voltage and frequency control More accurate power-sharing Better power quality and transient response Less circulating current among ICs	Secondary and tertiary control	[101], [62], [102], [103], [75], [91], [92], [93], [94]

The traditional Proportional Integral Derivative (PID)+Resonance (R) controller, Model Predictive Control (MPC), Fuzzy, adaptive fuzzy, neuro-fuzzy Logic Control (FLC), and Reinforcement Learning (RL) are the most popular control techniques in these three power-sharing strategies. MPC is the most popular alternative for PID+R methods. MPC in DG and ES application is studied in [121]–[126].

[121] provides a review of model predictive current control with the SVM modulation technique for the DGs. [122] uses MPC for PV applications. In this work, model predictive current control and model predictive voltage control are used for MPPT and DC droop control respectively.

One of the main issues in the MPC is the determination of the cost function [126]. Cost functions contain control objectives or target sets and the limitation sets [106], [126] and [127] categorize cost functions based on the control objectives and applications successively. The MPC can be adopted to optimize the switching function, which is called the Finite Control Set (FCS) MPC [107]. However, it may result in variable switching frequency, spreading the frequency spectrum and higher THD, so some modifications in the cost function are necessary [111], [118]. MPC with an external switching module works with the fixed switching frequency called Continuous Control Set (CCS) MPC [119]. The input of the cost function is an error signal that must be minimized. This error signal is the difference between the reference value and its future predicted value. The MPC methods implement the state-space model of the system to predict the future states and calculate the optimal control. As these methods utilize updated states in each sampling time, they are equipped with online optimization inherently [111]. On the other hand, generalized predictive control employs the system transfer function utilized in offline optimization [111].

The general MPC application in hybrid MGs summarized in TABLE 3. will be discussed in this part and other parts of the paper.

RL is a heuristic intelligent technique consisting of environment, agent, action, rewards, penalties, and states [128]. RL aims to learn how to maximize the rewards for the agent based on the rewards or penalties of its actions in predefined environment states [129]. Different studies implement RL to optimize the schedule of DGs or DSs based on their predicted product, energy price, and load demand [128]–[133].

FLC is another intelligent control technique which emulates human decision making [134]. FLC is used in the control of DSs and DGs to provide reference values [135]–[143] or tune the optimized parameters of PID+R regulators [144] in different studies. In summary, the popular FLC method is Mamdani with 3 to 7 triangular or trapezoidal membership functions.

The pros and cons of different control techniques are summarized in TABLE 4.

These three main concepts of power-sharing and their control techniques are discussed below.

1) VOLTAGE AND CURRENT CONTROL CONCEPT

Many studies have focused on this control objective, regarding IC and BIC control. Each IC in the MG has the grid-tied or the islanded operation mode. In the grid-tied mode, the ICs follow the main grid voltage; so in the control strategy, a current-controlled grid is followed. In the islanded mode, the priority is to provide a stable voltage, so the grid-forming strategy is applied. This strategy is voltage controlled. In this section, different strategies toward this concept will be discussed.

a: PID+R TECHNIQUE (DUAL LOOP)

In the grid-tied and islanded mode, apart from the synchronization method, the same procedure is applied in many papers using traditional dual loop PID+R controllers. A reference current or voltage value is tracked by an outer voltage loop and inner current loop in abc (natural frame), dq (synchronous reference frame), or $\alpha\beta$ (stationary reference frame)

TABLE 3. Proposed categorizations of MPC studies based on their applications in hybrid MGs BICs.

MPC Application	Control Objective in the Cost Function	Ref.
AC/DC VSC Control	Current, Voltage, Power	[58], [104], [105]
	Current, Voltage, Power, Switching function	[106], [107], [105], [108]
Coordinated Control in a Hybrid MG	Power balance in both grid-tied and islanded modes	[58], [109]
	Power balance in both grid-tied and islanded modes, Switching function	[59] [110]
Stability Analysis	LCL filter variations on system stability	[111]
Droop Control	Current, Voltage, Power	[109], [112], [113]
Virtual Synchronous Generator	Frequency, Voltage, Power	[114]–[117]
Power Quality	Current, Voltage	[118], [119]

TABLE 4. Comparison of different power-sharing control techniques.

Techniques	Pros	Cons	Ref.
PID+R	Less computational time Fixed switching frequency Easy to implement	Dependency on the mathematical analysis Dependency on the dynamics of the system Complicated control system in terms of the cascaded control structure, feedback loops, and PWM structure Time-consuming parameter tuning of PID+R Slow in the dynamic response	[123], [124] [128] [130] [145]
MPC	Multi-objective optimization control technique Fast transient response Simplifies the control structure by combining the modulator block	More computational burden Needs high sampling frequency FCS produces extra harmonics Difficulty and uncertainty in the determination of weighting factors in the cost function Dependent on the accuracy model of the system	[105], [106], [107], [106], [107], [111], [118], [119], [121]– [126]
RL	Able to learn without pre-required knowledge Able to combine with other techniques	Convergence dependency on the initialization	[128]–[133], [146]
FLC	Does not need an accurate mathematical model of the system Does not need an accurate model of training Easy technique for control of complicated systems Simple rule-based membership functions Less sensitivity to disturbances Able to combine with PID+R controllers	Time-consuming in setting the membership functions Not optimized in terms of identifying membership functions Complicated in increasing numbers of inputs and outputs	[128] [147], [135]–[144]

frame in the single or three-phase and the s or z domain [9], [148]–[161].

In [158] and [154], despite showing simulation results in various operation conditions, the experimental results are limited to the voltage output and THD. Studies in [152] compare the voltage steady-state error in experimental results in four control conditions: PID, PID+ R, PID+R+ load current feedback, and dq frame control with load current feedback in no-load, resistive, capacitive, and first-order nonlinear load. Its experimental results show better performance of PID+R+load current feedback; however, in non-linear load, especially for higher-order, the effects of the harmonics and EMI are increased. In [153], a limited setup result with harmonics and EMI effects is shown; in other words, it neglects different load types and transition conditions like load change. Digital control is applied in [156]; the results show the suitability of steady-state response but a weak transient response of the proposed control method.

The experiments in all the studies referenced were done on a scale of less than 10 kW. However, the required power scale in MGs is higher. This fact points out the limitation of a power-electronics device in practical application. Consequently, most studies in large power-scale prove their proposed control methods in simulations rather than in the experimental setup. The exception case is [159]. In this study, in the experiment, a power scale of 500 kW was used. A three-level three-phase full-bridge VSC with Gate

Turn-Off thyristor (GTO) switches was applied; however, GTO has the limitation of low switching frequency operation. The experiment with the switching frequency of 1620 Hz is utilized, whereas the low switching frequency deteriorates the output power quality.

The current-controlled technique is easy to implement with BICs. It eliminates the circulating current and decouples active and reactive power, which are its positive points but its function is dependent on the voltage supply; as a result, this technique is not suitable for a weak hybrid MG [11]. The voltage-controlled technique is capable of providing a stable voltage, so it is suitable for the islanded mode and a weak hybrid MG [11]. Easily circulating current, coupling active, and reactive power, easily influenced by the line and filter impedances in the droop technique are some of the negative points of this method [11].

b: MPC TECHNIQUE

MPC application in voltage-controlled and current-controlled concepts can be divided into FCS MPC, hybrid FCS MPC, CCS MPC, and hybrid CCS MPC. Hybrid types contain an outer PID+R loop in their control blocks, as shown in TABLE 5. [105]. TABLE 5. categorizes the references based on this division and compares them. The measuring values can be transformed to the reference power in the control block.

Reference [106] confirms that the steady-state and dynamic response and THD control of FCS MPC are better as

compared to the hybrid FCS MPC; however, the hybrid FCS MPC technique is more robust against parameter variations. On the other hand, [162] shows that the performance of the hybrid FCS MPC is better than that of FCS MPC regarding the LCL resonance frequency, stability, and sensitivity enhancement.

References [58], [59], [110] address the application of MPC in both the grid-tied and the isolated mode of the hybrid MG. The experiment in [58] is conducted in the hardware-in-the-loop in which case the performance of CCS MPC is better than that of a hybrid type in terms of THD and transition states. In a similar hybrid MG, [59] suggests implementing model predictive power control and model predictive voltage control for the DS converter and AC/DC BIC respectively. The ES converter acts as a master in the islanded mode. Its cost function is designed to minimize the DC-link voltage ripple and balance the DC-link current in the islanded and the grid-tied mode successively, considering SOC and DS current constraints. The connection or disconnection of the load side capacitor generates a spike current, which is not solved in this work. Also, the reference reactive power is assumed to be zero, which limits the AC/DC BIC application in ancillary service to the utility. Optimization of the ES lifetime is not addressed in [59], [110].

Prediction horizon is an important issue in MPC. Increasing the prediction horizons improves the system performance and its stability [127], but it leads to an increased computational burden [127]. Most studies use one horizon step [58], [104], [106], [107]. However, to compensate for the processing time delay of digital hardware, two horizon steps are widely accepted [162].

c: RL TECHNIQUE

RL technique is used in [146]. This study proposes the RL-based fuzzy PID to control the frequency in an MG. The MG consists of different RESs and ESs. The Fuzzy-PID is utilized to prepare flexible parameters. Seven trapezoidal membership functions are regraded for three parameters of PID, which are selected based on genetic algorithm optimization. RL defines the reward action in each interval. Comparison of the results of the RL-based fuzzy-PID with the fuzzy-PID and the classic PID shows that the transient response of the proposed technique is better in load change conditions. Less settling time and decline in undershoot are the merits of this technique; however, it has more overshoot.

d: FLC TECHNIQUE

FLC in the voltage-controlled concept is used in [163]. It implements and simulates FLC for the self-tuning of PI regulators for a VSC IC in the dq frame. The results confirm the flexibility of the FLC controller compared to classic PI regulators in load change conditions. FLC utilization in the current-controlled VSC is studied and simulated in [125], in which FLC provides a referenced component current in the AC side. DC-link error voltage and its derivative are the inputs of the FLC regulator.

2) DROOP CONTROL CONCEPT

Droop-based control is the most common control technique, which can be implemented in communication-less-based networks as well as in communication-based networks. As the AC/DC BIC VSC transfers the active power between AC sub-MG and DC sub-MG, it implements both AC and DC droops called a hybrid droop. In this section, all these droops are categorized into AC droop, DC droop, hybrid droop, and active droop.

a: AC DROOP

Common AC-droop is based on the dominant inductive or resistive characteristics of the line and filters [164], so it includes active power-frequency P-f and reactive power-voltage Q-V characteristic for inductive characteristics and P-V, Q-f for resistive type [165]. Studies in [166]–[168] focus on the AC droop based primary control using PID+R controllers in an islanded MG, in which different AC droop types of static and dynamic, voltage regulation improvement, dynamic voltage regulation improvement, and virtual frame are explained. Also, different control block diagrams regarding communication-based techniques, such as centralized, distributed, master-slave, and angle droop, are explained in [166], [169].

In terms of MPC application, [112] uses hybrid FCS MPC for AC-droop control of parallel VSCs. Virtual resistive and droop loop provide the reference voltage for the FCS MPC block. [109] implements AC-droop-based CCS MPC for the primary and secondary control level of AC/DC VSCs in an islanded hybrid MG. The primary level of MPC has a steady-state error in the output voltage frequency and magnitude, which is compensated by the secondary level MPC.

The study in [94] presents three different control levels of the islanded ACMG, focusing on power-sharing and power quality in load changes. This work proposed droop control for the first control level, which could reach the voltage and frequency in an acceptable limit but it was not successful to keep them at nominal values. So the multi-stage based H_∞ controller as the second control level was introduced, which was able to reach those values to their nominal amounts. This control technique improved power quality as well. To enhance the performance of the second layer, the HS optimization algorithm for weighting parameters of H_∞ was implemented.

b: DC DROOP

DC-droop is based on the DC voltage and power. Generally, AC voltage droop solutions are expandable to the DC-droop as well [78]. DC droop is applied in ESs and DGs, which are discussed in [51], [61], [62], [170]–[174].

FLC utilization for adaptive DC-droop control in DGs and DSs is studied in [175]–[177]. FLC inputs are DC-link error voltage and SOC of ESs. The FLC output is the adaptive resistance of the DC-droop. Results of hardware-in-the-loop show that the performance of FLC in the power-sharing and

TABLE 5. Comparison of MPC applications in VSC current-controlled and voltage-controlled techniques.

		Block Diagram representative of control technique	
		Hybrid FCS MPC	Hybrid CCS MPC
Type		Hybrid FCS MPC	Hybrid CCS MPC
Ref		[106], [107], [105], [110], [162]	[58], [105]
Control Loop Features and Performance	Control Loop Numbers	2	2
	Computational Effort	Low	High
	Modulator Stage	Not Needed	PWM or SVM
	THD	Moderate	Moderate
	Steady-State Response	Good	Good
	Dynamic Response	Good	Good
Type		FCS MPC	CCS MPC
Ref		[59], [106], [105], [110], [162]	[58], [104], [105]
Control Loop Features and Performance	Control Loop Numbers	1	1
	Computational Effort	Moderate	High
	Modulator Stage	Not Needed	PWM or SVM
	THD	Moderate	Low
	Steady-State Response	Good	Good
	Dynamic Response	Good	Good

equalizing SOC among DSs is better in different conditions. Despite the DC-link voltage spike in the transition condition from the constant voltage-controlled mode to the droop mode of DSs, FLC has no steady-state error in the DC-link voltage compared to the fixed DC-droop.

c: HYBRID DROOP

Hybrid-droop is utilized in BIC power-sharing control, which links the AC droop in the AC side to the DC-droop on the DC side. The coordination of these two droops P-f and P-V is used in the BIC control for proportional power-sharing of AC sub-MG and DC sub-MG respectively [178], [179]. As shown in Fig. 4, to make the AC frequency and the DC voltage comparable, normalized or per unit (p.u.) amount of them is used in the hybrid droop. It is described and compared in TABLE 6. [11], [14], [78], [97], [180].

Besides the normalized hybrid droop discussed earlier, [179] and [97] introduce a modified hybrid droop and voltage-current droop control for the power-sharing strategy in AC/DC BIC as well. The modified droop is based on the direct relationship between the AC frequency and the DC voltage. In this equation in TABLE 6., C_{DC} and T_S are DC common bus capacitors and switching periods respectively.

FLC application in the hybrid-droop control is studied and simulated in [181]. The FLC controller inputs are per-unit frequency change and the DC-link voltage per-unit change, whereas the output is the reference active power. The simulation results show that the proposed method has a suitable performance, but membership functions are not clarified in this study.

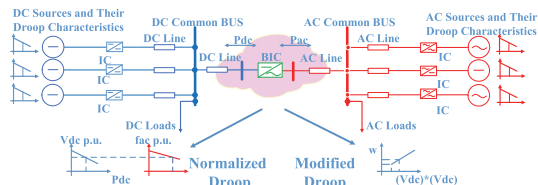


FIGURE 4. Hybrid Droop Scheme of BIC in a conventional hybrid MG.

Hybrid droop is not accurate enough in power-sharing. One practical problem of hybrid droop is measuring the frequency deviation. Equipment accuracy in the frequency deviation sensing is not sufficient for accurate power-sharing [50]. So, a voltage-controlled method that implements virtual impedance is proposed. In that method, the droop characteristic is achieved by measuring the AC side active power and the DC side voltage. The simulation results confirm the suitable steady-state response; however, noticeable oscillation in the DC voltage transient response needs to be declined.

Another way to enhance the accuracy of power-sharing is the high droop slopes of P-f and P-V, which results in instability, especially in weak MGs. As a result, adding an extra loop to modify d component of the reference voltage is suggested and simulated in [169].

The other problem in accurate power-sharing is related to the voltage. Although the frequency is a global variable, the voltage is not. In other words, as shown in Fig. 4, line resistance and impedance in DC and AC sub-MG between DGs and the common AC or DC-link in the hybrid MGs provide voltage drops. These voltage drops are not considered

TABLE 6. Comparison of different hybrid droop types in AC/DC BIC.

Droop type	Equation	Advantages	Disadvantages	Ref.
Normalized	$F_{p.u.} = \frac{F - 0.5(F_{Max} + F_{Min})}{0.5(F_{Max} - F_{Min})}$ $V_{DC\ p.u.} = \frac{V_{DC} - 0.5(V_{DC\ Max} + V_{DC\ Min})}{0.5(V_{DC\ Max} - V_{DC\ Min})}$	Easy to implement with one PI Good active power-sharing	Accuracy depending on the measuring device Increased loss in load change (continuous working)	[179] [14] [180] [50] [181]
	$F_{p.u.} = \frac{(F - F_{Max})}{(F_{Max} - F_{Min})}$ $V_{DC\ p.u.} = \frac{(V_{DC} - V_{DC\ Max})}{(V_{DC\ Max} - V_{DC\ Min})}$	Easy to implement with one PI Good active power-sharing Considering threshold zones to avoid overload or underload condition	Accuracy depending on the measuring device Line impedances are needed in [178] Inrush DC current in load change in [78]	[78] [178]
Modified	$w_0 - w = \left(\frac{m_x \times C_{DC}}{2 \times T_s}\right)(V_0 - V_{DC})(V_0 + V_{DC})$	Decoupled P and Q sharing Reduced mode transition loss Good active power-sharing	Accuracy depending on the measuring device More complex and costly	[179] [97]
Voltage-current	-	Better power-sharing functionality Required low bandwidth communication network	PR tuning difficulty Coordination tuning of two PRs Different control in rectifier or inverter mode	[179]

in the power-sharing control method; so, at imbalanced load or imbalanced line impedance conditions, it causes inaccuracy in power-sharing [178]. Moreover, increasing DGs power demand can result in shifting the system to an unstable zone [167]. Consequently, poor stability margin is another negative point of the communication-less droop technique addressed in many studies. Considering voltage drop [178], virtual impedance [165], [171], [182], [183], virtual P and Q frame control [184], communication-based control [185], and secondary control level [186] are the main solutions. In [173] and [174], the line and filter voltage drop is compensated by adding the voltage error signal to the reference voltage of droop [187] implements the same concept in the current-controlled mode.

In the virtual impedance method, by adding the virtual impedance in the control loop, the dominant impedance is controlled to be inductive [184], [188], or resistive [189]. The quantity of this virtual impedance is known [183]. As a result, the line and filter impedances are small enough to be dominated by the virtual impedance on the droop deviation voltage [185]. In the predominantly resistive output, the nonlinear power-sharing can be facilitated [183], [189]. It improves the overall system damping, current harmonic sharing among parallel ICs, and power-sharing in imbalanced loads or line impedances. References [190] and [174] add a virtual impedance by a feedforward loop to the P-V droop. References [171] and [172] propose a control system to minimize the circulating power. First, their experimental results reveal the effects of EMI. In [183], two single-phase full-bridge inverters are applied as the experiment setup. The implementation of a 7.5 kHz switching frequency has also resulted in the low power quality of the output voltage.

To minimize the circulating power between the AC and DC side of BIC and overstressed on DGs, e.g., some studies [78] proposed to apply boundaries in droop characteristics. These limitations are applied to overfrequency and under-frequency in AC and overvoltage and undervoltage in DC droops to force BIC to work in a fixed power mode, e.g., when the frequency in the AC part of BIC reaches its minimum amount, the BIC continues working as fixed power.

Harmonic-sharing is another issue that should be satisfied based on the load demand discussed in [165].

The hybrid droop in the case of multiple AC/DC BICs is modified based on the error-signal droop, which gives more accurate results [180]. Error-signal droop is the difference between normalized frequency and normalized DC voltage. In this method, BICs provide the reference power for both AC and DC sub-MG with the current-controlled mode explained in detail in [180]. Theoretically, considering the analog-digital conversion and sampling requirement, the voltage and frequency deviation boundaries of 2% and 5% are recommended but in practice, a slightly wider range (5% or higher for both) is possible [50], [180]. As the main grid link acts as a slack link, the droop control in the grid-tied operation is not that much crucial as in the islanded mode, regarding the power balance and stability issues [180].

Coordinated autonomous power management in a small hybrid MG consisting of back-to-back AC/DC VSCs as BIC with DC DSs is studied in [63]. AC/DC VSC connected to the PCC of the main grid works as a current-controlled mode to stabilize the DC-link voltage through tracking reference current angle in the main grid side. Another DC/AC VSC that connects the DC-link to the AC sub-MG works in a droop to transfer extra power to the AC or DC side. DC DSs work in constant power or droop [62] also studies primary level hybrid droop for similar MG with AC/DC and DC/DC VSCs. The process of general AC droop, general DC droop, and hybrid droop is explained. Besides, DS droop works based on the global supply-demand of the hybrid droop. The general DS droop based on the SOC condition of DSs in charging and discharging mode is discussed. To prevent unnecessary power circulation, and frequent charging/discharging of the DSs, the multilevel primary control is proposed. In this method, three different zones are introduced. The lower level is AC-droop-based ICs or DC-droop-based ICs that work separately in AC sub-MG or DC sub MG. The second level consists of hybrid-droop based AC/DC BIC in which AC and DC sub-MG transfer power to stabilize the AC frequency and the DC voltage. The higher level is DC-droop-based DS BIC, in which the global extra or deficit power is transferred to

the DSs. All these zones are determined by the normalized frequency and DC voltage. In the end, to avoid retrigger DSs in the transition mode, modifications in boundary zones are added.

Although the focus of this paper is on the conventional hybrid MG, as shown in Fig. 4, the complex configuration of the hybrid MG is also addressed in some papers. These complex hybrid MGs contain different configurations of AC and DC sub-MGs with AC or DC common bus. In this regard, [99] studies a decentralized coordinated power-sharing strategy in a hybrid MG with DC common bus, including multiple AC sub-MGs and DC sub-MGs that are connected by the DC common bus. DC common bus voltage is regulated by the DSs that are separated into a specific sub-MG. A new $P-V_{DC}^2$ DC droop characteristic is proposed for power-sharing among DSs in the main DC bus, whereas normalized hybrid droop is used in the AC/DC VSCs power-sharing strategy and a normalized V_{DC} droop characteristic is implemented in DC/DC VSCs in the DC sub-MGs. A coordinated power-sharing strategy is suggested based on the DC common bus voltage, AC sub-MGs frequencies, and DC sub-MGs voltages.

d: ACTIVE DROOP

Slow transient response, voltage deviations, the dependency of the DC droop on the output resistance, and the trade-off between power-sharing, frequency, and voltage deviations are the drawbacks of the communication-less-based droop [165]. Communication-based droop control is also called active droop. Active droop can be implemented in centralized, master-slave, average load sharing, and circular chain control [64], [75], [179], [191], [192]. In a centralized strategy based on every ICs droop characteristics, their reference currents or powers are transferred to them [165], [191]. In the master-slave, the master IC regulates the voltage, working as voltage-controlled, whereas other ICs work as slaves in the current-controlled mode [93], [165].

Master IC acts as a centralized controller, sending each ICs reference currents [165]. Considering the master IC role, three control schemes exist: 1- Dedicated master IC: the master IC is fixed; 2- Rotary: the master IC is arbitrarily selected; 3- High-crest current: the master IC is selected based on the maximized power supply ability among ICs [165]. Average load sharing is based on dividing the load among ICs [64]. The circular chain control concept is based on the AC power ring in the distribution power line; in this method, the study in the communication ring network is used among ICs [191], [192]. In this scheme, any IC can act as master IC controlling the voltage, whereas other ICs work as slaves in the current-controlled mode, tracking their previous reference current IC [191], [192].

Reference [185] employs an adaptive virtual impedance to get the Q reference value through the communication system on a 2 kVA prototype consisting of two ethernet-equipped VSCs. The experiment in this study confirms the suitable functionality of the proposed method in equally reactive sharing during the step load change in an unequal line impedance

condition. However, the test is limited to the two DGs with the same characteristics and the same ICs.

Primary control deviations are compensated through secondary level control. This control level is mainly equipped with a communication network. Reference [61] proposes the primary and secondary control level for a hybrid MG with AC/DC VSC and DC/DC DS VSC. After eliminating the deviation between the normalized frequency and the DC voltage by the secondary control in AC/DC VSC, it will be difficult for primary control to detect the frequency and the DC voltage deviation to determine the required power and its direction. Consequently, a virtual deviation and a normalization definition are introduced as the contribution of this work. This virtual deviation indicates the potential deviation, which is caused by the primary control. As a result, the primary hybrid droop can cooperate properly with the secondary control based on the simulation and hardware in the loop results.

Reference [43] improves the transient response in the transition mode with a shorter transient time and less transient peak in a hybrid MG, with the proposed interface topology of dual parallel AC/DC full-bridge VSCs between a slack DS-link and the PCC or AC-link. One BIC works in the current-controlled-mode, whereas the other works as the voltage-controlled-mode. In the grid-tied operation, converter 1 works as master, whereas in the islanded operation, converter 2 works as master. Dual parallel BICs provide seamless transition from grid-tied (current-controlled-mode) to islanded (voltage-controlled-mode) or vice versa. This study proposes an adaptive virtual impedance-based coordinated control structure for the voltage-controlled VSC in the $\alpha\beta$ frame in the grid-tied mode. To mitigate the harmonics and imbalanced voltage disturbances at PCC, the virtual impedance voltage drop is composed of three different components: positive sequence, negative sequence, and harmonic components. Since converter 1 works in the current-controlled mode, it rejects load harmonics; consequently, converter 2 has to provide the required harmonics, resulting in variation in the PCC voltage. As a result, converter 2 defines the reference current for converter 1 based on the power demand and mitigation of harmonics and imbalanced voltage disturbances in the islanded operation.

A coordinated droop control method for two back-to-back SST VSCs combined with a DS in a medium voltage hybrid distribution system studied in [16] is also applicable for a hybrid MG requiring high reliability. Reference [16] extracts the equivalent circuit model of the MMC based on [193]. In this study, the DS control is divided into constant power control in normal conditions and the voltage control mode in an abnormal condition. In other words, DS is implemented not only in smoothing the DGs output variations but also to provide slack DC-link voltage in abnormal operation to enhance the system stability. However, the efficient operating condition of DS and SOC are not considered in this study.

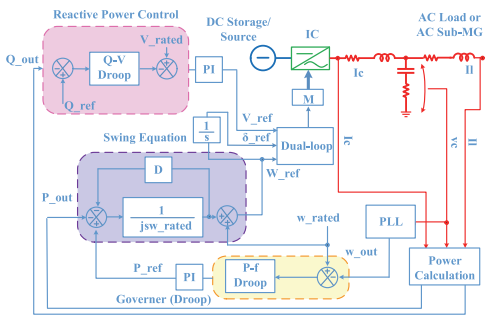


FIGURE 5. General VSG Control Diagram.

3) VIRTUAL SYNCHRONOUS GENERATOR (VSG)

Increasing penetration of the non-inertial DGs in the hybrid MG makes it vulnerable to frequency instability due to the drop in the rotating-physical-mass-sources inertia [194]. This can lead to a severe Rate Of Change Of Frequency (ROCOF). Then ROCOF relays operate against the islanding condition, and finally cascade effect of disconnecting DGs can happen [194]. To increase the DGs inertia for the enhancement of the hybrid MG stability, Distributed Storage (DS) in parallel with DG is proposed in [195]–[199], called Virtual Synchronous Generator (VSG). In some studies, it is also called Synchroverter, which refers to the VSC control [195], [200]. VSG emulates synchronous generator behavior through the swing equation, as shown in Fig. 5. The total procedure of simulating between the synchronous generator and VSG is defined in [195]. In [200], the transient condition of [195] is improved.

VSG (with or without droop) provides the required P or angle, whereas droop provides the required Q or voltage magnitude. To enhance the control system performance [196], [197] adopted inertia, [198], [201], [202] VSG with droop control techniques, in [46], [79], virtual inductance stator adjuster is proposed.

MPC applications using the VSG concept are investigated in [114]–[117], whereas [203] studies FLC utilization in VSG control.

All the studies mentioned focus on the VSG control of DG's or DS's ICs, whereas [56] brings the VSG concept into the BIC application in a hybrid MG. The aim is to reduce the required ultracapacitor size. This can be done by increasing the hybrid MG's inertia by employing a suitable control technique for the available synchronous generator and BIC as the DS in the AC side during the power disturbances. The combination of a synchronous generator and BIC as the short-term DS with the VSG technique is proposed to enhance the transient performance of the hybrid MG through controlling the BIC's output frequency. This study applies the islanded mode with power disturbances inputs, in which the hybrid MG is more fragile. The impedance line that generates deviation in the voltage in the synchronous generator and BIC is also considered. The results confirm a noticeable decrease in the variations of BIC active power in the transient

condition, leading to a decline in the ultracapacitor power variations, which results in the lower required short-term DSS capacity like ultra-capacitors.

B. POWER QUALITY AND HARMONICS CONTROL

There are so many factors that deteriorate the power quality in the MG, e.g., voltage unbalance, transient, harmonic distortion, nonlinear loads, DGs, voltage sags, and swells, under- and overvoltage, voltage notching, fault and outage, flicker and power electronic switches, which are some sources of power quality disturbance [204]–[208]. Bad quality of electrical power results in quick wear-out of the electric equipment, increasing the maintenance expenses, and even failure or shut- down of the system [209].

1) EMI REDUCTION CONTROL

EMI is referred to as radiated interference and conducted interference [210], whereas the latter is the focus of this part. High-frequency EMI is one source of pollution to the main grid that should comply with the Electro-Magnetic Compatibility (EMC) of nearby devices [211], [212].

The IEEE standard 1547 [213] determines the regulation for harmonic injection to the main grid. In this document, the acceptable percentage injection of different harmonic levels is clarified. Regarding EMI noise regulation, different EMC standards for different applications exist, such as the International Special Committee on Radio Interference CISPR32, which clarifies the conducted EMI limitations in the smart grid [266].

EMI is produced by high-switching frequency due to high $\frac{dv}{dt}$ or $\frac{di}{dt}$ at the switch's drain, the Common Mode (CM) current flowing in the phase and neutral wires, and returning through the ground [214], [215]. Differential Mode (DM) current as another source of EMI is mostly generated at normal switching operation flowing between the phase and the neutral [214]. In the hybrid MGs with non-isolated BIC, the low impedance CM path is generated between the grounded DC sub-MG and the grounded AC sub-MG [18]. In this system, AC sub-MG and DC sub-MG are coupled by the BIC and the ground [18].

EMI mitigation solutions can be divided into two main classes: to mitigate at the generation level and to decrease the generated leakage current along paths [214]. Most techniques in the latter apply the general concept of increasing the impedance method to tackle the leakage current [18]. As shown in Fig. 6, designing external or internal filters is a popular method to decline the EMI effects on the end receiver [215]. External filters are outside the noise source circuit, which is the power electronic circuit, whereas internal filters refer to the inside of the printed circuit board. Different types and designing processes and challenges are discussed in [209], [216], [217]. LCL and L types are the most commonly used passive filters in the studies demonstrated in Fig. 2.

At the generation-level solutions, the focus is on the IC's or BIC's switches. As shown in Fig. 6, it includes topologies and switching techniques [214], [211]. Different topologies are

possible by different circuit topologies discussed earlier and component specifications [214]. In the switching technique, the solutions are in the modulation control and soft transition techniques [214], [218], [219]. Some studies apply hybrid techniques that refer to the use of multiple solutions [210].

The external passive filter size is reduced by employing the external active filter. It can be applied as a feedforward filter and feedback filter explained in [214]. The stability issue is the main challenging topic in a feedback filter in real conditions with a nonideal component loop [215]. The lower frequency range of EMI is 150 kHz to 5 MHz, which is the dominant zone for disturbance mitigation [215]. This study [215] proposes a CM active feedback filter for off-line IC aiming to mitigate the low-frequency EMI. The CM noise current is measured, and the compensated noise voltage is injected into the power line by a voltage feeding transformer to reduce the EMI, which is a current-sense voltage-feedback active filter. Techniques shown in Fig. 6 can be divided into the power section and the control part. Different power-stage solutions are discussed in [212], [214]. Among the topics represented in Fig. 6, the red color parts as the circuit control of the designed topologies and PWM modulation can be employed through ICs and BICs control.

In the topology and circuit, the focus is on the rearrangement of the layout and circuit and grounding issue, e.g., by reduction of parasitic capacitors of the heat sink by different methods such as grounding [214].

In the PWM technique, it is common to apply the variable switching frequencies to spread the EMI noise spectrum [214]. Random carrier frequency, random PWM, and chaotic frequency modulation are some of the PWM techniques, which improve the EMI effect [214], [210].

2) POWER QUALITY CONTROL

Power quality objective in the AC sub-MG refers to the provision of sine current and voltage as the reference curves, whereas in the context of DC sub-MG, it refers to the reduction in the ripple, sag, and swell in the DC current and voltage [15]. Power factor, unbalance factor, and Total Harmonic Distortion (THD) are three main criteria for evaluating the power quality in the AC context [54], [220]. Based on the IEEE standard 141 [221] and 519 [222], the voltage unbalance factor and THD should be kept lower than 2% and 5% respectively in the utility distribution network [54].

Due to the less inertia of the MG in the islanded mode compared to that of the grid-tied, any changes like nonlinear or unbalanced loads can produce harmonic distortion [204], [205]. In the grid-tied mode, any unbalanced condition in the PCC can change the power quality of the MG.

Filters are the main tools to eliminate the harmonic distortions, which are classified into passive, active, and hybrid filters [206]. Passive filters contain different configurations of inductance, capacitance, and resistance, forming low-pass, high-pass, middle-pass, and middle-no pass filters, the structure, and functions of which are described in [206], [223]. Passive filters are not flexible in load variations; however,

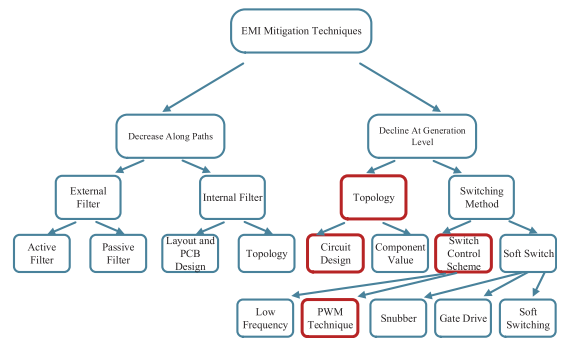


FIGURE 6. Classification of EMI Mitigation Techniques [214].

active filters have the desired dynamic response [206], [224]. Active filters are equipped with switches; in other words, ICs and BICs can work as active filters as well [2], [204]. The most widely used filters are the hybrid type, which leverages both active and passive filters. Different controllers like PI, PR, hysteresis, deadbeat, repetitive, H_∞ , the fuzzy, and neural-based controller can be applied to improve the power quality, which is discussed and compared in [204].

Reference [153] focuses on PR implementations and their role in the compensation of specific harmonic components. Specific harmonic elimination modulations like harmonic elimination Pulse Width Modulation (PWM) [225], [226] are other ways to eliminate harmonic components. In this case, [227] employs a null vector control technique with the conventional harmonic elimination PWM on two parallel VSCs to eliminate zero-sequence harmonic currents. Zero harmonics do not appear in line-to-line voltage, but they exist in each phase; so, in the case of parallel connection of inverters, they act as a zero-sequence harmonic voltage. This method decreases the zero-sequence circulating current, resulting in a decline in the related circulation power loss; however, it increases the switching loss.

Considering the low-frequency CM current, [228] continues studies on the test setup topology presented in [229]. A low-frequency CM voltage control loop to inject the duty cycle to the VSC is proposed. Split single-phase with grounded connection is applied on the AC side, whereas a bipolar DC-link with high grounding resistances is suggested for the DC side. The results confirm the DC-link voltage ripple decline. Also, in a hybrid system, [229] explains in detail how two-stage BIC can decouple the AC side ripples from the DC side noises. The test result confirms the stable operation of the proposed topology in different operating conditions of a rectifier, inverter, and transition. However, despite employing a low-frequency transformer at the PCC, the experimental results show low power quality and EMI noise in the ac voltage and current. Reference [18] proposes a two-stage interleaved BIC (AC/DC and DC/DC BIC) to decouple the CM voltage between the AC split-phase single-phase sub-MG and the bipolar DC sub-MG. The CM voltage control loop for DC/DC BIC is introduced.

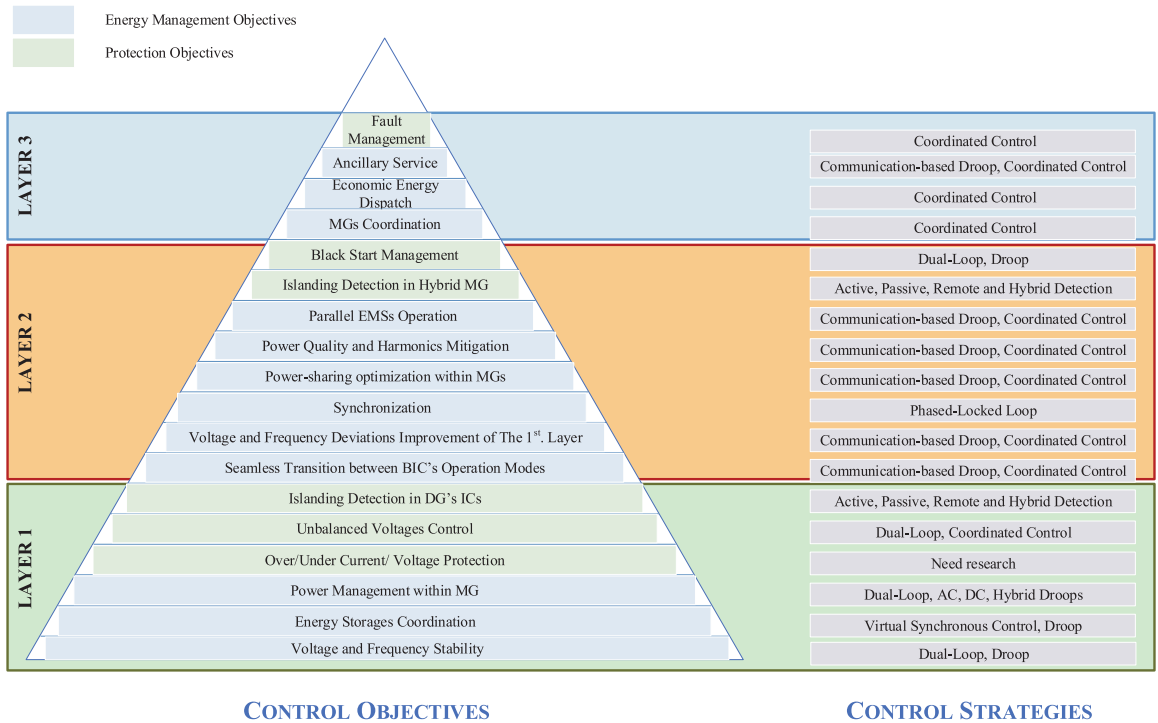


FIGURE 7. Proposed Classification of hybrid MG control objectives.

The power-sharing strategies contain the power factor objective implicitly by providing the required P and Q. THD and DC-links power quality are also considered in the power-sharing strategy. So most different control strategies for power-sharing can be used for power factor improvement, providing acceptable THD and suitable DC-link voltage as well.

Focusing on the role of AC/DC BIC's MPC in enhancing the power quality, [54] suggests using AC/DC BIC with DC sub-MG as a virtual active power filter. Implementing P-Q control in $\alpha\beta$ frame with MPC for AC sub-MG reference voltage, the required firing signals are produced. However, this study just focuses on power-sharing and THD as the power quality criteria. Studies in [118] focus on the required harmonics current control, whereas those in [119] address removal of low-order harmonics control of the current. Reference [118] suggests adding discrete-time filters in FCS MPC for a three-phase IC. The proposed cost function is the error currents in the $\alpha\beta$ frame. The discrete filter bandwidth can be tuned based on the desired output harmonics. Although the results confirm that load current harmonics are controllable by suitable discrete filter bandwidth, estimation of discrete filter coefficients in different load harmonics is a complicated task that is not covered in this study. Reference [119] proposes the two-step horizon hybrid FCS MPC in $\alpha\beta$ frame

for current-controlled ICs with LCL filter. Then the results with the same hybrid FCS MPC but one-step horizon and hybrid FCS MPC with two PI loops are compared. The results confirm that the proposed hybrid FCS MPC provides better performance regarding the THD; however, the average switching frequency is also higher in this method. The low average switching frequency and quite low THD of the output current is one of the interesting results of this study. Also, the assumption and implementation of 40 k Hz sampling frequency compared to 5.5 k HZ average switching frequency makes it easy to do the state-space modeling, FCS MPC model, and delay issues.

To evaluate PWM techniques on the power quality, [230] considers a three-phase full-bridge VSC and compares different techniques of CM-current-reduction PWM. Unipolar, bipolar and hybrid PWM are studied and compared on a 1 kW VSC with a load with the unity power factor and with various modulation indices in [231]. The studied criteria are the inductor's THD current, CM current, and zero-crossing distortion. The results demonstrate the good performance of bipolar PWM in the CM current and zero-crossing distortion, whereas unipolar is suitable regarding THD and zero-crossing distortion. Hybrid PWM has a suitable function in the THD and CM current.

C. ISLANDING DETECTION

When unintentional islanding conditions, e.g., a fault in the main grid happens, the MG should recognize it and change it to work in the islanded mode. Islanding detection is applied to detect the instant at which AC/DC BIC should switch from the grid-tied to the islanded mode. Based on the IEEE 1547-2003 [232], Islanding Detection (ID) should be recognized within 2 s after it happens [233], [234] and IEEE 929-1988 [235] clarifies the requirements for ID [236].

The ability of hybrid MGs to restore is called a black-start, which needs some strategies discussed in [237], [238]. Voltage and frequency control and stabilization, power management are the main tasks of black-start management [237].

The core concept of ID methods is based on monitoring and detecting parameters (like frequency, voltage, harmonics, phase shift) change and deciding if an islanded condition happens [234], [236]. ID methods are divided into remote detection and local detection. Local detection techniques are also classified into passive ID, active ID, and hybrid ID [234]. Passive ID is based on the measurement of slope changes of the PCC parameters. A suitable threshold for ID is the main criterion to differentiate the islanding mode [233], [234].

In the active ID, the main concept is related to the perturbation and observation technique. In the grid-tied mode, the MG inertia is so high that perturbation cannot result in considerable changes; however, in the islanded mode, a noticeable change happens [233], [234].

The remote ID needs a communication network. The comparisons among different ID techniques are shown in TABLE 7.

In [239], the evaluation criteria for different performances of ID methods are classified into the following four groups:

- Non-Detection Zone (NDZ) is the indicator of failure regions that the method cannot detect the islanding condition properly. This zone is described in the power mismatch space (in passive ID) or load parameter space (active ID) [240].
- Detection time is the time difference between disconnection from the utility and detection.
- The error detection ratio represents the false detection ratio to the total detections.
- Power quality is inevitable in the distortion injection techniques.

The overall aim of this work is to categorize the MG's objectives, classify them among three layers of functions and their control strategy. Fig. 7 summarizes the general categorization of this work. It should be noted that despite the noticeable importance of BIC protection, only a few studies have addressed that topic. As a result, no proven strategies are available yet.

V. FUTURE PROSPECTS

A. REAL-TIME FLEXIBILITY CONTROL

The growing complexity of control systems due to the increasing integration of renewable energy sources in the

power grid invokes a need for safer, faster yet reliable and economical testing methods, which do not compromise on the degree of detail [241]. The main disadvantage of typical analysis tools of MGs (software simulations, prototypes, and pilot projects) is the limited ability to test all interconnection issues, specifically in very small time steps [242]. In this context, real-time simulations and hardware-in-the-loop technologies are beneficial mainly because of their easily reconfigurable test environment and the possibility to determine exact values of control parameters and debug them [243], [244].

Some recent papers validate their methodologies in the control and optimization of hybrid AC/DC MGs through real-time simulation approaches [99], [245], [246], [247]. The study in [248] presented a comprehensive testbed for real-time multiagent systems for decentralized and distributed MG control. Authors in [249] also describe a range of possibilities for real-time MG testing. Real-time simulation is particularly beneficial for the comprehensive testing of interlinking converters of grid-tied hybrid MGs among the communication infrastructure and the protection system.

B. CYBERSECURITY

Cyber-physical systems, meaning integration of computation, communication, and physical processes as well as their security issues, are new research frontiers [250]. MGs are considered cyber-physical systems since they need advanced communication infrastructure to maintain their stability, therefore they are prone to cybersecurity issues as well [251]. Man-made incidents including cyber-physical attacks will significantly impact the stability and resiliency of the MG [252].

In the case of hybrid MGs, cyber-physical security and privacy issues would potentially have a significant effect on the central and distribution control structure. Therefore, advanced monitoring and real-time control systems for detecting attack scenarios and intrusion tolerance of these structures need to be developed in future research for the particular case of hybrid MGs.

C. UNBALANCED CONDITIONS CONTROL

From any unbalanced operation mode in PCC, faults, sudden load changes in the hybrid MG to malfunction of any capacitor or switches can lead to an unbalanced condition in the hybrid MG, e.g., an unbalanced voltage can lead to the unbalanced current, circulating current, and power loss in the hybrid MG. In this condition, providing a neutral point can help to provide a current path for unbalanced currents [258]. A fixed neutral point helps to prevent unbalanced and circulating currents, shifting the neutral point voltage, variable and unbalanced AC voltages, DC components in the AC side [258]. Four-leg VSC is the most common topology to provide a neutral point [151], [192]. The majority of researches have focused on the different control objectives in power management in symmetric sequences. So, asymmetric operation condition, especially in active power oscillation

TABLE 7. Comparison of ID techniques.

ID Methods	Applied Techniques	Advantages	Disadvantages	Ref.
Passive	Rate of change of transferred power with the utility Rate of change of frequency Rate of change of frequency over the power Change of utility impedance Harmonic distortions	Simple to implement Low cost Does not change the system's power quality Operates in less than 2 s	Large NDZs Almost high error detection rate	[234], [239] [253], [254]
Active	Disability in tracking reference reactive power Impedance measurement Phase shift (or frequency) Slide mode frequency shift Frequency drift	Small NDZ	Deteriorates the power quality The possibility of distortion signals interferences among multiple hybrid MGs	[234], [239] [253], [255]
Remote	SCADA Power Line Carrier Communication The signal produced by a disconnect	Almost Zero NDZ Needs less disturbance signal injection	Communication-based Lower reliability Expensive	[234], [239]
Hybrid	Combination of passive and active methods	Upgrade with signal processing analysis Low error detection ratio, Small NZD	Deteriorates less the power quality	[233], [234], [236], [239] [256],[257]

that has a direct impact on the DC-link voltage, is another important issue that needs to be studied [179].

The unbalanced condition originated from a fault condition and the required protection objectives are other topics for future research. Studies in [259] address the short-circuit detection in a back-to-back BIC. It employs a DC-link capacitor current change to detect the short-circuit. In [61], the parallel operation of BICs in an unbalanced grid fault focuses on stabilizing the DC-link voltage by supposing a redundant BIC. In [260], the current-controlled VSC in an MG in an unbalanced grid voltage and unbalanced fault condition is described, considering both the grid-tied and the islanded operation. The results show that the short-circuit current in the islanded operation mode is noticeably lower than in the grid-tied operation. Also, depending on the pre-fault IC condition (e.g., DG's generation), and fault type, the short-circuit current can be different in the direction, phase, and amplitude [260], [261]. All these aforementioned reasons make it impractical to implement the traditional protection functions like non-directional or directional overcurrent for the MG application in both the islanded and the grid-tied operation [260], [261]. In general, it is required to enhance the existing protection system to categorize the solutions in the future research into the following three solution categories: adaptive protection, communication-based protection, and customized logic-based scheme [261], [262].

D. TRANSITION MODE OF BIC

Transition mode can be divided into two categories: 1- from standalone to grid-tied connection or vice versa; 2- from inverter mode to rectifier, or vice versa. The former arises due to different control strategies; in the standalone mode, droop and voltage-controlled mode control and grid-tied current-controlled mode are implemented [179]. Through the transition mode, these two control systems should shift to each other. This control transition may produce inrush current and resonance in output filters [43]. Two parallel AC/DC BICs [43] and fault limiter implementation [179] can be solutions

here; however, no studies have proven their realizations in hybrid MG yet.

In the interchange between the rectifier and the inverter mode, the BIC current should be shifted in the other direction, which also means different control strategies.

In general, minimization of inrush current and the smooth transition currents and voltage for both groups are the main concerns requiring research.

E. ROBUSTNESS ANALYSIS

The variation or imbalanced condition in line and filter impedance may happen in practice, so the control system has to have minimized sensitivity toward the inputs of these disturbances. The robustness analysis for changes in line impedances and LCL filters was conducted for the H_∞ proposed controller technique and compared with the MPC technique in [94]. Also, both singular value decomposition (used for indicating the process noise index) and the bode analysis were performed to confirm the decomposition of system's singular value and phase margin to tolerate noises. The results show that the H_∞ controller is more robust than MPC. Another study of control parameter roles in the stability of the current-controlled grid-tied inverter in the grid impedance variation condition was conducted in [161]. The decomposition method clarifies the stable region in the z domain in the grid impedance uncertainty. To the best knowledge of the authors, little research has been done in this field. The robustness analysis of the influence of the communication system variables, e.g., the delay time in the communication-based control methods, is another research gap. As these conditions can happen, it is required to address them and to confirm experimentally.

F. CM CURRENT CONTROL

Low-frequency CM leakage current referred to as ground leakage current [228] is one of the issues that connects AC sub-MG to the DC sub-MG, which is dependent on both sides of the grounding system. This CM current increases

power loss and safety issues. Many studies have focused on the decline of the high-frequency EMI and the control of the power quality in the inverter mode of BIC such as PV connection. However, few studies have addressed the frequency noise and power quality in the rectifier mode of BIC on the DC side. Decoupling the AC side from the DC side by the two-stage BIC is an efficient way to decline the effects of EMI [229]; however, few studies consider the effects of AC side power change on the DC-link ripple and the harmonics produced [27]. This issue originates from an essential topic, i.e., lack of DC power quality regulations. Although some studies address the issue of DC power quality, the lack of a unit standard is a major topic. For instance, in [263] DC power quality evaluation is based on IEEE 1159 [264] and [265] points out some main criteria of DC power quality, but there are no common criteria to evaluate harmonics, EMI, DC-link ripple, CM voltage, etc.

VI. CONCLUSION

The growth of DGs is the main motivation to enhance the traditional grid to the MG, and the increasing rate of DC loads and sources is the main reason to choose the hybrid MG. The focus of this review was on the different control functions of BIC in the hybrid MG. The most studied function is power-sharing. Different control strategies toward power-sharing were investigated and categorized. The common power sharing strategy, which is droop, was classified based on AC, DC, or both types of energy, availability of the communication system, and coordinated control. Different techniques for different strategies of power-sharing function were compared, the PID+R controller technique is the most mature and widespread, whereas digital processor improvement opens a new door to apply heavily processing control techniques in a shorter time. In this way, different MPC techniques are the trend in the past eight years. Different MPC techniques have been implemented in power-sharing to find the optimum MPC control structure with optimized prediction horizon steps and weighting factors. Also, the RL technique is an interesting newcomer technique needing more research. Power variations interactions on the AC sub-MG and DC sub-MG in the presence of filter and line impedance disturbances are the other main issues to be implemented in practice.

However, despite the developed concept of the hybrid MG, it is evident that the main limitation consists in the low power rating of BIC. Our analysis demonstrated that the most typical power rating of the commercially available BICs is 10 kW, which is far from the power distribution scale. As a result, a major improvement in the wide bandgap technology, such as SiC and GaN, is required to improve the capability of the BICs and ICs applied to a large power scale.

DC-link capacitors are one of the weak points of the hybrid-MG with one-phase AC/DC BIC, which decreases its reliability. The first solution is an enhancement in capacitor technology with high operating temperature and high capacity with small volume. The other solution is to find control

techniques to separate double ripple frequency power in the DC-link. Results of different control studies have not yet provided overall solution to the issue.

CM voltage and current control in different operating modes, especially in unbalanced conditions, designing the optimized grounding circuit and EMI noise control as well as protection strategies are the future topics to be addressed.

REFERENCES

- [1] Enerdata, Grenoble, France. *Electrification and Decarbonisation Analyst Brief—February 2020 An In-Depth Look at Electrification Trends Worldwide*. [Online]. Available: <https://www.enerdata.net/publications/executive-briefing/world-electrification-decarbonisation.html>
- [2] Z. Zeng, H. Yang, R. Zhao, and C. Cheng, "Topologies and control strategies of multi-functional grid-connected inverters for power quality enhancement: A comprehensive review," *Renew. Sustain. Energy Rev.*, vol. 24, pp. 223–270, Aug. 2013.
- [3] E. Unamuno and J. A. Barrena, "Hybrid AC/DC microgrids—Part I: Review and classification of topologies," *Renew. Sustain. Energy Rev.*, vol. 52, pp. 1251–1259, Dec. 2015.
- [4] X. Wang, J. M. Guerrero, F. Blaabjerg, and Z. Chen, "A review of power electronics based microgrids," *J. Power Electron.*, vol. 12, no. 1, pp. 181–192, Jan. 2012.
- [5] J. M. Guerrero, M. Chandorkar, T.-L. Lee, and P. C. Loh, "Advanced control architectures for intelligent microgrids—Part I: Decentralized and hierarchical control," *IEEE Trans. Ind. Electron.*, vol. 60, no. 4, pp. 1254–1262, Apr. 2013.
- [6] Q. Fu, A. Nasiri, A. Solanki, A. Bani-Ahmed, L. Weber, and V. Bhavaraju, "Microgrids: Architectures, controls, protection, and demonstration," *Electr. Power Compon. Syst.*, vol. 43, no. 12, pp. 1453–1465, Jul. 2015.
- [7] T. Dragicevic, X. Lu, J. C. Vasquez, and J. M. Guerrero, "DC microgrids—Part II: A review of power architectures, applications, and standardization issues," *IEEE Trans. Power Electron.*, vol. 31, no. 5, pp. 3528–3549, May 2016.
- [8] B. Luis and E. Zubietta, "Are microgrids the future of energy?" *IEEE Electr. Mag.*, vol. 4, no. 2, pp. 37–44, Jun. 2016.
- [9] I. Roasto, T. Jalakas, and A. Rosin, "Bidirectional operation of the power electronic interface for nearly-zero energy buildings," in *Proc. 20th Eur. Conf. Power Electron. Appl. (EPE ECCE Europe)*, 2018, pp. 1–9.
- [10] F. Nejathkhan and Y. W. Li, "Overview of power management strategies of hybrid AC/DC microgrid," *IEEE Trans. Power Electron.*, vol. 30, no. 12, pp. 7072–7089, Dec. 2015.
- [11] X. Shen, D. Tan, Z. Shuai, and A. Luo, "Control techniques for bidirectional interlinking converters in hybrid microgrids: Leveraging the advantages of both AC and DC," *IEEE Power Electron. Mag.*, vol. 6, no. 3, pp. 39–47, Sep. 2019.
- [12] A. Gupta, S. Doolla, and K. Chatterjee, "Hybrid AC–DC microgrid: Systematic evaluation of control strategies," *IEEE Trans. Smart Grid*, vol. 9, no. 4, pp. 3830–3843, Jul. 2018.
- [13] H. W. D. Hettiarachchi, K. T. M. U. Hemapala, and A. G. B. P. Jayasekara, "Review of applications of fuzzy logic in multi-agent-based control system of AC-DC hybrid microgrid," *IEEE Access*, vol. 7, pp. 1284–1299, 2019.
- [14] G. Ding, F. Gao, S. Zhang, P. C. Loh, and F. Blaabjerg, "Control of hybrid AC/DC microgrid under islanding operational conditions," *J. Mod. Power Syst. Clean Energy*, vol. 2, no. 3, pp. 223–232, Sep. 2014.
- [15] T. Tricarico, G. F. Gontijo, M. Aredes, R. Dias, and J. M. Guerrero, "New hybrid-microgrid topology using a bidirectional interleaved converter as a robust power interface operating in grid-connected and islanded modes," *IET Renew. Power Gener.*, vol. 14, no. 1, pp. 134–144, Jan. 2020.
- [16] Y. Xu, Z. Zhai, X. Kang, M. Guo, and X. Ma, "Coordination control of medium-voltage hybrid AC/DC distribution," *J. Eng.*, vol. 2019, no. 16, pp. 910–916, Mar. 2019.
- [17] *International Standard International Standard*, Standard ISO 10426-5, 61010-1 Iec2001, 2006, p. 13.
- [18] F. Chen, R. Burgos, and D. Boroyevich, "A bidirectional high-efficiency transformerless converter with common-mode decoupling for the interconnection of AC and DC grids," *IEEE Trans. Power Electron.*, vol. 34, no. 2, pp. 1317–1333, Feb. 2019.

- [19] B. Yang, W. Li, Y. Gu, W. Cui, and X. He, "Improved transformerless inverter with common-mode leakage current elimination for a photovoltaic grid-connected power system," *IEEE Trans. Power Electron.*, vol. 27, no. 2, pp. 752–762, Feb. 2012.
- [20] K. S. Alatawi and M. A. Matin, "Power management for PV-battery based hybrid microgrid using WBG devices," *Proc. SPIE*, vol. 11126, Sep. 2019, Art. no. 111260L.
- [21] S. Dey, V. K. Bussa, and R. K. Singh, "Transformerless hybrid converter with AC and DC outputs and reduced leakage current," *IEEE J. Emerg. Sel. Topics Power Electron.*, vol. 7, no. 2, pp. 1329–1341, Jun. 2019.
- [22] M. Victor, F. Greizer, S. Bremicker, and U. Hübler, "Method of converting a direct current voltage from a source of direct current voltage, more specifically from a photovoltaic source of direct current voltage, into an alternating current voltage," U.S. Patent 7 411 802 B2, Aug. 12, 2008. [Online]. Available: <https://patents.google.com/patent/US7411802B2/en>
- [23] L. Zhang, K. Sun, Y. Xing, and M. Xing, "H6 transformerless full-bridge PV grid-tied inverters," *IEEE Trans. Power Electron.*, vol. 29, no. 3, pp. 1229–1238, Mar. 2014.
- [24] R. Rahimi, S. Farhangi, B. Farhangi, G. R. Moradi, E. Afshari, and F. Blaabjerg, "H8 inverter to reduce leakage current in transformerless three-phase grid-connected photovoltaic systems," *IEEE J. Emerg. Sel. Topics Power Electron.*, vol. 6, no. 12, pp. 910–918, Jun. 2018.
- [25] Y. Zhou and C. Ngai-Man Ho, "A review on microgrid architectures and control methods," in *Proc. IEEE 8th Int. Power Electron. Motion Control Conf. (IPEMC-ECCE Asia)*, May 2016, pp. 3149–3156.
- [26] G. Escobar, S. Pettersson, and N. Ho, "Method and apparatus for zero-sequence damping and voltage balancing," U.S. Patent 9 030US 854 B2, May 12, 2015. [Online]. Available: <https://patents.google.com/patent/US9030854B2/en>
- [27] G. Escobar, P. R. Martinez-Rodriguez, S. Iturriaga-Medina, J. Lopez-Sarabia, J. C. Mayo-Maldonado, and O. M. Micheloud-Vernack, "Mitigation of leakage-ground currents in transformerless grid-tied inverters via virtual-ground connection," *IEEE J. Emerg. Sel. Topics Power Electron.*, vol. 8, no. 3, pp. 3111–3123, Sep. 2020.
- [28] H. Wang, H. S.-H. Chung, and W. Liu, "Use of a series voltage compensator for reduction of the DC-link capacitance in a capacitor-supported system," *IEEE Trans. Power Electron.*, vol. 29, no. 3, pp. 1163–1175, Mar. 2014.
- [29] P. T. Krein, R. S. Balog, and M. Mirjafari, "Minimum energy and capacitance requirements for single-phase inverters and rectifiers using a ripple port," *IEEE Trans. Power Electron.*, vol. 27, no. 11, pp. 4690–4698, Nov. 2012.
- [30] M. A. Vitorino, L. F. S. Alves, R. Wang, and M. B. D. R. Correa, "Low-frequency power decoupling in single-phase applications: A comprehensive overview," *IEEE Trans. Power Electron.*, vol. 32, no. 4, pp. 2892–2912, Apr. 2017.
- [31] Y. Sun, Y. Liu, M. Su, W. Xiong, and J. Yang, "Review of active power decoupling topologies in single-phase systems," *IEEE Trans. Power Electron.*, vol. 31, no. 7, pp. 4778–4794, Jul. 2016.
- [32] S. Qin, Y. Lei, C. Barth, W.-C. Liu, and R. C. N. Pilawa-Podgurski, "A high power density series-stacked energy buffer for power pulsation decoupling in single-phase converters," *IEEE Trans. Power Electron.*, vol. 32, no. 6, pp. 4905–4924, Jun. 2017.
- [33] H. Wang, H. Wang, G. Zhu, and F. Blaabjerg, "An overview of capacitive DC-links-topology derivation and scalability analysis," *IEEE Trans. Power Electron.*, vol. 35, no. 2, pp. 1805–1829, Feb. 2020.
- [34] Y. Tang, W. Yao, P. C. Loh, and F. Blaabjerg, "Highly reliable transformerless photovoltaic inverters with leakage current and pulsating power elimination," *IEEE Trans. Ind. Electron.*, vol. 63, no. 2, pp. 1016–1026, Feb. 2016.
- [35] D. B. W. Abeywardana, B. Hredzak, and V. G. Agelidis, "An input current feedback method to mitigate the DC-side low-frequency ripple current in a single-phase boost inverter," *IEEE Trans. Power Electron.*, vol. 31, no. 6, pp. 4594–4603, Jun. 2016.
- [36] R. Chen, "DC capacitor minimization of single phase power conversion and applications," Ph.D. dissertation, Dept. Elect. Eng., Michigan State Univ., East Lansing, MI, USA, 2016.
- [37] T. Tricarico, M. Soares, G. Gontijo, D. Oliveira, F. Dieler, and M. Aredes, "Design, control and stability analysis of an interleaved DC converter for voltage interfacing application in microgrids," in *Proc. 22nd Congresso Brasileiro de Automática*, 2018, pp. 1–8.
- [38] X. Guo, Y. Yang, and X. Wang, "Optimal space vector modulation of current-source converter for DC-link current ripple reduction," *IEEE Trans. Ind. Electron.*, vol. 66, no. 3, pp. 1671–1680, Mar. 2019.
- [39] X. Guo, Y. Yang, and X. Zhang, "Advanced control of grid-connected current source converter under unbalanced grid voltage conditions," *IEEE Trans. Ind. Electron.*, vol. 65, no. 12, pp. 9225–9233, Dec. 2018.
- [40] M. Ashabani, Y. A.-R.-I. Mohamed, M. Mirsalim, and M. Aghashabani, "Multivariable droop control of synchronous current converters in weak Grids/Microgrids with decoupled dq-axes currents," *IEEE Trans. Smart Grid*, vol. 6, no. 4, pp. 1610–1620, Jul. 2015.
- [41] X. Guo, D. Xu, J. M. Guerrero, and B. Wu, "Space vector modulation for DC-link current ripple reduction in back-to-back current-source converters for microgrid applications," *IEEE Trans. Ind. Electron.*, vol. 62, no. 10, pp. 6008–6013, Oct. 2015.
- [42] X. Guo, N. Wang, J. Zhang, B. Wang, and M.-K. Nguyen, "A novel transformerless current source inverter for leakage current reduction," *IEEE Access*, vol. 7, pp. 50681–50690, 2019.
- [43] J. He, L. Du, B. Liang, Y. Li, and C. Wang, "A coupled virtual impedance for parallel AC/DC converter based power electronics system," *IEEE Trans. Smart Grid*, vol. 10, no. 3, pp. 3387–3400, May 2019.
- [44] R. Sedaghati and M. R. Shakerami, "A novel control strategy and power management of hybrid PV/FC/SC/battery renewable power system-based grid-connected microgrid," *Sustain. Cities Soc.*, vol. 44, pp. 830–843, Jan. 2019.
- [45] J. Wang, C. Jin, and P. Wang, "A uniform control strategy for the interlinking converter in hierarchical controlled hybrid AC/DC microgrids," *IEEE Trans. Ind. Electron.*, vol. 65, no. 8, pp. 6188–6197, Aug. 2018.
- [46] C.-K. Nguyen, T.-T. Nguyen, H.-J. Yoo, and H.-M. Kim, "Improving transient response of power converter in a stand-alone microgrid using virtual synchronous generator," *Energies*, vol. 11, no. 1, p. 27, Dec. 2017.
- [47] N. Chettibi, A. Mellit, G. Sulilgoi, and A. Massi Pavan, "Adaptive neural network-based control of a hybrid AC/DC microgrid," *IEEE Trans. Smart Grid*, vol. 9, no. 3, pp. 1667–1679, May 2018.
- [48] V. Mortezaei and H. Lesani, "Hybrid AC/DC microgrids: A generalized approach for autonomous droop-based primary control in islanded operations," *Int. J. Electr. Power Energy Syst.*, vol. 93, pp. 109–118, Dec. 2017.
- [49] A. A. A. Radwan and Y. A.-R.-I. Mohamed, "Networked control and power management of AC/DC hybrid microgrids," *IEEE Syst. J.*, vol. 11, no. 3, pp. 1662–1673, Sep. 2017.
- [50] M. Baharizadeh, H. R. Karshenas, and J. M. Guerrero, "Control strategy of interlinking converters as the key segment of hybrid AC–DC microgrids," *IET Gener., Transmiss. Distrib.*, vol. 10, no. 7, pp. 1671–1681, May 2016.
- [51] P. C. Loh, D. Li, Y. K. Chai, and F. Blaabjerg, "Autonomous control of interlinking converter with energy storage in hybrid AC–DC microgrid," *IEEE Trans. Ind. Appl.*, vol. 49, no. 3, pp. 1374–1382, Jun. 2013.
- [52] S. Peyghami, H. Mokhtari, and F. Blaabjerg, "Autonomous operation of a hybrid AC/DC microgrid with multiple interlinking converters," *IEEE Trans. Smart Grid*, vol. 9, no. 6, pp. 6480–6488, Nov. 2018.
- [53] T. Ma, M. H. Cintuglu, and O. A. Mohammed, "Control of a hybrid AC/DC microgrid involving energy storage and pulsed loads," *IEEE Trans. Ind. Appl.*, vol. 53, no. 1, pp. 567–575, Jan. 2017.
- [54] M. Khederzadeh and M. Sadeghi, "Virtual active power filter: A notable feature for hybrid AC/DC microgrids," *IET Gener., Transmiss. Distrib.*, vol. 10, no. 14, pp. 3539–3546, Nov. 2016.
- [55] X. Li, Z. Li, L. Guo, J. Zhu, Y. Wang, and C. Wang, "Enhanced dynamic stability control for low-inertia hybrid AC/DC microgrid with distributed energy storage systems," *IEEE Access*, vol. 7, pp. 91234–91242, 2019.
- [56] G. Melath, S. Rangarajan, and V. Agarwal, "A novel control scheme for enhancing the transient performance of an islanded hybrid AC–DC microgrid," *IEEE Trans. Power Electron.*, vol. 34, no. 10, pp. 9644–9654, Oct. 2019.
- [57] K. Sun, X. Wang, Y. W. Li, F. Nejabatkhah, Y. Mei, and X. Lu, "Parallel operation of bidirectional interfacing converters in a hybrid AC/DC microgrid under unbalanced grid voltage conditions," *IEEE Trans. Power Electron.*, vol. 32, no. 3, pp. 1872–1884, Mar. 2017.
- [58] J. Hu, Y. Shan, Y. Xu, and J. M. Guerrero, "A coordinated control of hybrid AC/DC microgrids with PV-wind-battery under variable generation and load conditions," *Int. J. Electr. Power Energy Syst.*, vol. 104, pp. 583–592, Jan. 2019.

- [59] Y. Shan, J. Hu, K. W. Chan, Q. Fu, and J. M. Guerrero, "Model predictive control of bidirectional DC–DC converters and AC/DC interlinking converters—A new control method for PV-wind-battery microgrids," *IEEE Trans. Sustain. Energy*, vol. 10, no. 4, pp. 1823–1833, Oct. 2019.
- [60] J. Liu, M. J. Hossain, J. Lu, F. H. M. Rafi, and H. Li, "A hybrid AC/DC microgrid control system based on a virtual synchronous generator for smooth transient performances," *Electr. Power Syst. Res.*, vol. 162, pp. 169–182, Sep. 2018.
- [61] C. Jin, J. Wang, and P. Wang, "Coordinated secondary control for autonomous hybrid three-port AC/DC/DS microgrid," *CSEE J. Power Energy Syst.*, vol. 4, no. 1, pp. 1–10, Mar. 2018.
- [62] P. Wang, C. Jin, D. Zhu, Y. Tang, P. C. Loh, and F. H. Choo, "Distributed control for autonomous operation of a three-port AC/DC/DS hybrid microgrid," *IEEE Trans. Ind. Electron.*, vol. 62, no. 2, pp. 1279–1290, Feb. 2015.
- [63] R. Majumder, "A hybrid microgrid with DC connection at back to back converters," *IEEE Trans. Smart Grid*, vol. 5, no. 1, pp. 251–259, Jan. 2014.
- [64] Y. Liu, Y. Fang, and J. Li, "Interconnecting microgrids via the energy router with smart energy management," *Energies*, vol. 10, no. 9, p. 1297, Aug. 2017.
- [65] T. Tricarico, G. Gontijo, M. Neves, M. Soares, M. Aredes, and J. Guerrero, "Control design, stability analysis and experimental validation of new application of an interleaved converter operating as a power interface in hybrid microgrids," *Energies*, vol. 12, no. 3, p. 437, Jan. 2019.
- [66] Y. Wang, Y. Li, Y. Cao, Y. Tan, L. He, and J. Han, "Hybrid AC/DC microgrid architecture with comprehensive control strategy for energy management of smart building," *Int. J. Electr. Power Energy Syst.*, vol. 101, pp. 151–161, Oct. 2018.
- [67] P. P. Dash and M. Kazerani, "Dynamic modeling and performance analysis of a grid-connected current-source inverter-based photovoltaic system," *IEEE Trans. Sustain. Energy*, vol. 2, no. 4, pp. 443–450, Oct. 2011.
- [68] A. A. A. Radwan and Y. A.-R.-I. Mohamed, "Power synchronization control for grid-connected current-source inverter-based photovoltaic systems," *IEEE Trans. Energy Convers.*, vol. 31, no. 3, pp. 1023–1036, Sep. 2016.
- [69] T. Geury, S. Pinto, and J. Gyselink, "Current source inverter-based photovoltaic system with enhanced active filtering functionalities," *IET Power Electron.*, vol. 8, no. 12, pp. 1–9, Dec. 2015.
- [70] S. Anand, S. K. Gundlapalli, and B. G. Fernandes, "Transformer-less grid feeding current source inverter for solar photovoltaic system," *IEEE Trans. Ind. Electron.*, vol. 61, no. 10, pp. 5334–5344, Oct. 2014.
- [71] Q. Wei, B. Wu, D. Xu, and N. R. Zargari, "An optimized strategy for PWM current source converter based wind conversion systems with reduced cost and improved efficiency," *IEEE Trans. Power Electron.*, vol. 33, no. 2, pp. 1202–1210, Feb. 2018.
- [72] P. Cossutta, M. P. Aguirre, A. Cao, S. Raffo, and M. I. Valla, "Single-stage fuel cell to grid interface with multilevel current-source inverters," *IEEE Trans. Ind. Electron.*, vol. 62, no. 8, pp. 5256–5264, Aug. 2015.
- [73] S. Sen and V. Kumar, "Microgrid control: A comprehensive survey," *Annu. Rev. Control*, vol. 45, pp. 118–151, Jan. 2018.
- [74] *IEEE Standard for the Testing of Microgrid Controllers*, IEEE Power Energy Soc., Piscataway, NJ, USA, 2018.
- [75] E. Unamuno and J. A. Barrena, "Hybrid AC/DC microgrids—Part II: Review and classification of control strategies," *Renew. Sustain. Energy Rev.*, vol. 52, pp. 1123–1134, Dec. 2015.
- [76] W. Feng, M. Jin, X. Liu, Y. Bao, C. Marnay, C. Yao, and J. Yu, "A review of microgrid development in the United States—A decade of progress on policies, demonstrations, controls, and software tools," *Appl. Energy*, vol. 228, pp. 1656–1668, Oct. 2018.
- [77] F. Martín-Martínez, A. Sánchez-Miralles, and M. Rivier, "A literature review of microgrids: A functional layer based classification," *Renew. Sustain. Energy Rev.*, vol. 62, pp. 1133–1153, Sep. 2016.
- [78] P. C. Loh, D. Li, Y. K. Chai, and F. Blaabjerg, "Autonomous operation of AC–DC microgrids with minimised interlinking energy flow," *IET Power Electron.*, vol. 6, no. 8, pp. 1650–1657, Sep. 2013.
- [79] J. Liu, Y. Miura, H. Bevrani, and T. Ise, "Enhanced virtual synchronous generator control for parallel inverters in microgrids," *IEEE Trans. Smart Grid*, vol. 8, no. 5, pp. 2268–2277, Sep. 2017.
- [80] B. Liang, L. Kang, J. He, F. Zheng, Y. Xia, Z. Zhang, Z. Zhang, G. Liu, and Y. Zhao, "Coordination control of hybrid AC/DC microgrid," *J. Eng.*, vol. 2019, no. 16, pp. 3264–3269, Mar. 2019.
- [81] X. Zhou, Y. Chen, L. Zhou, A. Luo, J. M. Guerrero, W. Wu, L. Yang, and W. Tan, "Power coordinated control method with frequency support capability for hybrid single/three-phase microgrid," *IET Gener., Transmiss. Distrib.*, vol. 12, no. 10, pp. 2397–2405, May 2018.
- [82] Y. Xia, W. Wei, M. Yu, Y. Peng, and J. Tang, "Decentralized multi-time scale power control for a hybrid AC/DC microgrid with multiple subgrids," *IEEE Trans. Power Electron.*, vol. 33, no. 5, pp. 4061–4072, May 2018.
- [83] L. Che, M. Shahidehpour, A. Alabdulwahab, and Y. Al-Turki, "Hierarchical coordination of a community microgrid with AC and DC microgrids," *IEEE Trans. Smart Grid*, vol. 6, no. 6, pp. 3042–3051, Nov. 2015.
- [84] A. Colet-Subirachs, A. Ruiz-Alvarez, O. Gomis-Bellmunt, F. Alvarez-Cuevas-Figueroa, and A. Sudria-Andreu, "Centralized and distributed active and reactive power control of a utility connected microgrid using IEC61850," *IEEE Syst. J.*, vol. 6, no. 1, pp. 58–67, Mar. 2012.
- [85] Y. Karimi, H. Oraee, and J. M. Guerrero, "Decentralized method for load sharing and power management in a hybrid single/three-phase-islanded microgrid consisting of hybrid source PV/battery units," *IEEE Trans. Power Electron.*, vol. 32, no. 8, pp. 6135–6144, Aug. 2017.
- [86] A. H. Yazdavar, M. A. Azzouz, and E. F. El-Saadany, "A novel decentralized control scheme for enhanced nonlinear load sharing and power quality in islanded microgrids," *IEEE Trans. Smart Grid*, vol. 10, no. 1, pp. 29–39, Jan. 2019.
- [87] S. K. Sahoo, A. K. Sinha, and N. K. Kishore, "Control techniques in AC, DC, and hybrid AC–DC microgrid: A review," *IEEE J. Emerg. Sel. Topics Power Electron.*, vol. 6, no. 2, pp. 738–759, Jun. 2018.
- [88] A. G. Tsikalakis and N. D. Hatziargyriou, "Centralized control for optimizing microgrids operation," in *Proc. IEEE Power Energy Soc. Gen. Meeting*, Jul. 2011, vol. 23, no. 1, pp. 241–248.
- [89] K. T. Tan, X. Y. Peng, P. L. So, Y. C. Chu, and M. Z. Q. Chen, "Centralized control for parallel operation of distributed generation inverters in microgrids," *IEEE Trans. Smart Grid*, vol. 3, no. 4, pp. 1977–1987, Dec. 2012.
- [90] I. V. Prasanna, D. Srinivasan, and S. K. Panda, "Design, analysis and implementation of a four-tier centralized control architecture for intelligent operation of grid-connected microgrids," in *Proc. IEEE Int. Conf. Power Electron., Drives Energy Syst. (PEDES)*, Dec. 2016, pp. 1–6.
- [91] M. A. Hossain, H. R. Pota, W. Issa, and M. J. Hossain, "Overview of AC microgrid controls with inverter-interfaced generations," *Energies*, vol. 10, no. 9, pp. 1–27, 2017.
- [92] D. Wang, X. Ma, P. Su, B. Liu, W. Du, and L. Wu, "Household microgrid interaction technology based on power router," *Energy Procedia*, vol. 158, pp. 6452–6457, Feb. 2019.
- [93] T. L. Vandoorn, J. D. M. D. Kooning, B. Meersman, and L. Vandevelde, "Review of primary control strategies for islanded microgrids with power-electronic interfaces," *Renew. Sustain. Energy Rev.*, vol. 19, pp. 613–628, Mar. 2013.
- [94] B. E. Sedhom, M. M. El-Saadawi, A. Y. Hatata, and A. S. Alsayyari, "Hierarchical control technique-based harmony search optimization algorithm versus model predictive control for autonomous smart microgrids," *Int. J. Electr. Power Energy Syst.*, vol. 115, Feb. 2020, Art. no. 105511.
- [95] A. Hirsch, Y. Parag, and J. Guerrero, "Microgrids: A review of technologies, key drivers, and outstanding issues," *Renew. Sustain. Energy Rev.*, vol. 90, pp. 402–411, Jul. 2018.
- [96] Y. E. García Vera, R. Dufo-López, and J. L. Bernal-Agustín, "Energy management in microgrids with renewable energy sources: A literature review," *Appl. Sci.*, vol. 9, no. 18, p. 3854, Sep. 2019.
- [97] N. Eghtedarpour and E. Farjah, "Power control and management in a hybrid AC/DC microgrid," *IEEE Trans. Smart Grid*, vol. 5, no. 3, pp. 1494–1505, May 2014.
- [98] H. Mahmood, D. Michaelson, and J. Jiang, "Decentralized power management of a PV/battery hybrid unit in a droop-controlled islanded microgrid," *IEEE Trans. Power Electron.*, vol. 30, no. 12, pp. 7215–7229, Dec. 2015.
- [99] Y. Xia, W. Wei, M. Yu, X. Wang, and Y. Peng, "Power management for a hybrid AC/DC microgrid with multiple subgrids," *IEEE Trans. Power Electron.*, vol. 33, no. 4, pp. 3520–3533, Apr. 2018.
- [100] L. Dong, T. Zhang, T. Pu, N. Chen, and Y. Sun, "A decentralized optimal operation of AC/DC hybrid microgrids equipped with power electronic transformer," *IEEE Access*, vol. 7, pp. 157946–157959, 2019.

- [101] Y. Xia, Y. Peng, P. Yang, M. Yu, and W. Wei, "Distributed coordination control for multiple bidirectional power converters in a hybrid AC/DC microgrid," *IEEE Trans. Power Electron.*, vol. 32, no. 6, pp. 4949–4959, Jun. 2017.
- [102] P. Lin, C. Jin, J. Xiao, X. Li, D. Shi, Y. Tang, and P. Wang, "A distributed control architecture for global system economic operation in autonomous hybrid AC/DC microgrids," *IEEE Trans. Smart Grid*, vol. 10, no. 3, pp. 2603–2617, May 2019.
- [103] A. Agrawal and R. Gupta, "Distributed coordination control of hybrid energy resources for power sharing in coupled hybrid DC/AC microgrid using paralleled IFCs/ILCs," *IET Smart Grid*, vol. 2, no. 1, pp. 89–105, Mar. 2019.
- [104] I. Roasto, O. Husev, M. Najafzadeh, T. Jalakas, and J. Rodriguez, "Voltage source operation of the energy-router based on model predictive control," *Energies*, vol. 12, no. 10, p. 1892, May 2019.
- [105] S. Mariéthoz and S. Almér, "Model predictive control a review of its applications in power electronics," *IEEE Ind. Electron. Mag.*, pp. 16–31, Mar. 2014.
- [106] Z. Zhang, F. Wang, T. Sun, J. Rodriguez, and R. Kennel, "FPGA-based experimental investigation of a quasi-centralized model predictive control for back-to-back converters," *IEEE Trans. Power Electron.*, vol. 31, no. 1, pp. 662–674, Jan. 2016.
- [107] J. B. Nørgaard, M. K. Graungaard, T. Dragicevic, and F. Blaabjerg, "Current control of LCL-Filtered grid-connected VSC using model predictive control with inherent damping," in *Proc. 20th Eur. Conf. Power Electron. Appl.*, Sep. 2018, pp. 1–11.
- [108] V. Yaramasu, M. Rivera, B. Wu, and J. Rodriguez, "Predictive control of four-leg power converters," in *Proc. IEEE Int. Symp. Predict. Control Electr. Drives Power Electron.*, Oct. 2015, pp. 121–125.
- [109] M. Jayachandran and G. Ravi, "Predictive power management strategy for PV/battery hybrid unit based islanded AC microgrid," *Int. J. Electr. Power Energy Syst.*, vol. 110, pp. 487–496, Sep. 2019.
- [110] M. J. Rana and M. A. Abido, "Energy management in DC microgrid with energy storage and model predictive controlled AC–DC converter," *IET Gener., Transmiss. Distrib.*, vol. 11, no. 15, pp. 3694–3702, Oct. 2017.
- [111] M. G. Judewicz, S. A. Gonzalez, J. R. Fischer, J. F. Martinez, and D. O. Carrica, "Inverter-side current control of grid-connected voltage source inverters with LCL filter based on generalized predictive control," *IEEE J. Emerg. Sel. Topics Power Electron.*, vol. 6, no. 4, pp. 1732–1743, Dec. 2018.
- [112] T. Dragicevic, "Model predictive control of power converters for robust and fast operation of AC microgrids," *IEEE Trans. Power Electron.*, vol. 33, no. 7, pp. 6304–6317, Jul. 2018.
- [113] Y. Shan, J. Hu, M. Liu, J. Zhu, and J. M. Guerrero, "Model predictive voltage and power control of islanded PV-battery microgrids with washout-filter-based power sharing strategy," *IEEE Trans. Power Electron.*, vol. 35, no. 2, pp. 1227–1238, Feb. 2020.
- [114] B. Long, Y. Liao, K. T. Chong, J. Rodriguez, and J. M. Guerrero, "MPC-controlled virtual synchronous generator to enhance frequency and voltage dynamic performance in islanded microgrids," *IEEE Trans. Smart Grid*, early access, Sep. 28, 2020, doi: 10.1109/TSG.2020.3027051.
- [115] C. Zheng, T. Dragicevic, and F. Blaabjerg, "Model predictive control based virtual inertia emulator for an islanded AC microgrid," *IEEE Trans. Ind. Electron.*, early access, Jul. 10, 2020, doi: 10.1109/TIE.2020.3007105.
- [116] S. Saadatmand, M. S. Sanjarinia, P. Shamsi, M. Ferdowsi, and D. C. Wunsch, "Neural network predictive controller for grid-connected virtual synchronous generator," 2019, *arXiv:1908.05199*. [Online]. Available: <http://arxiv.org/abs/1908.05199>
- [117] J. Jongdomkarn, J. Liu, and T. Ise, "Reliable fault ride-through ability?: A solution based on finite-set model predictive control," *IEEE J. Emerg. Sel. Top. Power Electron.*, vol. 8, no. 4, pp. 3811–3824, 2020.
- [118] P. Cortes, J. Rodriguez, D. E. Quevedo, and C. Silva, "Predictive current control strategy with imposed load current spectrum," *IEEE Trans. Power Electron.*, vol. 23, no. 2, pp. 612–618, Mar. 2008.
- [119] F. Piot, "Finite control set model predictive control for grid-connected NPC Converter with LCL filter and novel resonance damping method," *IEEE Trans. Ind. Electron.*, vol. 65, no. 4, pp. 2844–2852, Apr. 2018.
- [120] M. F. Zia, E. Elbouchikhi, and M. Benbouzid, "Microgrids energy management systems: A critical review on methods, solutions, and prospects," *Appl. Energy*, vol. 222, pp. 1033–1055, Jul. 2018.
- [121] W. R. Sultana, S. K. Sahoo, S. Sukchai, S. Yamuna, and D. Venkatesh, "A review on state of art development of model predictive control for renewable energy applications," *Renew. Sustain. Energy Rev.*, vol. 76, pp. 391–406, Sep. 2017.
- [122] M. B. Shadmand, R. S. Balog, and H. Abu-Rub, "Model predictive control of PV sources in a smart DC distribution system: Maximum power point tracking and droop control," *IEEE Trans. Energy Convers.*, vol. 29, no. 4, pp. 913–921, Dec. 2014.
- [123] Y. Shan, J. Hu, Z. Li, and J. M. Guerrero, "A model predictive control for renewable energy based AC microgrids without any PID regulators," *IEEE Trans. Power Electron.*, vol. 33, no. 11, pp. 9122–9126, Nov. 2018.
- [124] M. P. Akter, S. Mekhilef, N. M. L. Tan, and H. Akagi, "Model predictive control of bidirectional AC-DC converter for energy storage system," *J. Electr. Eng. Technol.*, vol. 10, no. 1, pp. 165–175, Jan. 2015.
- [125] U. Sandhya and P. Murari, "DC grid based wind power generation in a microgrid application: Modeling and simulation," *J. Eng. Sci.*, vol. 10, no. 10, pp. 206–214, 2019.
- [126] J. Rodriguez, M. P. Kazmierkowski, J. R. Espinoza, P. Zanchetta, H. Abu-Rub, H. A. Young, and C. A. Rojas, "State of the art of finite control set model predictive control in power electronics," *IEEE Trans. Ind. Informat.*, vol. 9, no. 2, pp. 1003–1016, May 2013.
- [127] S. Vazquez, J. Rodriguez, M. Rivera, L. G. Franquelo, and M. Norambuena, "Model predictive control for power converters and drives: Advances and trends," *IEEE Trans. Ind. Electron.*, vol. 64, no. 2, pp. 935–947, Feb. 2017.
- [128] B. C. Phan and Y. C. Lai, "Control strategy of a hybrid renewable energy system based on reinforcement learning approach for an isolated microgrid," *Appl. Sci.*, vol. 9, no. 19, p. 4001, Sep. 2019.
- [129] E. Kuznetsova, Y.-F. Li, C. Ruiz, E. Zio, G. Ault, and K. Bell, "Reinforcement learning for microgrid energy management," *Energy*, vol. 59, pp. 133–146, Sep. 2013.
- [130] J. Duan, Z. Yi, D. Shi, C. Lin, X. Lu, and Z. Wang, "Reinforcement-learning-based optimal control of hybrid energy storage systems in hybrid AC–DC microgrids," *IEEE Trans. Ind. Informat.*, vol. 15, no. 9, pp. 5355–5364, Sep. 2019.
- [131] A. N. Kozlov, N. V. Tomlin, D. N. Sidorov, E. E. S. Lora, and V. G. Kurbatsky, "Optimal operation control of PV-biomass gasifier-diesel-hybrid systems using reinforcement learning techniques," *Energies*, vol. 13, no. 10, p. 2632, May 2020.
- [132] A. O. Erick and K. A. Folly, "Reinforcement learning approaches to power management in grid-tied microgrids: A review," in *Proc. Clemson Univ. Power Syst. Conf. (PSC)*, Mar. 2020, pp. 1–6.
- [133] P. Kofinas, G. Vourous, and A. I. Dounis, "Energy management in solar microgrid via reinforcement learning using fuzzy reward," *Adv. Building Energy Res.*, vol. 12, no. 1, pp. 97–115, Jan. 2018.
- [134] O. Husev, S. Ivanets, and D. Vinnikov, "Neuro-fuzzy control system for active filter with load adaptation," in *Proc. 7th Int. Conference-Workshop Compat. Power Electron. (CPE)*, Jun. 2011, pp. 28–33.
- [135] W. V. H. Hasaranga, R. D. T. M. Hemarathne, M. D. C. P. K. Mahawithana, M. G. A. B. N. Sandanuwan, H. W. D. Hettiarachchi, and K. T. M. U. Hemapala, "A fuzzy logic based battery SOC level control strategy for smart micro grid," in *Proc. 3rd Int. Conf. Adv. Electr., Electron., Inf., Commun. Bio-Informat. (AEEICB)*, Feb. 2017, pp. 215–221.
- [136] H. Shao, Y. Wang, H.-M. Li, L.-D. Qin, and H.-S. Zhao, "A novel design of fuzzy logic control algorithm for hybrid energy storage system," in *Proc. 2nd IEEE Conf. Energy Internet Energy Syst. Integr. (EI2)*, Oct. 2018, pp. 1–4.
- [137] H. W. D. Hettiarachchi, K. T. M. U. Hemapala, and A. G. B. P. Jayasekara, "A fuzzy logic based power management system for an integrated AC-DC hybrid microgrid model," in *Proc. Moratuwa Eng. Res. Conf. (MERCon)*, May 2017, pp. 357–362.
- [138] B. N. Alajmi, K. H. Ahmed, S. J. Finney, and B. W. Williams, "Fuzzy-logic-control approach of a modified hill-climbing method for maximum power point in microgrid standalone photovoltaic system," *IEEE Trans. Power Electron.*, vol. 26, no. 4, pp. 1022–1030, Apr. 2011.
- [139] A. V. Kumar, P. M. Rao, B. S. Rao, A. V. Kumar, P. M. Rao, and B. S. Rao, "Modified voltage control strategy for DC network with distributed energy storage using fuzzy logic controller," *J. Eng. Sci.*, vol. 11, no. 1, pp. 249–255, 2020.
- [140] P. B. Nempu and N. S. Jayalakshmi, "Coordinated power management of the subgrids in a hybrid AC–DC microgrid with multiple renewable sources," *IETE J. Res.*, vol. 2063, pp. 1–11, Feb. 2020.

- [141] S. Das and A. K. Akella, "A fuzzy logic-based frequency control scheme for an isolated AC coupled PV-wind-battery hybrid system," *Int. J. Model. Simul.*, pp. 1–13, May 2019.
- [142] B. P. D. Souza, V. S. Zeni, E. T. Sica, C. Q. Pica, and M. V. Hernandez, "Fuzzy logic energy management system in islanded hybrid energy generation microgrid," in *Proc. Can. Conf. Electr. Comput. Eng.*, May 2018, pp. 1–5.
- [143] B. Liu, W. Wu, C. Zhou, C. Mao, D. Wang, Q. Duan, and G. Sha, "An AC–DC hybrid multi-port energy router with coordinated control and energy management strategies," *IEEE Access*, vol. 7, pp. 109069–109082, Aug. 2019.
- [144] M. S. Bisht and Sathans, "Fuzzy based intelligent frequency control strategy in standalone hybrid AC microgrid," in *Proc. IEEE Conf. Control Appl. (CCA)*, Oct. 2014, pp. 873–878.
- [145] S. Kouro, M. A. Perez, J. Rodriguez, A. M. Llor, and H. A. Young, "Model predictive control: MPC's role in the evolution of power electronics," *IEEE Ind. Electron. Mag.*, vol. 9, no. 4, pp. 8–21, Dec. 2015.
- [146] M. Esmaili, H. Shayeghi, H. M. Nejad, and A. Younesi, "Reinforcement learning based PID controller design for LFC in a microgrid," *COMPEL-Int. J. Comput. Math. Electr. Electron. Eng.*, vol. 36, no. 4, pp. 1287–1297, Jul. 2017.
- [147] M. N. Cirstea, A. Dinu, J. G. Khor, and M. McCormick, "Fuzzy logic fundamentals," in *Neural and Fuzzy Logic Control of Drives and Power Systems*, vol. 6, 1st ed. London, U.K.: Newnes, 2002, pp. 114–121.
- [148] I. Roasto, A. Rosin, and T. Jalakas, "Power electronic interface converter for resource efficient buildings," in *Proc. IECON-43rd Annu. Conf. IEEE Ind. Electron. Soc.*, Oct. 2017, pp. 3638–3643.
- [149] R. Teodorescu, F. Blaabjerg, and M. Liserre, "Proportional-resonant controllers. A new breed of controllers suitable for grid-connected voltage-source converters," in *Proc. Optim. 9th Conf. Optim. Elect. Electron. Equip.*, vol. 3, May 2004, pp. 9–14.
- [150] I. Vechiu, H. Camblong, G. Tapia, B. Dakyo, and O. Curea, "Control of four leg inverter for hybrid power system applications with unbalanced load," *Energy Convers. Manage.*, vol. 48, no. 7, pp. 2119–2128, Jul. 2007.
- [151] R. Lliuyacc, J. M. Mauricio, A. Gomez-Exposito, M. Savaghebi, and J. M. Guerrero, "Grid-forming VSC control in four-wire systems with unbalanced nonlinear loads," *Electr. Power Syst. Res.*, vol. 152, pp. 249–256, Nov. 2017.
- [152] D. Dong, T. Thacker, R. Burgos, F. Wang, and D. Boroyevich, "On zero steady-state error voltage control of single-phase PWM inverters with different load types," *IEEE Trans. Power Electron.*, vol. 26, no. 11, pp. 3285–3297, Nov. 2011.
- [153] R. Teodorescu, F. Blaabjerg, M. Liserre, and P. C. Loh, "Proportional-resonant controllers and filters for grid-connected voltage-source converters," *IEE Proc.-Electr. Power Appl.*, vol. 153, no. 5, pp. 750–762, Sep. 2006.
- [154] W. Ping, G. Lin, Z. Zhe, C. Liuye, and W. Wei, "Switch-mode AC stabilized voltage supply based on PR controller," in *Proc. 5th Int. Conf. Power Electron. Syst. Appl. (PESA)*, Dec. 2013, pp. 1–4.
- [155] L. Tien Phong, L. T. Phong, T. Hai, L. Tien Phong, L. T. Phong, and T. Hai, "Grid-connected control system for three-phase bidirectional DC/AC converter to exploit photovoltaic power generation," *Amer. J. Eng. Technol. Manag.*, vol. 2, no. 6, pp. 98–107, 2017.
- [156] X. Zhang, J. W. Spencer, and J. M. Guerrero, "Small-signal modeling of digitally controlled grid-connected inverters with LCL filters," *IEEE Trans. Ind. Electron.*, vol. 60, no. 9, pp. 3752–3765, Sep. 2013.
- [157] B. Li, W. Yao, L. Hang, and L. M. Tolbert, "Robust proportional resonant regulator for grid-connected voltage source inverter (VSI) using direct pole placement design method," *IET Power Electron.*, vol. 5, no. 8, p. 1367, 2012.
- [158] P. Student and A. Professor, "Bidirectional AC/DC converter using simplified PWM with feed-forward control," *Int. J. Innov. Res. Sci. Eng. Technol.*, vol. 5, no. 7, pp. 12426–12433, Jul. 2016.
- [159] M. M. Kanai, J. N. Nderu, and P. K. Hinga, "Modeling and analysis of AC-DC converter PID controller optimized with pattern search algorithm," *J. Sci. Technol.*, vol. 11, no. 2011, pp. 104–118, 2011.
- [160] N. Eghtedarpour and E. Farjah, "Control strategy for distributed integration of photovoltaic and energy storage systems in DC micro-grids," *Renew. Energy*, vol. 45, pp. 96–110, Sep. 2012.
- [161] J. Wang, I. Tyuryukanov, and A. Monti, "Design of a novel robust current controller for grid-connected inverter against grid impedance variations," *Int. J. Electr. Power Energy Syst.*, vol. 110, pp. 454–466, Sep. 2019.
- [162] T. Dragicevic, C. Zheng, J. Rodriguez, and F. Blaabjerg, "Robust quasi-predictive control of LCL-filtered grid converters," *IEEE Trans. Power Electron.*, vol. 35, no. 2, pp. 1934–1946, Feb. 2020.
- [163] P. B. Nempu, N. S. Jayalakshmi, K. Shaji, and M. Singh, "Fuzzy-PI controllers for voltage and frequency regulation of a PV-FC based autonomous microgrid," in *Proc. IEEE Int. Conf. Distrib. Comput., VLSI, Electr. Circuits Robot. (DISCOVER)*, Aug. 2019, pp. 1–6.
- [164] U. B. Tayab, M. A. B. Roslan, L. J. Hwai, and M. Kashif, "A review of droop control techniques for microgrid," *Renew. Sustain. Energy Rev.*, vol. 76, pp. 717–727, Sep. 2017.
- [165] J. M. Guerrero, L. Hang, and J. Uceda, "Control of distributed uninteruptible power supply systems," *IEEE Trans. Ind. Electron.*, vol. 55, no. 8, pp. 2845–2859, Aug. 2008.
- [166] E. Rokrok, M. Shafie-khah, and J. P. S. Catalao, "Review of primary voltage and frequency control methods for inverter-based islanded microgrids with distributed generation," *Renew. Sustain. Energy Rev.*, vol. 82, pp. 3225–3235, Feb. 2018.
- [167] Y. Mohamed and E. F. El-Saadany, "Adaptive decentralized droop controller to preserve power sharing stability of paralleled inverters in distributed generation microgrids," *IEEE Trans. Power Electron.*, vol. 23, no. 6, pp. 2806–2816, Nov. 2008.
- [168] E. Barklund, N. Pogaku, M. Prodanovic, C. Hernandez-Aramburo, and T. C. Green, "Energy management in autonomous microgrid using stability-constrained droop control of inverters," *IEEE Trans. Power Electron.*, vol. 23, no. 5, pp. 2346–2352, Sep. 2008.
- [169] R. Majumder, B. Chaudhuri, A. Ghosh, R. Majumder, G. Ledwich, and F. Zare, "Improvement of stability and load sharing in an autonomous microgrid using supplementary droop control loop," *IEEE Trans. Power Syst.*, vol. 25, no. 2, pp. 796–808, May 2010.
- [170] Y.-C. Jeung, D. D. Le, and D.-C. Lee, "Analysis and design of DC-bus voltage controller of energy storage systems in DC microgrids," *IEEE Access*, vol. 7, pp. 126696–126708, 2019.
- [171] J. M. Guerrero, N. Berbel, J. Matas, L. G. De Vicuña, and J. Miret, "Decentralized control for parallel operation of distributed generation inverters in microgrids using resistive output impedance," in *Proc. IECON Ind. Electron. Conf.*, Nov. 2006, vol. 54, no. 2, pp. 5149–5154.
- [172] J. M. Guerrero, J. Matas, L. Garcia de Vicuña, M. Castilla, and J. Miret, "Decentralized control for parallel operation of distributed generation inverters using resistive output impedance," *IEEE Trans. Ind. Electron.*, vol. 54, no. 2, pp. 994–1004, Apr. 2007.
- [173] Y. Zeng, "Droop control of parallel-operated inverters," Ph.D. dissertation, Dept. Autom. Control Syst. Eng., Univ. Sheffield, Sheffield, U.K., 2015.
- [174] Q.-C. Zhong and Y. Zeng, "Universal droop control of inverters with different types of output impedance," *IEEE Access*, vol. 4, pp. 702–712, 2016.
- [175] N. L. Diaz, T. Dragicevic, J. C. Vasquez, and J. M. Guerrero, "Intelligent distributed generation and storage units for DC microgrids—A new concept on cooperative control without communications beyond droop control," *IEEE Trans. Smart Grid*, vol. 5, no. 5, pp. 2476–2485, Sep. 2014.
- [176] Y. Fu, Z. Zhang, Y. Mi, Z. Li, and F. Li, "Droop control for DC multi-microgrids based on local adaptive fuzzy approach and global power allocation correction," *IEEE Trans. Smart Grid*, vol. 10, no. 5, pp. 5468–5478, Sep. 2019.
- [177] M. Mosayebi, S. M. Sadeghzadeh, J. M. Guerrero, and M.-H. Khooban, "Stabilization of DC nanogrids based on non-integer general type-II fuzzy system," *IEEE Trans. Circuits Syst. II, Exp. Briefs*, vol. 67, no. 12, pp. 3108–3112, Dec. 2020.
- [178] M. Baharizadeh, H. R. Karshenas, and J. M. Guerrero, "An improved power control strategy for hybrid AC-DC microgrids," *Int. J. Electr. Power Energy Syst.*, vol. 95, pp. 364–373, Feb. 2018.
- [179] S. M. Malik, X. Ai, Y. Sun, C. Zhengqi, and Z. Shupeng, "Voltage and frequency control strategies of hybrid AC/DC microgrid: A review," *IET Gener., Transmiss. Distrib.*, vol. 11, no. 2, pp. 303–313, Jan. 2017.
- [180] P. C. Loh, D. Li, Y. K. Chai, and F. Blaabjerg, "Autonomous operation of hybrid microgrid with AC and DC subgrids," *IEEE Trans. Power Electron.*, vol. 28, no. 5, pp. 2214–2223, May 2013.
- [181] A. Gupta, D. K. Jain, and S. Dahiya, "Management of power exchange between hybrid microgrids using intelligent control," in *Proc. IEEE 6th Int. Conf. Power Syst. (ICPS)*, Mar. 2016, pp. 1–6.

- [182] A. Micallef, M. Apap, C. Spiteri-Staines, and J. M. Guerrero, "Mitigation of harmonics in grid-connected and islanded microgrids via virtual admittances and impedances," *IEEE Trans. Smart Grid*, vol. 8, no. 2, pp. 651–661, Mar. 2017.
- [183] Q. C. Zhong, "Control of parallel-connected inverters to achieve proportional load sharing," *IFAC Proc. Volumes*, vol. 44, no. 1, pp. 2785–2790, 2011.
- [184] T. Wu, Z. Liu, J. Liu, S. Wang, and Z. You, "A unified virtual power decoupling method for droop-controlled parallel inverters in microgrids," *IEEE Trans. Power Electron.*, vol. 31, no. 8, pp. 5587–5603, Aug. 2016.
- [185] H. Mahmood, D. Michaelson, and J. Jiang, "Accurate reactive power sharing using adaptive virtual impedances in an islanded micro-grid," *J. Power Electron.*, vol. 30, no. 3, pp. 1605–1617, 2015.
- [186] M. Savaghebi, A. Jalilian, J. C. Vasquez, and J. M. Guerrero, "Secondary control for voltage quality enhancement in microgrids," *IEEE Trans. Smart Grid*, vol. 3, no. 4, pp. 1893–1902, Dec. 2012.
- [187] M. A. Aboushal, M. M. Zakaria, M. M. Z. Moustafa, M. M. Zakaria, M. M. Z. Moustafa, and M. M. Zakaria, "Original article a new unified control strategy for inverter-based micro-grid using hybrid droop scheme," *Alexandria Eng. J.*, vol. 58, no. 4, pp. 1229–1245, Dec. 2019.
- [188] Y. Wei Li and C.-N. Kao, "An accurate power control strategy for power-electronics-interfaced distributed generation units operating in a low-voltage multibus microgrid," *IEEE Trans. Power Electron.*, vol. 24, no. 12, pp. 2977–2988, Dec. 2009.
- [189] J. He and Y. W. Li, "Analysis, design, and implementation of virtual impedance for power electronics interfaced distributed generation," *IEEE Trans. Ind. Appl.*, vol. 47, no. 6, pp. 2525–2538, Nov. 2011.
- [190] Q.-C. Zhong, "Robust droop controller for accurate proportional load sharing among inverters operated in parallel," *IEEE Trans. Ind. Electron.*, vol. 60, no. 4, pp. 1281–1290, Apr. 2013.
- [191] R. P. S. Chandrasena, F. Shahnia, A. Ghosh, and S. Rajakaruna, "Dynamic operation and control of a hybrid nanogrid system for future community houses," *IET Gener., Transmiss. Distrib.*, vol. 9, no. 11, pp. 1168–1178, Aug. 2015.
- [192] I. Vechiu, H. Camblog, G. Tapia, B. Dakyo, and O. Curea, "Control of four leg inverter for hybrid power system applications with unbalanced load," *Energy Convers. Manag.*, vol. 162, pp. 169–182, Sep. 2007.
- [193] H. Saad, S. Denetiere, J. Mahseredjian, P. Delarue, X. Guillaud, J. Peralta, and S. Nguereu, "Modular multilevel converter models for electromagnetic transients," *IEEE Trans. Power Del.*, vol. 29, no. 3, pp. 1481–1489, Jun. 2014.
- [194] P. Tielens, and D. Van Hertem, "Grid inertia and frequency control in power systems with high penetration of renewables," in *Proc. Symp. Electr. Power Eng.*, Delft, The Netherlands, 2012, vol. 39, no. 2, pp. 1–6.
- [195] Q.-C. Zhong and G. Weiss, "Synchronverters: Inverters that mimic synchronous generators," *IEEE Trans. Ind. Electron.*, vol. 58, no. 4, pp. 1259–1267, Apr. 2011.
- [196] J. Alipoor, Y. Miura, and T. Ise, "Power system stabilization using virtual synchronous generator with alternating moment of inertia," *IEEE J. Emerg. Sel. Topics Power Electron.*, vol. 3, no. 2, pp. 451–458, Jun. 2015.
- [197] Y. Xiang-zhen, S. Jian-hui, D. Ming, L. Jin-wei, and D. Yan, "Control strategy for virtual synchronous generator in microgrid," in *Proc. 4th Int. Conf. Electr. Utility Deregulation Restructuring Power Technol. (DRPT)*, Jul. 2011, pp. 1633–1637.
- [198] D. Chen, Y. Xu, and A. Q. Huang, "Integration of DC microgrids as virtual synchronous machines into the AC grid," *IEEE Trans. Ind. Electron.*, vol. 64, no. 9, pp. 7455–7466, Sep. 2017.
- [199] S. S. H. Yazdi, J. Milimonfared, S. H. Fathi, K. Rouzbehi, and E. Rakhshani, "Analytical modeling and inertia estimation of VSG-controlled type 4 WTGs: Power system frequency response investigation," *Int. J. Electr. Power Energy Syst.*, vol. 107, pp. 446–461, May 2019.
- [200] Q.-C. Zhong, P.-L. Nguyen, Z. Ma, and W. Sheng, "Self-synchronized synchronverters: Inverters without a dedicated synchronization unit," *IEEE Trans. Power Electron.*, vol. 29, no. 2, pp. 617–630, Feb. 2014.
- [201] M. Guan, W. Pan, J. Zhang, J. Cheng, X. Zheng, and Q. Hao, "Synchronous generator emulation control strategy for voltage source converter (VSC) stations," *IEEE Trans. Power Syst.*, vol. 30, no. 6, pp. 3093–3101, Nov. 2015.
- [202] T. Shintai, Y. Miura, and T. Ise, "Reactive power control for load sharing with virtual synchronous generator control," in *Proc. 7th Int. Power Electron. Motion Control Conf.*, vol. 2, Jun. 2012, pp. 846–853.
- [203] A. Karimi, Y. Khayat, M. Naderi, T. Dragicevic, R. Mirzaei, F. Blaabjerg, and H. Bevrani, "Inertia response improvement in AC microgrids: A fuzzy-based virtual synchronous generator control," *IEEE Trans. Power Electron.*, vol. 35, no. 4, pp. 4321–4331, Apr. 2020.
- [204] V. Lavanya and N. S. Kumar, "A review: Control strategies for power quality improvement in microgrid," *Int. J. Renew. Energy Res.*, vol. 8, no. 1, pp. 150–165, 2018.
- [205] F. Hosen-Zdeh, A. Edrisian, and M. R. Naseh, "Power quality improvement in distributed generation resources using UPQC," *Int. J. Renew. Energy Res.*, vol. 4, no. 3, pp. 795–800, 2014.
- [206] A. Chauhan and R. Thakur, "Power quality improvement using passive & active filters," *Int. J. Eng. Trends Technol.*, vol. 36, no. 3, pp. 130–136, 2016.
- [207] K. Nikum, R. Saxena, and A. Wagh, "Effect on power quality by large penetration of household non linear load," in *Proc. IEEE 1st Int. Conf. Power Electron., Intell. Control Energy Syst. (ICPEICES)*, Jul. 2016, pp. 1–5.
- [208] K. K. Weng, W. Y. Wan, R. K. Rajkumar, and R. K. Rajkumar, "Power quality analysis for PV grid connected system using PSCAD/EMTDC," *Int. J. Renew. Energy Res.*, vol. 5, no. 1, pp. 121–132, 2015.
- [209] D. Dong, "AC-DC bus-interface bi-directional converters in renewable energy systems," Ph.D. dissertation, Dept. Elect. Eng., Virginia Polytech. Inst. State Univ., Blacksburg, VA, USA, 2012.
- [210] T. Cui, Q. Ma, P. Xu, and P. Zhang, "EMI mitigation in switching power converters combining closed-loop gate drive and chaotic frequency modulation technique," *IET Power Electron.*, vol. 12, no. 12, pp. 3033–3040, Oct. 2019.
- [211] D. Dong, F. Luo, X. Zhang, D. Boroyevich, and P. Mattavelli, "Grid-interface bidirectional converter for residential DC distribution systems—Part 2: AC and DC interface design with passive components minimization," *IEEE Trans. Power Electron.*, vol. 28, no. 4, pp. 1667–1679, Apr. 2013.
- [212] M. R. Yazdani, H. Farzanehfard, and J. Faiz, "Classification and comparison of EMI mitigation techniques in switching power converters—A review," *J. Power Electron.*, vol. 11, no. 5, pp. 767–777, Sep. 2011.
- [213] *Standard for Interconnection and Interoperability of Distributed Energy Resources with Associated Electric Power Systems Interfaces*, IEEE Standard Assoc., Piscataway, NJ, USA, 2018.
- [214] K. Mainali and R. Oruganti, "Conducted EMI mitigation techniques for switch-mode power converters: A survey," *IEEE Trans. Power Electron.*, vol. 25, no. 9, pp. 2344–2356, Sep. 2010.
- [215] K. Mainali and R. Oruganti, "Design of a current-sense voltage-feedback common mode EMI filter for an off-line power converter," in *Proc. IEEE Power Electron. Spec. Conf.*, Jun. 2008, pp. 1632–1638.
- [216] V. Tarateeraseth, "EMI filter design: Part III: Selection of filter topology for optimal performance," *IEEE Electromagn. Compat. Mag.*, vol. 1, no. 2, pp. 60–73, 2nd Quart., 2012.
- [217] S. Ye, W. Eberle, and Y.-F. Liu, "A novel EMI filter design method for switching power supplies," *IEEE Trans. Power Electron.*, vol. 19, no. 6, pp. 1668–1678, Nov. 2004.
- [218] M. R. Yazdani and H. Farzanehfard, "Conducted electromagnetic interference analysis and mitigation using zero-current transition soft switching and spread spectrum techniques," *IET Power Electron.*, vol. 5, no. 7, pp. 1034–1041, Aug. 2012.
- [219] X. Wang, Y. Sun, T. Li, and J. Shi, "Active closed-loop gate voltage control method to mitigate metal-oxide semiconductor field-effect transistor turn-off voltage overshoot and ring," *IET Power Electron.*, vol. 6, no. 8, pp. 1715–1722, Sep. 2013.
- [220] M. Hamzeh, A. Ghazanfari, H. Mokhtari, and H. Karimi, "Integrating hybrid power source into an islanded MV microgrid using CHB multilevel inverter under unbalanced and nonlinear load conditions," *IEEE Trans. Energy Convers.*, vol. 28, no. 3, pp. 643–651, Sep. 2013.
- [221] *IEEE Recommended Practice for Electric Power Distribution for Industrial Plants*, IEEE Standard 141, Dec. 1993.
- [222] *IEEE Recommended Practice and Requirements for Harmonic Control in Electric Power Systems*, IEEE Standard 519, Mar. 2014.
- [223] G. W. Chang, H. J. Su, L. Y. Hsu, H. J. Lu, Y. R. Chang, Y. D. Lee, and C. C. Wu, "A study of passive harmonic filter planning for an AC microgrid," in *Proc. IEEE Power Energy Soc. Gen. Meeting*, Jul. 2015, pp. 28–31.

- [224] I. M. Safwat and W. Xiaohua, "Comparative study between passive PFC and Active PFC based on buck-boost conversion," in *Proc. IEEE 2nd Adv. Inf. Technol., Electron. Automat. Control Conf. (IAEAC)*, no. 1, Mar. 2017, pp. 45–50.
- [225] M. S. A. Dahidah, G. Konstantinou, and V. G. Agelidis, "A review of multilevel selective harmonic elimination PWM: Formulations, solving algorithms, implementation and applications," *IEEE Trans. Power Electron.*, vol. 30, no. 8, pp. 4091–4106, Aug. 2015.
- [226] Y. Sahali and M. K. Fellah, "Selective harmonic eliminated pulse-width modulation technique (SHE PWM) applied to three-level inverter/converter," in *Proc. IEEE Int. Symp. Ind. Electron.*, vol. 2, Jun. 2003, pp. 1112–1117.
- [227] T.-P. Chen, "Zero-sequence circulating current reduction method for parallel HEPWM inverters between AC bus and DC bus," *IEEE Trans. Ind. Electron.*, vol. 59, no. 1, pp. 290–300, Jan. 2012.
- [228] F. Chen, R. Burgos, D. Boroyevich, and X. Zhang, "Low-frequency common-mode voltage control for systems interconnected with power converters," *IEEE Trans. Ind. Electron.*, vol. 64, no. 1, pp. 873–882, Jan. 2017.
- [229] D. Dong, I. Cvetkovic, D. Boroyevich, W. Zhang, R. Wang, and P. Mattavelli, "Grid-interface bidirectional converter for residential DC distribution systems—Part one: High-density two-stage topology," *IEEE Trans. Power Electron.*, vol. 28, no. 4, pp. 1655–1666, Apr. 2013.
- [230] C.-C. Hou, C.-C. Shih, P.-T. Cheng, and A. M. Hava, "Common-mode voltage reduction pulsewidth modulation techniques for three-phase grid-connected converters," *IEEE Trans. Power Electron.*, vol. 28, no. 4, pp. 1971–1979, Apr. 2013.
- [231] Y. Xia and R. Ayyanar, "Comprehensive comparison of THD and common mode leakage current of bipolar, unipolar and hybrid modulation schemes for single phase grid connected full bridge inverters," in *Proc. IEEE Appl. Power Electron. Conf. Expo. (APEC)*, Mar. 2017, pp. 743–750.
- [232] *IEEE Interconnecting Distributed Resources with Electric Power Systems*, IEEE Standard 1547, Jun. 2003.
- [233] A. Pouryekt, V. K. Ramachandramurthy, N. Mithulananthan, and A. Arulampalam, "Islanding detection and enhancement of microgrid performance," *IEEE Syst. J.*, vol. 12, no. 4, pp. 3131–3141, Dec. 2018.
- [234] P. Mahat, Z. Chen, and B. Bak-Jensen, "Review of islanding detection methods for distributed generation," in *Proc. 3rd Int. Conf. Electr. Utility Deregulation Restructuring Power Technol.*, Apr. 2008, pp. 2743–2748.
- [235] *IEEE Recommended Practice for Utility Interface of Residential and Intermediate Photovoltaic (PV) Systems*, IEEE Standard 929, May 1987.
- [236] P. Mahat, Z. Chen, and B. Bak-Jensen, "A hybrid islanding detection technique using average rate of voltage change and real power shift," *IEEE Trans. Power Del.*, vol. 24, no. 2, pp. 764–771, Apr. 2009.
- [237] O. Palizban, K. Kauhaniemi, and J. M. Guerrero, "Microgrids in active network management—Part II: System operation, power quality and protection," *Renew. Sustain. Energy Rev.*, vol. 36, pp. 440–451, Aug. 2014.
- [238] Z. Xu, P. Yang, Q. Zheng, and Z. Zeng, "Study on black start strategy of microgrid with PV and multiple energy storage systems," in *Proc. 18th Int. Conf. Electr. Mach. Syst. (ICEMS)*, Oct. 2015, pp. 402–408.
- [239] C. Li, C. Cao, Y. Cao, Y. Kuang, L. Zeng, and B. Fang, "A review of islanding detection methods for microgrid," *Renew. Sustain. Energy Rev.*, vol. 35, pp. 211–220, Jul. 2014.
- [240] M. E. Ropp, M. Begovic, A. Rohatgi, G. A. Kern, R. H. Bonn, and S. Gonzalez, "Determining the relative effectiveness of islanding detection methods using phase criteria and nondetection zones," *IEEE Trans. Energy Convers.*, vol. 15, no. 3, pp. 290–296, 3rd Quart., 2000.
- [241] A. S. Vijay, S. Doolla, and M. C. Chandorkar, "Real-time testing approaches for microgrids," *IEEE J. Emerg. Sel. Topics Power Electron.*, vol. 5, no. 3, pp. 1356–1376, Sep. 2017.
- [242] R. AhmadiAhangar, A. Rosin, A. N. Niaki, I. Palu, and T. Korotko, "A review on real-time simulation and analysis methods of microgrids," *Int. Trans. Electr. Energy Syst.*, vol. 29, no. 11, 2019, Art. no. e12106.
- [243] A. Mohamed, V. Salehi, and O. Mohammed, "Real-time energy management algorithm for mitigation of pulse loads in hybrid microgrids," *IEEE Trans. Smart Grid*, vol. 3, no. 4, pp. 1911–1922, Dec. 2012.
- [244] C. M. Colson and M. H. Nehrir, "Comprehensive real-time microgrid power management and control with distributed agents," *IEEE Trans. Smart Grid*, vol. 4, no. 1, pp. 617–627, Mar. 2013.
- [245] H. Shi, F. Zhuo, H. Yi, F. Wang, D. Zhang, and Z. Geng, "A novel real-time voltage and frequency compensation strategy for photovoltaic-based microgrid," *IEEE Trans. Ind. Electron.*, vol. 62, no. 6, pp. 3545–3556, Jun. 2015.
- [246] A. Kirakosyan, E. F. El-Saadany, M. S. E. Moursi, A. H. Yazdavar, and A. Al-Durra, "Communication-free current sharing control strategy for DC microgrids and its application for AC/DC hybrid microgrids," *IEEE Trans. Power Syst.*, vol. 35, no. 1, pp. 140–151, Jan. 2020.
- [247] P. Yang, M. Yu, Q. Wu, N. Hatzigiorgiou, Y. Xia, and W. Wei, "Decentralized bidirectional voltage supporting control for multi-mode hybrid AC/DC microgrid," *IEEE Trans. Smart Grid*, vol. 11, no. 3, pp. 2615–2626, May 2020.
- [248] M. H. Cintuglu, T. Youssef, and O. A. Mohammed, "Development and application of a real-time testbed for multiagent system interoperability: A case study on hierarchical microgrid control," *IEEE Trans. Smart Grid*, vol. 9, no. 3, pp. 1759–1768, May 2018.
- [249] W. Shi, N. Li, C.-C. Chu, and R. Gadh, "Real-time energy management in microgrids," *IEEE Trans. Smart Grid*, vol. 8, no. 1, pp. 228–238, Jan. 2017.
- [250] D. Ding, Q.-L. Han, Y. Xiang, X. Ge, and X.-M. Zhang, "A survey on security control and attack detection for industrial cyber-physical systems," *Neurocomputing*, vol. 275, pp. 1674–1683, Jan. 2018.
- [251] T. Vu, B. Nguyen, Z. Cheng, M.-Y. Chow, and B. Zhang, "Cyber-physical microgrids: Toward future resilient communities," *arXiv*, pp. 1–12, 2019. [Online]. Available: <https://arxiv.org/abs/1912.05682>
- [252] S. Poudel, Z. Ni, and N. Malla, "Real-time cyber physical system testbed for power system security and control," *Int. J. Electr. Power Energy Syst.*, vol. 90, pp. 124–133, Sep. 2017.
- [253] S. Raza, H. Mokhlis, H. Arof, J. A. Laghari, and L. Wang, "Application of signal processing techniques for islanding detection of distributed generation in distribution network: A review," *Energy Convers. Manage.*, vol. 96, pp. 613–624, May 2015.
- [254] Z. Ye, A. Kolwalkar, Y. Zhang, P. Du, and R. Walling, "Evaluation of anti-islanding schemes based on nondetection zone concept," *IEEE Trans. Power Electron.*, vol. 19, no. 5, pp. 1171–1176, Sep. 2004.
- [255] R. S. Kunte and W. Gao, "Comparison and review of islanding detection techniques for distributed energy resources," in *Proc. 40th North Amer. Power Symp.*, Sep. 2008, pp. 1–8.
- [256] S. D. Kermany, M. Joorabian, S. Deilami, and M. A. S. Masoum, "Hybrid islanding detection in microgrid with multiple connection points to smart grids using fuzzy-neural network," *IEEE Trans. Power Syst.*, vol. 32, no. 4, pp. 2640–2651, Jul. 2017.
- [257] V. Menon and M. H. Nehrir, "A hybrid islanding detection technique using voltage unbalance and frequency set point," *IEEE Trans. Power Syst.*, vol. 22, no. 1, pp. 442–448, Feb. 2007.
- [258] Q.-C. Zhong, L. Hobson, and M. G. G. Jayne, "Classical control of the neutral point in 4-wire 3-phase DC-AC converters," *Electr. Power Qual. Util. J.*, vol. 6, no. 2, pp. 73–81, 2005.
- [259] A. Mohamed, S. Vanteddu, and O. Mohammed, "Protection of bidirectional AC-DC/DC-AC converter in hybrid AC/DC microgrids," in *Proc. IEEE Southeastcon*, Mar. 2012, vol. 25, no. 3, pp. 1–6.
- [260] J. Jia, G. Yang, A. Nielsen, and P. Ronne-Hansen, "Study of control strategies of power electronics during faults in microgrids," in *Hybrid-Renewable Energy Systems in Microgrids: Integration, Developments and Control*, vol. 7, 1st ed. Denmark: Elsevier, 2018, pp. 109–146.
- [261] J. Shiles, E. Wong, S. Rao, C. Sanden, M. A. Zamani, M. Davari, and F. Katiraei, "Microgrid protection: An overview of protection strategies in North American microgrid projects," in *Proc. IEEE Power Energy Soc. Gen. Meeting*, Jul. 2017, pp. 1–5.
- [262] S. Mirsaedi, X. Dong, S. Shi, and D. Tzelepis, "Challenges, advances and future directions in protection of hybrid AC/DC microgrids," *IET Renew. Power Gener.*, vol. 11, no. 12, pp. 1495–1502, Oct. 2017.
- [263] G. Van den Broeck, J. Stuyts, and J. Driesen, "A critical review of power quality standards and definitions applied to DC microgrids," *Appl. Energy*, vol. 229, pp. 281–288, Nov. 2018.
- [264] *IEEE Recommended Practice for Power Quality Data Interchange Format (PQDIF)*, IEEE Power Energy Soc., Piscataway, NJ, USA, 2019.
- [265] G. S. Rawat and S. Suhag, "Survey on DC microgrid architecture, power quality issues and control strategies," in *Proc. 2nd Int. Conf. Inventive Syst. Control (ICISC)*, Jan. 2018, pp. 500–505.
- [266] *CISPR/CIS/A Electromagnetic Compatibility of Information Technology Equipment, Multimedia Equipment and Receivers*, IEC CISPR Standard 32, Mar. 2015.



MAHDIEH NAJAFZADEH (Student Member, IEEE) received the B.Sc. degree in power electrical engineering from the Water and Power University of Technology (Shahid Beheshti), in 2006, and the M.Sc. degrees in power electrical engineering and power electronics and electrical machinery from the K. N. Toosi University of Technology, Tehran, Iran, in 2015. She is currently pursuing the Ph.D. degree from the Tallinn University of Technology, Tallinn, Estonia.

She worked as an Electrical Power Substation Designer in low-voltage and high-voltage parts (research and development section) from Sane Shargh, Moham Shargh Group, Mashhad, Iran, from 2006 to 2012. Her research interest includes the design and control of power electronics converters, including modeling, design, simulation, and application of control systems in converters.



ROYA AHMADIAHANGAR (Member, IEEE) received the M.Sc. and Ph.D. degrees in power system engineering from the Babol University of Technology (Ranked 1st, 2017–2019, Times Magazine), Babol, Iran, in 2009 and 2014, respectively.

She has been currently a Postdoctoral Researcher with the Department of Electrical Power Engineering and Mechatronics, Tallinn University of Technology, Estonia, since 2018. She has authored or coauthored one book and five book chapters, as well as more than 40 published articles on the power system and smart grids. Her research interests include the integration of DER in smart grids, demand response and demand-side flexibility, AI applied to smart grid and planning, and management of power systems. In her Ph.D. studies, she was awarded the Iranian Ministry of Science Scholarship for Ph.D. studies (Merit Scholarship) and Ranked 1st in the Ph.D. program.



OLEKSANDR HUSEV (Senior Member, IEEE) received the B.Sc. and M.Sc. degrees in industrial electronics from Chernihiv State Technological University, Chernihiv, Ukraine, in 2007 and 2008 respectively. He defended his Ph.D. thesis at the Institute of Electrodynamics, National Academy of Science of Ukraine, in 2012.

He is currently a Senior Researcher with the Department of Electrical Engineering and Mechatronics, Tallinn University of Technology. He has over 100 publications. He holds several patents. His research interests include power electronics systems; design of novel topologies, control systems based on a wide range of algorithms, including modeling, design, and simulation; applied design of power converters; and control systems and application and stability investigation.



INDREK ROASTO (Member, IEEE) received the M.Sc. and Ph.D. degrees in electrical engineering from the Tallinn University of Technology (TalTech), Tallinn, Estonia, in 2005 and 2009, respectively.

He was with the Gdynia Maritime Academy, Poland, as a Postdoctoral Researcher, in 2013. He is currently a Senior Researcher with TalTech. He has over 100 publications and owns five utility models and two patents in the field of power electronics. His research interests include digital control of switching power converters, interfacing renewable energy sources, and power quality in microgrid.



TANEL JALAKAS (Member, IEEE) received the Ph.D. studies in electrical engineering from the Tallinn University of Technology (TalTech), in 2010. He is currently a Senior Researcher with the Department of Electrical Power Engineering and Mechatronics, TalTech. His main research interest includes the design of power electronic converters for renewable energy sources.



ANDREI BLINOV (Senior Member, IEEE) received the M.Sc. degree in electrical drives and power electronics and the Ph.D. degree, with a dissertation devoted to the research of switching properties and performance improvement methods of high-voltage IGBT-based dc-dc converters, from the Tallinn University of Technology, Tallinn, Estonia, in 2008, and 2012, respectively. After the Ph.D. studies, he has spent two years working as a Postdoctoral Researcher at the KTH Royal Institute of Technology, Sweden. He is currently a Senior Researcher with the Department of Electrical Power Engineering and Mechatronics, Tallinn University of Technology. His research interests include switch-mode power converters, new semiconductor technologies, and energy storage systems.

...

Publication II

Roasto, I.; Husev, O.; Najafzadeh, M.; Jalakas, T.; Rodriguez, J. Voltage source operation of the energy-router based on model predictive control. *Energies*, 2019, 12 (10), 1892.

Article

Voltage Source Operation of the Energy-Router Based on Model Predictive Control

Indrek Roasto ^{1,*}, Oleksandr Husev ¹, Mahdiyyeh Najafzadeh ¹, Tanel Jalakas ¹ and Jose Rodriguez ²

¹ Department of Electrical Power Engineering and Mechatronics, Tallinn University of Technology, 19086 Tallinn, Estonia; oleksandr.husev@taltech.ee (O.H.); mahdieh.najafzadeh@taltech.ee (M.N.); tanel.jalakas@taltech.ee (T.J.)

² Department of Electronics, Universidad Andrés Bello (UNAB), Santiago 8320000, Chile; jose.rodriguez@unab.cl

* Correspondence: indrek.roasto@ieee.org

Received: 8 April 2019; Accepted: 12 May 2019; Published: 17 May 2019



Abstract: The energy router (ER) is regarded as a key component of microgrids. It is a converter that interfaces the microgrid(s) with the utility grid. The energy router has a multiport structure and bidirectional energy flow control. The energy router concept can be implemented in nearly zero energy buildings (NZEB) to provide flexible energy management. We propose a concept where ER is working as a single grid-forming converter with a predefined voltage reference. The biggest challenge is to maintain regulated voltage and frequency inside the NZEB in the idle operation mode, where traditional regulators, e.g., proportional-resonant (PR), proportional-integral-derivative (PID), will not meet the control design requirements and could have unstable behavior. To gain the stability of the system, we propose model predictive control (MPC). The design of the MPC algorithm is explained. A simulation software for power electronics (PLECS) is used to simulate the proposed algorithm. Finally, the simulation results are verified on an experimental prototype.

Keywords: energy router; model predictive control; voltage source inverter; idle mode; nearly zero energy building

1. Introduction

The steadily increasing penetration of renewable energy sources (RES) in the utility grid is a current trend in electrical energy technology. This has launched a paradigm shift in energy production. Centralized production and distribution are moving towards a multi-sourced mesh network, also called the Internet of Energy (IoE) [1]. Similar to the Information Internet, the IoE has a potential for massive innovation, cost reductions and productivity enhancements in the industry [2]. Nevertheless, the increasing penetration of RES is also a source for many technical challenges that are still to be overcome. Well-known issues of the utility grid are the voltage/frequency disturbances caused by the chaotic nature of RES. One way to maintain the power balance is by utilizing energy storage (ES). Batteries that are the most robust and flexible ES technology are still too expensive. Currently, the price of an ES system (including Li-ion batteries, power electronics, taxes, installation etc.) is about 630 \$/kWh on average [3]. Although there are many other ES technologies, e.g., pumped hydro power, compressed air, power-to-gas, none of them meet all of the following requirements: Robustness, reliability, and economic feasibility [1].

Alternatively, the power balance in the utility grid can be maintained also via smart energy management. The key element here is a power electronic converter called an energy router (ER). The concept of ER introduced by National Science Foundation Future Renewable Electric Energy Delivery Management (NSF FREEDM) Systems Center in 2010 [2] presented a solid state transformer (SST) based ER concept and

described the IoE architecture. The operation of the energy router in the microgrids has been described in many papers. Complementary energy exchange via ER between adjacent microgrids is addressed in [1]. It is based on the idea that adjacent microgrids may have complementarity in terms of the pattern of energy production and consumption, which can be utilized to compensate for each other's instant energy deficiency. In [4] the ER control strategy inside a microgrid consisting of photovoltaic energy, a battery ES and electric vehicles is studied. In [5] focus is on the use of a hybrid converter as an ER in a DC nanogrid scenario. An application scenario of the ER for low-voltage and small-capacity users in households is presented in [6].

In our paper, the energy router concept will be implemented in nearly zero energy buildings (NZEB) to provide flexible energy management. Typically, the NZEB consists of energy sources, loads and storages. It possesses independent controls and can operate either in grid connected or islanded mode. Regarding these features, NZEB can be seen as a hybrid nanogrid [7,8]. The main goal of the ER is to maintain regulated voltage and frequency inside the NZEB in all operation modes. In addition, the ER could provide many active functions such as:

- Power control (active and reactive power injection/absorption);
- voltage control (compensation of voltage sags and peaks, control of voltage harmonics, frequency control inside the building);
- current control (harmonic cancelation, short-circuit current limitation);
- simplifies integration of distributed energy sources (provides DC and AC ports control);
- protection functions (island detection, frequency, voltage and current monitoring, short circuit protection);
- increased reliability (modular structure, redundant supply, on/off-grid operation).

Providing stable frequency and voltage in the microgrid with distributed generation could be challenging. Traditionally, the frequency and voltage were connected to each other through rotating masses, e.g., synchronous generators. A variation in the load changes the frequency of the generator, which will also change the grid voltage. Today, power electronics are used to interface loads, sources and storage. This decouples the grid from sources and the system becomes inertialess. Inertialess grids are characterized by fast dynamical processes where voltage and frequency are not dependent on each other [9]. A well-known solution to this problem is the droop control, which emulates the operation of a rotating generator [9–11]. Droop controls allow for connection to many micro sources in parallel and share power proportionally between each other.

However, most conventional power electronic converters in household, residential or office buildings are not compatible with the droop control and new power converters need to be installed. Our goal was to design an ER for the NZEB that would be applicable in conventional buildings with minimal cost and modifications. In this case, the droop control is not a convenient solution. We proposed a solution where ER is working as a single grid-forming converter with a predefined voltage reference [12,13]. All micro sources in the NZEB must be grid followers, i.e., they are current controlled and inject power synchronously with the grid.

A single-phase back to back converter topology was selected for the realization of the concept. It inherently includes DC and AC ports (Figure 1), which makes it a suitable candidate for micro- and nanogrids [14]. The ER connects to the grid via the input inverter Inv1. At this port, power quality is the most important requirement regulated by multiple norms. This is also a bidirectional port that allows energy injection back to the grid. The second port is a DC port to access energy storage, local energy generation, DC-loads etc. The third port is a bidirectional AC port with the grid-forming inverter Inv2, which is connected to the house appliances, as shown in Figure 1. In the case of NZEB, house appliances not only include loads but also storage and sources. House appliances work as grid followers that either consume or generate power synchronously with the grid.

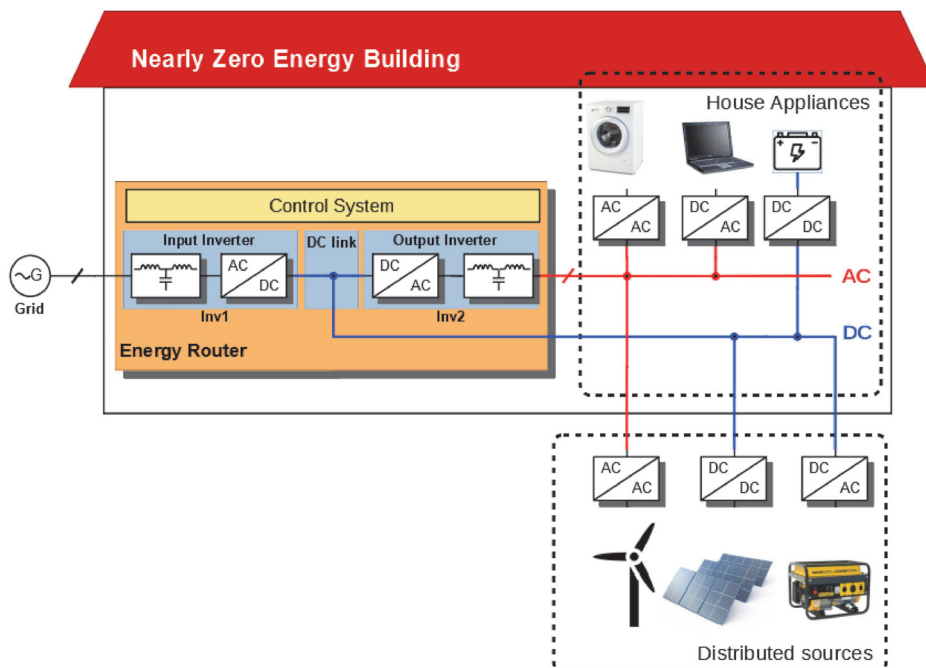


Figure 1. The structure of the energy router for a nearly zero energy building (NZEB).

In [13] all possible operation modes of the proposed ER were described. The goal of our paper is to focus in detail on the control and stability issues of the building side inverter Inv2 in the voltage source operation mode and the idle operation mode in particular. This mode is a very important and expected to be utilized often. One of the biggest challenges is the idle (no-load) operation where traditional regulators, e.g., proportional-resonant (PR), PID, will not meet the control design requirements. To gain the stability of the system, we propose model predictive control (MPC) for Inv2. The paper first analyzes the stability issues of Inv2 in different load conditions with a conventional regulator in order to identify the problem. Then the MPC algorithm is proposed as an alternative solution. It is explained in Section 3. Optimal parameters are tuned by means of simulation in Section 4. Finally, the simulation results are verified on an experimental prototype.

2. Voltage Source Operation of the Output Inverter

We propose a concept where the ER operates as a single grid-forming converter. The ER has back to back topology with fixed DC-link. This paper focuses on the output inverter, which is emulating the behavior of the grid for the house appliances. Figure 2 shows a simplified model of the output inverter, which consists of a single-phase full-bridge, a DC voltage source, an LCL filter, and a load. In this paper, we assume that a load has a simple resistance R_L . The most demanding operation point of the output inverter is the no-load operation. This situation happens when the load exactly matches the generation of the NZEB and no power is taken from the grid. In the no-load operation, Inv2 should still provide sinusoidal output voltage like a grid.

To analyze the stability of the system, a small signal model of the inverter was derived. The inverter can be seen as a duty-cycle controlled voltage source, as shown in Figure 2.

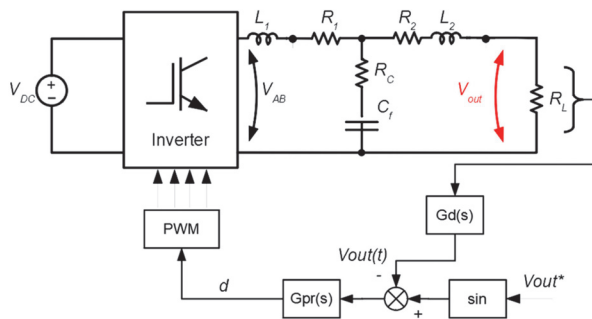


Figure 2. Model of the energy router (ER) output inverter with LCL filter and proportional-resonant (PR) voltage regulator.

The dynamics of the system is defined by the LCL filter, which will be the plant. The state space equations of the plant are:

$$\begin{cases} \frac{dx(t)}{dt} = A \cdot x(t) + B \cdot u(t) \\ y(t) = Cx(t) + Eu(t) \end{cases} \quad (1)$$

where

$$A = \begin{bmatrix} \frac{-(R_1+R_C)}{L_1} & \frac{R_C}{L_1} & -\frac{1}{L_1} \\ \frac{R_C}{L_2} & -\frac{(R_2+R_C+R_L)}{L_2} & \frac{1}{L_2} \\ \frac{1}{C_f} & -\frac{1}{C_f} & 0 \end{bmatrix}, C = [0 \quad R_L \quad 0], B = \begin{bmatrix} \frac{1}{L_1} \\ 0 \\ 0 \end{bmatrix}, E = 0 \quad (2)$$

and the state, input and output vectors are defined as:

$$x(t)^T = [i_1(t) \quad i_2(t) \quad v_C(t)] \quad (3)$$

$$u(t) = [v_{AB}(t)] \quad (4)$$

$$y(t) = v_{out}(t) \quad (5)$$

After simplification and Laplace transform, the transfer function of the plant is derived:

$$G_{vv}(s) = \frac{v_{out}}{v_{ab}} = \frac{R_L + C_f \cdot R_C \cdot R_L s}{a_3 s^3 + a_2 s^2 + a_1 s + a_0} \quad (6)$$

where

$$a_3 = C_f L_1 L_2,$$

$$a_2 = C_f L_1 R_2 + C_f L_2 R_1 + C_f L_1 R_C + C_f L_2 R_C + C_f L_1 R_L,$$

$$a_1 = L_1 + L_2 + C_f R_1 R_2 + C_f R_1 R_C + C_f R_2 R_C + C_f R_1 R_L + C_f R_C R_L,$$

$$a_0 = R_1 + R_2 + R_L.$$

In the case of ER most of the presented works simply use droop control, where the grid frequency and voltage are formed jointly by distributed sources [14,15]. In this case, the idle operation of the ER represents no difficulties. However, it is a major problem in the case of a single grid-forming inverter. Different structures of control systems have been proposed for grid-connected inverters [16–18]. The same algorithms can be used for a grid-off inverter like ER. One of the most used inverter control approaches is the dual-loop: The outer loop with slower dynamics in the time domain and the

inner loop with very fast response to control the current. Regarding this inner current control loop, its controller can be classified as nonlinear and linear. Hysteresis [19], predictive [20,21] and dead beat controller [22–24] types belong to the first controller’s group, presenting high robustness and fast dynamic response. On the other hand, linear current controllers such as proportional-integral (PI) based, PR based or repetitive controller based have been successfully used [25–28]. The PR controller, first proposed in [26], is quite a simple and attractive solution in the case of abc-naturally or $\alpha\beta$ -stationary reference implementation frames because it can overcome two well-known drawbacks of the conventional PI controller: Inability to track a sinusoidal reference with zero steady-state error and poor disturbance rejection capability. Many detailed studies addressing that type of controller have been reported.

In our work, the PR controller is selected as a reference controller. Figure 2 depicts the closed loop control system with a PR controller.

The PR controller is defined by the equation below:

$$G_{PR}(s) = K_P + K_R \frac{2w_c s}{s^2 + 2w_c s + w_o^2} \quad (7)$$

where K_P, K_R , and w_c, w_o are proportional gain, integral gain, cut-off frequency, and resonance frequency respectively. Assuming a digital delay of one sampling period, the closed-loop transfer function in a discrete domain can be derived as:

$$G_{closed\ loop}(z) = \frac{G_{PR}(z) \times G_{VV}(z)}{1 + G_{PR}(z) \times G_D(z) \times G_{VV}(z)} \quad (8)$$

where $G_D(z)$ is the digital delay transfer function. It can be calculated as follows:

$$G_D(z) = z^{-1} \quad (9)$$

The pole-zero map of the closed-loop system with different load resistance values is presented in Figure 3. Results of the study of the pole-zero map behavior indicate a tendency of poles directed towards the right-half plane when the load resistance is increased.

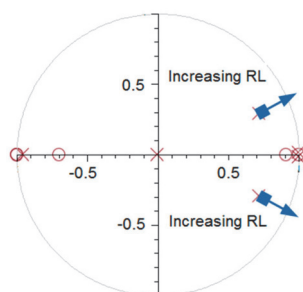


Figure 3. Pole-zero tendency map in Z-domain for different load resistance values.

3. Indirect Model Predictive Control Proposed for Voltage Source Mode

The study of the pole-zero map of the closed loop system showed that the conventional PR regulator has a tendency towards instability with the decreasing load. Thus, the PR control cannot be used in the idle mode.

Among nonlinear methods, MPC, which is a well-known approach from the 1980s, has attracted high interest [20,21]. However, the complexity of MPC imposes limitations to its utilization in power electronics. With the progress of computational resources, it becomes more and more feasible for industrial applications in power electronics [29–32].

MPC is a family of controllers that explicitly uses the model of the system to be controlled. In general, MPC defines the control action by minimizing a cost function that describes the desired system behavior. This cost function compares the predicted system output with a reference. The predicted outputs are computed from the system model. In general, for each sampling time the MPC controller calculates a control action sequence that minimizes the cost function, but only the first element of this sequence is applied to the system [31]. Typically, system identification is used to improve the accuracy of the MPC. System identification methods have been extensively studied for energy efficient buildings [33,34]. In this paper we study ER in idle mode. Thus, we only have predefined passive components of the LCL filter and in the case of acceptable tolerance (10%–20%) we do need any identification.

Many research papers have addressed the grid-connected systems [34–39]. At the same time, none of them address no-load or idle operation of the inverter. In the ER concept, this mode has to be realized to provide a reference output voltage. Our paper is devoted to indirect MPC (iMPC) study of an inverter operating in voltage source mode. The simulations demonstrate the effect of iMPC in no-load operation, while the experiments also show a power step from a no-load to a loaded operation. Thus, iMPC is able to control the output voltage with and without the load. The iMPC design procedure is described below.

Figure 4 shows the output filter along with the control system structure. The main purpose of the control system is to provide the output voltage $v_{out}(t)$ according to the reference sinusoidal signal. This signal along with measured currents in inductors $i_{L1}(t)$, $i_{L2}(t)$, and DC-link voltage $v_{dc}(t)$ is given to the iMPC block.

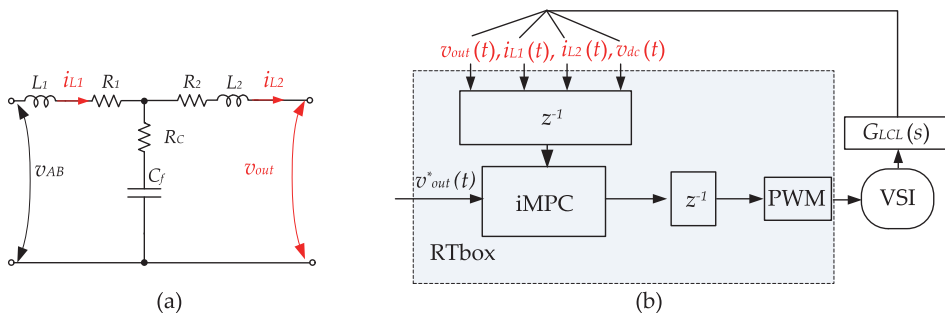


Figure 4. Equivalent circuit of the output filter (a) along with the control system structure (b).

This signal along with measured currents in inductors $i_{L1}(t)$, $i_{L2}(t)$, and DC-link voltage $v_{dc}(t)$ is given to the iMPC block. In a very general case of iMPC, the dynamic system is represented by the continuous vector of state space variables:

$$x(t) = [i_{L1}(t), i_{L2}(t), v_{cf}(t)]^T \tag{10}$$

After deriving the measured values, the first step is to estimate the grid current value during the next samples in the discrete time domain:

$$x(n + 1) = F \cdot x(n) + G u(n) \tag{11}$$

where $u(n)$ is the input vector

$$u(n) = [v_{ab}(n), v_{out}(n)]^T \tag{12}$$

and F and G are dynamic matrixes that correspond to a discrete small signal model of the LCL filter. The dynamic matrixes are as follows:

$$F = \begin{bmatrix} f_1 & f_2 & f_3 \\ f_4 & f_5 & f_6 \\ f_7 & f_8 & 1 \end{bmatrix} \quad (13)$$

$$G = \begin{bmatrix} g_1 & 0 \\ 0 & g_4 \\ 0 & 0 \end{bmatrix} \quad (14)$$

where

$$f_1 = 1 - (R_1 + R_C) \frac{T_S}{L_1}; f_2 = \frac{R_C T_S}{L_1}; f_3 = -\frac{T_S}{L_1} \quad (15)$$

$$f_4 = \frac{R_C T_S}{L_2}; f_5 = 1 - (R_2 + R_C) \frac{T_S}{L_2}; f_6 = \frac{T_S}{L_2} \quad (16)$$

$$f_7 = \frac{T_S}{C_f}; f_8 = -\frac{T_S}{C_f} \quad (17)$$

$$g_1 = \frac{T_S}{L_1}; g_4 = -\frac{T_S}{L_2} \quad (18)$$

and T_S is the sampling time.

It should be noted that the capacitor voltage of the output filter is not measured; it can be predicted as well, taking into account current across inductors and initial voltage that is assumed to be zero during the start-up process. The predicted capacitor value $v_c(n + 1)$ can be derived from Equations (10)–(18).

Finally, the output voltage can be predicted as:

$$v_{out}(n + 1) = v_c(n + 1) - \frac{(i_{L2}(n + 1) - i_{L2}(n))}{-g_4}. \quad (19)$$

It is obvious that it depends on the further output inverter voltage $v_{ab}(n + 1)$ and the measured parameters. As a result, the voltage error can be estimated:

$$\Delta v_{out}(i) = v_{out}(i) - v_{out_ref}(i), \quad (n + 1 \geq i \geq n + p). \quad (20)$$

Finally, to select the optimal sequence of the applied inverter voltage, the cost function $J[d]$ is introduced:

$$J[d] = |\Delta v_{out}(n + 1)| + I + |\Delta v_{out}(n + p)|. \quad (21)$$

The function quantizes estimations of different summarized output voltage errors. And each of those estimations can be associated with a possible scenario d , which could occur at the prediction horizon. As any MPC method is associated with a fixed switching frequency, a finite number of scenarios was considered as well. This process is illustrated in Figure 5.

It should be mentioned that in any case, the output inverter voltage is expected to be close to the sinusoidal reference signal. Some deviation from the reference value is required to smooth the output voltage in the case of load connection and to avoid resonance oscillation in the output filter. Also, it provides compensation of the voltage drop across the inductors. Based on this, a specific possible reference voltage $v_{ib}(i, d)$ during the cost function evaluation is expressed as:

$$v_{ab}(i, d) = v_{out_ref}(i) + \Delta v_{ab}(i, d). \quad (22)$$

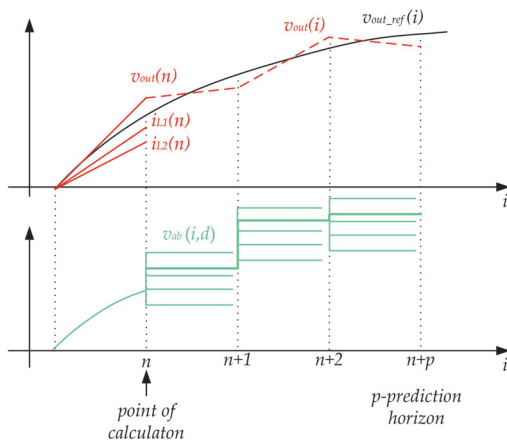


Figure 5. Proposed indirect model predictive control (iMPC) approach.

4. Optimal Parameters Selection of iMPC

The main criterion of the quality of the grid current is the total harmonic distortion (THD) factor. At the same time, from the above description, it is evident that it depends on the horizon prediction p and the voltage quantizing d . Due to the nonlinearity of the discussed control, the most suitable tuning approach is simulation. The PLECS (4.2.6, Plexim GmbH, Zurich, Switzerland) simulation software was used in our work. Table 1 shows the main inverter parameters used for the simulation and final experimental verification.

Table 1. Components and parameters of the inverter used for simulation and experiments.

Parameter	Value
Power step in experiments	0–700 W
Input DC voltage V_{IN}	400 V
Output AC RMS voltage V_{OUT}	230 V
Inverter side inductor L_1	1.44 mH
Resistance of L_1 windings R_1	0.05 Ω
Output side inductor L_2	0.6 mH
Resistance of L_2 windings R_2	0.03 Ω
Filter capacitor C_f	9.6 μF
Resistance of C_f R_C	0.5 Ω
Sampling frequency f_s	20 kHz
Switching frequency f_{SW}	20 kHz

According to Equation (22), the output voltage value was selected close to the reference output voltage value $v_{out}(i)$ with respective voltage deviations $\Delta v_{ab}(i,d)$. During each sampling, 21 possible output voltage deviation values were considered. This number is constant from sample by sample. But the possible minimum and maximum value can be different:

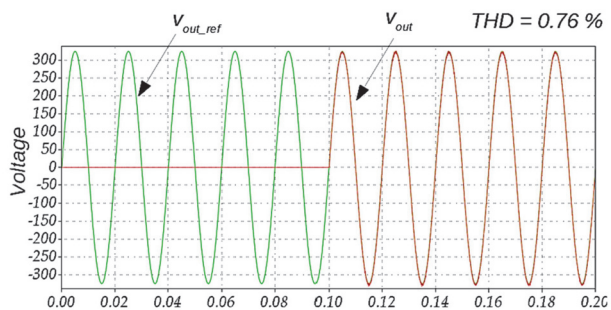
$$-\Delta v_{ab_max} < \Delta v_{ab}(i,d) < \Delta v_{ab_max} \tag{23}$$

Figure 6 shows the simulation results with different Δv_{ab_max} values. The reference root mean square (RMS) output voltage was set to 230 V.

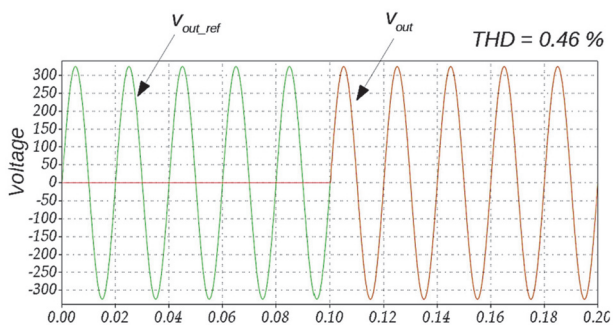
Figure 6 shows two waveforms. The first waveform corresponds to the ideal sinusoidal reference output voltage v_{out_ref} . At the moment of time 0.1 s, transistors start operating. It can be seen that a decrease in the output voltage deviation leads to an improvement of the THD of the output voltage.

Both simulation results were derived for the horizon prediction $p = 1$. This is the simplest case and requires minimum calculation resources. Figure 7 shows the output voltage under different deviation voltage values at the horizon prediction $p = 2$. No significant improvements of the THD can be observed while the calculation complexity increases noticeably. Since 21 possible output voltage deviation values were considered, the overall iteration number N can be simply calculated as:

$$N = 21^p \tag{24}$$

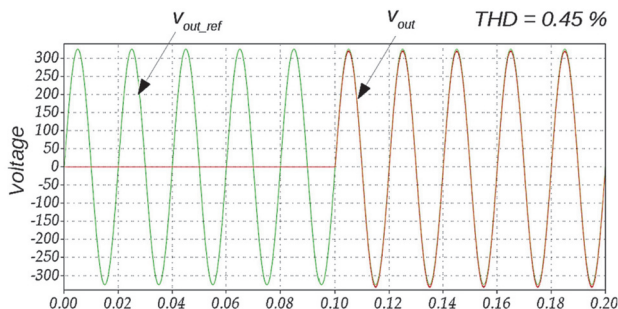


(a)



(b)

Figure 6. Output voltage waveforms under different deviation voltage values for the horizon prediction $p = 1$: $\Delta v_{ab_max} = 40$ V (a), $\Delta v_{ab_max} = 5$ V (b).



(a)

Figure 7. Cont.

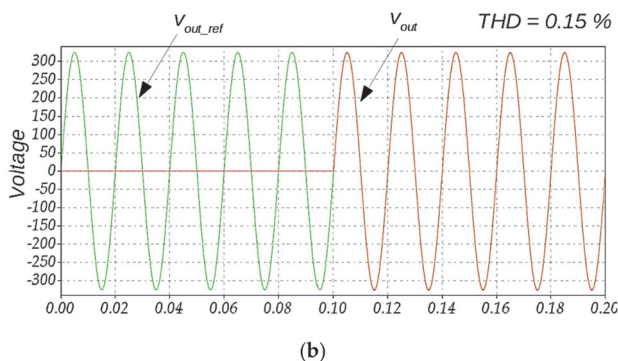


Figure 7. Output voltage waveforms under different deviation voltage values for the horizon prediction $p = 2$: $\Delta v_{ab_max} = 40$ V (a), $\Delta v_{ab_max} = 5$ V (b).

It means that in the case $p = 1$ we have only 21 iterations, but in the case $p = 2$ we have 441 iterations. Thus, the simplest case from the practical aspect, the horizon prediction $p = 1$, should be used in a real microcontroller.

The non-significant impact of the horizon prediction on the output voltage waveform can be explained by a simplified model without a capacitor voltage measurement. At the same time, this approach has no redundancy and is feasible for practical application.

5. Experimental Verification

To verify the simulation results, an experimental study was conducted. Figure 8 shows the experimental prototype of the ER. It is a single-phase back to back converter with a three-port structure: Two AC ports and one DC port. Table 1 shows the experimental parameters. The inverters are based on isolated gate bipolar transistors (IKW40N65F5). The control system has six sensors: Input voltage, current, DC-link voltage, output voltage, and both inductor currents. The current sensors are based on the Hall effect current transducer ACS712 and the voltage sensors are based on the precision optically isolated voltage sensor ACPL-C87A. Rapid control platform RT Box from PLECS was used as a control system. The control system was first simulated and then used for the real demonstration.

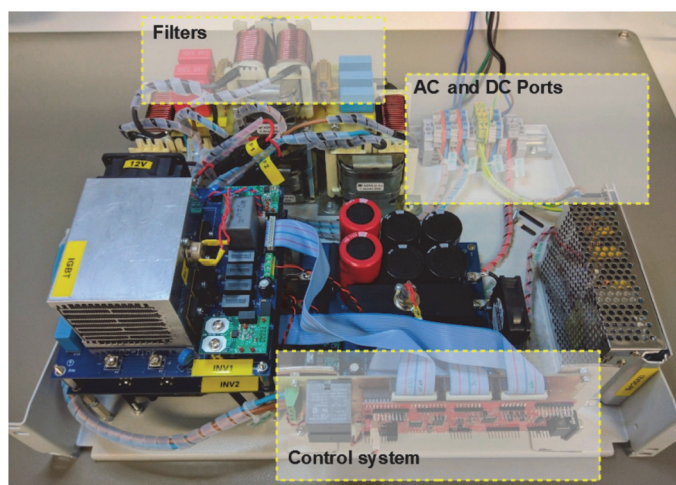


Figure 8. Experimental prototype of the energy router.

In the first experiment the instable operation of the PR regulator in the idle mode was demonstrated. Since the unstable operation is a non-controllable process and could easily damage the hardware, we conducted this experiment with reduced power and voltage levels. In the idle operation the PR regulator is not able to provide sinusoidal voltage, as shown in Figure 9. The sinusoidal voltage shape is restored after the load is switched on.

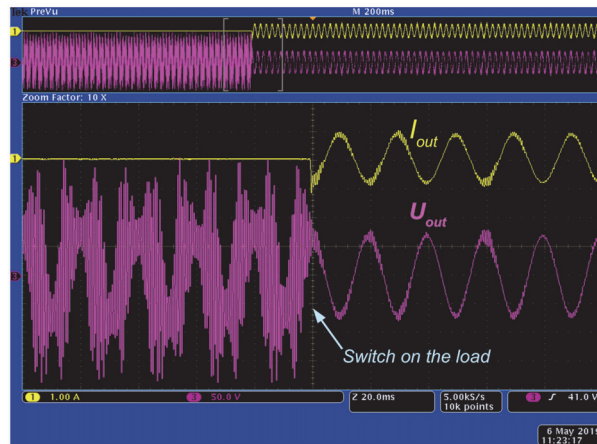


Figure 9. Unstable operation of the PR regulator in the idle mode.

In the following experiment, the performance of the iMPC algorithm in the idle mode was tested. In this mode, the load of the NZEB exactly matched the generation and no power was needed from the grid, i.e., the ER was operating in no load mode. Nevertheless, it should still sustain sinusoidal output with the grid frequency. The iMPC algorithm successfully fulfilled this task, as depicted in Figure 10. The RMS value of the output voltage was about 230 V while the current was zero.

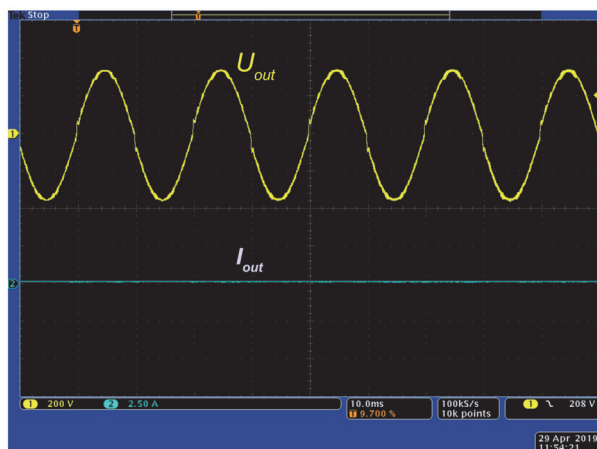


Figure 10. ER output voltage in idle operation mode.

The NZEB is characterized by highly dynamic properties. The load and generation can change rapidly. The ER should be able to respond to those changes by keeping its output voltage stable and sinusoidal. To test these properties, a load step from 0 to 700 W was added to the output of the ER. Figure 11 shows the result of the load step. The current jumped from 0 to about 3.5 A_{rms} while the voltage remained stable at 230 V_{rms} and 50 Hz.

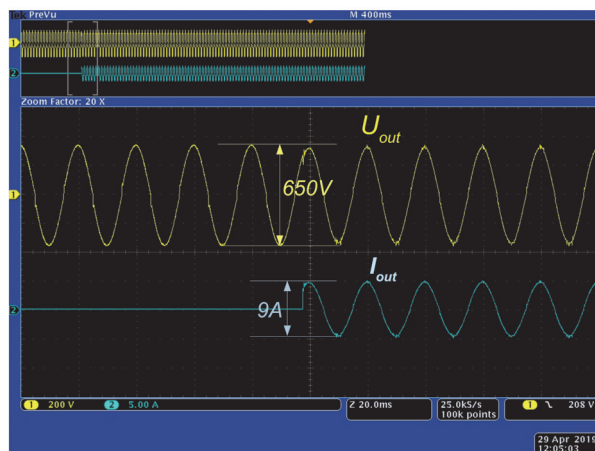


Figure 11. Inverter output voltage and current at the power step from 0 to 700 W.

6. Conclusions

The energy router (ER) can be considered as a key element of the micro- and nanogrids. Through smart energy management the power balance in the micro- and nanogrids can be maintained without utilizing oversized and expensive batteries. Among other active functions, the ER's goal is to maintain regulated voltage and frequency inside the micro- or nanogrid. In this paper we studied the ER role in the nearly zero energy buildings (NZEB), which can be seen as a hybrid nanogrid. Typically, droop control will be implemented in such systems. However, most conventional power electronic converters in residential or office buildings are not compatible with droop control and new power converters need to be installed. Our goal was to design an ER for the NZEB that would be applicable in conventional buildings with minimal cost and modifications. We proposed a solution where the ER is working as a single grid-forming converter with predefined voltage reference. In this case the most challenging operation point is the idle operation that happens when the load exactly matches the generation within the NZEB.

PR control is a well-known algorithm to regulate sinusoidal signals. Typically, it is used in voltage or current controlled inverters. However, PR control has its limitations. This paper shows that the PR control tends towards instability in small or no-load operation. Thus, it cannot be used in the case of a single grid forming inverter, it should be able to deliver sinusoidal voltage also in idle mode. Our proposal is to use indirect model predictive control (iMPC), which gave good results in both idle and loaded operation mode. The tuning procedure of the iMPC method was explained. As a result, it was found that the dependency between the quality of the output voltage and the horizon prediction p is small. It is shown that the most optimal p value is the simplest case $p = 1$. Increasing the horizon prediction level would only slightly improve the THD of the output voltage but significantly increase the calculation burden of the controller. The experimental results verified that the proposed iMPC method is capable of regulating the output voltage in both idle and loaded operation mode and it can handle the fast-dynamic nature of NZEB.

The further research includes study of the proposed iMPC method in the case of real non-linear loads in NZEB. In this case also system identification will become an important research topic.

Author Contributions: Conceptualization, O.H.; formal analysis, O.H. and M.N.; funding acquisition, I.R.; investigation, I.R. and M.N.; methodology, O.H.; project administration, I.R.; supervision, I.R.; validation, T.J.; writing—original draft, I.R., O.H. and M.N.; writing—review and editing, J.R.

Funding: This research was supported by the Estonian Research Council grant PUT1680, and co-financed by the Estonian Centre of Excellence in Zero Energy and Resource Efficient Smart Buildings and Districts, ZEBE, grant 2014-2020.4.01.15-0016 funded by the European Regional Development Fund.

Conflicts of Interest: The authors declare no conflict of interest.

References

1. Liu, Y.; Fang, Y.; Li, J. Interconnecting microgrids via the energy router with smart energy management. *Energies* **2017**, *10*, 1297.
2. Huang, A.Q.; Crow, M.L.; Heydt, G.T.; Zheng, J.P.; Dale, S.J. The future renewable electric energy delivery and management (FREEDM) system: The energy internet. *IEEE* **2011**, *99*, 133–148. [[CrossRef](#)]
3. Fu, R.; Remo, T.; Margolis, R. 2018 U.S. Utility-Scale Photovoltaics Plus-Energy Storage System Costs Benchmark. Report of National Renewable Energy Laboratory. Available online: www.nrel.gov/publications (accessed on 22 March 2019).
4. Liu, Y.; Li, Y.; Liang, H.; He, J.; Cui, H. Energy routing control strategy for integrated microgrids including photovoltaic, battery-energy storage and electric vehicles. *Energies* **2019**, *12*, 302. [[CrossRef](#)]
5. Ray, O.; Mishra, S. Integrated hybrid output converter as power router for renewable-based nanogrids. In Proceedings of the In IECON 2015—41st Annual Conference of the IEEE Industrial Electronics Society, Yokohama, Japan, 9–12 November 2015; pp. 001645–001650.
6. Zhen, L.; Penghua, L.; Wanxing, S.; Songhuai, D.; Qing, D.; Zhipeng, L. Research on a household energy router for energy internet. In Proceedings of the 2018 13th IEEE Conference on Industrial Electronics and Applications (ICIEA), Wuhan, China, 31 May–2 June 2018; pp. 952–957.
7. Hagh, M.T.; Aghdam, F.H. Smart hybrid nanogrids using modular multiport power electronic interface. In Proceedings of the 2016 IEEE Innovative Smart Grid Technologies—Asia (ISGT-Asia), Melbourne, Australia, 28 November–1 December 2016; pp. 618–623.
8. Mishra, S.; Ray, O. Advances in nanogrid technology and its integration into rural electrification in India. In Proceedings of the 2014 International Power Electronics Conference (IPEC-Hiroshima 2014—ECCE ASIA), Hiroshima, Japan, 18–21 May 2014; pp. 2707–2713.
9. Pedrasa, M.; Spooner, T. A survey of techniques used to control microgrid generation and storage during island operation. Available online: <https://pdfs.semanticscholar.org/01f7/e8ceb853c7bc1073ad390b3dc6736ca31c41.pdf> (accessed on 29 April 2019).
10. Engler, A.; Soutlanis, N. Droop control in LV-grids. In Proceedings of the 2005 International Conference on Future Power Systems, Amsterdam, The Netherlands, 18 November 2005; p. 6.
11. Shoeiby, B.; Davoodnezhad, R.; Holmes, D.G.; McGrath, B.P. A resonant current regulator based microgrid control strategy with smooth transition between islanded and grid-connected modes. In Proceedings of the 2014 IEEE 5th International Symposium on Power Electronics for Distributed Generation Systems (PEDG), Galway, Ireland, 24–27 June 2014.
12. Roasto, I.; Rosin, A.; Jalakas, T. Power electronic interface converter for resource efficient buildings. In Proceedings of the IECON 2017—43rd Annual Conference of the IEEE Industrial Electronics Society, Beijing, China, 29 October–1 November 2017; pp. 3638–3643.
13. Roasto, I.; Rosin, A.; Jalakas, T. Multiport interface converter with an energy storage for nanogrids. In Proceedings of the IECON 2018—44th Annual Conference of the IEEE Industrial Electronics Society, Washington, DC, USA, 21–23 October 2018; pp. 6088–6093.
14. Majumder, R. A hybrid microgrid with dc connection at back to back converters. *IEEE Trans. Smart Grid* **2014**, *5*, 251–259. [[CrossRef](#)]
15. Boroyevich, D.; Cvetkovic, I.; Dong, D.; Burgos, R.; Wang, F.; Lee, F. Future electronic power distribution systems a contemplative view. In Proceedings of the 2010 12th International Conference on Optimization of Electrical and Electronic Equipment, Basov, Romania, 20–22 May 2010; pp. 1369–1380.
16. Blaabjerg, F.; Teodorescu, R.; Liserre, M.; Timbus, A.V. Overview of control and grid synchronization for distributed power generation systems. *IEEE Tran. Ind. Electron.* **2006**, *53*, 1398–1409. [[CrossRef](#)]
17. Timbus, A.; Liserre, M.; Teodorescu, R.; Rodriguez, P.; Blaabjerg, F. Evaluation of current controllers for distributed power generation systems. *IEEE Trans. Power Electron.* **2009**, *24*, 654–664. [[CrossRef](#)]
18. Zeng, Z.; Yang, H.; Zhao, R.; Cheng, C. Topologies and control strategies of multi-functional grid-connected inverters for power quality enhancement: A comprehensive review. *Renew. Sust. Energ. Rev.* **2013**, *24*, 223–270. [[CrossRef](#)]

19. Husev, O.; Chub, A.; Romero-Cadaval, E.; Roncero-Clemente, C.; Vinnikov, D. Hysteresis current control with distributed shoot-through states for impedance source inverters. *Int. J. Circuit Theory Appl.* **2015**, *44*, 783–797. [[CrossRef](#)]
20. Rodriguez, J.; Kolar, J.; Espinoza, J.; Rivera, M.; Rojas, C. Predictive torque and flux control of an induction machine fed by an indirect matrix converter with reactive power minimization. In Proceedings of the 2010 IEEE International Symposium on Industrial Electronics, Bari, Italy, 4–7 July 2010; pp. 3177–3183.
21. Kennel, R.; Linder, A. Predictive control of inverter supplied electrical drives. Proceedings of 2000 IEEE 31st Annual Power Electronics Specialists Conference. Conference Proceedings (Cat. No.00CH37018), Galway, Ireland, 23 June 2000.
22. Gholami-Khesht, H.; Monfared, M. Deadbeat direct power control for grid connected inverters using a full-order observer. In Proceedings of the 2015 4th International Conference on Electric Power and Energy Conversion Systems (EPECS), Sharjah, UAE, 24–26 November 2015; pp. 1–5.
23. Buso, S.; Caldognetto, T.; Brandao, D.I. Oversampled dead-beat current controller for voltage source converters. In Proceedings of the 2015 IEEE Applied Power Electronics Conference and Exposition (APEC), Charlotte, NC, USA, 15–19 March 2015; pp. 1493–1500.
24. Wang, L.; Ertugrul, N.; Kolhe, M. Evaluation of dead beat current controllers for grid connected converters. In Proceedings of the IEEE PES Innovative Smart Grid Technologies, Tianjin, China, 21–24 May 2012; pp. 1–7.
25. Jiao, J.; Nelms, R.M. Regulating output impedance using a PI controller to improve the stability of a single phase inverter under weak grid. In Proceedings of the 2016 IEEE 16th International Conference on Environment and Electrical Engineering (EEEIC), Florence, Italy, 7–10 June 2016; pp. 1–6.
26. Sato, Y.; Ishizuka, T.; Nezu, K.; Kataoka, T. A new control strategy for voltage-type PWM rectifiers to realize zero steady-state control error in input current. *IEEE Trans. Ind. Appl.* **1998**, *34*, 480–486. [[CrossRef](#)]
27. Chattopadhyay, R.; De, A.; Bhattacharya, S. Comparison of PR controller and damped PR controller for grid current control of LCL filter based grid-tied inverter under frequency variation and grid distortion. In Proceedings of the 2014 IEEE Energy Conversion Congress and Exposition (ECCE), Pittsburgh, PA, USA, 14–18 September 2014; pp. 3634–3641.
28. Husev, O.; Roncero-Clemente, C.; Makovenko, E.; Pimentel, S.P.; Vinnikov, D.; Martins, J. Optimization and implementation of the proportional-resonant controller for grid-connected inverter with significant computation delay. *IEEE Trans. Ind. Electron.* **2019**, *1*. [[CrossRef](#)]
29. Cutler, R.; Ramaker, B.L. Dynamic Matrix Control—A Computer Control Algorithm. Available online: <https://www.infona.pl/resource/bwmeta1.element.ieee-art-000004232009> (accessed on 20 April 2019).
30. Richalet, J.; Rault, A.; Testud, J.D.; Papon, J. Model predictive heuristic control: applications to industrial processes. *Automatica* **1978**, *14*, 413–428. [[CrossRef](#)]
31. Vazquez, S.; Rodriguez, J.; Rivera, M.; Franquelo, L.G.; Norambuena, M. Model Predictive control for power converters and drives: Advances and trends. *IEEE Trans. Ind. Electron.* **2017**, *64*, 935–947. [[CrossRef](#)]
32. Rodriguez, J.; Kazmierkowski, M.P.; Espinoza, J.; Zanchetta, P.; Abu-Rub, H.; Young, H.A.; Rojas, C.A. State of the art of finite control set model predictive control in power electronics. *IEEE Trans. Ind. Inf.* **2013**, *9*, 1013–1016. [[CrossRef](#)]
33. Anas, A.; Ellis, M.J.; Bernal, J.E.T.; Wenzel, M.J. Practice-Oriented System Identification Strategies for MPC of Building Thermal and HVAC Dynamics. Available online: <https://docs.lib.purdue.edu/cgi/viewcontent.cgi?article=1254&context=ihpbc> (accessed on 21 April 2019).
34. Ellis Matthew, J.; Alanqar, A. Formulation and Application of an Economic Model Predictive Control Scheme for Thermostats. Available online: <https://docs.lib.purdue.edu/cgi/viewcontent.cgi?article=1262&context=ihpbc> (accessed on 18 April 2019).
35. Zhang, Z.; Li, Z.; Kazmierkowski, M.P.; Rodriguez, J.; Kennel, R. Robust predictive control of three-level npc back-to-back converter pmsg wind turbine systems with revised predictions. *IEEE Trans. Power Electron.* **2018**, *33*, 9588–9598.
36. Zhang, X.; Tan, L.; Xian, J.; Zhang, H.; Ma, Z.; Kang, J. Direct grid-side current model predictive control for grid-connected inverter with LCL filter. *IET Power Electron.* **2018**, *11*, 2450–2460. [[CrossRef](#)]

37. Moreno, J.C.; Huerta, J.M.E.; Gil, R.G.; González, S.A. A robust predictive current control for three-phase grid-connected inverters. *IEEE Trans. Ind. Electron.* **2009**, *56*, 1993–2004. [[CrossRef](#)]
38. Wang, X.; Zou, J.; Peng, Y.; Xie, C.; Li, K.; M, J.; Zapata, G. Elimination of zero sequence circulating currents in paralleled three-level T-type inverters with a model predictive control strategy. *IET Power Electron.* **2008**, *11*, 2573–2581. [[CrossRef](#)]
39. Yang, G.; Hao, S.; Fu, C.; Chen, Z. Model predictive direct power control based on improved T—Type Grid Connected Inverter. *IEEE J. Emerg. Sel. Top. Power Electron.* **2018**, *7*, 252–260. [[CrossRef](#)]



© 2019 by the authors. Licensee MDPI, Basel, Switzerland. This article is an open access article distributed under the terms and conditions of the Creative Commons Attribution (CC BY) license (<http://creativecommons.org/licenses/by/4.0/>).

Publication III

M. Najafzadeh, O. Husev, R. Strzelecki, I. Roasto, N. Strzelecka, D. Vinnikov. Grid-Forming Operation of Energy-Router Based on Model Predictive Control with Improved Dynamic Performance. *Energies*, 2022, Accepted for Publication.

Article

Grid-Forming Operation of Energy-Router Based on Model Predictive Control with Improved Dynamic Performance

Mahdieh Najafzadeh ¹, Natalia Strzelecka ^{2,*}, Oleksandr Husev ¹, Indrek Roasto ¹, Kawsar Nassereddine ³, Dmitri Vinnikov ¹ and Ryszard Strzelecki ⁴

¹ Department of Electrical Power Engineering and Mechatronics, Tallinn University of Technology, 19086 Tallinn, Estonia; mahdieh.najafzadeh@taltech.ee (M.N.); oleksandr.husev@taltech.ee (O.H.); indrek.roasto@ieee.org (I.R.); dmitri.vinnikov@taltech.ee (D.V.)

² Faculty of Electrical Engineering, Gdynia Maritime University, 81-225 Gdynia, Poland

³ Faculty of Engineering, Lebanese University, Beirut 6573, Lebanon; nassereddinejana@gmail.com

⁴ Faculty of Electrical and Control Engineering, Gdańsk University of Technology, 80-233 Gdańsk, Poland; ryszard.strzelecki@pg.edu.pl

* Correspondence: n.strzelecka@we.umg.edu.pl

Abstract: The focus of this study is on the grid-forming operation of the Energy Router (ER) based on Model Predictive Control (MPC). ER is regarded as a key component of microgrids. It is a converter that interfaces the microgrid (s) with the utility grid. The ER has a multiport structure and bidirectional energy flow control. The ER concept can be implemented in Nearly Zero-Energy Buildings (NZEB) to provide flexible energy control. A concept is proposed where the ER works as a single grid-forming converter. The challenge is to keep the predefined reference voltage and frequency inside the NZEB in all possible modes, including the idle operation mode, current sources, and nonlinear load control. To gain stability and output voltage quality, the MPC is proposed. The design of the modified MPC algorithm with improved dynamics performance is explained. PLECS software is utilized to verify the proposed algorithm. The results demonstrate the suitable performance of the proposed control method in terms of total harmonic distortion of the output voltage. The influence of weighting coefficients is evaluated, showing the higher impact of the capacitor filter voltage on lowering the total harmonics distortion of the output voltage. Finally, the capability of the control system toward step change in the reference value is evaluated.

Keywords: energy router; current sources; nonlinear load; grid-forming control; bidirectional power flow control; model predictive control



Citation: Najafzadeh, M.; Strzelecka, N.; Husev, O.; Roasto, I.; Nassereddine, K.; Vinnikov, D.; Strzelecki, R. Grid-Forming Operation of Energy-Router Based on Model Predictive Control with Improved Dynamic Performance. *Energies* **2022**, *15*, 4010. <https://doi.org/10.3390/en15114010>

Academic Editor: Nicu Bizon

Received: 24 April 2022

Accepted: 26 May 2022

Published: 30 May 2022

Publisher's Note: MDPI stays neutral with regard to jurisdictional claims in published maps and institutional affiliations.



Copyright: © 2022 by the authors. Licensee MDPI, Basel, Switzerland. This article is an open access article distributed under the terms and conditions of the Creative Commons Attribution (CC BY) license (<https://creativecommons.org/licenses/by/4.0/>).

1. Introduction

The steadily increasing penetration of renewable energy sources (RESs) in the utility grid is a current trend [1,2], which, in turn, is a source of many technical challenges that need to be overcome. The voltage/frequency disturbances caused by the chaotic nature of RES in the utility grid are widely known.

The solution is to shift the responsibility to the local prosumer. Accordingly, in many countries, governments have set strict regulations on grid energy injection. This consists of the limitations of the power injected into the grid produced by RES in local households. Near Zero-Energy Building (NZEB) is a concept regarding reductions in energy consumption in households. This is achieved in several ways, including energy-saving technologies, modern heating systems, and modern power electronics facilities. New power electronics facilities ensure zero energy consumption by means of energy flow control between RESs, storage batteries and loads. The announced priorities are drifting from mass RESs used for grid balancing.

A more recent concept is the so-called smart communities, which take advantage of the Smart Grid (SG), allowing for effective demand-side management. SGs require

general-purpose power electronic converters (in both dc and ac), micro-storage systems installed at the residential level, advanced metering infrastructure, and the optimal use of information and communication technology [3]. In this regard, the trend moves toward the concept of energy routers (ERs) or hubs [4].

The concept of ER, introduced by the NSF FREEDM Systems Center in 2010 [2], introduces an SST-based ER concept and describes the IoE architecture. In this way, a flexible and two-directional energy flow will be the future of the distribution network [5,6]. The main tool is the ER, which manages the power flow between the subnet, main grid, RESs and other components. The further development of the concept for microgrids application is addressed in many papers. Complementary energy exchange by means of ER between neighboring microgrids is addressed in [6,7]. The control strategy of ER inside a microgrid with different energy sources, loads and battery ES is studied in [8]. Work [9] studied the utilization of a hybrid converter as an ER in a case of dc nanogrid. The conceptual architecture of the ER in a residential application and different power-electronics architectures are discussed in [4]. Finally, paper [10] is devoted to the ER as a power management tool in the case of low-voltage residential applications. The further extension of this approach consists of ER utilization for the NZEB concept. It has to provide flexible energy management in the case of different loads, energy sources, and battery storage. In advance of the grid-connected mode, the islanded mode, when the main grid is disconnected, has to be realized. In conclusion, the NZEB corresponds to the hybrid nanogrid [11,12], while the goal of the ER is to maintain a stable output voltage in all operation modes. Active and reactive power control, voltage control, current control, and protection functions are just a few of the active functions that an ER could have [4].

Figure 1 shows a single-phase multiport converter topology that is selected to realize the interface between the external grid and internal load. Inherently, it has dc and ac terminals, which make similar micro-and nanogrids converters [13]. Two dc–dc interface converters allow for energy storage and local energy generation sources to be connected. In addition, dc loads can be connected to the dc-port. The different dc-load connection to the dc-port of the ER and the proposed control technique is studied in [14]. The output ac port is directly connected to the house appliances. Appliances in the NZEB are considered as “grid followers”, only. At the same time, it is well-known that different types of load have to be considered, including light load and non-linear loads. The basic operation modes of the considered ER are described in [15]. This work studies the quality of the grid-forming operation in extremely nonlinear conditions and small current sources. Enhancing the classic linear controller to nonlinear control technique (MPC) and, specifically, the cost function of the proposed MPC with the filter capacitor voltage of the output side is the main contribution of this work. The next section concentrates on the conventional grid-following solution and the limitations of the conventional control system. The proposed indirect MPC is explained in the following sections. Finally, the parameter selections and the simulation results for different scenarios are described. The robustness test results in case of a drop in the reference voltage are also demonstrated.

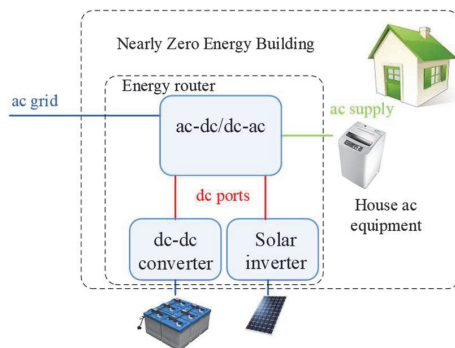


Figure 1. Energy router for NZEB.

2. Conventional Grid-Forming Control Systems and Problem Definition

Figure 2 shows the electrical circuit diagram of the ER. The measured signals are marked in red. One of the conventional control systems of the ER is shown in Figure 3. It has a conventional Phase-Locked Loop (PLL) block that provides synchronization to the primary grid [16]. The traditional Second-Order Generalized Integrator (SOGI) regulator is used [17]. The grid side reference current is derived by means of a simple proportional-integral (PI) controller, in combination with the instantaneous value of the output current. This provides the instantaneous power balance between the output side and the grid side, which, in turn, mitigates the power ripple across the dc-link capacitor and improves the dynamic of the system. Finally, a conventional proportional-resonant (PR) controller is used for grid current control. Thus, the grid-side control operation is ensured (Figure 3a).

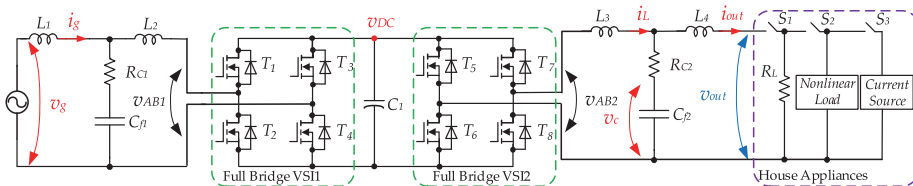


Figure 2. Back-to-back mode circuit diagram of the proposed energy router.

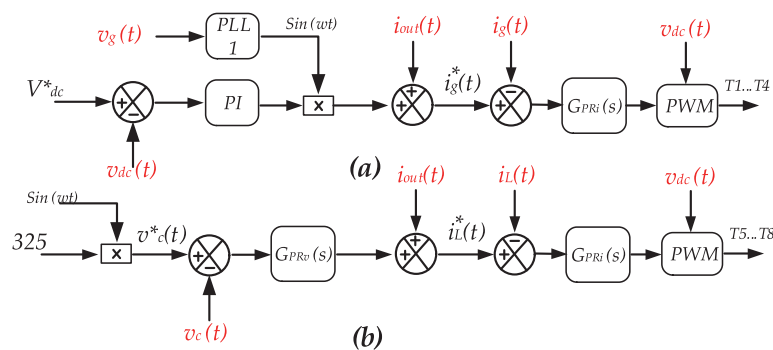


Figure 3. The conventional control system structure of the ER primary grid-side VSI1 control (a) and output side grid-forming VSI2 control (b).

The PR controller is a key element of the discussed grid-side control system. To provide the proper dynamic, it has to be the fastest and most properly tuned chain in the control loop [18].

The output control has a more complex structure. The classical definition of the grid-forming operation is derived from the microgrid application and has high-level and low-level control components. The low-level algorithm has to provide the output voltage according to the reference value. An example of the output voltage control structure is illustrated in Figure 3b. The initial goal of the output side controller is to provide sinusoidal output voltage under any output load. As a result, a consumer recognizes this as a normal grid. It typically has current and voltage control loops [19–23]. The internal structure can differ. In the three-phase system, the dq rotating frame is often used, while resonant controllers are mostly used for a single-phase system. In both cases, the most attention should be paid to the stable operation of the system. The current control loop is usually tuned as a fast control loop, while the voltage control loop has a damped dynamic.

The high-level algorithm provides the power-sharing control in the case of several power sources working in parallel. First and foremost, this is achievable through Droop control [24–28]. It is a well-known and verified approach.

The virtual impedance [29,30] method and its derivation can also be applied for this purpose. Finally, a relatively novel approach, based on the synchronverter concept, was proposed in [31–33]. The goal of a high-level algorithm is to provide different amplitudes and frequencies of the reference voltage across the filter capacitor. It enables the stable operation of the microgrid. However, this is beyond the scope of this work.

In the classical approach, the voltage at the Point of Common Coupling (PCC) is not under direct control. It is assumed that only linear loads with sinusoidal current sources can be connected to the PCC. At the same time, it is obvious that this assumption is not acceptable in household applications where ER is connected to different low-power loads and current sources. It is clear that the PCC obtains higher harmonics from appliances such as solar microinverters and other nonlinear loads and current sources.

This paper is focused on how to improve the voltage shape in the PCC when the ER is used with different loads and current sources. In addition, the robustness of the system toward external noises and perturbations is another criterion that should be considered. Different control methods were studied to compensate the system disturbances [34,35]. In this paper, the ER control robustness is evaluated in the final step.

3. Grid-Forming Operations Based on Indirect Model Predictive Control

Model Predictive Control (MPC) is a well-known approach in power electronics from the 1980s [36]. Despite the complexity of the MPC, which imposes limitations on its utilization in power electronics, the progress of computational resources makes it increasingly feasible for industrial applications [37,38]. According to the most recent research, this can be used in a variety of power electronics fields [39–47]. MPC is categorized into two types: Finite Control Set (FCS) MPC and Continuous Control Set (CCS) MPC. FCS MPC provides optimized switching states; as a result, it can provide a variable switching frequency, resulting in higher THD [48]. On the other hand, CCS MPC produces the required duty cycles for modulators with a fixed switching frequency, ending with a lower THD [40,49]. Considering the priority of a lower THD in the grid forming operation, CCS MPC matches our control application.

Figure 4 shows the proposed control system. The control system for the primary side of the ER is shown in Figure 4a. Only one modification concerns an additional PLL block. It provides a pure sinusoidal reference current that is equal to the fundamental harmonic of the output current. It will provide only a sinusoidal grid current under any shape of the output current. All non-active harmonics will be circulated between the DC-link and the secondary side of the ER.

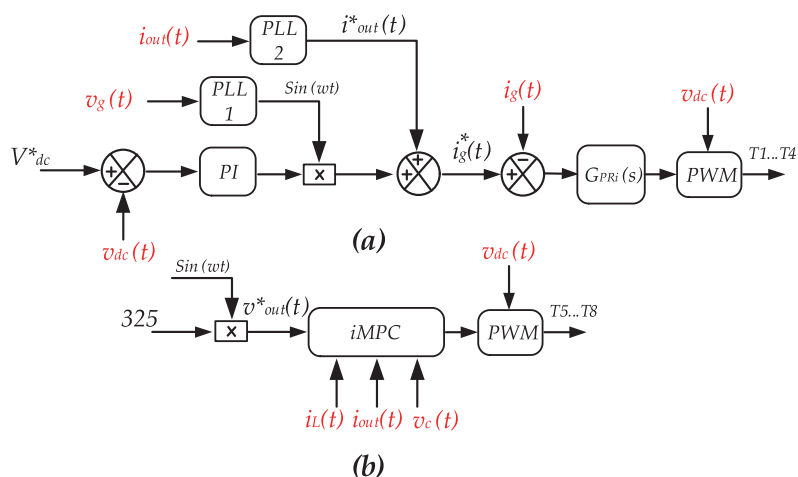


Figure 4. The proposed control system structure of the ER primary grid-side VSI1 control (a) and output side grid-forming VSI2 control (b).

Figure 4b shows the part of the control system that is formed in response to the grid-forming operation. In a very general case, the MPC says what the control action should be by trying to minimize: a cost function that describes the target of the control system.

The proposed approach was partially studied in [50] for the unidirectional power flow control mode. In our case, the main goal of the proposed control system was to maintain the output voltage shape according to the reference sinusoidal signal under any type of load or current source that can be connected from the house side. Different from the classical approach, where only the voltage across the filter capacitor is controlled, MPC allows for control of both voltages across the capacitor and the output voltage, even without direct measurement of the last value. It turns out that, in our case, the cost function J is defined as:

$$J[d] = k_{out}|\Delta v_{out}(n+1)| + k_c|\Delta v_c(n+1)| + \dots + k_{out}|\Delta v_{out}(n+p)| + k_c|\Delta v_c(n+p)| \quad (1)$$

It contains a voltage error across the filter capacitor and an error of the output voltage, along with corresponding weighting coefficients. It also has p elements that are defined by horizon prediction. The function quantizes the estimations of different summarized outputs and capacitor voltage errors. Each of those estimations corresponds to the possible scenario d , which could occur at the prediction horizon.

The measurement system provides the dc-link voltage, the voltage across the filter capacitor and currents in the inductors. If you want to conduct any more calculations, you need to use the indirect MPC and the dynamic model of the system shown in Figure 5.

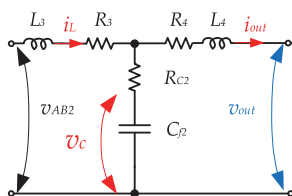


Figure 5. The dynamic model of the secondary side part of the ER used for iMPC.

The dynamic system is represented by the continuous vector of the measured parameters:

$$x(t) = [i_L(t), i_{out}(t), v_c(t)]^T, \quad (2)$$

After the measured signal discretization, the discontinuous set of the measured values is derived:

$$x(i) = [i_L(i), i_{out}(i), v_c(i)]^T, \quad (3)$$

After obtaining the measured values, the first step is to calculate the voltage at the PCC point based on a simple equation:

$$v_{out}(n) = v_c(n) - (i_L(n) - i_{out}(n)) \times R_{C2} - \frac{L_3}{T_S} (i_{out}(n) - i_{out}(n-1)) - R_4 \times i_{out}(n), \quad (4)$$

where T_S is the sampling time, L_3, L_4, C_{f2} are parameters of the output filter, R_3, R_4, R_{C2} are parasitic resistances.

To calculate the grid current value during the next samples in the discrete-time domain:

$$x(n+1) = F \cdot x(n) + G u(n), \quad (5)$$

$$u(n) = [v_{AB}(n), v_{out}(n)]^T \quad (6)$$

where F and G are matrices that correspond to the dynamic model of the system and sampling frequency:

$$F = \begin{bmatrix} f_1 & f_2 & f_3 \\ f_4 & f_5 & f_6 \\ f_7 & f_8 & f_9 \end{bmatrix}, \quad (7)$$

$$G = \begin{bmatrix} g_1 & 0 \\ 0 & g_4 \\ 0 & 0 \end{bmatrix}, \quad (8)$$

$$f_1 = 1 - (R_3 + R_{C2}) \frac{T_S}{L_3}; f_2 = \frac{R_{C2} T_S}{L_3}; f_3 = -\frac{T_S}{L_3}; \quad (9)$$

$$f_4 = \frac{R_{C2} T_S}{L_4}; f_5 = 1 - (R_4 + R_{C2}) \frac{T_S}{L_4}; f_6 = \frac{T_S}{L_4}; \quad (10)$$

$$f_7 = \frac{T_S}{C_{f2}}; f_8 = -\frac{T_S}{C_{f2}}; f_9 = 1; \quad (11)$$

$$g_1 = \frac{T_S}{L_3}; g_4 = -\frac{T_S}{L_4}, \quad (12)$$

The proposed approach provides us a reference output voltage in the PCC. To make sure the control system works properly, the voltage across the capacitor is set as follows:

$$v_c^*(t) = v_{out}^*(t) - (i_L(t) - i_{out}^*(t)) \times R_{C2} + L_4 \frac{d}{dt} i_{out}^*(t) + R_4 \times i_{out}^*(t), \quad (13)$$

In the further step, the voltage across the capacitor of the output filter is calculated as a function of the applied inverter voltage. The same concerns the output voltage in the PCC, which can be estimated similarly to Equation (4). As a result, the proposed control system keeps the capacitor voltage and the voltage in the PCC under control, considering the difference between them.

Finally, possible errors are calculated:

$$\Delta v_{out}(n+1) = v_{out}(n+1) - v_{out}^*(n+1); \Delta v_c(n+1) = v_c(n+1) - v_c^*(n+1); \quad (14)$$

The flow chart diagram for the case $p = 2$ is shown in Figure 6. Firstly, the variables are measured, and then the output voltage is estimated.

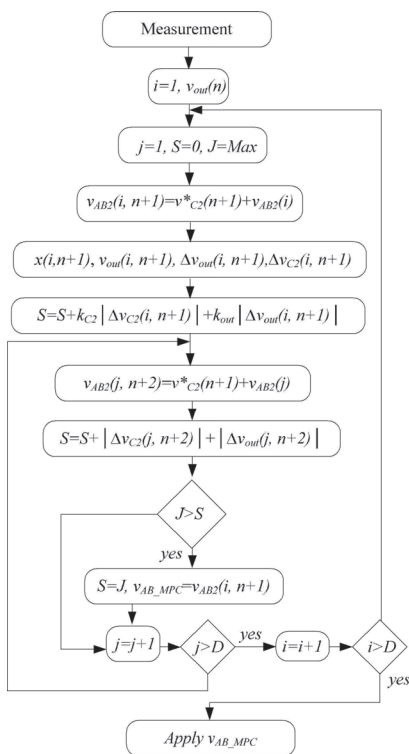


Figure 6. The procedure of activity diagram of the proposed iMPC in the case of $p = 2$.

Based on this estimated state, the predicted state of the system at $n + 1$ is calculated for all the possible output inverter values v_{AB2} combinations.

It should be mentioned that, in any case, the output inverter voltage is expected to be close to the sinusoidal reference signal. $v_{AB2(i)}$ is an example of a possible reference voltage that could be used to figure out the cost function:

$$v_{AB2}(n + 1) = v_c^*(n + 1) + \Delta v_{AB2}(i), \tag{15}$$

Finally, the combination of voltages on the output inverter that minimizes (1) is stored and will be used at the start of the next test.

4. Optimal Parameters Selection

The main criterion for the quality evaluation of the output voltage is the THD. At the same time, from the above description, it is evident that the resulting THD depends on the horizon prediction p , weighting coefficients, and the voltage quantizing d . Due to the nonlinearity of the control, the most suitable tuning approach is achieved by simulation. In this work, the PLECS simulation tool was used as the simulation environment.

The parameters of the prototype are shown in Table 1. They are used for simulation and experimental tests.

Table 1. Components and parameters of the ER.

Parameter	Value
Input RMS ac voltage V_{IN}	230 V
Output ac RMS voltage V_{OUT}	230 V
Output power	0.3–3.6 kW
Dc-link capacitor C_1	0.8 mF
Grid side inductor filter L_1	0.6 mH
Grid side second inductor filter L_2	1.44 mH
Grid side capacitor filter C_{f1} R_{C1}	3 μ F, 0.8 Ohm
Output side inductor filter L_3	1.44 mH
Output side second inductor filter L_4	0.6 mH
Output side capacitor filter C_{f2} R_{C2}	9.6 μ F, 0.8 Ohm
Switching frequency f	25 kHz
Sampling frequency f	25 kHz

First of all, based on previous research [50], it is assumed that the horizon prediction $p = 2$ is optimal. Increasing p even more will not make a big difference in THD, but it will make the calculations a lot more complicated. According to Equation (15), the output voltage value is selected, close to the present reference voltage value with respect to voltage deviations. During each sampling, five possible output voltage deviation values are individually considered and verified. This number is constant from sample to sample, which is limited by the calculation resources. However, the possible minimum and maximum values can be different:

$$-\Delta v_{AB2_max} < \Delta v_{AB2}(i, d) < \Delta v_{AB2_max}, \quad (16)$$

It is well known that the voltage difference between the filter capacitor and the PCC is defined by the parasitic resistance R_4 (Figure 5), inductance L_4 and current. The maximum and minimum voltages that can be applied to the inverter can be flexible and changed slightly based on the peak current.

In conclusion, the most significant parameters for evaluation are the weighting coefficients. The idea of these coefficients consists of a priority setting between the quality of the output capacitor voltage and the quality of the PCC voltage. On the one hand, it is evident that the PCC is more important than the voltage across the capacitor, which is an internal parameter. However, this parameter that can be directly measured, and direct control of it could improve both the capacitor and the PCC.

A simulation was performed to study the influence of these coefficients. Figure 7 shows the simulation results in the case of $k_{out} = 0, k_c = 1$. This means that only the quality of the capacitor voltage is considered in the cost function estimation. At the very beginning, the DC-link is charged and a 529 W simple resistive load is connected at 0.25 s. At 0.35 s, the nonlinear 180 W load is connected. To emulate a highly nonlinear load, a resistor with a half-bridge diode with an LC filter is assumed. It can be seen that, at the resistive load, both the capacitor and the PCC voltage have a good shape, without significant distortions. At the nonlinear load connection, both voltages have distortions. However, it is evident that the capacitor voltage is less distorted. The grid current is also distorted by the nonlinear load connection.

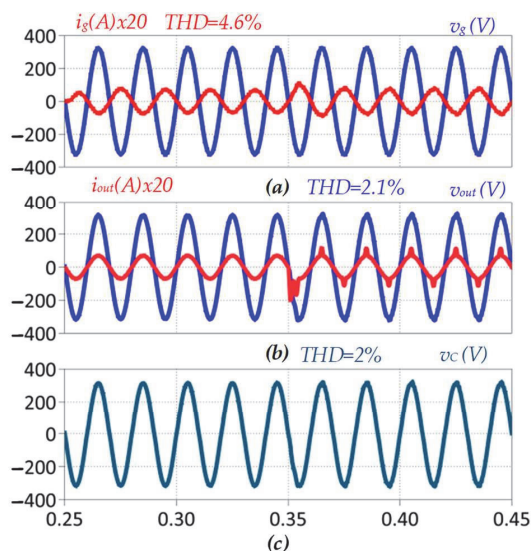


Figure 7. Voltage and current shape at the main grid (a), output (b), and capacitor of the filter (c) with $k_{out} = 0, k_c = 1$.

The opposite situation is shown in Figure 8. In this case, the predicted capacitor voltage is not considered in the cost function estimation. It can be seen from Figure 8 that with a simple resistive load, the quality of the PCC voltage and the capacitor voltage is good, but the situation changes under a nonlinear load. Both shapes are more distorted compared to Figure 7 results. However, the THD of the grid current remains constant.

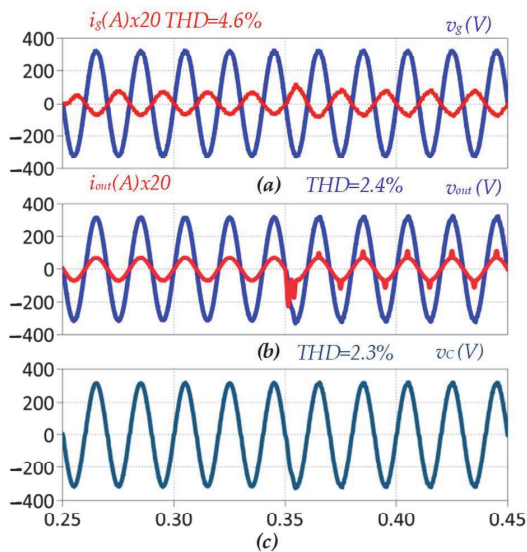


Figure 8. Voltage and current shape at the main grid (a), output (b), and capacitor of the filter (c) with $k_{out} = 1, k_c = 0$.

The simulation results of different coefficients k_{out}, k_c show the influence of the weighting coefficients k_{out}, k_c on the THD of output voltage and capacitor voltage. It is assumed that $k_{out} + k_c = 1$ under nonlinear load. The results show that different values of k_{out} and

k_c have no significant impact on THD, but lower k_{out} improves the output voltage and capacitor voltage quality. As a result, we continue the simulation with $k_{out} = 0.2$, $k_c = 0.8$ as optimal values. The higher impact of k_c proves the improved performance of the proposed iMPC compared to [50], in which the proposed cost function includes just k_{out} .

Figure 9 shows the simulation of the whole system under different load conditions with $k_{out} = 0.2$, $k_c = 0.8$. It includes an idle mode, a simple resistive load, and a nonlinear load. They are utilized in this case. This figure demonstrates the steady-state pictures with a better resolution as well as the dynamic behavior of the main grid, ac output, and the capacitor. This figure shows that the proposed iMPC can work because the THD of the output voltage and the grid current are in the range that they should be.

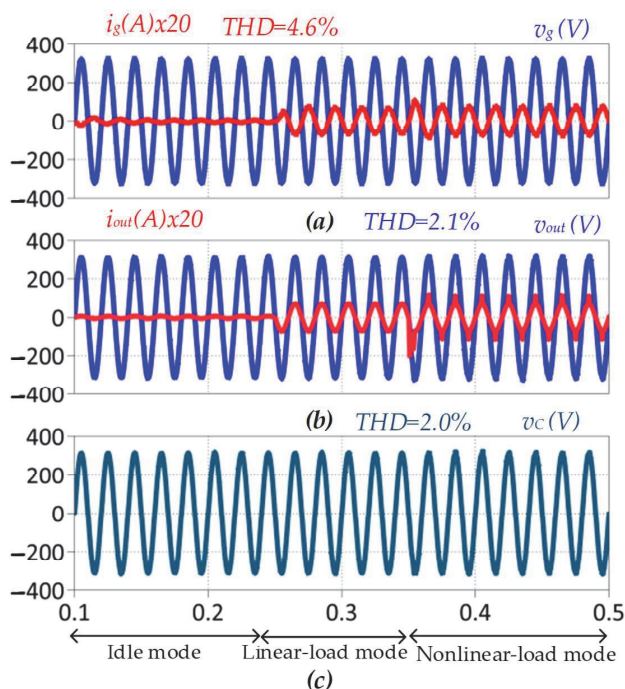


Figure 9. Voltage and current shape transitions at the main grid (a), output (b), and filter capacitor (c) with $k_{out} = 0.2$ and $k_c = 0.8$ in idle mode, linear load, and nonlinear load.

The next scenario evaluates the iMPC performance in the opposite power flow in a low-power solar microinverter connection. Figure 10 demonstrates the simulation results in idle mode with a current-source connection. The results confirm the good performance of the iMPC in terms of grid-forming. However, the high THD of the grid current implies the necessity of improvements in current control on the VSI1 side. The last case is the most complex and reveals a problem with any grid configured by power electronics. The high switching frequency current harmonics fluctuate between the ER and the microinverter.

The next level is the robustness evaluation of the proposed iMPC. As the grid-forming inverter must also work in droop control in the case of multiple loads and sources connection, the proposed control technique needs to be capable of tracking voltage with step changes. As a result, we test the iMPC performance in this case. In this scenario, we make a step-change in the reference value of the output voltage peak from 325 V to 305 V. The grid voltage and current, load voltage and current and filter capacitor voltage are depicted in Figure 11. In this case, grid current THD is 4.8%, however the iMPC provides voltage with THD of 2.2%. The total simulation results, in terms of the THD, are summarized in Table 2.

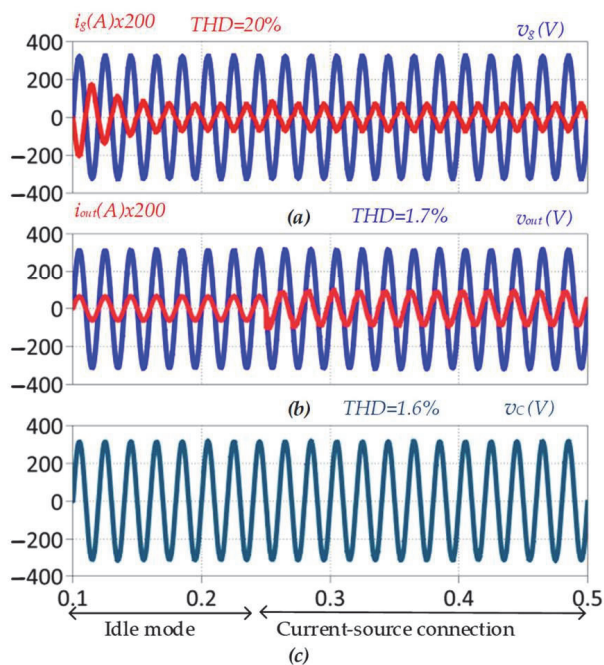


Figure 10. Voltage and current shape transition at the main grid (a), output (b), capacitor of the filter (c) with $k_{out} = 0.2$, $k_c = 0.8$ in idle mode, and current-source connection.

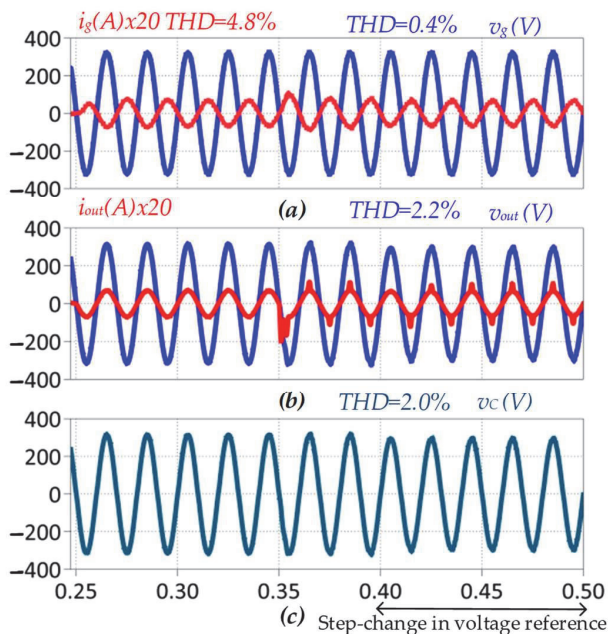


Figure 11. Voltage and current shape at the main grid (a), output (b), and capacitor of the filter (c) in case of drop voltage reference with $k_{out} = 0.2$, $k_c = 0.8$.

Table 2. Comparison of THD results of the ER parameters for different scenarios.

Scenario	Parameter	THD (%)
linear and nonlinear load with $k_{out} = 0.0$ and $k_c = 1.0$	Grid current i_g	4.6
	Output voltage v_{out}	2.1
	Filter capacitor voltage v_c	2.0
linear and nonlinear load with $k_{out} = 1.0$ and $k_c = 0.0$	Grid current i_g	4.6
	Output voltage v_{out}	2.4
	Filter capacitor voltage v_c	2.3
linear and nonlinear load with $k_{out} = 0.2$ and $k_c = 0.8$	Grid current i_g	4.6
	Output voltage v_{out}	2.1
	Filter capacitor voltage v_c	2.0
current-source connection with $k_{out} = 0.2$ and $k_c = 0.8$	Grid current i_g	20
	Output voltage v_{out}	1.7
	Filter capacitor voltage v_c	1.6
Step change in reference from 230 V to 210 V with $k_{out} = 0.2$ and $k_c = 0.8$	Grid current i_g	4.8
	Output voltage v_{out}	2.2
	Filter capacitor voltage v_c	2.0

It can be seen that the proposed control approach is capable of maintaining the sinusoidal voltage in the PCC under any type of load that can be connected on the house side. Moreover, it underlines that the ER requires modification on the VSI1 side to maintain an acceptable quality of the injected current on the local grid under any load from the consumer side. Finally, bidirectional operation is possible without significant PCC voltage distortion.

5. Conclusions

This work studies the energy-router-based back-to-back inverter in grid-forming mode. The conventional PR regulator for grid-forming of the energy router has limitations in terms of its idle mode, nonlinear loads and current sources. This paper proposes an enhanced iMPC to improve the output voltage quality of the energy router. To improve the THD of the output voltage, a prediction horizon of two is suggested. Increasing the number of voltage deviations in each horizon will improve the output voltage quality at the expense of a higher processing burden on the microcontroller at each sampling time. Considering this issue, a voltage deviation of five is implemented, with a total of 25 loops in each sampling time. The simulation results for four different modes of idle mode, linear load, nonlinear load, and low-power current source show the higher impact of filter capacitor voltage on the THD of the output voltage. The results confirm that the proposed technique can control the steady-state and dynamic performance of the energy router in a grid-forming operation. In addition, the high THD of the grid current in the current-source connection proves the necessity of improvements in grid-following side control of the ER.

Future research can be conducted regarding the experimental verification of the proposed technique in different operation scenarios.

Author Contributions: Conceptualization: R.S.; Formal analysis: N.S. and M.N.; Validation: M.N. and N.S.; Methodology: O.H.; Visualization M.N., I.R. and K.N.; Investigation: M.N. and N.S.; Writing—original draft: M.N. and K.N.; Resources: I.R. and K.N.; Writing—review and editing: R.S. and D.V.; Supervision: D.V. and O.H.; Project administration: R.S.; Funding acquisition: N.S. All authors have read and agreed to the published version of the manuscript.

Funding: The project is financed by the “program of the Ministry of Science and Higher Education “Regional Excellence Initiative” in the years 2019–2022 project number 006/RID/2018/19 grant amount 11,870,000 PLN”, realized in the GDYNIA MARITIME UNIVERSITY, POLAND.

Institutional Review Board Statement: Not applicable.

Informed Consent Statement: Not applicable.

Data Availability Statement: Not applicable.

Conflicts of Interest: The authors declare no conflict of interest.

References

1. Liu, Y.; Fang, Y.; Li, J. Interconnecting microgrids via the energy router with smart energy management. *Energies* **2017**, *10*, 1297. [CrossRef]
2. Huang, A.Q.; Crow, M.L.; Heydt, G.T.; Zheng, J.P.; Dale, S.J. The future renewable electric energy delivery and management (FREEDM) system: The energy internet. *Proc. IEEE* **2011**, *99*, 133–148. [CrossRef]
3. Roncero-Clemente, C.; Vilhena, N.; Delgado-Gomes, V.; Romero-Cadaval, E.; Martins, J.F. Control and operation of a three-phase local energy router for prosumers in a smart community. *IET Renew. Power Gener.* **2020**, *14*, 560–570. [CrossRef]
4. Martins, J.F.; Romero-Cadaval, E.; Vinnikov, D.; Malinowski, M. Transactive Electronics Power Energy: Challenges. *IEEE Power Electron. Mag.* **2022**, *9*, 20–32. [CrossRef]
5. Liu, Y.; Li, J.; Wu, Y.; Zhou, F. Coordinated Control of the Energy Router-Based Smart Home Energy Management System. *Appl. Sci.* **2017**, *7*, 943. [CrossRef]
6. Fu, R.; Remo, T.; Margolis, R.; Fu, R.; Remo, T.; Margolis, R. 2018 U.S. Utility-Scale Photovoltaics-Plus-Energy Storage System Costs Benchmark. 2018. Available online: <https://www.nrel.gov/docs/fy19osti/71714.pdf> (accessed on 21 November 2018).
7. Liu, Y.; Chen, X.; Wu, Y.; Yang, K.; Zhu, J.; Li, B. Enabling the Smart and Flexible Management of Energy Prosumers via the Energy Router with Parallel Operation Mode. *IEEE Access* **2020**, *8*, 35038–35047. [CrossRef]
8. Liu, Y.; Li, Y.; Liang, H.; He, J.; Cui, H. Energy Routing Control Strategy for Integrated Microgrids Including Photovoltaic, Battery-Energy Storage and Electric Vehicles. *Energies* **2019**, *12*, 302. [CrossRef]
9. Ray, O.; Mishra, S. Integrated Hybrid Output Converter as Power Router for Renewable-based Nanogrids. In Proceedings of the ECON 2015—41st Annual Conference of the IEEE Industrial Electronics Society, Yokohama, Japan, 9–12 November 2015; pp. 1645–1650.
10. Zhen, L.; Penghua, L.; Wanxing, S.; Songhuai, D.; Qing, D.; Zhipeng, L. Research on a household energy router for energy internet. In Proceedings of the 2018 13th IEEE Conference on Industrial Electronics and Applications (ICIEA), Wuhan, China, 31 May–2 June 2018; pp. 952–957. [CrossRef]
11. Tarafdar, M.H.; Hamzeh, F. Aghdam Smart Hybrid Nanogrids Using Modular Multiport Power Electronic Interface. In Proceedings of the 2016 IEEE Innovative Smart Grid Technologies—Asia (ISGT-Asia), Melbourne, VIC, Australia, 28 November–1 December 2016; pp. 11–16.
12. Mishra, S.; Ray, O. Advances in nanogrid technology and its integration into rural electrification in India. In Proceedings of the 2014 International Power Electronics Conference (IPEC-Hiroshima 2014—ECCE ASIA), Hiroshima, Japan, 18–21 May 2014; pp. 2707–2713. [CrossRef]
13. Majumder, R. A hybrid microgrid with dc connection at back to back converters. *IEEE Trans. Smart Grid* **2014**, *5*, 251–259. [CrossRef]
14. Najafzadeh, M.; Husev, O.; Roasto, I.; Jalakas, T. Improved DC-Link Voltage Transient Response and Stability Issues in Energy Router with Fuzzy Logic Control Method. In Proceedings of the 2020 IEEE 61th International Scientific Conference on Power and Electrical Engineering of Riga Technical University (RTUCon), Riga, Latvia, 5–7 November 2020.
15. Roasto, I.; Rosin, A.; Jalakas, T. Multiport Interface Converter with an Energy Storage for Nanogrids. In Proceedings of the IECON 2018—44th Annual Conference of the IEEE Industrial Electronics Society, Washington, DC, USA, 21–23 October 2018; Volume 1, pp. 6088–6093.
16. Najafzadeh, M.; Roasto, I.; Jalakas, T. Energy Router Based Energy Management System for Nearly Zero Energy Buildings. In Proceedings of the 2019 IEEE 60th International Scientific Conference on Power and Electrical Engineering of Riga Technical University (RTUCon), Riga, Latvia, 7–9 October 2019.
17. Yang, Y.; Hadjidemetriou, L.; Blaabjerg, F.; Kyriakides, E. Benchmarking of Phase Locked Loop based Synchronization Techniques for Grid-Connected Inverter Systems. In Proceedings of the 9th International Conference on Power Electronics—ECCE Asia, Seoul, Korea, 1–5 June 2015; pp. 2167–2174.
18. Husev, O.; Roncero-Clemente, C.; Makovenko, E.; Pimentel, S.P.; Vinnikov, D.; Martins, J. Optimization and Implementation of the Proportional-Resonant Controller for Grid-Connected Inverter with Significant Computation Delay. *IEEE Trans. Ind. Electron.* **2020**, *67*, 1201–1211. [CrossRef]
19. Rocabert, J.; Luna, A.; Blaabjerg, F.; Rodriguez, P. Control of Power Converters in AC Microgrids. *IEEE Trans. Power Electron.* **2012**, *27*, 4734–4749. [CrossRef]
20. Hossain, M.J.A.J.; Pota, H.R.; Issa, W.; Hossain, M.J.A.J. Overview of AC microgrid controls with inverter-interfaced generations. *Energies* **2017**, *10*, 1300. [CrossRef]
21. Unamuno, E.; Barrera, J.A. Hybrid ac/dc microgrids—Part II: Review and classification of control strategies. *Renew. Sustain. Energy Rev.* **2015**, *52*, 1123–1134. [CrossRef]
22. Malik, S.M.; Ai, X.; Sun, Y.; Zhengqi, C.; Shupeng, Z. Voltage and frequency control strategies of hybrid AC/DC microgrid: A review. *IET Gener. Transm. Distrib.* **2017**, *11*, 303–313. [CrossRef]

23. Loh, P.C.; Li, D.; Chai, Y.K.; Blaabjerg, F. Autonomous control of interlinking converter with energy storage in hybrid AC-DC microgrid. *IEEE Trans. Ind. Appl.* **2013**, *49*, 1374–1382. [[CrossRef](#)]
24. Tayab, U.B.; Roslan, M.A.B.; Hwai, L.J.; Kashif, M. A review of droop control techniques for microgrid. *Renew. Sustain. Energy Rev.* **2017**, *76*, 717–727. [[CrossRef](#)]
25. Guerrero, J.M.; de Vicuña, L.G.; Matas, J.; Castilla, M. Output Impedance Design of Parallel-Connected UPS Inverters with Wireless Load-Sharing Control. *IEEE Trans. Ind. Electron.* **2005**, *52*, 1126–1135. [[CrossRef](#)]
26. Zhang, H.; Zhou, J.; Sun, Q.; Guerrero, J.M.; Ma, D. Data-Driven Control for Interlinked AC/DC Microgrids Via Model-Free Adaptive Control and Dual-Droop Control. *IEEE Trans. Smart Grid* **2017**, *8*, 557–571. [[CrossRef](#)]
27. Mahmood, H.; Michaelson, D.; Jiang, J. Decentralized Power Management of a PV/Battery Hybrid Unit in a Droop-Controlled Islanded Microgrid. *IEEE Trans. Power Electron.* **2015**, *30*, 7215–7229. [[CrossRef](#)]
28. Wang, J.; Dong, C.; Jin, C.; Lin, P.; Wang, P. Distributed Uniform Control for Parallel Bidirectional Interlinking Converters for Resilient Operation of Hybrid AC/DC Microgrid. *IEEE Trans. Sustain. Energy* **2022**, *13*, 3–13. [[CrossRef](#)]
29. He, J.; Li, Y.W.; Guerrero, J.M.; Blaabjerg, F.; Vasquez, J.C. An Islanding Microgrid Power Sharing Approach Using Enhanced Virtual Impedance Control Scheme. *IEEE Trans. Power Electron.* **2013**, *28*, 5272–5282. [[CrossRef](#)]
30. Jiang, X.y.; He, C.; Jermsittiparsert, K. Online optimal stationary reference frame controller for inverter interfaced distributed generation in a microgrid system. *Energy Rep.* **2020**, *6*, 134–145. [[CrossRef](#)]
31. Zhong, Q.C.; Weiss, G. Synchronverters: Inverters that mimic synchronous generators. *IEEE Trans. Ind. Electron.* **2011**, *58*, 1259–1267. [[CrossRef](#)]
32. Liu, J.; Hossain, M.J.; Lu, J.; Rafi, F.H.M.; Li, H. A hybrid AC/DC microgrid control system based on a virtual synchronous generator for smooth transient performances. *Electr. Power Syst. Res.* **2018**, *162*, 169–182. [[CrossRef](#)]
33. Arghir, C.; Jouini, T.; Dörfler, F. Grid-forming control for power converters based on matching of synchronous machines. *Automatica* **2018**, *95*, 273–282. [[CrossRef](#)]
34. Wang, J.; Rong, J.; Yu, L. Dynamic prescribed performance sliding mode control for DC–DC buck converter system with mismatched time-varying disturbances. *ISA Trans.* **2022**; *in press*. [[CrossRef](#)]
35. Wang, J.; Rong, J.; Yang, J. Adaptive Fixed-Time Position Precision Control for Magnetic Levitation Systems. *IEEE Trans. Autom. Sci. Eng.* **2022**, 1–12. [[CrossRef](#)]
36. Kouro, S.; Perez, M.A.; Rodriguez, J.; Llor, A.M.; Young, H.A. Model Predictive Control: MPC’s Role in the Evolution of Power Electronics. *IEEE Ind. Electron. Mag.* **2015**, *9*, 8–21. [[CrossRef](#)]
37. Rodriguez, J.; Kolar, J.; Espinoza, J.; Rivera, M.; Rojas, C. Predictive Torque and Flux Control of an Induction Machine fed by an Indirect Matrix Converter with Reactive Power Minimization. In Proceedings of the 2010 IEEE International Symposium on Industrial Electronics, Bari, Italy, 4–7 July 2010; pp. 3177–3183.
38. Kennel, R.; Linder, A. Predictive control of inverter supplied electrical drives. In Proceedings of the 2000 IEEE 31st Annual Power Electronics Specialists Conference. Conference Proceedings (Cat. No. 00CH37018), Galway, Ireland, 23 June 2000; pp. 761–766.
39. Zhuikov, V.; Pavlov, V.; Strzelecki, R.G. *Preemptive Control Systems for Valve Converters*; Nauk. Dumka: Kiev, Ukraine, 1991; 240p.
40. Rodriguez, J.; Kazmierkowski, M.P.; Espinoza, J.R.; Zanchetta, P.; Abu-Rub, H.; Young, H.A.; Rojas, C.A. State of the art of finite control set model predictive control in power electronics. *IEEE Trans. Ind. Inform.* **2013**, *9*, 1003–1016. [[CrossRef](#)]
41. Falkowski, P.; Sikorski, A. Finite Control Set Model Predictive Control for Grid-Connected AC–DC Converters with LCL Filter. *IEEE Trans. Ind. Electron.* **2018**, *65*, 2844–2852. [[CrossRef](#)]
42. Wojciechowski, D.; Strzelecki, R. Sensorless predictive control of three-phase parallel active filter. In Proceedings of the AFRICON 2007, Windhoek, South Africa, 26–28 September 2007.
43. Hu, J.; Shan, Y.; Guerrero, J.M.; Ioinovici, A.; Chan, K.W.; Rodriguez, J. Model predictive control of microgrids—An overview. *Renew. Sustain. Energy Rev.* **2021**, *136*, 110422. [[CrossRef](#)]
44. Wojciechowski, M.; Strzelecki, R.; Benysek, G. Predictive Control System of the Shunt Active Power Filter. In Proceedings of the 2008 International Biennial Baltic Electronics Conference (BEC2008), Tallinn, Estonia, 6–8 October 2008.
45. Wojciechowski, D.; Strzelecki, R. Predictive Control of Active Filter System with LCL Coupling Circuit. In Proceedings of the 2010 International Power Electronics Conference, Sapporo, Japan, 21–24 June 2010.
46. Lee, J.; Lee, J.; Moon, H.; Lee, K. An Improved Finite-Set Model Predictive Control Based on Discrete Space Vector Modulation Methods for Grid-Connected Three-Level Voltage Source Inverter. *IEEE J. Emerg. Sel. Top. Power Electron.* **2018**, *6*, 1744–1760. [[CrossRef](#)]
47. Wang, F.; Xie, H.; Chen, Q.; Davari, S.A.; Rodríguez, J.; Kennel, R. Parallel Predictive Torque Control for Induction Machines Without Weighting Factors. *IEEE Trans. Power Electron.* **2020**, *35*, 1779–1788. [[CrossRef](#)]
48. Wang, J.; Yang, H.; Liu, Y.; Rodriguez, J. Low-cost Multi-step FCS-MPCC for PMSM Drives Using a DC Link Single Current Sensor. *IEEE Trans. Power Electron.* **2022**, *37*, 11034–11044. [[CrossRef](#)]
49. Najafzadeh, M.; Ahmadihangar, R.; Husev, O.; Roasto, I.; Jalakas, T.; Blinov, A. Recent Contributions, Future Prospects and Limitations of Interlinking Converter Control in Hybrid AC/DC Microgrids. *IEEE Access* **2021**, *9*, 7960–7984. [[CrossRef](#)]
50. Roasto, I.; Husev, O.; Najafzadeh, M.; Jalakas, T.; Rodriguez, J. Voltage Source Operation of the Energy-Router Based on Model Predictive Control. *Energies* **2019**, *12*, 1892. [[CrossRef](#)]

Publication IV

M. Najafzadeh, I. Roasto, T. Jalakas. "Energy Router Based Energy Management System for Nearly Zero Energy Buildings", 2019 IEEE 60th International Scientific Conference on Power and Electrical Engineering of Riga Technical University (RTUCON), Riga, Latvia, 2019, pp. 1–6, DOI: 0.1109/RTUCON48111.2019.8982366.

Energy Router Based Energy Management System for Nearly Zero Energy Buildings

1st Mahdiyyeh Najafzadeh
Department of Electrical Power
Engineering and Mechatronics
Tallinn University of Technology
Tallinn, Estonia
mahdieh.najafzadeh@taltech.ee

2nd Indrek Roasto
Department of Electrical Power
Engineering and Mechatronics
Tallinn University of Technology
Tallinn, Estonia
indrek.roasto@taltech.ee

3rd Tanel Jalakas
Department of Electrical Power
Engineering and Mechatronics
Tallinn University of Technology
Tallinn, Estonia
tanel.jalakas@taltech.ee

Abstract— Nearly Zero Energy Buildings (NZEBs) in the building sector, one of the most energy intensive fields in the modern world, are facing new challenges. These extremely energy efficient buildings can produce their own energy whereas local storage and sources are needed. To meet those goals, new technologies and control principles must be developed and implemented. Energy usage could be best optimized by a central energy management system (EMS). This paper proposes an energy router-based EMS for NZEBs. The concept and its features will be explained and analyzed. The energy router has many tasks, e.g. energy routing, system protection and reliability, voltage regulation. However, the focus of this paper will be on the power quality at the point of common coupling (PCC). Modern households are overwhelmed by the nonlinear electrical loads, which are lowering the power quality in the grid. The power quality is a serious issue also in NZEB. This paper will demonstrate how an energy router can be used to control reactive and active power and compensate current harmonics at the PCC. The system behavior will be simulated and verified by the experimental prototype.

Keywords— Power Factor Correction, Energy Management System, Near Zero Energy Buildings, harmonic compensation.

I. INTRODUCTION

Increasing rate of greenhouse gas emissions is one of the concerns that motivates humans to find appropriate solutions. The growing penetration of electrical technology in human life is inevitable and human habits are very difficult to change. These are the reasons for a steadily increasing rate of electricity consumption. The US Energy Information Administration has estimated a 56% rise of global electrical consumption from 2010 to 2040 [1]. Moreover, according to research, up to 40% of total electrical consumers are residential and commercial buildings, i.e. buildings contribute about 40% of the greenhouse gas emission [2][3]. In EU, 75% of the buildings are energy inefficient. However, 0.3-1% of the buildings are renovated annually, which results in energy savings of 5-6% and reduction of greenhouse gas emission of about 5%[3]. Thus, this sector has a great potential to save energy and reduce greenhouse gas emission. As a result, in the buildings sector, a paradigm shift has been launched from conventional buildings toward Nearly Zero Energy Buildings (NZEBs).

In October 2014, the European Council adopted the climate and energy framework for 2030. The key targets for 2030 [22]:

- 40% cuts in greenhouse gas emissions (from 1990 levels);
- 32% share for renewable energy;
- 32.5% improvement in energy efficiency.

To achieve those targets, both production and consumption sides must be taken care by finding alternative “green” electrical energy sources and reducing energy consumption. Consequently, the European Council established a new rule for all public buildings to be NZEB after December 2018, for all new buildings to be NZEB after 2020 and all existing ones from 2050 [23]. Based on the Energy Performance of the Building Directive, NZEBs are high-energy-performance buildings that meet their required electrical energy through on-site or nearby renewable energy resources [3]. Thus, NZEBs can use Distributed Generation (DG) and Distributed storage (DS) [2]. By utilizing DG, DS makes it possible to achieve annual energy balance, i.e. NZEBs feed back to the grid the same amount of energy that they have used. Additionally, based on the European Committee for standardization, electricity consumption should be reported not only annually but also weekly. This allows getting more accurate load profile model of a building [4].

Typically, DGs such as photovoltaic panels or wind generators in NZEB have an intermittent nature, thus they have strong impact on the power quality. Moreover, nonlinear loads inside the NZEB will consume a large amount of reactive power, which will increase transmission losses and reduce the power quality further [1]-[5]. Thus, to manage the generation and consumption in an optimized and efficient way, the NZEB needs an energy management system (EMS). The EMS could eliminate power quality problems and manage energy flow among DG and DS and loads [6]-[7].

Based on the literature, the EMS could be divided into distributed and central energy management systems, as shown **Error! Reference source not found.** In [8] an energy router (ER) based EMS for microgrids is explained. It is proposed to use solid state transformers as ERs. The ER is capable of generating AC and DC voltage and communicating through an open-standard-based communication interface. The EMS will be distributed between all devices connected to the microgrid, i.e. every connection to the microgrid should be done through the ER. Since there is no central control, this type can be classified as distributed EMS. By scaling this concept down to

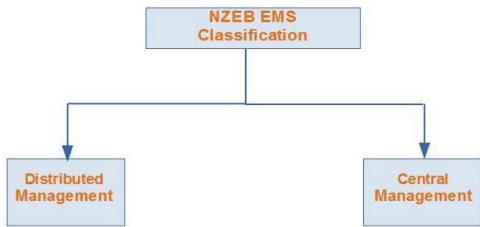


Fig. 1. EMS classification of NZEBs.

a building size it would mean that all DG, DS and loads in a house should be interfaced with smart power electronic converters that could maintain regulated voltage and frequency in all operation modes. This clearly requires major changes in the available infrastructure and does not suit for conventional buildings.

An alternative concept that is more suitable for conventional buildings could be classified as a central EMS. The main idea here is to connect a smart power electronic converter to the point of common coupling (PCC) of the building and leave everything else inside the building unchanged. Many papers address the increase of reliability and self-independence via a central EMS [24][25] [13].

We propose to use an ER as the central EMS for the NZEB. The general structure and operation modes of the concept are reported in [9]. The concept includes a single phase back-to-back type converter at the PCC. This converter can act as an EMS to manage all DC and AC sources, storages and loads. It provides AC and DC distribution buses. As a result, the EMS can connect, measure and manage an energy flow between the consumers and provides flexible protection against faults, e.g. grid blackout, short circuit, overload etc. The main improvement of the proposed EMS is providing voltage-controlled output (on the building side) that allows all local sources to run in on-grid and off-grid modes. By implementing ER to NZEB, it becomes an independent entity that acts as a controllable smart load for the main grid [9][10][11][12]. Moreover, ER allows implementing various active functions like [2][9][10] [13]:

- power control (active and reactive power);
- AC voltage control (compensation of voltage sags and peaks, harmonic control);
- AC current control (harmonic cancelation, short-circuit current limitation);
- DC link voltage control;
- Grid synchronization;
- integration of distributed generation (MPP tracking, energy storage);
- protection functions (island detection, frequency, voltage and current monitoring, short circuit protection);
- improved reliability (modular structure, redundant power supply).

The central EMS must be able to provide power quality at the PCC and inside the NZEB. In our latest study [10], we addressed building related power quality issues. In this paper,

we demonstrate how an ER based EMS can provide power quality at the PCC of the NZEB. The mathematical model of the system will be used to tune regulators and estimate the stability margin. The simulation results are shown and verified by an experimental prototype.

II. ENERGY ROUTER BASED ENERGY MANAGEMENT SYSTEM FOR NZEB

Typically, the microgrid below 20 kW is classified as a nanogrid [2][3][14][15]. The NZEB with proper EMS can behave as the nanogrid. Having both DC and AC distribution buses available, the NZEB can be seen as a hybrid nanogrid [2]. **Error! Reference source not found.** shows the proposed concept of EMS for the NZEB. The main benefit of the ER based EMS is that it is combining EMS and power electronics in one device. Thus, the EMS has close control over the hardware, power quality and energy flow at the PCC. ER can have multi port structure that simplifies DS and implementation of renewable sources in NZEBs. Moreover, through smart EMS it can convert a conventional NZEB into off-grid capable buildings, i.e. emulate grid in an islanded mode so that all DG and loads in the building could continue working.

The proposed ER structure consists of three levels (**Error! Reference source not found.**): power electronic, communication and energy management level. The power electronic level can consist of two back to back full bridge converters used to manage the energy flow between the main grid and the residential building. The communication level is used to communicate between the main grid and the EMS. The EMS acts as the main key in the NZEB, it controls the power electronic level in order to manage the NZEB's power consumption in an efficient way.

The proposed ER consists of three different ports: two AC single phase ports and a DC port [9]. The first AC port is connected to the main grid by the grid side inverter. The second AC port is connected to the building side through a load inverter. DC loads, sources and storage connect to the DC-port by a DC-DC converter [9]. The grid inverter and load inverter are connected by a common DC-link. The grid inverter connects the NZEB to the distribution grid and controls the

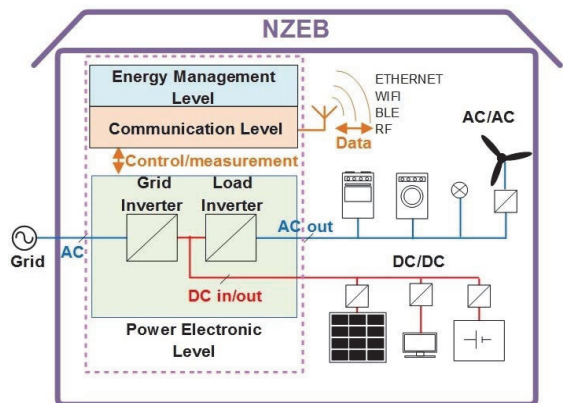


Fig. 2. Proposed concept of the NZEB.

power flow and quality [16]. It also acts as a synchronous

rectifier with power factor correction (PFC). This inverter controls the grid current. By controlling the grid current, it can manage the sent active and reactive power to the grid [9]. From the viewpoint of the distribution grid, the whole NZEB is considered as a DG; if it injects the extra electrical energy to the grid. There are different methods to satisfy the desired active and reactive power of the grid such as master-slave control, average current sharing control and droop control. The most popular method is droop control since it does not need critical communication links among ERs and the distribution grid [26].

The load inverter is a voltage controlled sine wave inverter that emulates the behavior of the grid. In [10] more detailed information about the operation of a load inverter can be found. Our focus here is on grid inverter operation and power quality issues at the PCC.

III. MODEL OF THE SYSTEM

The standard IEEE1547 defines the requirements for the power quality of the distributed resources when they are connected to the grid. The total harmonic distortion (THD) of the grid current should be smaller than 5%. In addition, the power factor must be greater than 0.9 since reactive power consumption from the grid increases transmission losses. Thus, ER should only inject and consume sinusoidal current (THD < 5%) aligned with the line voltage.

Different types of PFC could be used in the NZEB EMS like passive type (adding passive components like inductance or capacitance) or active PFC. Passive components are bulky and the passive PF filter could correct the power factor only to 0.86 [17]. An ER based EMS enables active PFC without addition of extra components. With active PFC, a higher PF could be reached [18][19].

A. Model of the Plant

The ER consists of a back-to-back converter with two AC and one DC port. The active PFC is only involving the input stage of the topology; thus the output inverter can be omitted from the model for simplicity. The plant of the ER consists of an LCL filter and a full-bridge inverter, as shown in Fig. 3. An LCL filter is used to eliminate the high switching frequency. State space equations can model the dynamic behavior of the plant. The plant space state equations are defined as:

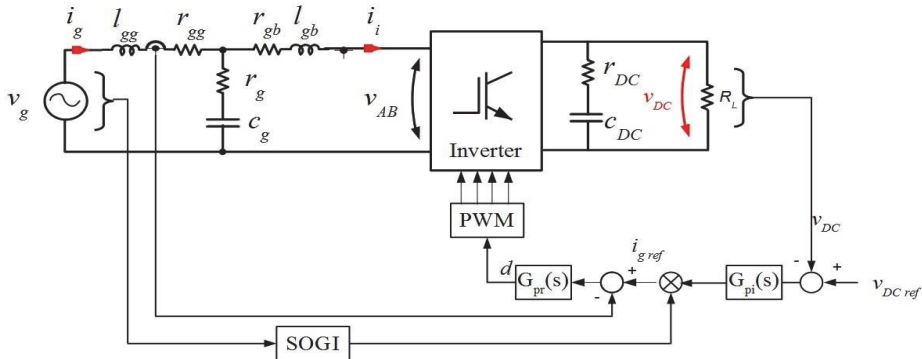


Fig. 3. Model of the plant and the control system.

$$\begin{cases} \frac{dx(t)}{dt} = A \cdot x(t) + B \cdot u(t) \\ y(t) = Cx(t) + Eu(t), \end{cases} \quad (1)$$

where $x(t)$, $u(t)$ and $y(t)$ are state space parameters, inputs and output, respectively. These matrixes are:

$$x(t)^T = [i_g(t) \quad i_i(t) \quad v_c(t)], \quad (2)$$

$$u(t) = [v_{AB}(t)], \quad (3)$$

$$y(t) = i_g(t), \quad (4)$$

$$A = \begin{bmatrix} -(r_g + r_{gg}) & r_g & -\frac{1}{l_{gg}} \\ l_{gg} & l_{gg} & -\frac{1}{l_{gg}} \\ r_g & -\frac{1}{l_{gb}} & \frac{1}{l_{gb}} \\ l_{gb} & -\frac{1}{l_{gb}} & \frac{1}{l_{gb}} \\ \frac{1}{c_g} & -\frac{1}{c_g} & 0 \end{bmatrix}, \quad (5)$$

$$C = [1 \quad 0 \quad 0], B = \begin{bmatrix} 0 \\ -1 \\ l_{gb} \\ 0 \end{bmatrix}, E = 0,$$

After simplifying the above equations, the inverter voltage to the grid current transfer function is derived as:

$$G_{igv}(s) = \frac{i_g(s)}{v_{AB}(s)} \quad (6)$$

where:

$$\begin{aligned} i_g(s) &= c_g r_g s + 1, v_{AB}(s) = (c_g l_{gb} l_{gg}) s^3 + \\ &(c_g l_{gb} r_g + c_g l_{gg} r_g + c_g l_{gb} r_{gg} + c_g l_{gg} r_{gb}) s^2 + \\ &(l_{gg} + l_{gb} + c_g r_g r_{gg} + c_g r_g r_{gb} + c_g r_{gb} r_{gg}) s + \\ &r_{gb} + r_{gg} \end{aligned} \quad (7)$$

B. Model of the Controller

The PFC is just one of many features of the proposed ER based EMS. The control algorithm of the PFC consists of the DC-link voltage and an input current regulation loop, as shown in Fig. 3. The DC-link voltage is regulated by the PI regulator that stabilizes it at 400 V. The DC-link voltage loop programs current reference for a proportional resonant (PR)

current regulator.

To synchronize the input current with the grid voltage, a second order generalized integrator (SOGI) based PLL was implemented. It extracts the phase and the amplitude from the grid voltage v_g . The SOGI output is multiplied with the current amplitude. As a result, sinusoidal grid current reference will be derived and fed to the current regulator [12].

PR regulator transfer function [20][21] is expressed as:

$$G_{PR}(s) = K_{pg} + K_i \frac{2\omega_c s}{s^2 + 2\omega_c s + \omega_0^2} \quad (8)$$

where K_{pg} is the proportional gain, K_i is the integral gain, ω_0 is the grid frequency (rad/s) and ω_c is the cutoff frequency. To mitigate higher harmonics available in the grid voltage, harmonic compensations is used. The harmonic compensator transfer function is

$$G_{HC}(s) = \sum_{h=3,5,7,9} K_{hi} \frac{2\omega_c s}{s^2 + 2\omega_c s + (h\omega_0)^2} \quad (9)$$

where K_{hi} is the integral gain of the corresponding harmonic, h is the number of the harmonic to be compensated.

In this work, a digital delay of one sample time considered is defined as:

$$G_D(z) = z^{-1} \quad (10)$$

So the close loop system in discrete time is obtained as follows:

$$G_{closed\ loop}(z) = \frac{G_{PR}(z) \times G_{igv}(z)}{1 + G_{PR}(z) \times G_D(z) \times G_{igv}(z)} \quad (11)$$

The closed loop system is stable as there are no poles in the right half plane (Fig. 4).

IV. SIMULATION OF THE ER OPERATION

A. Simulation and experimental parameters

Table 1 shows parameters used in the simulation and experiment.

B. Computer simulation

The simulations were carried out with the PLECS software. A distorted grid voltage with injected 5th harmonic was used to check the PR regulator operation. A residential load about 0.9 kW was considered. Fig. 5 shows both the grid current and voltage without a PFC regulator. As Fig. 5 shows, the grid inverter acts as a full bridge diode rectifier in this condition, the grid current THD is 140% i.e. totally unacceptable. DC link voltage alternates between 323 and 313v. Fig. 6 represents the same parameters with a PR controller. Comparison of the two former figures confirms the output controlled-parameters improvement in the grid current and the DC link voltage. The results were obtained through an ER in the NZEB at the PCC. The power factor correction forces the current to be sinusoidal and in phase with the grid voltage, as shown in Fig. 6. The THD of the grid current is 2%, which is within acceptable

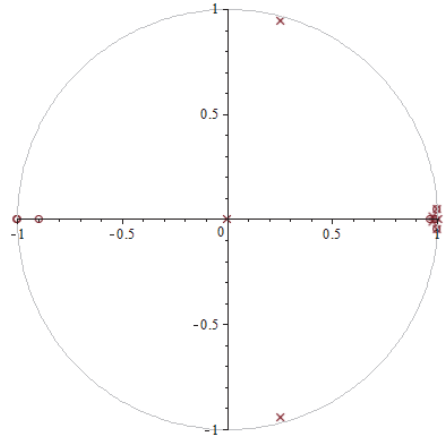


Fig. 4. Pole zero plot of the PR controller and the plant transfer function.

TABLE 1. SIMULATION AND EXPERIMENT PARAMETERS.

Symbol	Parameter	Value
v_g	Input voltage (RMS)	230 V, 50 Hz
l_{gg}	Grid -side LCL inductor	0.6 mH
r_{gg}	Series resistor of the inductor	0.1 Ω
c_{DC}	HV DC-link capacitor	400 μ F
g_b	Inverter -side LCL filter inductor	1.44 mH
r_{gb}	Series resistor of the inductor	0.1 Ω
c_g	LCL filter capacitor	3 μ F
U_{dc}	DC link voltage	400 V
P_{out}	Output power	1 kW
F_{sw}	Switching frequency	20 kHz

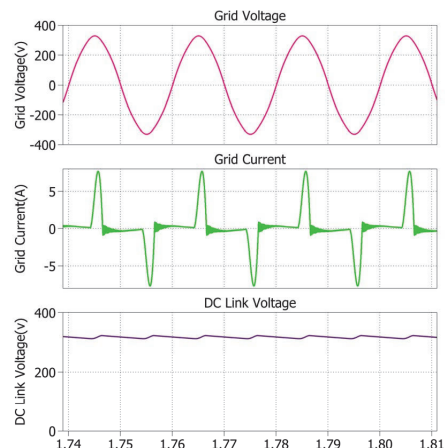


Fig. 5. Grid Voltage and Current, DC Link Voltage without PFC.

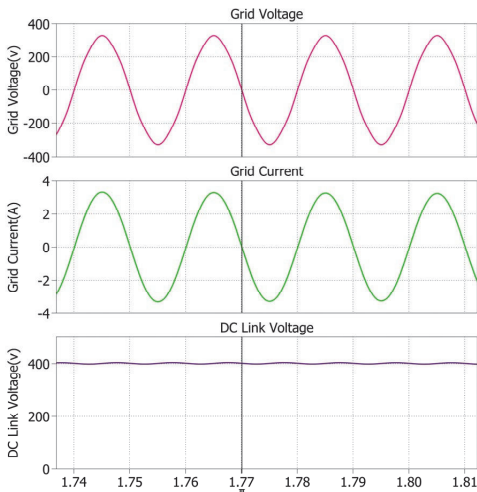


Fig. 6. Grid voltage and current, DC Link voltage based on the PR controller.

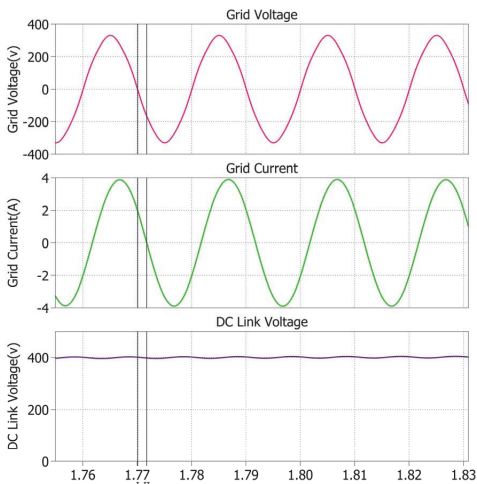


Fig. 7. Grid voltage and current, DC Link voltage at 30 degree.

limits. The DC voltage has 4% fluctuation, which is also acceptable.

To test the reactive power control function of the ER based EMS, a 30 degree phase shifted current reference was fed to the PR regulator, as shown in Fig. 7. The grid current remains sinusoidal with the phase lag of 30 deg. Thus, the converter is acting as a pure inductive load and is consuming reactive power.

V. EXPERIMENTAL RESULT

The simulation results were verified on an experimental prototype. The experimental setup of the ER for the NZEB consists of two full-bridge IGBT inverters connected to each other via a 400 V DC link, as shown in Fig. 8. The experiments were carried out at 0.9 kW power.

Fig. 9 depicts two LCL filters with specification in Table 1 implemented to decrease the harmonic component. Control

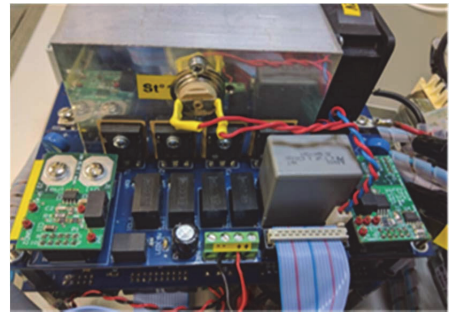


Fig. 8. EMS Hardware Prototype.



Fig. 9. NZEB EMS grid and load-side LCL filters.

system hardware is realized in PLECS RTbox Rapid Control Prototype that enables PLECS power electronics simulation software to be interfaced with real devices. Output signals of voltage and current sensors are directly connected to the analog inputs of the RT box rapid control prototype system and IGBT drivers to the digital outputs. The proposed control system is able to correct PFC, as the experimental result in Fig. 10 shows.

VI. CONCLUSIONS

The increasing penetration of DS and DG along with continuously increasing number of nonlinear loads in modern households has made power quality one of the major concerns. To guarantee power quality in the NZEB, an energy

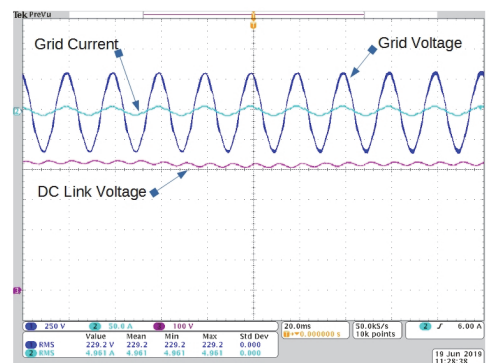


Fig. 10. Grid voltage and current.

management system is needed. The key technology here is the ER based EMS concept. In this paper we focused on the active rectifier, which will be the input stage of the ER. The ER based EMS can be implemented as an active or reactive power regulator. The EMS was first modeled and then simulated and implemented on the prototype. The proposed ideas were confirmed by the simulation and experimental results.

ACKNOWLEDGMENT

This research was co-financed by the Estonian Research Council grant PUT1680 and by the Estonian Centre of Excellence in Zero Energy and Resource Efficient Smart Buildings and Districts, ZEBE, grant 2014- 2020.4.01.15-0016 funded by the European Regional Development Fund.

REFERENCES

- [1] P. Arbolea *et al.*, "Efficient energy management in smart micro-grids: ZERO grid impact buildings," *IEEE Trans. Smart Grid*, vol. 6, no. 2, pp. 1055–1063, 2015.
- [2] I. Roasto, T. Jalakas, and A. Rosin, "Bidirectional Operation of the Power Electronic Interface for Nearly-Zero Energy Buildings Acknowledgments Keywords Control Structures Basic Control Structures," *2018 20th Eur. Conf. Power Electron. Appl. (EPE'18 ECCE Eur.)*, 2018.
- [3] L. Martirano, E. Habib, A. Giuseppi, and A. Di Giorgio, "Nearly zero energy building model predictive control for efficient heating," *2018 IEEE Ind. Appl. Soc. Annu. Meet. IAS 2018*, pp. 1–6, 2018.
- [4] K. Doubleday *et al.*, "Integrated distribution system and urban district planning with high renewable penetrations," *Wiley Interdiscip. Rev. Energy Environ.*, no. March 2018, pp. 1–15, 2019.
- [5] K. Nikum, R. Saxena, and A. Wagh, "Effect on power quality by large penetration of household non linear load," *1st IEEE Int. Conf. Power Electron. Intell. Control Energy Syst. ICEPICES 2016*, pp. 1–5, 2017.
- [6] D. Dong, F. Luo, X. Zhang, D. Boroyevich, and P. Mattavelli, "Grid-interface bidirectional converter for residential DC distribution systems - Part 2: AC and DC interface design with passive components minimization," *IEEE Trans. Power Electron.*, vol. 28, no. 4, pp. 1667–1679, 2013.
- [7] L. Martirano *et al.*, "Demand Side Management in Microgrids for Load Control in Nearly Zero Energy Buildings," *IEEE Trans. Ind. Appl.*, vol. 53, no. 3, pp. 1769–1779, 2017.
- [8] A. Q. Huang, M. L. Crow, G. T. Heydt, J. P. Zheng, and S. J. Dale, "The future renewable electric energy delivery and management (FREEDM) system: The energy internet," *Proc. IEEE*, vol. 99, no. 1, pp. 133–148, 2011.
- [9] A. R. Indrek Roasto, Tanel Jalakas, "Control of Bidirectional Grid- Forming Inverter for Nearly Zero Energy Buildings," pp. 1–6, 2018.
- [10] Roasto, Husev, Najafzadeh, Jalakas, and Rodriguez, "Voltage Source Operation of the Energy-Router Based on Model Predictive Control," *Energies*, vol. 12, no. 10, p. 1892, 2019.
- [11] I. Cvetkovic *et al.*, "A testbed for experimental validation of a low-voltage DC nanogrid for buildings," *15th Int. Power Electron. Motion Control Conf. Expo. EPE-PEMC 2012 ECCE Eur.*, p. LS7c.5-1-LS7c.5-8, 2012.
- [12] I. Roasto, A. Rosin, and T. Jalakas, "Multiport Interface Converter with an Energy Storage for Nanogrids," *IECON 2018 - 44th Annu. Conf. IEEE Ind. Electron. Soc.*, vol. 1, pp. 6088–6093.
- [13] R. Majumder, A. Ghosh, G. Ledwich, and F. Zare, "Power management and power flow control with back-to-back converters in a utility connected microgrid," *IEEE Trans. Power Syst.*, vol. 25, no. 2, pp. 821–834, 2010.
- [14] E. Hamatwi, I. E. Davidson, J. Agee, and G. Venayagamoorthy, "Model of a hybrid distributed generation system for a DC nano-grid," *Clemson Univ. Power Syst. Conf. PSC 2016*, pp. 1–8, 2016.
- [15] S. Teleke, L. Oehlerking, and M. Hong, "Nanogrids with energy storage for future electricity grids," *2014 IEEE PES T&D Conf. Expo.*, pp. 1–5, 2014.
- [16] I. Roasto, A. Rosin, and T. Jalakas, "Power electronic interface converter for resource efficient buildings," in *Proceedings IECON 2017 - 43rd Annual Conference of the IEEE Industrial Electronics Society*, 2017.
- [17] I. M. Safwat and W. Xiaohua, "Comparative study between Passive PFC and Active PFC based on Buck-Boost Conversion," no. 1, pp. 45–50, 2017.
- [18] Y. S. Kim, W. Y. Sung, and B. K. Lee, "Comparative performance analysis of high density and efficiency PFC topologies," *IEEE Trans. Power Electron.*, vol. 29, no. 6, pp. 2666–2679, 2014.
- [19] K. Raggl, T. Nussbaumer, G. Doerig, J. Biela, and J. W. Kolar, "Comprehensive design and optimization of a high-power-density single-phase boost PFC," *IEEE Trans. Ind. Electron.*, vol. 56, no. 7, pp. 2574–2587, 2009.
- [20] W. Ping, G. Lin, Z. Zhe, C. Liuye, and W. Wei, "Switch-mode AC stabilized voltage supply based on PR controller," *2013 5th Int. Conf. Power Electron. Syst. Appl. PESA 2013*, pp. 1–4, 2013.
- [21] G. Zeng and T. W. Rasmussen, "Design of current-controller with PR-regulator for LCL-filter based grid-connected converter," *2nd Int. Symp. Power Electron. Distrib. Gener. Syst. PEDG 2010*, pp. 490–494, 2010.
- [22] "Homepage of European Council," [Online]. https://ec.europa.eu/clima/policies/strategies/2030_sv..
- [23] "NEARLY ZERO ENERGY BUILDINGS DEFINITIONS ACROSS EUROPE," [Online]. http://bpie.eu/uploads/lib/document/attachment/128/BPIE_fa_csheet_nZEB_definitions_across_Europe.pdf
- [24] S. I. Ganesan, D. Pattabiraman, R. K. Govindarajan, M. Rajan, and C. Nagamani, "Control Scheme for a Bidirectional Converter in a Self-Sustaining Low-Voltage DC Nanogrid," *IEEE Trans. Ind. Electron.*, vol. 62, no. 10, pp. 6317–6326, 2015.
- [25] S. Mishra and O. Ray, "Advances in nanogrid technology and its integration into rural electrification in India," in *2014 International Power Electronics Conference (IPEC-Hiroshima 2014 - ECCE ASIA)*, 2014, no. c, pp. 2707–2713.
- [26] U. B. Tayab, M. A. Bin Roslan, L. J. Hwai, and M. Kashif, "A review of droop control techniques for microgrid," *Renew. Sustain. Energy Rev.*, vol. 76, no. May 2016, pp. 717–727, 2017.

Mahdiyyeh Najafzadeh received her M.Sc in power electronics and electric machinery engineering from K.N. Toosi University of Technology, Tehran, Iran in 2016. In 2018, she entered Tallinn University of Technology. Her research interest is design and control of power electronics converters, including modeling, design, simulation and application of control systems in converters.

Publication V

M. Najafzadeh, O. Husev, I. Roasto, T. Jalakas. "Improved DC-Link Voltage Transient Response and Stability Issues in Energy Router with Fuzzy Logic Control Method", 2020 IEEE 60th International Scientific Conference on Power and Electrical Engineering of Riga Technical University (RTUCON), Riga, Latvia, 2020, pp. 1–6, DOI: forthcoming.

Improved DC-Link Voltage Transient Response and Stability Issues in Energy Router with Fuzzy Logic Control Method

Mahdieh Najafzadeh, Oleksandr Husev, Indrek Roasto, Tanel Jalakas
Power Engineering and Mechatronics department
Tallinn University of Technology
Tallinn, Estonia
mahdieh.najafzadeh@taltech.ee

Abstract—This work proposes an intelligent control method for ensuring the Direct Current (DC) link voltage stability and for improving the DC-link voltage transient response in a residential Energy Router (ER). This ER is an interface among the main grid, local AC or DC loads and sources. When connecting different loads to the DC-link, the classic Proportional Integrator Derivative (PID) controller has been unable to provide a stable DC-link voltage. In this study, the PID controller will be compared with the proposed fuzzy logic controller in different DC load levels. The results prove the enhanced functionality of the proposed control method.

Keywords—energy router; fuzzy logic control; DC-link control;

I. INTRODUCTION

Increasing penetration of renewable energy sources (RES) and power electronics devices in the main grid have created challenges. One issue relates to the intermittent nature of RES which requires complicated control systems. The growing application of power electronics devices in both sources and loads is another concern that has made the control and modeling of systems more complex. The traditional design of the control system requires a mathematical model of that system. The more complicated the system is the less effective the mathematical model is [1]. Nonlinear systems are other challenges that limit the application of the mathematical model and classical linear controllers [2]. Fuzzy logic control (FLC) can be implemented on a nonlinear system. FLC uses a nonlinear control method. In other words, it is a model-free approach for complex system control [3][4]. The basic underlying concept is using linguistic variables instead of numbers for computing systems. Although using linguistic variables are not as precise as numbers, they are closer to human intuition [5]. So FLC is an intelligent control system, which emulates human behavior in the tuning of fuzzy logic controller [6][2]. This method has been implemented in a different configuration of sources and loads e.g. [4] suggested this method to control the fuel cell to prolong its lifetime. The method is used in a DC microgrid consist of a storage system, wind turbine, fuel cell, and loads. FLC is also used in [7] to manage the batteries to enhance their life in a DC microgrid. The microgrid contains photovoltaic (PV) panels, batteries, loads. In this work, two different FLCs are considered for charging and discharging the current reference of batteries. The main target of this work is to limit the battery's state of the charge (SOC) level

in a predefined margin. A similar study is also conducted in [8] within an isolated hybrid microgrid consist of a wind turbine, PV, and diesel generator. FLC is used to provide the AC bus reference current in the d-q frame. Then the results are compared to PI regulators. Previous proposed FLCs were multiple inputs-single-output (MISO). In [3] a single input- single output (SISO) FLC is proposed. This FLC is used for controlling the ultracapacitor (UC) with batteries in a battery- UC hybrid energy storage system. Battery system management with FLC is studied in different work such as [9][10][11], and [12]. FLC is implemented in a configuration of battery, PV, and wind turbine with FLC is studied in [9]. A hybrid microgrid consists of PV, fuel cell, hydrogen electrolyzer system, and some AC and DC loads with wind and battery are studied in [10]. [12] suggested using FLC to provide modified virtual resistance of the droop controller based on the SOC. In this work, two operation modes of MPPT and DC-link voltage in the battery are studied. FLC is used to control the charging and discharging current of the battery system to extract the MPPT in both PV and wind. FLC in control of the battery system in a multiport energy router is suggested in [13]. Another study for DC-link voltage control in a wind farm is done in [14], in this work, the difference voltage between DC-link voltage and its reference value is used as input of FLC to provide d reference wind current in the d-q frame. In this paper, a MISO FLC is used to stabilize the DC-link voltage. FLC is also applied in AC microgrid to control the frequency in [15]. In this study, FLC is used to provide the PID gain to stabilize the frequency. FLC in an adaptive droop controller in a DC microgrid is discussed in [16]. In all cases, it is observed that FLC is more flexible in the presence of disturbance. In this paper, a MISO FLC is used to stabilize the DC bus voltage. The general control block of the system with FLC is shown in Fig. 1.

II. SYSTEM DESCRIPTION

The Energy Router (ER) proposed for Nearly Zero Energy Building (NZEB) application is based on a single-phase back-to-back Voltage Source Inverter (VSI) topology, as shown in Fig. 2. Different operation modes in various conditions have been studied in [17]. Different loads and sources can be

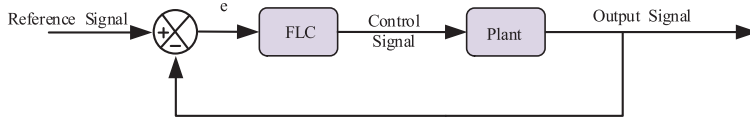


Fig. 1. General control block of a system with FLC.

connected to the DC or AC buses. The grid side inverter or VSI1 based on the PR controller works synchronously with the grid [18]. The Power Factor Correction (PFC) algorithm based on a PI regulator draws a sinusoidal grid current and steps up the dc-link voltage to 400 V. The NZEB side inverter or VSI2 works as grid forming. It produces a stable voltage on the AC bus. Model Predictive Control (MPC) is implemented in NZEB or load side converter to provide stable AC bus voltage in different operating conditions like no-load and nonlinear loads. More details in the implementation of the MPC controller can be found in [19]. PFC based PI regulator has fixed and inflexible coefficients that limit its application in various operation conditions [20]. In this case, without any DC load, the PI regulator works well with PR and MPC controller. However, in case of adding some DC loads to the DC bus, the system is going to be unstable. That is due to the linear nature of the PI regulator and disability to provide stable DC-link voltage in a wide range of loads. As a result, an intelligent control method such as FLC is suggested to be implemented instead of a regular PI controller, as shown in Fig. 2. FLC can decide and adjust its output based on its inputs in a nonlinear way that it will explain in detail.

III. DESIGN OF FUZZY LOGIC CONTROLLER

FLC includes five steps: the determination of the required parameters, fuzzification, knowledgebase, logic interface (rules), and defuzzification [1][6]. Our proposed FLC has two inputs: DC-link-voltage error-signal and its derivative value which shows the trend of the error signal. This input helps FLC

to make different decisions based on the instantaneous slope of the error signal. FLC output is the derivative of the reference grid current which is demonstrated in Fig. 3. To clarify more, a sample of the error signal is demonstrated in Fig. 4. As shown in this fig., four different operation conditions are explained in Table 1. The target is to stabilize the error signal around zero, so e.g. in point 1 the error signal is positive which shows the DC link voltage is bigger than the reference value, also the positive instantaneous slope demonstrates the increasing rate of the error signal; as a result, the reference grid current should be decreased to decrease the error signal. In point 2, the error signal is equal to point 1 but the slope is negative which shows the decreasing trend of it so it is not needed to change the grid reference current. FLC adjusts the sign and amount of output based on the sign and amounts of its inputs; e.g. if the error signal is positive high

TABLE 1. SPECIFICATIONS OF FOUR DIFFERENT CONDITIONS.

	Error signal	The derivative of the error signal	Preferred grid reference current derivative
Point 1	+v	+	Decrease(-)
Point 2	+v	-	Zero(0)
Point 3	-v	-	Increase(+)
Point 4	-v	+	Zero(0)

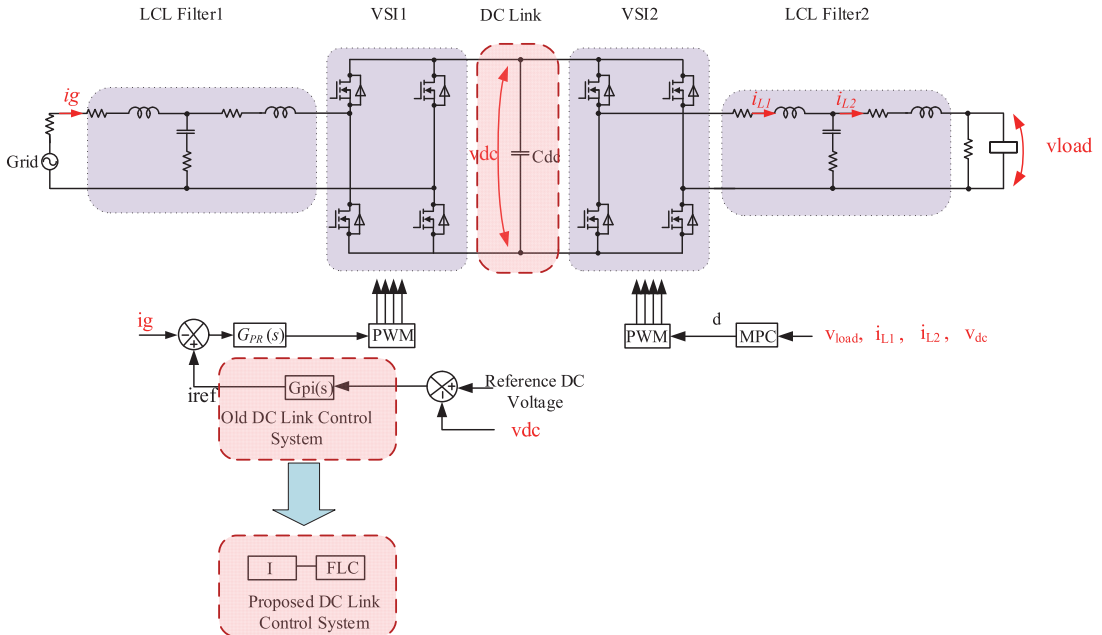


Fig. 2. The proposed NZEB energy router topology.

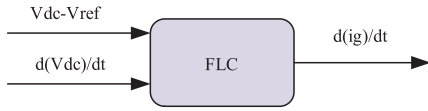


Fig. 3. FLC inputs and output.

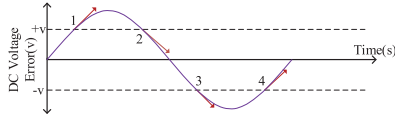


Fig. 4. A sample of the error signal.

and the trend is also positive high so it should set its output to high negative to regulate fast enough its output.

In this paper, the Mamdani method is used. Seven different intervals for each input and the output membership functions are considered that are called as negative high (NH), negative medium (NM), negative small (NS), zero (Z), positive small (PS), positive medium (PM) and positive high (PH). A sample membership function curve for the input error signal is shown in Fig. 5. As an inevitable charging and discharging nature of the DC link capacitor, the DC link voltage has variations. The accepted variation is assumed at ± 4 V (for the nominal value of 400 V), about this area is set to zero zones in error signal membership function. Variations of more than ± 30 V is categorized in high areas. Small zones are categorized to less than ± 10 V. Medium zones (negative and positive) are devoted to the areas between small and high zones. Based on different loads, the DC-link voltage decline and its slope vary. The more DC load is, the more sudden reduction in DC voltage at the connecting time will happen. Also, the more grid reference current is required. In this case, the controller must adjust its

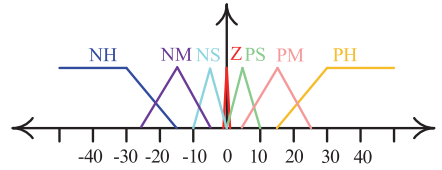


Fig. 5. Membership function of error DC-link voltage signal.

output in high zones to regulate the fast changes in DC voltage. In case of low DC load, the drop in DC voltage is lower and the controller must set its output in medium zones. The main tool to provide this desired behavior of the controller is the table rule. Table rules for low load and high load are depicted in Table 2 and Table 3 respectively.

The fuzzy output surface is also demonstrated in Fig. 6.

IV. SIMULATION RESULT

The simulation is carried out in PLECS software. The system specifications are depicted in Table 4. The simulation is performed for different DC loads as shown in Table 5. In all cases at $t = 0.35$ s, the DC load is added then at $t = 0.5$ s the NZEB load is inserted to the system. A 106 W resistive load is implemented in the NZEB side. The results for small DC load with PI and FLC are demonstrated in Fig. 7. and Fig. 8. In both regulators, DC-link voltage reaches 400 V smoothly. Grid current THD is 2% with FLC and 8.4% with the PI regulator. Also, in both cases, the NZEB side voltage is sinusoidal and stable, which shows that FLC can work well with MPC. In scenario 2 as shown in Fig. 9. and Fig. 10., grid current THD in

TABLE 2. TABLE RULES FOR LOW LOAD.

Error Signal Derivative / Error Signal	Negative high	Negative medium	Negative small	zero	Positive small	Positive medium	Positive high
Negative high	PH	PH	PH	PH	PH	PH	PM
Negative medium	PH	PM	PS	PS	PS	Z	Z
Negative small	PM	PS	PS	PS	Z	PS	Z
zero	PS	Z	Z	Z	Z	Z	NS
Positive small	Z	Z	Z	NS	NS	NS	NM
Positive medium	Z	Z	NS	NS	NS	NM	NH
Positive high	NM	NH	NH	NH	NH	NH	NH

TABLE 3. TABLE RULES FOR HIGH LOADS.

Error Signal Derivative / Error Signal	Negative high	Negative medium	Negative small	zero	Positive small	Positive medium	Positive high
Negative high	PH	PH	PH	PH	PH	PH	PH
Negative medium	PH	PM	PM	PM	PS	PS	PS
Negative small	PM	PM	PS	PS	Z	Z	Z
zero	PS	PS	Z	Z	Z	NS	NS
Positive small	Z	Z	Z	NS	NS	NM	NM
Positive medium	NS	NS	NS	NM	NM	NM	NH
Positive high	NH	NH	NH	NH	NH	NH	NH

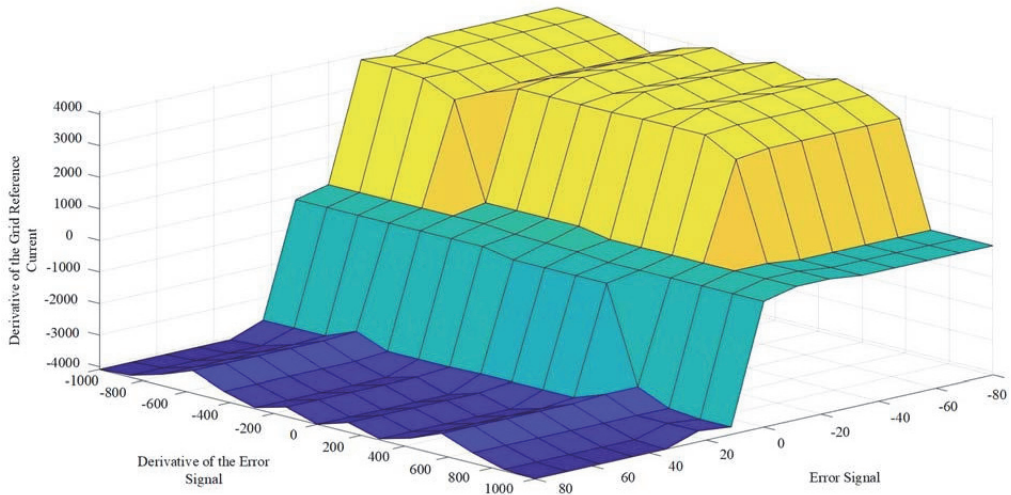


Fig. 6. Output surface of high load FLC.

PI and FLC regulator are 3.5% and 3% respectively. In this regard, the results in this scenario are similar. The results in this scenario are sinusoidal with acceptable THD. However, comparing the DC-link voltages in two cases (PI and FLC regulators) of scenario 3, (Fig. 11, Fig. 12) shows that PI cannot and the FLC can provide a stable DC-link voltage in high DC load. THD of the grid current with the FLC regulator is 0.8% which is acceptable.

V. CONCLUSIONS

FLC relies on the experience rather than on a mathematical model which makes it easy to implement in complicated systems. The simulation results of this work showed FLC's ability to enhance the control of DC-link voltage in the presence of different DC loads. Comparing FLC with PI regulator results

confirm its ability to provide more stable DC-link voltage and better power quality of the grid current that is another advantage of this regulator. The nonlinear nature of the FLC helps to tune it for a wide range of loads and disturbances.

ACKNOWLEDGMENT

This research was co-financed by the Estonian Research Council grants PUT1680, PRG675 and by the Estonian Centre of Excellence in Zero Energy and Resource Efficient Smart Buildings and Districts, ZEBE, grant 2020- 2020.4.01.15-0016 funded by the European Regional Development Fund.

TABLE 4. SPECIFICATIONS OF THE SYSTEM.

Symbol	Parameter	Value
v_g	Grid and Load side voltage (RMS)	230 V, 50 Hz
l_{gg}	Grid -side LCL inductor	0.6 mH
r_{gg}	Series resistor of the inductor	0.1 Ω
c_{DC}	DC-link capacitor	1000 μ F
g_b	Load -side LCL filter inductor	1.44 mH
r_{gb}	Series resistor of the inductor	0.1 Ω
c_g	LCL filter capacitor	3 μ F
U_{dc}	DC link voltage	400 V
P_{out}	NZEB Output power	106 W
F_{sw}	Switching frequency	20 kHz
P_{DC}	DC link power	0.004, 0.4, 4 kW

TABLE 5. THREE DIFFERENT DC LOAD SCENARIOS.

Scenario	Load Type	DC Load Power (W)
1	Low Load	$P_{DC} = 4$
2	Medium Load	$P_{DC} = 400$
3	High Load	$P_{DC} = 2000$

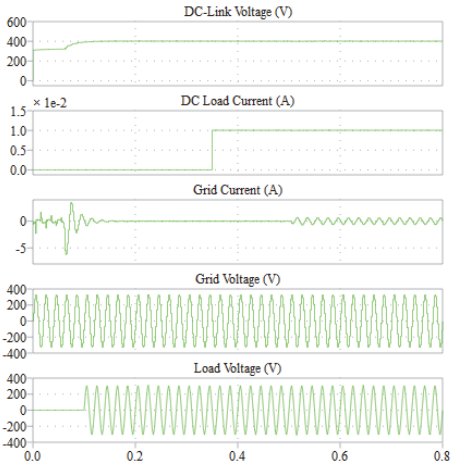


Fig. 7. Simulation results for scenario 1 with PI regulator.

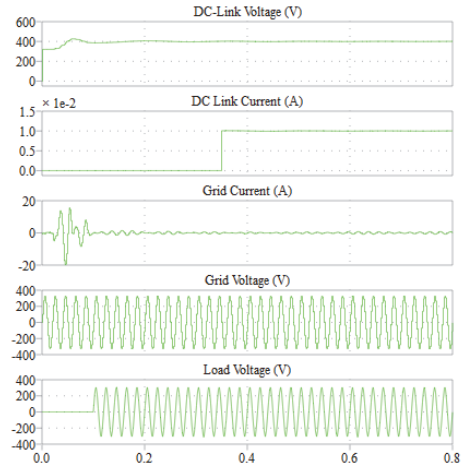


Fig. 8. Simulation results for scenario 1 with FLC.

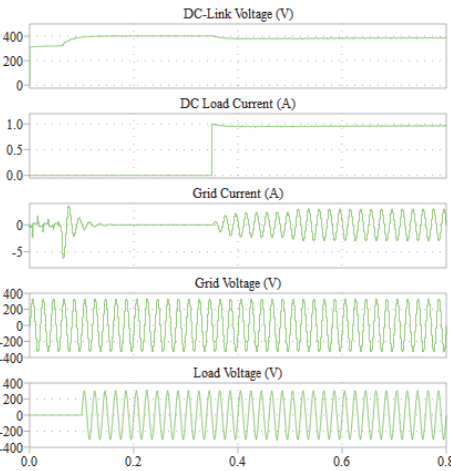


Fig. 9. Simulation results for scenario 2 with PI regulator.

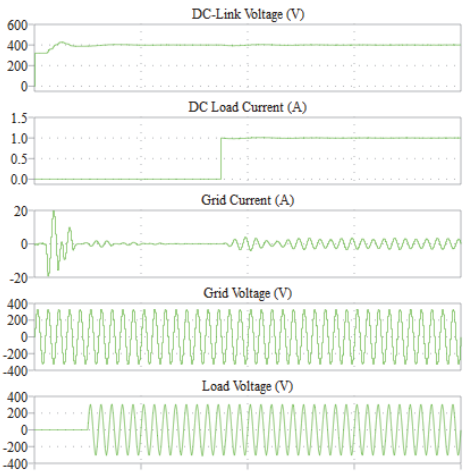


Fig. 10. Simulation results for scenario 2 with FLC.

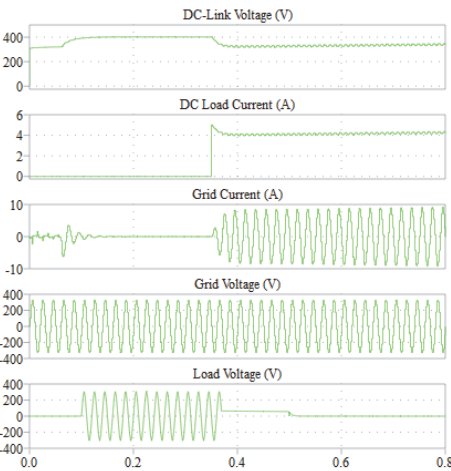


Fig. 11. Simulation results for scenario 3 with PI regulator.

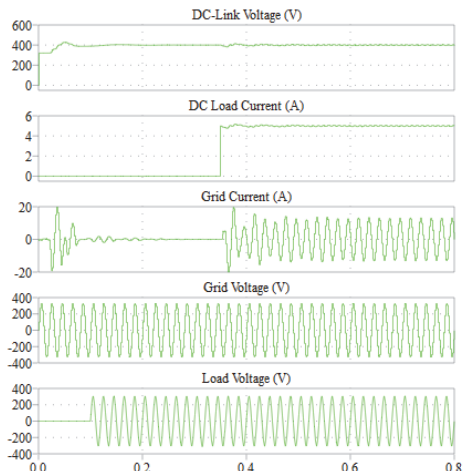


Fig. 12. Simulation results for scenario 3 with FLC.

References

- [1] "Neural and Fuzzy Logic Control of Drives and Power Systems," *Neural Fuzzy Log. Control Drives Power Syst.*, 2002.
- [2] O. Husev, S. Ivanets, and D. Vinnikov, "Neuro-fuzzy control system for active filter with load adaptation," *2011 7th Int. Conf. Compat. Power Electron. CPE 2011 - Conf. Proc.*, pp. 28–33, 2011.
- [3] R. Bhosale and V. Agarwal, "Fuzzy logic control of the ultracapacitor interface for enhanced transient response and voltage stability of a dc microgrid," *IEEE Trans. Ind. Appl.*, vol. 55, no. 1, pp. 712–720, Jan. 2019.
- [4] A. Hajizadeh, M. Soltani, and L. E. Norum, "Intelligent power control of DC microgrid," *2017 IEEE 17th Int. Conf. Ubiquitous Wirel. Broadband, ICUWB 2017 - Proc.*, vol. 2018-Janua, pp. 1–5, 2018.
- [5] A. V. Kumar, P. M. Rao, B. S. Rao, A. Vinod Kumar, P. Maheswara Rao, and B. Srinivasa Rao, "Modified Voltage Control Strategy for DC Network with Distributed Energy Storage using Fuzzy Logic Controller Page No : 249," vol. 11, no. 1, pp. 249–255, 2020.
- [6] V. P. Vinod and A. Singh, "A Comparative Analysis of PID and Fuzzy Logic Controller in an Autonomous PV-FC Microgrid," *2018 Int. Conf. Control. Power, Commun. Comput. Technol. ICCPCT 2018*, pp. 381–385, 2018.
- [7] W. V. H. Hasaranga, R. D. T. M. Hemarathne, M. D. C. P. K. Mahawithana, M. G. A. B. N. Sandanuwan, H. W. D. Hettiarachchi, and K. T. M. U. Hemapala, "A Fuzzy logic based battery SOC level control strategy for smart Micro grid," *Proc. 3rd IEEE Int. Conf. Adv. Electr. Electron. Information, Commun. Bio-Informatics, AEEICB 2017*, pp. 215–221, 2017.
- [8] H. P. H. Anh, L. V. Truong, and C. Van Kien, "Advanced intelligent fuzzy control of standalone pv-wind-diesel hybrid system," *Proc. 2019 Int. Conf. Syst. Sci. Eng. ICSSE 2019*, no. 2012, pp. 129–135, 2019.
- [9] M. Nagaiah and K. C. Sekhar, "Analysis of fuzzy logic controller based bi-directional DC-DC converter for battery energy management in hybrid solar/wind micro grid system," *Int. J. Electr. Comput. Eng.*, vol. 10, no. 3, pp. 2271–2284, 2019.
- [10] P. Bhat Nempu and N. S. Jayalakshmi, "Coordinated Power Management of the Subgrids in a Hybrid AC–DC Microgrid with Multiple Renewable Sources," *IETE J. Res.*, vol. 2063, 2020.
- [11] S. Sinha, D. V. Tekumalla, and P. Bajpai, "Fuzzy Logic Controlled Power Sharing among Energy Storage Devices in Multiple Standalone DC Microgrids," *Proc. 2019 IEEE PES Innov. Smart Grid Technol. Eur. ISGT-Europe 2019*, pp. 1–5, 2019.
- [12] N. L. Diaz, T. Dragicevic, J. C. Vasquez, and J. M. Guerrero, "Intelligent distributed generation and storage units for DC microgrids - A new concept on cooperative control without communications beyond droop control," *IEEE Trans. Smart Grid*, vol. 5, no. 5, pp. 2476–2485, Sep. 2014.
- [13] B. Liu *et al.*, "An AC–DC Hybrid Multi-Port Energy Router With Coordinated Control and Energy Management Strategies," *IEEE Access*, vol. 7, pp. 109069–109082, Aug. 2019.
- [14] "DC GRID BASED WIND POWER GENERATION IN A MICROGRID APPLICATION: MODELING AND SIMULATION 1 Undralla Sandhya, 2 Pakki Murari."
- [15] M. S. Bisht and Sathans, "Fuzzy based intelligent frequency control strategy in standalone hybrid AC microgrid," *2014 IEEE Conf. Control Appl. CCA 2014*, pp. 873–878, 2014.
- [16] Y. Fu, Z. Zhang, Y. Mi, Z. Li, and F. Li, "Droop Control for DC Multi-Microgrids Based on Local Adaptive Fuzzy Approach and Global Power Allocation Correction," *IEEE Trans. Smart Grid*, vol. 10, no. 5, pp. 5468–5478, 2018.
- [17] I. Roasto, A. Rosin, and T. Jalakas, "Multiport Interface Converter with an Energy Storage for Nanogrids," *IECON 2018 - 44th Annu. Conf. IEEE Ind. Electron. Soc.*, vol. 1, pp. 6088–6093.
- [18] I. Roasto, A. Rosin, and T. Jalakas, "Power electronic interface converter for resource efficient buildings," in *Proceedings IECON 2017 - 43rd Annual Conference of the IEEE Industrial Electronics Society*, 2017.
- [19] Roasto *et al.*, "Voltage Source Operation of the Energy-Router Based on Model Predictive Control," *Energies*, vol. 12, no. 10, p. 1892, 2019.
- [20] X. yan Jiang, C. He, and K. Jermisitiparsert, "Online optimal stationary reference frame controller for inverter interfaced distributed generation in a microgrid system," *Energy Reports*, vol. 6, pp. 134–145, Nov. 2020.

Mahdieh Najafzadeh received her M.Sc in power electronics and electric machinery engineering from K.N. Toosi University of Technology, Tehran, Iran in 2016. In 2018, she entered Tallinn University of Technology. Her research interest is design and control of power electronics converters, including modeling, design, simulation and application of control systems in converters.

Publication VI

M. Najafzadeh, O. Husev, I. Roasto, D. Vinnikov. "DC Nano grid Control in the Residential Energy Router with the Presence of Constant Power Loads", IEEE 7th International Energy Conference (ENERGYCON'2022) Riga, Latvia, 2022, pp. 1–6, DOI: forthcoming.

DC Nano grid Control in the Residential Energy Router with the Presence of Constant Power Loads

Mahdieh Najafzadeh
Power Engineering and Mechatronics
department
Tallinn University of Technology
Tallinn, Estonia
mahdieh.najafzadeh@taltech.ee

Oleksandr Husev
Power Engineering and Mechatronics
department
Tallinn University of Technology
Tallinn, Estonia
oleksandr.husev@taltech.ee

Indrek Roasto
Power Engineering and Mechatronics
department
Tallinn University of Technology
Tallinn, Estonia
indrek.roasto@taltech.ee

Dmitri Vinnikov
Power Engineering and Mechatronics
department
Tallinn University of Technology
Tallinn, Estonia
dmitri.vinnikov@taltech.ee

Abstract— Increasing penetration of DC-based electronics loads has highlighted the idea of DC -grid which is more efficient. Furthermore, DC -grid provides the distributed generators utilization that mostly is DC -based. As a result, in this study, we propose the combination of DC nano grid to the traditional AC-nano grid to the distribution system of a house using a power-electronics- interface called an energy router. However, interactions of multiple DC - DC and AC - DC converters in the nano grid make challenges in the stability of the system and control of it. Constant power loads are one of the main challenges since they are highly nonlinear and they behave as negative resistor from the feeder-side point of view. Consequently, we propose a nonlinear control technique to control the DC nano grid with the presence of constant power load in a residential application.

Keywords— constant power load; energy router; DC -link control; feeder-side control, fuzzy logic control, nonlinear load

I. INTRODUCTION

Technological improvement in the field of power electronic and digital signal processors results in growing penetration of power-electronics-based distributed generators (DGs) and loads in the grid, leading to upgrade the traditional grid to a smart grid. The smart grid contains multiple controllable entities as microgrids[1][2]. As the majority of electronics-based loads and DGs such as renewable resources and energy storages are DC -based, the idea of DC microgrid has been promoted [3]–[6]. DC microgrid application has been studied in buildings, data centers, aircraft, ships [7]–[9]. The absence of reactive power, power quality, harmonics, and frequency control are some of the positive aspects of DC microgrid control [8][10]. Furthermore, the lack of realistic regulations and framework for DC microgrid used to be one of the negative issues. However the solutions have been developed based on various applications such as buildings, power plants, low-voltage distribution systems, medium voltage distribution systems for ships in IECSSG4, IEEE946, IEEE1547, EMerge Alliance and NFPA70 standards [11][12].

On the other side, the increasing number of switched-based converters in loads and sources makes multi-level converter systems with different challenges [13]. In a multi-level converter system, different loads and sources are interconnected via different-level converters. When power electronics converters tightly control the output voltages, they

behave as Constant Power Load (CPL) [13]. In household applications, many sensitive electrical devices exist e.g. LEDs, laptops, computer screens, brushless DC drive-based equipment, any battery charger with 5v DC output in cellphones, tablets [12]. These loads require a switched-based converter to regulate their inputs, as a result, they commonly work in higher switching frequencies. These devices act as a CPL in the system. An increasing number of CPLs are one of the main challenges in the DC microgrids. Different solutions are available: passive damping, active damping. Passive damping contains different filters for damping the oscillations. Active damping is implemented by the control tool.

In this work, we focus on the DC nano grid in residential nano grid considering CPLs. We suggest an active damping technique that is more efficient and does not need to add extra filters to the system. As the power level in residential applications is less than 20 kW, it is called nano grid [14]. Also, since the existing system is AC, the combination of the DC nano grid and AC nano grid is a feasible upgrade for the existing houses. As a result, the case study is a residential hybrid nano grid including AC and DC nano grids. The main key in the energy control of the residential hybrid nano grid is called an energy router. Energy router (ER) is a power-electronics interface among the residential DC nano grid, AC nano grid, and the main grid [15]. The energy router concept and its challenges are studied in [16]–[18]. The main focus of this study is on the nonlinear voltage control of the DC nano grid in the energy router considering CPLs. Adding CPLs in the DC -side of the energy router results in a high THD current of the inverters which is higher than the limit standard of the AC-grid. As a result, we suggest implementing a nonlinear control technique as Fuzzy Logic Control (FLC). FLC emulates human intuition. The positive aspect of this technique is no requirement for the complex mathematical model of the system [19][20].

II. CONSTANT POWER LOAD IN ENERGY ROUTER

A CPL consumes a constant power load despite different voltages. The voltage-current characteristic of a CPL is depicted in Fig.1. The CPL current can be described by.

$$i_{CPL} = \frac{P_{CPL}}{v_{CPL}} \quad (1)$$

Where p_{CPL} is the power of CPL. v_{CPL} is the voltage of CPL and i_{CPL} is the current of CPL. So at a given operating point

$$\frac{\partial i_{CPL}}{\partial v_{CPL}} = -\frac{P_{CPL}}{V_{CPL}^2} = \frac{1}{r_{eq}} \quad (2)$$

Where r_{eq} is the equivalent resistor. So by approximation

$$i_{CPL} = -\frac{P_{CPL}}{V_{CPL}^2} v_{CPL} + 2\frac{P_{CPL}}{V_{CPL}} \quad (3)$$

Consequently, the small-signal model of the CPL is composed of a negative equivalent resistor ($r_{eq} = \frac{V_{CPL}^2}{P_{CPL}}$) parallel with a constant current source ($I_{CPL} = 2\frac{P_{CPL}}{V_{CPL}}$) depicted in Fig.2. As a result, CPLs have not only nonlinear behavior but also negative resistance. The constant current source does not affect the stability but the negative resistor characteristic makes it difficult to dampen the oscillations and destabilizes the DC or AC microgrid [21]. Consequently, stability issue is the main challenge in microgrids. Different stability criteria are studied such as Middlebrook, gain

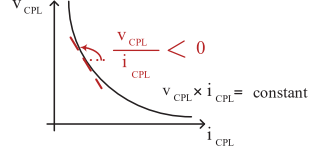


Fig. 1 Voltage-current characteristic of a CPL.

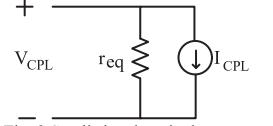


Fig. 2 Small signal equivalent circuit of a CPL.

margin and phase margin, passivity based criterion [22], To stabilize the system passive and active methods are suggested [23]. Passive techniques contain passive routes to dampen the oscillations of negative resistor. Active damping methods implements control techniques to damp the oscillation. The benefit of the active method is that it does not require any additional circuit resulting to less power loss. In this study we suggest FLC technique to control the DC-grid voltage and damp the oscillations of CPL negative resistor.

III. ENERGY ROUTER DESCRIPTION AND THE PROPOSED CONTROL TECHNIQUE

The ER structure for residential application contains two back-to-back single-phase full-bridge converters interconnecting by a DC-link. Through this DC-link, all DC-based DGs and loads and storages are connected forming a DC-nano grid [24][25]. Three extra relays are used to main grid-connection, DC-nano grid-connection and to bypass the back-to-back converters. The ER topology is demonstrated in Fig.3.

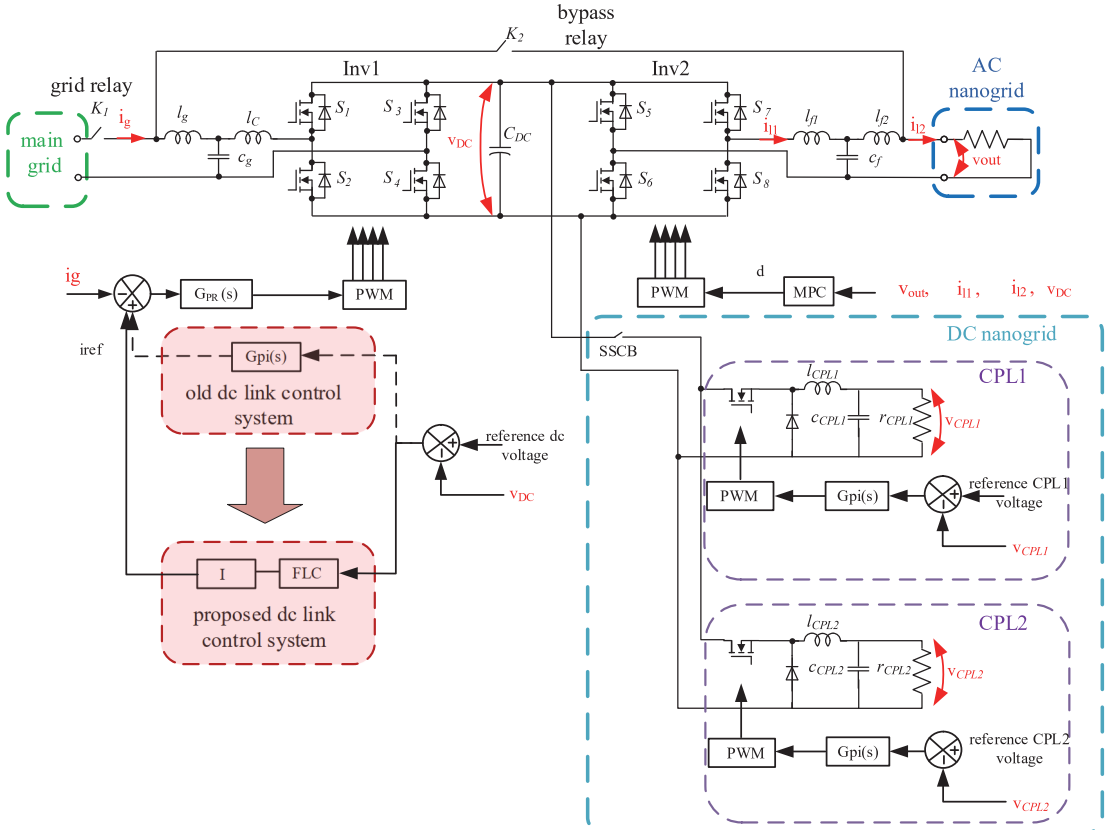


Fig. 3 The energy router topology and the proposed control technique.

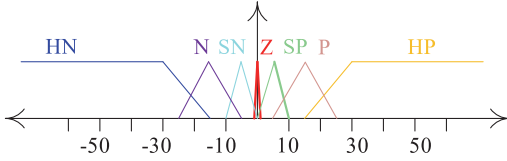


Fig. 4 Membership functions for error signal of DC-voltage.

The PR regulator provides the switching function for Inv1 in current-controlled mode. The reference current for PR regulator was provided by a simple PI regulator. However, with adding CPLs in the DC -side the Inv1 current has higher than 5% THD. As a result, we proposed the FLC instead of the PI regulator.

FLC has five steps which are the determination of parameters, fuzzification, knowledgebase, rules, and defuzzification [8], [26]–[29]. As described in [30] and shown in Fig. 3, FLC inputs are the error signal of DC nano grid voltage and its slope. The reason is the sinusoidal double-frequency ripple of the DC -link voltage which is required to get distinguished between the negative slope and positive slope of the voltage. The output of the FLC is the grid-current reference derivative. The FLC output with an integrator provides the reference current amplitude from the main grid. Mamdani method is a popular method in similar applications implemented in the simulation code. Seven triangular membership functions are utilized for inputs and output. These membership functions are called Highly Negative (HN), Negative (N), Small negative (SN), Zero (Z), Small Positive (SP), Positive (P), and Highly Positive (HP). The membership functions for DC -link error voltage are shown in Fig.4. The knowledge for table rules is to change the grid-current slope to maintain the DC -voltage in Z interval, e.g. if the DC -voltage error is in HP and the slope of it is in the Z range, it means the grid-current needs to get decreased in small value so the slope of the grid-current is required to be in SN. The utilized table rule is demonstrated in Table. I.

IV. SIMULATION RESULTS

The PLECS software is implemented for the simulation. The system parameters used in the simulation are shown in Table II.

Two CPLs with the power of 80 and 200 W are connected to the DC -link. To simulate a CPL, a resistor with a buck converter is utilized. The buck switching frequency is

TABLE I. TABLE RULES FOR DC-VOLTAGE CONTROL

Error Signal \ Derivative Error Signal	HN	N	SN	Z	SP	P	HP
HN	HP	HP	HP	HP	HP	HP	P
N	HP	P	SP	SP	SP	Z	Z
SN	P	SP	SP	SP	Z	SP	Z
Z	PS	Z	Z	Z	Z	Z	NS
SP	Z	Z	Z	SN	SN	SN	N
P	Z	Z	SN	SN	SN	N	HN
HP	N	HN	HN	HN	HN	HN	HN

assumed high enough to tightly control the resistor voltage. PI regulator is used to control the CPL output voltage. The CPL power and control parameters are depicted in Table II.

The simulation is done with the classic PI regulator for DC -voltage control and with the proposed FLC. The classical PI regulator parameters for DC -voltage control are shown in Table II. The PR regulator parameters are chosen based on [31]. To evaluate the compatibility of the proposed FLC technique with the Model Predictive Control (MPC), we

TABLE II. SYSTEM SPECIFICATIONS

Symbol	Parameter	Value
AC Grid Side Parameters		
v_g	Grid side voltage (RMS)	230 V, 50 Hz
l_g	Grid -side LCL inductor	0.6 mH
l_c	Converter -side LCL filter inductor	1.44 mH
c_g	LCL filter capacitor	3 μ F
r_c	Series resistor of the inductor	0.001 Ω
DC Side Parameters		
c_{DC}	DC side capacitor	2000 μ F
v_{DC}	DC link voltage	400 V
P_{CPL1}	CPL1 power	80 W
P_{CPL2}	CPL2 power	200 W
k_p	Prportional Parameter	0.25
k_i	Integrator Parameter	0.25
CPLs Parameters		
F_{sw}	Switching frequency	60 kHz
v_{CPL}	CPL voltage	20 V
k_p	Prportional Parameter	0.2
k_i	Integrator Parameter	0.8
r_{CPL1}	Resistor of the CPL1	5 Ω
l_{CPL1}	LC filter inductor of CPL1	0.1 mH
c_{CPL1}	LC filter capacitor of CPL1	1000 μ F
r_{CPL2}	Resistor of the CPL2	2 Ω
l_{CPL2}	LC filter inductor of CPL2	0.1 mH
c_{CPL2}	LC filter capacitor of CPL2	1000 μ F
AC Load Side Parameters		
v_{load}	Load side voltage (RMS)	230 V, 50 Hz
l_{l2}	Load -side LCL inductor	0.6 mH
l_{l1}	Converter -side LCL filter inductor	1.44 mH
c_f	LCL filter capacitor	9.6 μ F
r_f	Series resistor of the inductor	0.001 Ω
$P_{I_{out}}$	AC Output power	105 W
General Parameters		
F_{sw}	Switching frequency	20 kHz

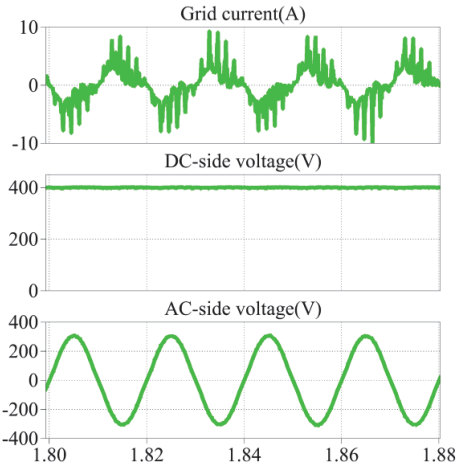


Fig. 5 Simulation results of the classic PI regulator in steady-state.

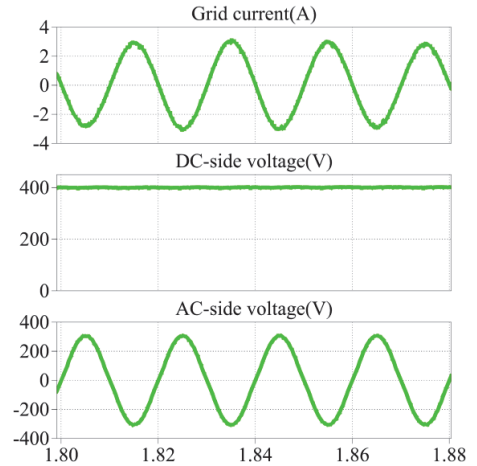


Fig. 6 Simulation results of the classic FLC regulator in steady-state.

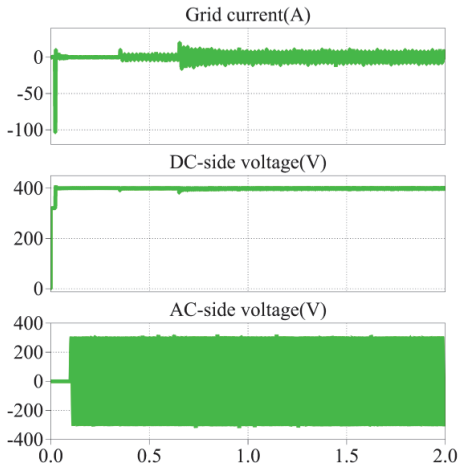


Fig. 7 The transient results with the classic PI regulator.

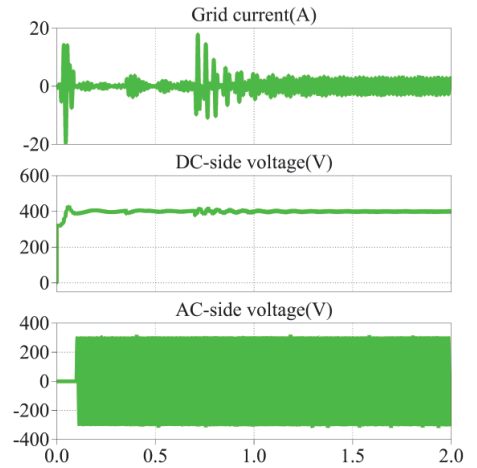


Fig. 8 The transient results with the proposed FLC technique.

connect a 105 W AC resistor load to the AC nano grid by the Inv2 in voltage-controlled mode. The details of the MPC were studied in [32].

The main grid current, DC nano grid voltage, and AC nano grid voltage in steady-state for the classical PI and the proposed FLC techniques are shown in Fig. 5 and Fig. 6 respectively.

The grid-current THD in the classical PI regulator and the proposed FLC are 7.1% and 2.1% successively. This shows the combination of PI+PR regulators cannot provide an acceptable current and it has limitations regarding different DC-load types. However, the THD of grid current in the FLC technique works well with PR regulator for simple resistor-type and CPL type. The DC-side voltage in both techniques track well 400 V, demonstrating the stability of the DC nano grid. The AC nano grid voltage in both methods is sinusoidal which confirms the MPC works well.

Fig. 7 and Fig. 8 demonstrate the transient behavior of the grid-current, DC-link voltage, and the AC-voltage with classic PI and the proposed FLC at the time of starting, CPL1, CPL2, and AC-load connection. The grid-current results show despite the better steady-state performance of FLC, in the transient state this method needs improvements.

Fig. 9 and Fig. 10 demonstrate the CPLs' voltage behavior within the ER system using PI and FLC techniques. The results show the PI regulators of CPLs track better the reference voltage with FLC implementation. This issue can be studied in the future work.

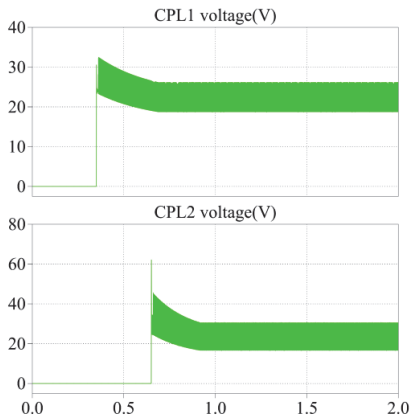


Fig. 9 CPLs voltages in classic PI regulator method.

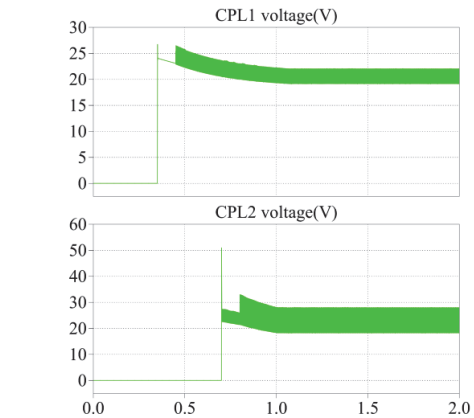


Fig. 10 CPLs voltages in the proposed FLC method.

V. CONCLUSION

Due to the increasing utilization of electronics load with CPL characteristics and their negative effects on the stability of grids, we studied CPL effects on the energy router performance in a residential application. Since the performance of classical linear control has limitations, we propose FLC application for DC-voltage control. The simulation results of the proposed technique with the presence of CPLs in the energy router show the better performance of the FLC technique compared with the classical PI regulator. The combination of AC-load connection with Inv2 in voltage-controlled mode via MPC confirms the compatibility of FLC and MPC application in the control system.

The future work is to study and suggest the solutions to improve the grid-current transient response using FLC in the presence of CPLs in DC nano grid of energy router.

ACKNOWLEDGMENT

This research was co-financed by the Estonian Research Council grant PRG675 and by the Estonian Centre of Excellence in Zero Energy and Resource Efficient Smart Buildings and Districts, ZEBC, grant 2020- 2020.4.01.15-0016 funded by the European Regional Development Fund.

REFERENCES

- [1] H. M. Hussain, A. Narayanan, P. H. J. Nardelli, and Y. Yang, "What is energy internet? concepts, technologies, and future directions," *IEEE Access*, vol. 8, no. iv, pp. 183127–183145, 2020, doi: 10.1109/ACCESS.2020.3029251.
- [2] K. Wang *et al.*, "A survey on energy internet: Architecture, approach, and emerging technologies," *IEEE Syst. J.*, vol. 12, no. 3, pp. 2403–2416, 2018, doi: 10.1109/JSYST.2016.2639820.
- [3] T. Dragicevic, J. M. Guerrero, J. C. Vasquez, and D. Skrlac, "Supervisory control of an adaptive-droop regulated DC microgrid with battery management capability," *IEEE Trans. Power Electron.*, vol. 29, no. 2, pp. 695–706, 2014, doi: 10.1109/TPEL.2013.2257857.
- [4] T. Dragicevic, X. Lu, J. C. Vasquez, and J. M. Guerrero, "DC Microgrids - Part I: A Review of Control Strategies and Stabilization Techniques," *IEEE Trans. Power Electron.*, vol. 31, no. 7, pp. 4876–4891, 2016, doi: 10.1109/TPEL.2015.2478859.
- [5] N. V. Kurdkandi *et al.*, "A New Transformer-Less Common Grounded With, Three-level Grid-tied Inverter," *Trans. ENERGY Convers.*, vol. 36, no. 3, pp. 1896–1909, 2021.
- [6] N. Hassan Pour and K. Varesi, "A New Non-Isolated High Gain DC-DC Converter Suitable for Renewable Energies," *2019 10th Int. Power Electron. Drive Syst. Technol. Conf. PEDSTC 2019*, pp. 747–751, 2019, doi: 10.1109/PEDSTC.2019.8697239.
- [7] Y. C. Jeung, D. D. Le, and D. C. Lee, "Analysis and Design of DC-Bus Voltage Controller of Energy Storage Systems in DC Microgrids," *IEEE Access*, vol. 7, pp. 126696–126708, 2019, doi: 10.1109/ACCESS.2019.2939176.
- [8] M. Najafzadeh, R. Ahmadihangar, O. Husev, I. Roasto, T. Jalakas, and A. Blinov, "Recent Contributions, Future Prospects and Limitations of Interlinking Converter Control in Hybrid AC/DC Microgrids," *IEEE Access*, vol. 9, pp. 7960–7984, 2021, doi: 10.1109/access.2020.3049023.
- [9] H. Maschinchi Maheri, D. Vinnikov, A. Chub, and V. Sidorov, "Topology Morphing Control of Low-Cost PV Microconverters," in *International (EPE-PEMC) Power Electronics and Motion Control*, 2021, pp. 857–863.
- [10] T. Hemmati, M. G. Marangalu, N. V. Kurdkandi, A. Khoshkbar-Sadigh, S. H. Hosseini, and H. K. Jahan, "Topology Review of Grid-Connected Multilevel Inverters Supplied by Photovoltaic Panels using Switched-Capacitor Based Circuits," in *Proceedings of the IEEE International Conference on Industrial Technology*, 2021, vol. 2021-March, pp. 508–513, doi: 10.1109/ICIT46573.2021.9453484.
- [11] K. K. Nandini, N. S. Jayalakshmi, and V. K. Jadoun, "An overview of DC Microgrid with DC distribution system for DC loads," *Mater. Today Proc.*, vol. 51, pp. 635–639, 2022, doi: 10.1016/j.matpr.2021.06.093.
- [12] J. P. Leonard, "Nonlinear Modeling of DC Constant Power Loads with Frequency Domain Volterra Kernels," Florida State University, 2014.
- [13] A. M. Rahimi and A. Emadi, "Active damping in DC/DC power electronic converters: A novel technique to overcome the problems of constant power loads," *IEEE Trans. Ind. Electron.*, vol. 56, no. 5, pp. 1428–1439, 2009, doi: 10.1109/TIE.2009.2013748.
- [14] I. Roasto, T. Jalakas, and A. Rosin, "Bidirectional Operation of the Power Electronic Interface for Nearly-Zero Energy Buildings," 2018.
- [15] C. Roncero-Clemente, N. Vilhena, V. Delgado-Gomes, E. Romero-Cadaval, and J. F. Martins, "Control and operation of a three-phase local energy router for prosumers in a smart community," *IET Renew. Power Gener.*, vol. 14, no. 4, pp. 1–11, 2020, doi: 10.1049/iet-rpg.2019.0589.
- [16] J. F. Martins, E. Romero-Cadaval, D. Vinnikov, and M. Malinowski, "Transactive Electronics Power Energy: Challenges," no. February, pp. 20–32, 2022.
- [17] C. Balda, A. Mantooth, R. Blum, and P. Tenti, "Cybersecurity and Power Electronics," *IEE Power Electronics Magazine*, no. December, pp. 37–43, 2017.
- [18] S. Zhao, J. Umuhoza, Y. Zhang, J. Moquin, C. Farnell, and H. A. Mantooth, "Analysis and optimization of a high-efficiency residential energy harvesting system with dual half-bridge converter," in *Applied Power Electronics Conference and Exposition - APEC*, 2017, no. 1, pp. 2838–2844, doi: 10.1109/APEC.2017.7931100.
- [19] V. P. Vinod and A. Singh, "A Comparative Analysis of PID and Fuzzy Logic Controller in an Autonomous PV-FC Microgrid," *2018 Int. Conf. Control. Power. Commun. Comput. Technol. ICCPCCT 2018*, pp. 381–385, 2018, doi: 10.1109/ICCPCCT.2018.8574237.

- [20] B. Liu *et al.*, "An AC-DC Hybrid Multi-Port Energy Router With Coordinated Control and Energy Management Strategies," *IEEE Access*, vol. 7, pp. 109069-109082, Aug. 2019, doi: 10.1109/access.2019.2933469.
- [21] S. Singh, A. R. Gautam, and D. Fulwani, "Constant power loads and their effects in DC distributed power systems: A review," *Renew. Sustain. Energy Rev.*, vol. 72, no. January, pp. 407-421, 2017, doi: 10.1016/j.rser.2017.01.027.
- [22] L. Hamefors, A. G. Yepes, A. Vidal, and J. Doval-Gandoy, "Passivity-based controller design of grid-connected VSCs for prevention of electrical resonance instability," *IEEE Trans. Ind. Electron.*, vol. 62, no. 2, pp. 702-710, 2015, doi: 10.1109/TIE.2014.2336632.
- [23] M. K. AL-Nussairi, R. Bayindir, S. Padmanaban, L. Mihet-Popa, and P. Siano, "Constant power loads (CPL) with Microgrids: Problem definition, stability analysis and compensation techniques," *Energies*, vol. 10, no. 10, 2017, doi: 10.3390/en10101656.
- [24] M. Najafzadeh, I. Roasto, and T. Jalakas, "Energy Router Based Energy Management System for Nearly Zero Energy Buildings," 2019.
- [25] M. Najafzadeh, D. Vinnikov, O. Husev, T. Jalakas, and I. Roasto, "DC-link Capacitor Minimization In Residential Energy Router Through Battery Utilization," pp. 1-6, 2021, doi: 10.1109/cpe-powereng50821.2021.9501173.
- [26] M. M. M. N. Cirstea, A. Dinu, J. G. Khor and Newnes, *Neural and Fuzzy Logic Control of Drives and Power Systems*. 2002.
- [27] A. V. Kumar, P. M. Rao, B. S. Rao, A. Vinod Kumar, P. Maheswara Rao, and B. Srinivasa Rao, "Modified Voltage Control Strategy for DC Network with Distributed Energy Storage using Fuzzy Logic Controller," *J. Eng. Sci.*, vol. 11, no. 1, pp. 249-255, 2020, [Online]. Available: www.jespublication.com.
- [28] S. Das and A. K. Akella, "A fuzzy logic-based frequency control scheme for an isolated AC coupled PV-wind-battery hybrid system," *Int. J. Model. Simul.*, vol. 00, no. 00, pp. 1-13, 2019, doi: 10.1080/02286203.2019.1613063.
- [29] W. V. H. Hasaranga, R. D. T. M. Hemarathne, M. D. C. P. K. Mahawithana, M. G. A. B. N. Sandanuwan, H. W. D. Hettiarachchi, and K. T. M. U. Hemapala, "A Fuzzy logic based battery SOC level control strategy for smart Micro grid," *Proc. 3rd IEEE Int. Conf. Adv. Electr. Electron. Information, Commun. Bio-Informatics, AEEICB 2017*, pp. 215-221, 2017, doi: 10.1109/AEEICB.2017.7972416.
- [30] M. Najafzadeh, O. Husev, I. Roasto, and T. Jalakas, "Improved DC-Link Voltage Transient Response and Stability Issues in Energy Router with Fuzzy Logic Control Method."
- [31] O. Husev, C. Roncero-Clemente, E. Makovenko, S. P. Pimentel, D. Vinnikov, and J. Martins, "Optimization and Implementation of the Proportional-Resonant Controller for Grid-Connected Inverter with Significant Computation Delay," *IEEE Trans. Ind. Electron.*, vol. 67, no. 2, pp. 1201-1211, 2020, doi: 10.1109/TIE.2019.2898616.
- [32] Roasto *et al.*, "Voltage Source Operation of the Energy-Router Based on Model Predictive Control," *Energies*, vol. 12, no. 10, p. 1892, 2019, doi: 10.3390/en12101892.

Publication VII

M. Najafzadeh, O. Husev, I. Roasto, D. Vinnikov, T. Jalakas. "DC-link Capacitor Minimization In Residential Energy Router Through Battery Utilization", CPE POWERENG 2021, Italy, Florence. pp. 1–6, DOI: forthcoming.

DC-link Capacitor Minimization In Residential Energy Router Through Battery Utilization

Mahdieh Najafzadeh
Power Engineering and Mechatronics
department
Tallinn University of Technology
Tallinn, Estonia
mahdieh.najafzadeh@taltech.ee

Oleksandr Husev
Power Engineering and Mechatronics
department
Tallinn University of Technology
Tallinn, Estonia
oleksandr.husev@taltech.ee

Indrek Roasto
Power Engineering and Mechatronics
department
Tallinn University of Technology
Tallinn, Estonia
indrek.roasto@taltech.ee

Dmitri Vinnikov
Power Engineering and Mechatronics
department
Tallinn University of Technology
Tallinn, Estonia
dmitri.vinnikov@taltech.ee

Tanel Jalakas
Power Engineering and Mechatronics
department
Tallinn University of Technology
Tallinn, Estonia
tanel.jalakas@taltech.ee

Abstract—Ac to dc conversion in a single-phase ac-dc voltage source converters and current source converters produce double frequency ripple power on the dc side. This ripple power multiplies the dc-link capacitor size by increasing its operating temperature. Different active and passive solutions are suggested to decouple this ripple power. In this paper, by reviewing the charging-current frequency effect on the li-ion battery performance and its lifetime, we find out ripple-power utilization for charging li-ion battery can be practical. As a result, we propose to decouple the ripple power by the Li-ion battery in a residential energy router system. This energy router system is an interface among the main grid, loads, renewable energy resources, and energy storage of a house.

Keywords—li-ion battery, energy router, active decoupling, double-frequency ripple.

I. INTRODUCTION

The utilization of Renewable Energy Resources (RESs) at the distribution level has been boomed during the last ten years [1]. RESs are an alternative green energy supply for an annual load growth of 2.5% [2]. RESs proximity to the load increases efficiency, as a result, they contribute to decrease pollution, increase efficiency, and an alternative resource to the growing load demand [3], [4].

The residential scale of RESs exploitation upgrades the traditional house to the Nearly or Net Zero Energy Building (NZEB) [5], [6]. In an NZEB the sum of production and consumption of the load is almost zero [5]. The main key in NZEB is the residential Energy Router (ER) that interfaces the main grid with residential loads, RESs, and Energy Storages (ESs) [7], [8], [9]. As RESs are intermittent, ESs are used with RESs to exploit the maximum of the RESs' energy. ESs play an important role in ancillary service support e.g. peak load shifting, dynamic local voltage support, short-term frequency smoothing [10].

The ER consists of multiple converters interconnected by a common dc-link. As dc-link capacitors are the main element in these systems, they are called capacitor-supported systems [11]. These capacitors play an important role in power balance, ripple voltage limitation, and short-term energy storage in the ER [12]. However, capacitors are the most fragile elements in the ER which decreases its reliability [12], [13].

The common and low-cost candidate for dc capacitors is the electrolytic capacitor. However, electrolytic dc-link capacitors are the most susceptible elements in capacitor-supported systems. Their lifetime is dependent on the ripple current and temperature; besides, they have high Equivalent Series Resistance (ESR) and Equivalent Series Inductance (ESL) [14], [15], [11]. One way to increase the reliability of the system is by decreasing the ripple power and declining the operating temperature. This method is applicable by decoupling the ripple power. Two main approaches to decouple the ripple power are passive and active techniques as discussed in many studies [16], [17], [18], [19].

Another solution to enhance the reliability of the capacitor-supported systems is replacing the electrolytic capacitor with the film capacitor. High current ripple capability, high operating temperature, and small ESR are the main merits of film capacitors; however, their energy density is less than electrolytic capacitors and their cost is higher [14]. Many pieces of research have been done, replacing the film capacitor with the electrolytic capacitor [15].

In this study, we work on decoupling the ripple power by ESs utilization. First, the charging-discharging technique's effect on ES's performance is reviewed.

Lithium-ion batteries are the common types of ESs in nano and microgrids. The traditional charging method is Constant Current (CC) and Constant Voltage (CV); however, there are some issues in terms of efficiency and lifetime [20]. The useful lifetime of a battery is defined based on the charging-discharging cycles by the faded capacity [21]. Some studies have been done to clarify the effect of charging-current frequency on battery performance [20], [21], [22], [23]. The research in [22] shows that ripple frequency lower than 10 Hz has the worst degradation effects in long term, whereas, ripple higher than 100 Hz has a less degradation effect compared to below 10 Hz charging-current effect. This study provides capacity fade curves according to the frequency charge cycle between 50 to 147 days. It confirms the least capacity fade happened in 100Hz among selected frequencies. Study in [20] studies on the frequency charging current effects on the charging and discharging time, efficiency, and temperature

Residential energy router

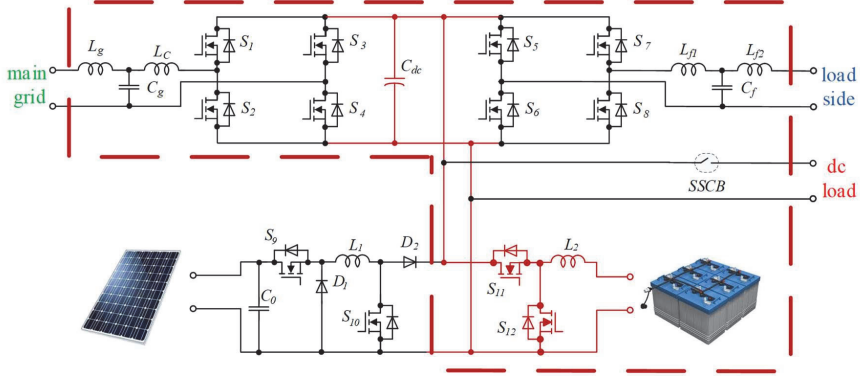


Fig. 1. The ER Case Study Topology.

rise in the li-ion battery. This study compares CC-CV, 1 Hz, 1 kHz, and pulse current charge technique on ES performance. It confirms the better performance of 100 Hz in terms of higher discharging capacity, better efficiency, and less rise in temperature. Research in [23] confirmed the same results regarding the capacity fade. To sum up, referred to these studies double-frequency charging current has fewer degradation effects on the battery performance among the selected frequency ranges. However, more precise research is needed to determine the optimized frequency of the charging current.

Implementation of the ripple power to charge and discharge the battery is one active decoupling technique that can help us to utilize a lower dc-link capacitor.

In conclusion, in this paper, li-ion battery utilization is introduced as an active decoupling technique for 100 Hz ripple current to decline the dc-link capacitor size.

II. SYSTEM DESCRIPTION

The main ER concept and operation modes are discussed in [24]. The comprehensive ER topology consists of two back-

to-back full-bridge converters that connect the main grid to the residential loads (or other grids) by a dc-link. PV and battery are connected to the dc-link by noninverting buck-boost and bidirectional converter successively. ac and dc loads can be connected to the ac side and dc-link respectively. The whole ER system is depicted in Fig. 1. As a result, the ER is an intelligent multi-port connector that connects ac loads, dc loads, PV, battery, and the main grid.

The Voltage Source Inverters (VSIs) in the ER contains different voltage components in their ports: ac and dc. This issue makes some double-grid-frequency sinusoidal mismatch power on the dc side as shown in (1) [25]. This ripple power should be absorbed by the dc-link capacitor. As a result, these capacitors stabilize the dc-link voltage by providing this energy balance in the dc-link[11].

$$p_{ac}(t) = v_{ac}(t) \times i_{ac}(t) = V_{ac} \sin(\omega t) \times I_{ac} \sin(\omega t + \theta) = \frac{V_{ac} \times I_{ac}}{2} (1 + \cos(2\omega t + \theta))$$

$$p_{ripple} = \frac{V_{ac} \times I_{ac}}{2} \cos(2\omega t + \theta) \quad (1)$$

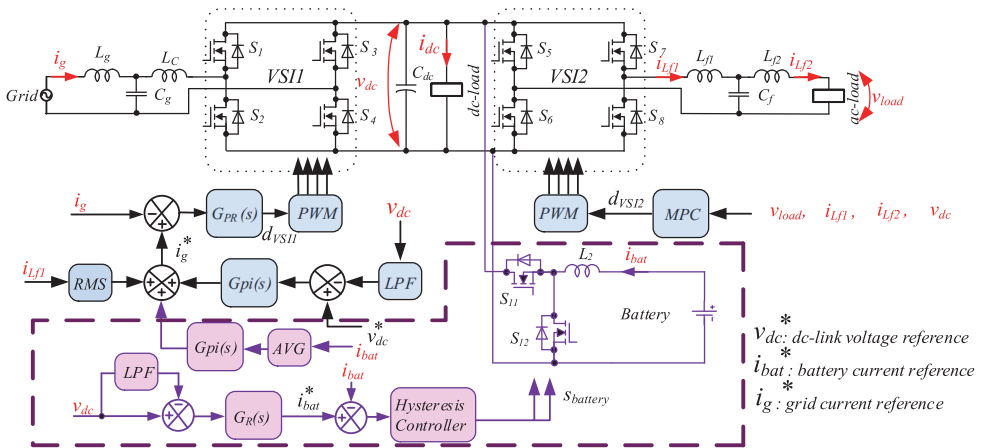


Fig. 2. The Proposed Control Block in the Dashed Line.

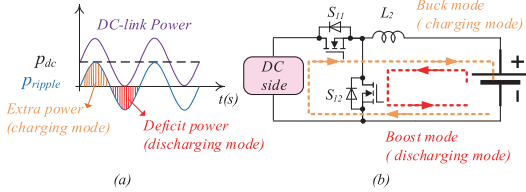


Fig. 3. a) dc-link Power and its Components. b) Buck and Boost Operation of the Battery Converter.

TABLE 1. OPERATION MODES OF BATTERY CONVERTOR

Operation Mode	On-state	Off-state (Freewheeling mode)
Buck	MOSFETS _{S11}	Diode S ₁₂
Boost	MOSFETS _{S12}	Diode S ₁₁

Where:

p_{ac} is the total transferred power.

v_{ac} and i_{ac} are the instantaneous ac-side voltage and current respectively.

V_{ac} and I_{ac} are the RMS value of the ac-side voltage and current respectively.

ω and θ are the grid frequency in radian and ac-side current phase angle.

p_{ripple} is the ripple component of the total transferred power.

This ripple power is the main constraint in capacitor sizing [26], [27]. Based on the conclusion in [26] the required dc-link capacitor size is determined by (2).

$$c = \frac{s}{w \times V_{DC} \times \Delta v} \quad (2)$$

Where:

s is ac side apparent power that is: $s = V_{ac} \times I_{ac}$

w is grid frequency in radian.

V_{DC} is the average dc-link voltage.

Δv is the allowable dc-link voltage ripple.

This formula shows for the determined ac-dc transferred power, fixed ac-side frequency, and fixed dc-link voltage, reduction in the dc voltage ripple results in increasing the dc-link capacitor. As a result, controlling this ripple voltage helps us to provide an ac-dc power balance with a less dc-link capacitor.

In this work, we focus on two back-to-back VSIs and battery which are separated with a dashed line in Fig. 1. The grid side converter is current-controlled by Proportional Resonance (PR) regulator, whereas, the load side converter is voltage-controlled by Model Predictive Control (MPC) regulator. More information can be found in [28].

The battery is connected to the dc-link by a bidirectional half-bridge converter. The target is to control the charge and discharge current of the battery to compensate for the dc-link ripple voltage in (2). In this study, the simplified equivalent circuit of the battery is utilized.

The proposed control structure for the li-ion battery will be discussed in the next part.

III. PROPOSED CONTROL TECHNIQUE

The bidirectional converter of the battery is current-controlled. The proposed control concept is based on [29] that

is dc-link voltage ripple control. The dc-link voltage is measured then by a low pass filter, the double-frequency component of the dc-link voltage is provided. The Resonance R controller and repetitive controller are two ways to compensate for this ripple power[30]. In this study, a PR harmonic compensator is utilized for double frequency compensation to produce the reference signal for battery current. (3) describes the PR harmonic compensator transfer function.

$$G_R(s) = k_p + \frac{k_R \times s}{s^2 + (2 \times \pi \times 100)^2} \quad (3)$$

k_p and k_R are the proportional and resonant coefficients respectively. The hysteresis controller is used for providing the modulator signals.

The whole control block is demonstrated in Fig. 2. More information about grid-side converter and load-side converter control design are available in [28]. The proposed control technique with battery utilization is separated by the dashed line in Fig. 2. The Low Pass Filter (LPF) is a simple filter with a 30 Hz cutoff frequency. The main merits of this control technique are easy implementation and no need for tuning effort.

Looking into details of the battery's converter control, Fig. 3.a demonstrates the dc-link power based on (1) that consists of dc power p_{dc} and ripple power p_{ripple} . To compensate the ripple power, battery is charged when the extra power exists in the dc-link, and the deficit power in the dc-link is provided by discharging the battery. In the buck mode of the battery's converter, the extra power in dc-link charges the battery, S_{11} and freewheeling diode of S_{12} operate in this mode. In the boost mode, S_{12} and freewheeling diode of S_{11} provide the deficit power in dc-link as demonstrated in TABLE 1. These two operation modes during their MOSFETs operations are demonstrated in Fig. 3.b.

The control co-efficiencies are depicted in TABLE 2.

IV. SIMULATION RESULTS

PLECS 4.4 software is used for the simulation. The ER system specifications are specified in TABLE 3.

It is assumed that the peak load of a residential house is about 5 kW. Considering this assumption, the simulation is carried out for the worst operation condition at peak load. As a result, the simulation is carried out with this scenario: at $t_1=0.25$ sec $p_1=1650$ w ac load, $t_2=0.35$ sec an extra $p_2=1650$ w ac load, then $t_3=0.55$ sec an extra $p_3=2300$ w ac, and finally $t_4=0.7$ sec $p_4=1000$ w dc load are added to the system. The simulation is done for the aforementioned scenario with the active decoupling method and without it. In this study the

TABLE 2. CONTROL PARAMETERS VALUE.

Symbol	Parameter	Value
PR Compensator		
k_R	Resonance gain	50
k_p	Proportional gain	2
PI Regulator in Battery Current Averaging Loop		
k_i	Integrator gain	0.5
k_p	Proportional gain	0.5

TABLE 3. THE ER SYSTEM SPECIFICATIONS.

Symbol	Parameter	Value
Ac Grid Side Parameters		
v_g	Grid side voltage (RMS)	230 V, 50 Hz
l_g	Grid -side LCL inductor	0.6 mH
l_c	Converter -side LCL filter inductor	1.44 mH
c_g	LCL filter capacitor	3 μ F
r_c	Series resistor of the inductor	0.001 Ω
Dc Side Parameters		
v_{dc}	dc link voltage	400 V
P_{dc}	dc link power	1000 W
Ac Load Side Parameters		
v_{load}	Load side voltage (RMS)	230 V, 50 Hz
l_{f2}	Load -side LCL inductor	0.6 mH
l_{f1}	Converter -side LCL filter inductor	1.44 mH
c_f	LCL filter capacitor	9.6 μ F
r_f	Series resistor of the inductor	0.001 Ω
P_{1out}	Ac Output1 power	1650 W
P_{2out}	Ac Output2 power	1650 W
P_{3out}	Ac Output3 power	2300 W
General Parameters		
F_{sw}	Switching frequency	30 kHz

TABLE 4. THE COMPARISON OF THE REQUIRED DC-LINK CAPACITOR IN TWO METHODS WITH 5.6 kW LOAD.

Method	Implemented C_{dc}	Voltage Ripple Δv
Without battery utilization	2000 μ F	4 v
With battery utilization	400 μ F	1 v

accepted dc-link voltage variation is limited to ± 2 v. Considering this limitation, the proposed technique is simulated for different capacitors. The results prove a decrease in the dc-link capacitor from 2000 μ F to 400 μ F. The simulation results of the traditional control with a 2000 μ F dc-link capacitor are shown in Fig. 4, Fig. 6, and Fig. 8. As Fig. 4 demonstrates, the 2000 μ F dc-link capacitor with the traditional control technique is capable of providing sinusoidal grid current with an acceptable THD of 1.9%. Dc-link voltage, dc-link voltage reference, and dc-load current are depicted in Fig. 6 which shows the maximum of ± 2 v ripple in dc-link voltage. The average value of the dc-link capacitor is 400 v for the final step loads as demonstrated in Fig. 6. The dc-link voltage varies between 402 to 398 v as shown in Fig. 6. Ac load voltage and current in Fig. 8 shows they are sinusoidal. Load current THD is 2.7% which is acceptable. Also, Fig. 6 depicts the ripple dc-link voltage of 4 v in steady-state which is within the acceptable limit.

The proposed control results with 400 μ F are demonstrated in Fig. 5, Fig. 7, and Fig. 9. As we can see in Fig. 5, the grid current is sinusoidal with the THD of 0.5%. Fig. 7 demonstrates the dc-link voltage and its reference and

dc-load current on the left side and the zoomed one on the right side. The battery starts working at 0.25 s so as we can observe in Fig. 7 the voltage ripple in no-load is about 3 v before battery utilization. However, the steady-state dc-link ripple voltage is 1 v in full-load operating condition. The steady-state dc voltage is varied between 399.6 and 400.3 v. The overall transient voltage is varied between 392 to 406 v in both control techniques in Fig. 6 and Fig. 7. The load voltage and current are shown in Fig. 9. THD of the load current is 2.7% which is less than 5%. Sinusoidal grid current and load current and steady-state value of the dc-link voltage confirm the suitable performance of the PR regulator in double-frequency harmonic compensation. The grid current THD in traditional and the proposed control technique are 1.9% and 0.5% respectively, the load current THD in both conditions is 2.7%. This issue depicts the better performance of the proposed technique in the ER power-factor-correction function.

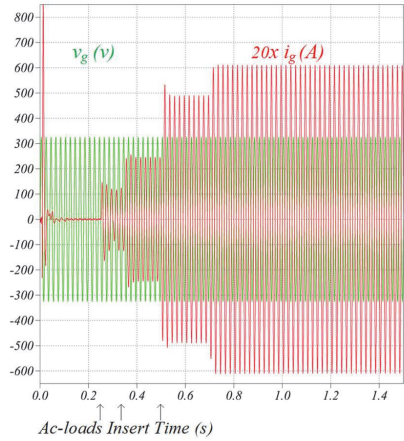


Fig. 4. Grid Voltage v.s. Grid Current Simulation Results of the Traditional Control with c_{dc} 2000 μ F.

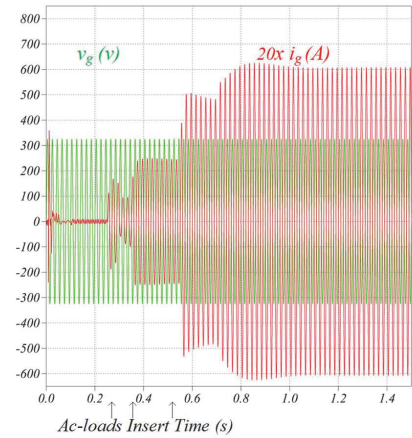


Fig. 5. Grid Voltage v.s. Grid Current Simulation Results of the Proposed Control with c_{dc} 400 μ F.

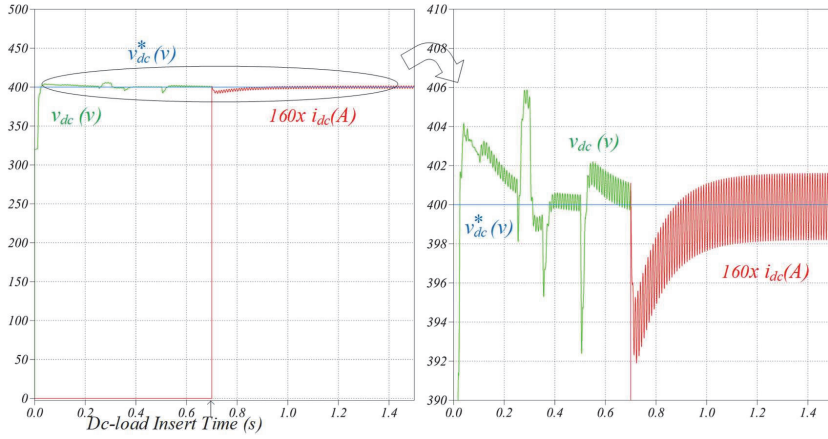


Fig. 6. De-link Voltage and De-load Current Simulation Results of the Traditional Control with c_{dc} 2000 μF .

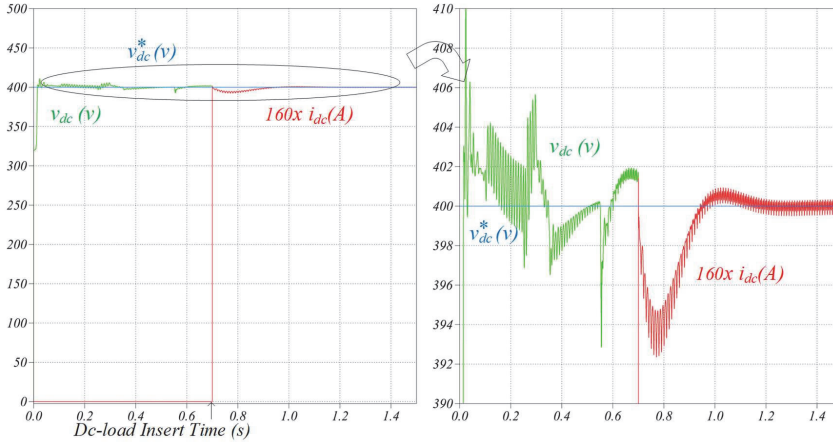


Fig. 7. De-link Voltage and De-load Current Simulation Results of the Proposed Control with c_{dc} 400 μF .

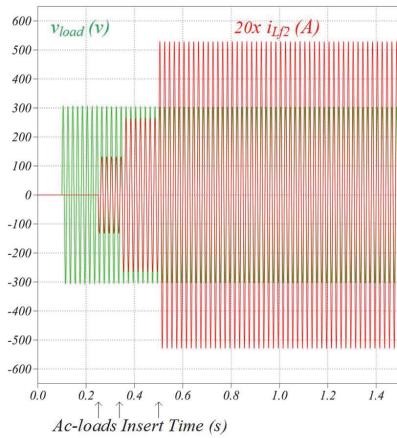


Fig. 8. Ac-load Side Voltage v.s. Ac-load Side Current Simulation Results of the Traditional Control with c_{dc} 2000 μF .

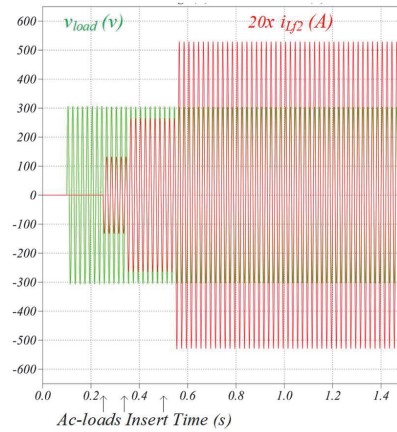


Fig. 9. Ac-load Side Voltage v.s. Ac-load Side Current Simulation Results of the Proposed Control c_{dc} 400 μF .

The summarized result is shown in Table 4 that confirms the capability of the proposed control technique to decrease the dc-link capacitor by 80% of the primary value.

V. CONCLUSION

Battery utilization as an active low-frequency decoupling technique is introduced in this study. A short review of low-frequency charging influence on the battery performance and lifetime proves the less performance degradation and less temperature rise in 100 and 120 Hz charging current frequency in comparison to the traditional CV-CC method. The results of the proposed control method prove the capability of battery utilization as decoupling double-frequency ripple voltage in dc-link voltage. The results demonstrate the compatibility of the proposed control technique with MPC as well. The capacitor in the proposed method decreases to 20% of the primary capacitor. The 1 v variation of dc-link voltage in full load steady-state in the proposed technique compared to the 4 v in the traditional method confirms the better performance of the proposed technique with the less dc-link capacitor.

ACKNOWLEDGMENT

This research was co-financed by the Estonian Research Council grants PUT1680, PRG675 and by the Estonian Centre of Excellence in Zero Energy and Resource Efficient Smart Buildings and Districts, ZEBE, grant 2020-2020.4.01.15-0016 funded by the European Regional Development Fund.

REFERENCES

- [1] M. Crenes, "Electrification and Decarbonisation - Analyst brief - Enerdata."
- [2] S. Sen and V. Kumar, "Microgrid control: A comprehensive survey," *Annu. Rev. Control*, vol. 45, pp. 118–151, Jan. 2018.
- [3] N. Shabbir, R. Ahmadihangar, L. Kütt, M. N. Iqbal, and A. Rosin, "Forecasting Short Term Wind Energy Generation using Machine Learning," pp. 0–3, 2020.
- [4] V. Sidorov, A. Chub, D. Vinnikov, and A. Bakaer, "An Overview and Comprehensive Comparative Evaluation of Constant-Frequency Voltage Buck Control Methods for Series Resonant DC-DC Converters," *IEEE Open J. Ind. Electron. Soc.*, vol. 2, no. November 2020, pp. 1–1, 2020.
- [5] M. A. Hannan *et al.*, "A review of internet of energy based building energy management systems: Issues and recommendations," *IEEE Access*, vol. 6, pp. 38997–39014, Jul. 2018.
- [6] R. Ahmadihangar, O. Husev, A. Blinov, H. Karami, and A. Rosin, "Development of a Battery Sizing Tool for Nearly Zero Energy Buildings," *IECON Proc. (Industrial Electron. Conf.)*, vol. 2020-Octob, no. 856602, pp. 5149–5154, 2020.
- [7] D. Wang, X. Ma, P. Su, B. Liu, W. Du, and L. Wu, "Household microgrid interaction technology based on power router," *Energy Procedia*, vol. 158, pp. 6452–6457, 2019.
- [8] M. H. Dadashi-Rad, A. Ghasemi-Marzbali, and R. A. Ahangar, "Modeling and planning of smart buildings energy in power system considering demand response," *Energy*, vol. 213, p. 118770, 2020.
- [9] M. B. Sanjareh, M. H. Nazari, G. B. Gharehpetian, R. Ahmadihangar, and A. Rosin, "Optimal scheduling of HVACs in islanded residential microgrids to reduce BESS size considering effect of discharge duration on voltage and capacity of battery cells," *Sustain. Energy, Grids Networks*, vol. 25, p. 100424, 2021.
- [10] M. Farrokhabadi, S. Konig, C. A. Canizares, K. Bhattacharya, and T. Leibfried, "Battery Energy Storage System Models for Microgrid Stability Analysis and Dynamic Simulation," *IEEE Trans. Power Syst.*, vol. 33, no. 2, pp. 2301–2312, 2018.
- [11] H. Wang, H. S. H. Chung, and W. Liu, "Use of a series voltage compensator for reduction of the dc-link capacitance in a capacitor-supported system," *IEEE Trans. Power Electron.*, vol. 29, no. 3, pp. 1163–1175, 2014.
- [12] H. Wang, H. Wang, G. Zhu, and F. Blaabjerg, "An Overview of Capacitive DC-Links-Topology Derivation and Scalability Analysis," *IEEE Trans. Power Electron.*, vol. 35, no. 2, pp. 1805–1829, 2020.
- [13] H. Wang and F. Blaabjerg, "Reliability of capacitors for DC-link applications in power electronic converters - An overview," *IEEE Trans. Ind. Appl.*, vol. 50, no. 5, pp. 3569–3578, 2014.
- [14] R. Chen, "DC Capacitor Minimization of Single Phase Power Conversion and Applications," Michigan State University, 2016.
- [15] M. Salcone and J. Bond, "Selecting film bus link capacitors for high performance inverter applications," *2009 IEEE Int. Electr. Mach. Drives Conf. IEMDC '09*, pp. 1692–1699, 2009.
- [16] Y. Tang *et al.*, "Highly Reliable Transformerless Photovoltaic Inverters with Leakage Current and Pulsating Power Elimination," *IEEE Trans. Ind. Electron.*, vol. 63, no. 2, pp. 1016–1026, 2016.
- [17] M. Mellincovsky, V. Yuhimenko, M. M. Peretz, and A. Kuperman, "Analysis and Control of Direct Voltage Regulated Active DC-Link Capacitance Reduction Circuit," *IEEE Trans. Power Electron.*, vol. 33, no. 7, pp. 6318–6332, 2018.
- [18] A. Mutovkin, V. Yuhimenko, M. Mellincovsky, S. Schacham, and A. Kuperman, "Control of Direct Voltage Regulated Active DC-Link Capacitance Reduction Circuits to Allow Plug-and-Play Operation," *IEEE Trans. Ind. Electron.*, vol. 66, no. 8, pp. 6527–6537, 2019.
- [19] Y. Tang, Z. Qin, F. Blaabjerg, and P. C. Loh, "A Dual Voltage Control Strategy for Single-Phase PWM Converters with Power Decoupling Function," *IEEE Trans. Power Electron.*, vol. 30, no. 12, pp. 7060–7071, 2015.
- [20] L. R. Chen, S. L. Wu, D. T. Shieh, and T. R. Chen, "Sinusoidal-ripple-current charging strategy and optimal charging frequency study for Li-ion batteries," *IEEE Trans. Ind. Electron.*, vol. 60, no. 1, pp. 88–97, 2013.
- [21] K. Uddin, A. D. Moore, A. Barai, and J. Marco, "The effects of high frequency current ripple on electric vehicle battery performance," *Appl. Energy*, vol. 178, pp. 142–154, 2016.
- [22] M. Uno and K. Tanaka, "Influence of high-frequency charge-discharge cycling induced by cell voltage equalizers on the life performance of lithium-ion cells," *IEEE Trans. Veh. Technol.*, vol. 60, no. 4, pp. 1505–1515, 2011.
- [23] T.-H. Kim *et al.*, "Analytical Study on Low-Frequency Ripple Effect of Battery Charging," in *IEEE Vehicle Power and Propulsion Conference*, 2012, pp. 809–811.
- [24] I. Roasto, A. Rosin, and T. Jalakas, "Multiport Interface Converter with an Energy Storage for Nanogrids," *IECON 2018 - 44th Annu. Conf. IEEE Ind. Electron. Soc.*, vol. 1, pp. 6088–6093.
- [25] S. Dusmez and A. Khaligh, "Generalized technique of compensating low-frequency component of load current with a parallel bidirectional DC/DC converter," *IEEE Trans. Power Electron.*, vol. 29, no. 11, pp. 5892–5904, 2014.
- [26] P. T. Krein, R. S. Balog, and M. Mirjafari, "Minimum energy and capacitance requirements for single-phase inverters and rectifiers using a ripple port," *IEEE Trans. Power Electron.*, vol. 27, no. 11, pp. 4690–4698, 2012.
- [27] M. Najafzadeh, R. Ahmadihangar, O. Husev, I. Roasto, T. Jalakas, and A. Blinov, "Recent Contributions, Future Prospects and Limitations of Interlinking Converter Control in Hybrid AC/DC Microgrids," *IEEE Access*, vol. 9, pp. 7960–7984, 2021.
- [28] Roasto *et al.*, "Voltage Source Operation of the Energy-Router Based on Model Predictive Control," *Energies*, vol. 12, no. 10, p. 1892, 2019.
- [29] E. Makovenko, D. Ommikov, C. Roncero-clemente, E. Romero-Cadaval, and D. Vinnikov, "Three-Level Single-Phase Quasi-Z Source Inverter With Active Power Decoupling Circuit," *Int. Conf. MICRO/NANOTECHNOLOGIES ELECTRON DEVICES EDM*, pp. 497–502, 2017.
- [30] S. Chen, Y. M. Lai, S. C. Tan, and C. K. Tse, "Analysis and design of repetitive controller for harmonic elimination in PWM voltage source inverter systems," *IET Power Electron.*, vol. 1, no. 4, pp. 497–506, 2008.

Curriculum vitae

Personal data

Name: Mahdiyyeh Najafzadeh
Date of birth: 14 June 1983
Place of birth: Iran
Citizenship: Iran

Contact data

E-mail: mahdieh6280@gmail.com

Education

2018–2022 Tallinn University of Technology – PhD
2012–2015 K.N. Toosi University of Technology – MSC
2001–2006 Shahid Beheshti University (Power and Water University of Technology) – BSC
1995–2001 National Organization for Development of Exceptional Talents (Sampad) – High school

Language competence

English Fluent
Persian Native
Germany Beginner
Arabic Beginner
Estonian Beginner

Professional employment

2013–2018 Arya Rahab Pazzh- Electrical engineering supervisor
2007–2012 Sane Shargh - Moham Shargh Group - R&D, L.V & H.V Electrical Substation Designer

Elulookirjeldus

Isikuandmed

Nimi: Mahdiyyeh Najafzadeh
Sünniaeg: 14. juuni 1983
Sünnikoht: Iraan
Kodakondsus: Iraani

Kontaktandmed

E-post: mahdieh6280@gmail.com

Hariduskäik

2018–2022 Tallinna Tehnikaülikool – PhD
2012–2015 K.N. Toosi University of Technology – MSC
2001–2006 Shahid Beheshti University (Power and Water University of Technology) – BSC
1995–2001 Rahvusvaheline organisatsioon erakordsete talentide arendamiseks (Sampad) – keskharidus

Keelteoskus

Inglise keel Kõrgtase
Pärsia keel Kõrgtase
Saksa keel Algtase
Araabia keel Algtase
Eesti keel Algtase

Teenistuskäik

2013–2018 Arya Rahab Pazzh- elektrotehniline juhendaja
2007–2012 Sane Shargh - Moham Shargh Group - R&D, L.V & H.V
Elektrialajaama projekteerija

ISSN 2585-6901 (PDF)
ISBN 978-9949-83-836-3 (PDF)